THEORETICAL AND EMPIRICAL APPROACHES TO EXAMINING THE INTERPLAY BETWEEN VASCULAR CONSTRAINTS AND PLANT RESPONSES TO ENVIRONMENTAL HETEROGENEITY

dissertation

submitted by

Alexandra M. Thorn

In partial fulfillment of the requirements
for the degree of

Doctor of Philosophy

in

Biology

TUFTS UNIVERSITY

February 2012

ADVISER: Colin M. Orians

Abstract

Environmental heterogeneity is ubiquitous in natural ecosystems, and plants, like other organisms, are constrained by their ability to make use of patchily distributed resources and to respond to localized stressors. Plants have developed numerous plastic responses to deal with environmental heterogeneity, but many of these responses are constrained by vascular architecture—the anatomical arrangement of the xylem and phloem. At the same time, vascular constraints—called sectoriality—are expected to have different effects on allocation of resources depending on the level of environmental heterogeneity. I combine modeling and empirical approaches to understanding ways that sectoriality interacts with plant responses to heterogeneity. The first two data chapters (Chapters 2 and 3) measure the movement of locally supplied isotopically labeled nitrate in basil, under different patchy scenarios. Chapter 2 shows that partial defoliation can cause increased crossover of nitrate between sectors. Chapter 3 shows that changes to local water uptake in the presence of a nitrate patch can affect inter-sector allocation. The third data chapter (Chapter 4) simulates water flow into, and transpiration and photosynthesis by high light leaves in trees whose crowns are otherwise shaded. The results of Chapter 4 suggest that sectoriality can constrain photosynthesis, but only when water is limited. The fourth data chapter (Chapter 5) examines crown morphology in understory saplings, to assess whether species with different wood types (and therefore different levels of sectoriality) use different strategies for branch biomass allocation in response to light gradients. The results of Chapter 5 did not support the hypothesized effect sectoriality on allocation patterns, suggesting that explanations are needed for the overall similarity between deciduous trees of

different wood types. The final data chapter (Chapter 6) presents a model for the effects of sectoriality on root proliferation in a nitrogen patch. The model output suggests interaction roles for xylem and phloem sectoriality in shaping root allocation. The model from Chapter 6 may be particularly useful for designing and interpretting experiments on nutrient foraging by plant roots. In the concluding chapter (Chapter 7), the results of the various data chapters are tied together and future research directions are suggested.

Acknowledgements

I thank my advisor Colin Orians for the central role he has played in my development of this dissertation, as well as in my development as a scholar. Thanks also go to the members of my graduate committee: Michael Reed, George Ellmore, and Stephen Levine from Tufts, and to my outside examiner Nathan Phillips from Boston University. All of these mentors have helped to shape the direction and final presentation of my doctoral research. In addition, I thank Sara Lewis, who was on my entrance committee, Francie Chew and Jan Pechenik, who were on my examination committee, and Phil Starks with whom the Orians lab shared lab meetings for the first two years of my time at Tufts. Francie and Phil have played particularly important mentoring roles outside of my committee.

The Tufts Department of Biology has served as my academic family since 2005, and it is impossible to thank all of the individuals from the department who have helped me at so many points along the way. Particular thanks go to the members of the Orians Lab, a.k.a. PRESH (Plant Responses to Environmental Stress and Heterogeneity): the graduate students Ben Babst, Minda Berbeco, Colleen Butler, and Tegan Morton; the post docs Coco Gomez and Selena Ahmed; and our numerous undergraduate researchers and assistants. Special thanks go to undergraduates Matilda Singleton, Caroline Roma, Margaux Birdsall, and Eliza McFarland, all of whom have provided direct assistance in the development of my research. My acknowledgements would not be complete without thanking the department staff, who have kept everything running smoothly for me during my years at Tufts: Phil Bibb, Liz Palmer, Eileen Magnant, Karin Murpy, Tony Keevan, and Michael Grossi.

The doctoral process is a period of particular emotional trials. It is therefore extremely valuable to have a strong network of friends. I have been particularly fortunate in this regard. I first thank my various housemates over these past six years (order from most recent to most distant): Chandra, Hanna, Reisa, Janna, Allie, Adam, Gabe, Julia, Jay, Regina, and to "Butterers" Mark Dulcey, Davis Droll, Tara Edwards, Beth Parkhurst. Fondest memories of roommate, landlady, and friend Marian Walke of the Buttery, who touched so many lives. Many other friends have offered various forms of support. I wish to name a few who have contributed most directly. Lori Campbell, in addition to being an awesome friend and great listener, has patiently watched me give practice presentations on a number of occasions. Eric Downs helped guide my systems thinking early my doctoral program. John Kraemer helped me to learn the R language. Alec Heller helped me become a more sophisticated programmer. Special thanks go to Justin Kao for editorial comments, for advice on everything from from time management to job applications, and for refusing to let me forget how wonderful LaTeX is for typsetting. In addition, thanks to many friends within the biology department who have provided more than an occasional helping hand: David Desrochers, Sasha Keyel, Jocelin Müller, Amy Yu, and many others.

Thank you to my family and family friends. Special thanks to my cousin Debbie Armstrong, to Patty Wallens and Jeff McCormack (the parents of my fiancé, Tim), and to the Furman clan and others I see at the CLAC gatherings at the Furman cabin each Columbus day weekend.

Last, but certainly not least, I thank my parents, Mary Furman and Charles Thorn, and my fiancé, Tim McCormack. Mama, Da and Tim, you have all done so much I know that I cannot possibly thank you properly. In particular, thank you for the stabilizing role in the long and winding road that has lead to the completion of my doctorate. This dissertation is a superior product for the continued role you have played in the life of its author.

This work was supported by the Tufts Department of Biology, the Tufts

Graduate School of Arts and Sciences, NSF REU (grant DBI 1005082 and DBI 0649190), and USDA National Institute of Food and Agriculture (Grant number 2007-35302-18351).

Table of Contents

List of Tables

List of Figures

CHAPTER 1

Introduction

Environmental heterogeneity is a ubiquitous characteristic of natural ecosystems, and growth of any organism is constrained by its ability to effectively make use of patchily distributed resources. This fact poses a particular adaptive problem for sessile organisms, such as plants. A great deal of research, therefore, has focused on the question of what strategies plants use to maximize acquisition of nutrients, water, and light in localized patches (Hodge 2006, Campbell et al. 1991). Observed responses to environmental heterogeneity have included tropisms (Takahashi 1994, Takano et al. 1995, Hangarter 1997), selective growth in high quality patches (Campbell et al. 1991, Robinson 1994, Hodge 2006), plasticity of local tissue development (Sack et al. 2003, Hodge 2006), dynamic changes to nutrient uptake rates (Hodge 2006), and changes to the hydraulic properties of leaves (Sack et al. 2003, Sack and M. 2006), roots (Gloser et al. 2007), and stems (Zwieniecki et al. 2003).

At the same time, it has also been noted that plant vascular architecture can limit the movement of resources needed for many of these responses (Watson and Casper 1984). Vascular constraints apply to both xylem transport of nutrients and water from the soil, and phloem transport of carbohydrates and other organic materials from photosynthesizing tissue to other parts of the plant. In general, each root only has direct connections to some parts of the crown, and each branch only has direct connections to some parts of the root system, a phenomenon called sectoriality. The ability to move resources outside of these direct connections varies according to species-specific anatomy, developmental

stage, and environmental context.

In this thesis, I use a combination of theoretical and empirical approaches to examine the interrelationship between vascular architecture and plant responses to environmental heterogeneity. To appreciate why sectoriality exists, and how it can constrain plant growth, it is essential to describe how resources are transported within xylem and within phloem. In this introductory chapter, I provide a general background on xylem and phloem transport processes within and between sectors, and introduce some ways in which sectoriality and heterogeneity responses interact to shape resource allocation and growth. I conclude this chapter with an overview of the approaches used in subsequent chapters to address a number of questions about the relationship between sectoriality and plant responses to heterogeneity.

1.1 Xylem and phloem overview

Long distance transport by xylem and phloem transport both rely on the bulk flow of sap. The hydraulic processes determining patterns of flow are mathematically understood using an hydraulic analogy to Ohm's law for electrical conductance. Below, I present an overview of plant hydraulics and the Ohm's law analogy, followed by an overview of transport processes in xylem and phloem.

1.1.1 Plant hydraulics and the Ohm's law analogy

Bulk flows in a hydraulic system are driven by differences in water potential (Ψ), i.e. the potential energy of water. Water moves from areas of higher Ψ to areas of lower Ψ. In plants, the overall water potential (Ψ_{total}) for any part of the plant is determined by the sum three components: the gravitational potential ($\Psi_{gravity}$), the pressure potential ($\Psi_{pressure}$), and the osmotic potential ($\Psi_{osmotic}$). $\Psi_{gravity}$ increases with elevation and $\Psi_{pressure}$ increases with hydrostatic or turgor pressure, the pressure that results from the compression of water in a confined space. $\Psi_{osmotic}$ becomes more negative as the concentration of solutes in

the water increases, but is only relevant to the flow of water across membranes (Taiz and Zeiger 2002).

Rates of water flow, or flux (Q), from along water potential gradients increase with the magnitude of the gradient and decrease with the hydraulic resistance (R). The flux and hydraulic resistance are related to the change in water potential ($\Delta\Psi$) between the two points by the Ohm's law analogy, where $\Delta\Psi$ is analogous to voltage, Q is analogous to current, and R is analogous to electrical resistance (Tyree and Ewers 1991):

$$\Delta\Psi = Q \times R \tag{1.1.1}$$

Hydraulic resistances across cell membranes are determined by the permeability of that membrane, and resistances along the length of xylem and phloem conduits are determined by the friction of the conduit. The resistance of a conduit can be approximated by Poiseuille's law, which states that the resistance per unit length of a cylindrical tube is inversely proportional to the fourth power of the diameter of the tube (d^4). Actual resistances of xylem and phloem conduits always higher than Poiseuille's law predictions, but the relationship provides a useful approximation for relating conduit anatomy to expected resistance.

Application of Ohm's law permits computation of whole plant hydraulic properties from the properties of individual components. When sap flux is considered across a number of plant components sequentially, the hydraulic resistance is simply the sum of the resistances across each component. When flux occurs through multiple components in parallel, e.g. the sap flow through the many xylem and phloem conduits in a vascular bundle, the overall conductance (the inverse of R) is the sum of the conductances for each component. Similarly, it can be shown that under steady-state conditions, the change in Ψ across a number of plant components in sequence is equal to the sum of the water potential changes across all components individually (Tyree and Ewers 1991).

1.1.2 Xylem overview

Xylem conducts water, mineral nutrients, and other molecules from the roots to the crown. The primary driving force for xylem transport is leaf water potential, which changes dynamically as a function of leaf water content.

During photosynthesis, water is lost from the leaves by transpiration from the stomatal pores, specialized structures open to permit the entry of carbon dioxide into internal air spaces. Since the internal air spaces are always close to 100% humidity, a great deal of water is lost per unit carbon dioxide fixed (typically $\sim$500 mol water / mol CO_2). As water vapor is lost, evaporation from the surface of mesophyll cells draws down the water content of these cells, increasing the concentration of solutes in the cytoplasm and decreasing the leaf osmotic potential. As leaf osmotic potential decreases, water is drawn from the xylem itself (Taiz and Zeiger 2002). The result is tension in the xylem water column and a gradient from more positive water potential in the roots to more negative water potential in the leaves (Taiz and Zeiger 2002).

Xylem conduits—vessels in angiosperms and tracheids in gymnosperms—are made up of the walls of dead cells. Since there are no membranes to cross, osmotic water potentials do not affect long distance transport in the xylem. Instead, as water is drawn into the leaves by transpiration, tension develops in the continuous column of xylem water from roots to leaves. The overall result is a water potential gradient from roots to leaves, driving the upward flow of water (Taiz and Zeiger 2002). The same gradients can also drive any lateral, or "tangential" flow between adjacent xylem elements (Ellmore et al. 2006).

In some cases, especially in herbaceous species and young trees, a secondary driver for xylem transport is generated by positive pressure in the root xylem. This pressure results when the concentration of mineral nutrients and other osmotically active molecules in the root xylem is greater than the concentration in the soil, osmotically drawing water into the root interior (Taiz and Zeiger 2002).

In the continually changing conditions of a natural ecosystem, the hydraulic

properties of the various plant components are not fixed. The total $\Delta\Psi$ between soil and leaves (and between different portions of the crown or different portions of the root system) depends on external factors such as soil moisture, root osmotic potential relative to the soil solution, atmospheric humidity, and leaf temperature. Gradients can shift due to changes in the hydraulic resistances of various tissues.

Transpiration from the leaves is modulated by opening and closure of stomatal pores in response to light environment and water availability (Tyree and Ewers 1991, Taiz and Zeiger 2002, Sack and M. 2006). When the water supply is plentiful, leaves in high light fix more carbon, and therefore lose more water, than leaves experiencing lower light levels. High light can also directly influence evaporation by changing the leaf temperature. At the same time, partial defoliation, e.g. as leaves are removed by leaf-chewing herboves, decreases the photosynthetic leaf area, and therefore the rate of transpiration, although water loss can initially increase due to evaporation from wound sites.

In the roots, water enters through the physiologically active surface near the root tips (Taiz and Zeiger 2002), and so hydraulic resistance decreases as this surface area increases, e.g. with increased root branching and proliferation in a nutrient patch (Hodge 2004). Since water entering the root tips must cross the membranes of living cells, the hydraulic resistance can be modulated at shorter time scales by the density of aquaporins (protein channels that conduct water) in these membranes. Aquaporin density has been shown to vary dynamically in response to nutrient availability, oxygen availability, salt or chemical stress, and day-night cycles. In general, root resistance tends to increase in stressful conditions (Javot and Maurel 2002).

While dynamic changes to the traits of the leaves and roots can generate differences in Ψ between parallel xylem streams, transport along lateral gradients is constrained by stem hydraulic properties. In the stems, resistance to axial and tangential flow depends on the dimensions, interconnections, and arrangement of xylem conduits: tracheids and vessels (Orians et al. 2005*a*). Vessels, the

Figure 1.1: Xylem vessel elements in *Quercus*. Light micrograph of a stained tangential section of oak (*Quercus*), showing the vessel elements of two parallel xylem vessels, and the tapered perforation plates separating them. Modified from http://www2.auckland.ac.nz/info/schools/nzplants/con_vascular.htm (retrieved 2008).

primary conduits in most angiosperms, are tube-shaped structures made up of the walls of stacks of dead cells called vessel elements (Fig. 1.1). Across species, maximum vessel lengths vary from several centimeters to many meters, and vessel diameters range from 25 to 500μm (Taiz and Zeiger 2002, Sperry 2003). Xylem sap moves from one vessel to another, axially or tangentially, through lateral pits in the end-walls and along the length of vessels (Fig. 1.2; Taiz and Zeiger 2002).

The hydraulic resistance associated with individual vessels (or individual pits) can be modeled by Poiseuille's law. Thus, interspecies variation in vessel diameter can have a large influence on xylem resistance (Tyree and Ewers 1991). Greater vessel lengths and larger vessel diameters promote axial flow, and thus a greater proportion of resources carried along direct pathways, as compared to indirect (tangential) pathways. The result is a more sectored distribution of resources by the xylem, all else held equal (Zanne et al. 2006*b*). At the same time, transfer of sap between parallel vessels is constrained by the number pits per vessel and the area of these pits (Hacke et al. 2006).

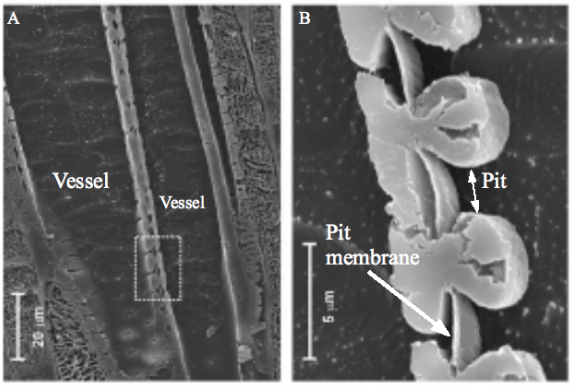

Modified from Choat (2004)

Figure 1.2: Electron micrograph of pit field connecting two xylem vessels. A) The two vessels, labeled, showing pit field in wall between them. B) Magnification of the boxed portion of vessel wall from (A), showing individual pits and the thin "membrane" of cell wall in each. Modified from Choat et al. (2004).

Xylem sectoriality also depends upon the overall configuration of vessels relative to their neighbors, an attribute that varies considerably among species (Ellmore et al. 2006, Zanne et al. 2006*b*). In herbaceous plants, vessels are located in discrete vascular bundles (Scarpella and Meijer 2004), an arrangement that will tend to result in higher sectoriality than is seen in woody species, where vessels are spread throughout the sapwood (Orians et al. 2005*a*). The functional segregation of bundles in herbaceous species may be reduced, however, by contact between different bundles at different heights along the stem, as is clearly documented in a number of species, e.g. tomato (Zwieniecki et al. 2003) and various members of the mint family (Gupta and Bhambie 1977).

Thus the degree to which xylem sap crosses between parallel vessels is determined by species specific arrangement of the vessels as well as by environmental heterogeneity. Patterns of transport in the stems are also influenced by environmental factors that affect the vascular tissue directly. For instance, when sap tension is high or freezing occurs, bubbles called embolisms can form in the xylem stream. These can expand to fill entire conduits, a process called cavitation. By blocking portions of the conductive tissue, cavitation results in increased resistance to axial flow through all or part of the stem. Similarly, mechanical damage to vascular tissue can increase axial resistance directly, as well as increasing the chance of embolism formation and cavitation.

Finally, in addition to the various factors affecting bulk flow of xylem between sectors, specialized transfer cells may influence sectoriality of xylem transport. These cells have been documented to move mineral nutrients from one xylem stream to another, e.g. to provide high nutrient xylem sap to young expanding leaves with relatively low transpiration (Pate and Jeschke 1995). However, it is not known whether these cells play a role in the lateral distribution of nutrients.

1.1.3 Phloem overview

The phloem conducts carbohydrates and other materials from carbon "sources," such as photosynthesizing leaves, to "sinks," such as the roots, young leaves, and developing flowers and fruits. In contrast to xylem vessels, phloem conduits (sieve tubes in angiosperms) are made up of living cells. Individual cells ("sieve tube elements") in a sieve tube are connected by specialized structures called plasmodesmata, so—as in the xylem—material does not need to cross a cell membrane to pass from one sieve tube element to the next (Fig. 1.3). The driving force behind long distance transport in the phloem is pressure gradients resulting from differences in the osmotic properties of sources and sinks. Loading of carbohydrates at sources results in osmotic influx of water into the phloem, increasing the local pressure potential. Export at the sinks results in efflux of water and so decreases local pressure potential (Taiz and Zeiger 2002). Tissues that are growing or more physiologically active tend to be stronger sinks and thus receive a larger portion of the phloem sap compared to weaker sinks fed by the same set of sieve tubes.

Xylem and phloem differ in sap flow rates and internal pressure. Movement through the phloem is generally slower, ranging from 0.3 to 1.5 m/hr, as compared to rates of 0.3 to 45 m/hr through the xylem (Taiz and Zeiger 2002). Furthermore, while xylem sap is generally under tension during transpiration, phloem sap is continually under positive pressure. As a result, material in phloem sap can leak from one sieve tube, to be actively taken up

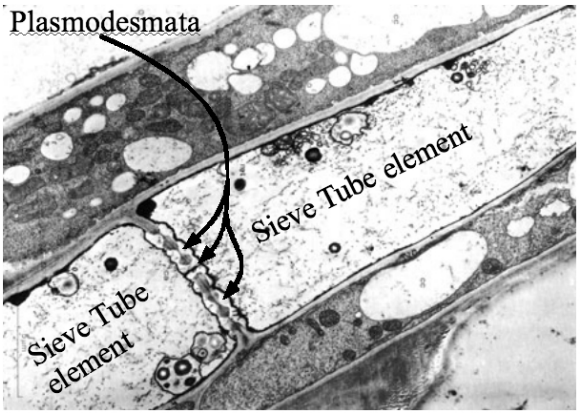

Figure 1.3: Sieve tube elements. Micrograph of a pair adjacent of sieve tube elements with plasmodesmata connecting them. Modified from http://www.unis.org/UNIScienceNet/IBHbio3_knowledge.html (retrieved 2008).

later, sometimes by a different sieve tube (Thorpe et al. 2005). This process has been hypothesized to provide an alternative pathway for lateral transfer of resources(Orians et al. 2005*a*).

In general, the mechanistic basis for phloem sectoriality is less well understood than xylem sectoriality. Experimental studies on recovery from asymmetrical damage (Shea and Watson 1989, Murphy and Watson 1996) and movement of isotopically labeled carbon (Preston 1998, Bledsoe and Orians 2006) show that movement of materials between parallel phloem sieve tubes occurs in some species more than others, but the processes whereby carbon moves laterally are not known. The documentation of sieve pore areas connecting parallel sieve tubes (Esau 1969) suggests that bulk flow might play a role, e.g. enabling strong source leaves in high light to supply carbon to the entire root system. However, it is not known how important bulk flow is relative to leakage and re-uptake, or activity of specialized transfer cells, which can move material between phloem streams as well as between xylem streams (Pate and Jeschke 1995).

1.2 Interactions between sectoriality and heterogeneity responses

Physiological responses to environmental heterogeneity are expected both to influence the inter-sector movement of resources and to be constrained by vas-

cular sectoriality. As noted above, local physiological changes in response to environmental heterogeneity have various effects on the pressure gradients that drive vascular transport within and between sectors. Active photosynthesis increases transpirational pull in the xylem and source strength in the phloem. Patchy distribution of water changes the soil water potential around different portions of the root system. Increased local root growth increases sink strength, as does the uptake of certain mineral nutrients (e.g. nitrate), which must be actively taken up from the soil. Finally, increased root conductance in high quality patches is expected to result in less negative water potentials in the connected xylem, potentially driving inter-sector flow.

At the same time, vascular constraints are expected to limit the ability of plants to effectively respond to environmental heterogeneity. Many of the responses to high quality patches are costly in terms of resources supplied by other structures. Selective growth of roots in a nutrient patch requires carbon fixed in the leaves, and selective growth of shoots in a high light patch requires nutrients and water from the roots. Active uptake of nitrate may be limited if only part of the crown can supply carbohydrate to roots in a high nitrate patch. Similarly, carbon fixation by the leaves is impossible without a steady supply of water to replace evapotranspiration losses. Logically, these inputs can be maximized if the vascular system permits resource supply to individual roots from the entire crown, and to individual branches from the entire root system.

1.3 Sectoriality research approaches to date

Most sectoriality studies to date have fallen into one of two broad categories: either they expose plants to patchy treatments and check for the subsequent growth responses, or they use specific artificial means to examine the limits to inter-sector resource allocation. Experiments exposing plants to patchy treatments and observing subsequent patterns of growth have included partial defoliation treatments (e.g. Shea and Watson 1989, Price and Hutchings 1992, Murphy and Watson 1996), and patchy nutrient treatments (e.g. Gloser et al. 2008).

These experiments examine the ecological consequences of sectoriality, but the emphasis on end-result can make it difficult to understand what processes underlie the effects of heterogeneity on growth.

More artificial approaches provide a more detailed picture. These manipulations have included dye studies, isotopic studies, and direct hydraulic measurements. In dye studies, colored dye is applied to a cut portion of the plant, where it can enter the xylem, and its subsequent distribution is observed (e.g. Kozlowski and Winget 1963, Larson et al. 1994, Orians et al. 2000, 2004). Isotope studies are similar in design, but have the advantages of using the natural uptake pathways of the plant (which do not damage the plant, and so are more representative of real transport patterns, and of permitting transport by phloem as well as xylem). This approach has been used to observe the subsequent distribution of isotopically labeled carbon applied isolated leaves (e.g. Murphy and Watson 1996, Preston 1998) or nutrients (notably nitrogen and phosphorus) applied to parts of the root system (e.g. Rinne and Langston 1960, Orians et al. 2004, Zanne et al. 2006*a*). Direct hydraulic conductance measurements provide a physical description of xylem resistance to transport along the most direct route, which is then compared to the resistance when the direct route is blocked, e.g. by application of epoxy over the direct outflow path (e.g. Zwieniecki et al. 2003, Orians et al. 2005*b*, Ellmore et al. 2006, Zanne et al. 2006*b*).

Another category of experiment has included efforts to evaluate the ability of plants to overcome specific interruptions of their transport pathways. For instance, in "saw cut" experiments in trees, where sawcuts are made partway through the stem, at different levels, and from different directions (e.g. Mackay and Weatherly 1973, Sperry et al. 1993), which interrupts xylem transport. Similarly, and partial girdling cuts through a portion of the phloem, while leaving the xylem intact (e.g Peel 1963). Saw cuts and girdling have been used to remove direct pathways of transport while leaving indirect pathways in place. This class of experiments is similar to the defoliation and patchy nutrient treatments in that they involve an asymmetrical treatment and evaluation of sub-

sequent processes. On the other hand, the damage is quite drastic, and has been carefully designed to uncover properties of vascular function rather than to understand ecological functioning, so in some ways they can also be seen as falling into the category of artificial approaches.

None of the above approaches quite address the question of how sectoriality constraints change under patchy environmental conditions, and what the consequences are for plant performance. Observations of growth patterns demonstrate sectoriality effects, but the ability to regrow after partial damage or to respond to a high quality patch also depends on intrinsic growth rates, availability of stored resources, and other environmental resilience traits beyond vascular architecture. Labeling studies could in principle be combined with environmental heterogeneity treatments, but generally are not (Bledsoe and Orians 2006, with a few exceptions, e.g.). Hydraulics studies reveal the physical limits of what a system can do, but do not indicate the degree to which these limits are physiologically relevant. Double saw cut experiments provide some physiological insights into the physical limitations of xylem transport, but leave open the question of how transport is affected by less extreme asymmetries.

A great deal remains to be done to tease apart the ecological relevance of sectoriality within an environmental context. One key limitation of research to date has been the absence of a theoretical framework for quantitatively predicting the effects of particular forms of environmental heterogeneity. When combined with labeling studies with environmentally patchy treatments, such a framework would provide the ability to assess whether allocation patterns are more or less than what would be expected based on our existing knowledge, thereby both evaluating the usefulness of the model and placing quantitative results into a more specific context. This thesis aims to provide such a framework, with preliminary validation, as well as providing some applications in answering specific questions about plant responses to light and nutrient heterogeneity.

1.4 Specific questions and approaches

This thesis presents a theoretical framework for understanding the interrelationships between sectoriality and environmental heterogeneity. Theoretical and empirical approaches are used to assess the usefulness of the framework and its limitations, and results are presented from theoretical studies to assess the possible effects of sectoriality in specific environmental contexts. Environmental heterogeneity scenarios considered include partial defoliation and patchy nutrients and light. Here I outline the specific questions and approaches used in Chapters 2-6.

In the first two data chapters (Chapter 2 and Chapter 3) I evaluate the predictive usefulness of a novel modeling framework for understanding nitrate allocation in basil (*Ocimum basilicum*, L., Lamiaceae). Chapter 2 ("Partial defoliation and hydraulic integration in *Ocimum basilicum*: Testing a model for sectored xylem flow using 15N labeling", in press at the *American Journal of Botany*) evaluates the usefulness of the xylem sectoriality model in predicting the crown distribution of nitrate following partial defoliation. Chapter 3 ("Patchy nitrate promotes inter-sector flow and 15N allocation in *Ocimum basilicum*: A model and an experiment," in press at *Functional Plant Biology*) uses the same modeling approach to investigate the predicted effects of changes in root hydraulics with patchy nitrate on the distribution of nitrate in the crown of basil. In each of these chapters, model outputs based on estimated values for physiological traits are compared to observed patterns of labeled nitrogen movement.

Chapters 4 and 5 investigate the role of sectoriality in aboveground performance of understory trees. Chapter 4 ("Modeling the influence of differential sectoriality on the photosynthetic responses of understory saplings to patchy light and water availability", published in *Trees—Structure and Function*) uses the same modeling framework as the previous two chapters in a strict theoretical approach to the question of whether sectoriality is likely to limit photosynthesis in understory trees by constraining the supply of water to leaves in a high light patch. Chapter 5 ("Do stem inclination and branch asymmetry

play different roles in canopy displacement for trees of different wood types?: An observational analysis of understory trees") presents the results of an exploratory crown morphology study to evaluate a new hypothesis for how patterns of crown growth to optimize light capture might differ between sectored and intergrated tree species.

The final data chapter (Chapter 6, "Modeling sectored resource allocation in patchy soils: A new perspective on root precision and nutrient foraging by plants") uses a new modular plant model to tie together the consequences of xylem and phloem sectoriality in a whole plant growth model. The model used in this chapter combines the xylem model used in Chapters 1–3 with a similar model for phloem sectoriality and a modular physiological growth model. This framework is used to simulate patterns of resource allocation and growth for plants exposed to long-term nutrient patches. Thus, sectoriality is related to patterns of root proliferation in nutrient patches, which have been shown to differ between species. Chapter 6 is particularly timely given current renewed interest in root foraging following recent meta-analyses showing that the popular hypothesis of a precision-scale tradeoff in root growth patterns is not supported by the literature (Kembel and Cahill 2005, Kembel et al. 2008).

In the concluding chapter (Chapter 7), I tie together the findings of Chapters 2–6. I place my theoretical and empirical results in the context of previous research on sectoriality and responses to environmental heterogeneity and suggest future research directions that would build on my findings.

CHAPTER 2

Partial defoliation and hydraulic integration in *Ocimum basilicum* (Lamiaceae): Testing a model for sectored xylem flow using ^{15}N labeling

Authors: Alexandra M. Thorn and Colin M. Orians

Published: 2011 *American Journal of Botany*, 98: 1816–1824

2.1 Abstract

Premise of the study: Xylem sectoriality limits nutrient translocation throughout the plant, which may constrain growth following partial defoliation by herbivores. To date, the implications for nutrient allocation have not been measured, and sectoriality studies lack a modeling framework for relating intersector transport to the hydraulic properties of the stem.

Methods: We present an Ohm's law model for sectoriality of xylem transport in basil (*Ocimum basilicum* L.), which we parameterized and tested using hydroponically grown split-root basil, pruned to two branches. To evaluate xylem resistance, we forced KCl solution through excised stems along either direct or indirect pathways. To examine the effect of partial defoliation on nutrient allocation, we applied ^{15}N-NO_3 to one half of the root system after one of three defoliation treatments: uniform, orthostichous to label, or opposite the label.

Key results: In support of our model, we found a tight correlation between total water uptake and total leaf area and between the actual and predicted proportions of water taken up from the labeled container. Significantly more ^{15}N accumulated in orthostichous than in opposite sector leaves for the uniform and

opposite defoliation treatments, but not for the orthostichous defoliation treatment. Across individuals, ^{15}N distribution varied as predicted by the model, but there was generally 10% more ^{15}N crossover than predicted.

Conclusions: These results support our model and suggest high potential integration for *O. basilicum*. The fact that our model consistently underestimated the rate of crossover suggests that other mechanisms are also in play. Future research should evaluate possible mechanisms for this mixing, including the role of transporters in specialized transfer cells.

2.2 Introduction

In vascular plants, the distribution of newly acquired nutrients from a particular root depends on the anatomical configuration of xylem and phloem, as well as on tissue demand for the nutrients, transpirational demand, and source-sink dynamics. Depending on the physical arrangement of xylem vessels and phloem sieve tubes, species differ in the ability to transport resources between parallel pathways, a limitation called sectoriality (Price et al. 1992, Orians et al. 2004, Zanne et al. 2006*a*). These constraints are expected to limit the ability of plants to respond to heterogeneous ecological factors such as patchy nutrients, partial shading, or partial defoliation by herbivores. The importance of vascular architecture to nutrient allocation has been demonstrated in a variety of species. For example, Zanne et al. (2006*a*) showed that in tomato the distribution of ^{15}N applied as nitrate or ammonium to an isolated lateral root depends on leaf biomass, developmental stage, and most strongly on vascular connections. Similar patterns have been observed in other species, but the relative importance of sectoriality to resource distribution is variable (Orians et al. 2004, 2005*a*, Ellmore et al. 2006, Zanne et al. 2006*b*, Gloser et al. 2008). For instance, Orians et al. (2004) showed that ^{15}N accumulation in branches of tree seedlings was tightly correlated with branch dry mass for integrated species (those with low sectoriality), but that this correlation was much weaker for sectored species.

A probable mechanism relating resource distribution to leaf biomass is vari-

ation in transpirational pull among leaves of different sizes (Siebrecht et al. 2003, Zanne et al. 2006*a*). In addition to the observations by Zanne et al. (2006*a*) that ^{15}N accumulation correlated with leaf size in tomato, Siebrecht et al. (2003) noted greater nutrient allocation to young leaves in poplar without a corresponding change to the xylem concentration of these nutrients, indicating that rate of bulk flow through the xylem was central to nutrient delivery. Furthermore, there is strong evidence that changes to flow within the xylem stream can modify nutrient allocation between sectors. When the roots of one sector are deprived of water, nutrients move freely from sectors still receiving water to other water-deprived sectors of the plant (Orians et al. 2005*a*). If resource distribution is indeed determined by transpirational pull, then changes to transpiration that are confined to a single sector—that would result from localized defoliation by herbivores—would be expected to modify the sectoriality of resource distribution.

Non-uniform defoliation by herbivores is common in nature. Large leaf chewing insects such as older caterpillars of Manduca sexta routinely remove large fractions of the leaf biomass in tomato plants, removing entire leaves over the course of a few hours (personal observation), and mammalian browsers can have a similarly rapid effect on small plants. Herbivore growth, survival, and behavioral responses to physical and chemical heterogeneity within the crown can further contribute to patchy defoliation (e.g., Suomela et al. 1995, Rodriguez-Saona et al. 2009, Roslin et al. 2006, Takeuchi et al. 2009). Herbivore preferences are influenced by a branch's immediate physical environment, as well as on the presence or absence of signals and defense compounds induced by previous herbivory and constrained by vascular architecture (Orians and Jones 2001). Defense compounds often deter herbivory, especially by generalists, although some specialist herbivores can be attracted by these compounds (Orians et al. 2011). Despite extensive research on the importance of vascular architecture to heterogeneity of leaf chemistry as noted already, and to subsequent patterns of carbon allocation and growth (Thomas and Watson 1988,

Shea and Watson 1989, Horton and Lacey 1994), little attention has been paid to the details of how nutrient allocation changes after an asymmetrical defoliation event. The present study addresses this question via artificial defoliation treatments in basil (*Ocimum basilicum*; Lamiaceae).

Plants in the Lamiaceae provide an ideal system for studying the effects of sectoriality on resource allocation and growth. These species are characterized by a square stem, vascular bundles in the four corners of the stem, and opposite-leaf growth habit. Each leaf or branch is fed by the two adjacent vascular bundles (Rinne and Langston 1960, Murphy and Watson 1996, Preston 1998). *Ocimum* species, including *O. basilicum* have been characterized as having unilacular, one-traced nodal anatomy, with adjacent bundles fusing to form a single trace entering each leaf, suggesting that the nodes are a likely site for intersector crossover (Gupta and Bhambie 1977). The symmetrical growth pattern permits easy comparison of leaves or branches from different sectors while controlling for position and age. Under uniform conditions, these species display strong sectoriality of carbon and nutrient movement (Rinne and Langston 1960, Murphy and Watson 1996). For instance, in *Mentha piperita*, the strongest labeling occurring in the leaf halves directly supplied by the labeled vascular bundle connected to roots receiving ^{32}P-phosphate (Rinne and Langston 1960). Similarly, when a single leaf was labeled with ^{14}C in Coleus rehneltianus, roots with direct vascular connections to the labeled leaf were primarily labeled (Murphy and Watson 1996). These sectored patterns appear not to be rigidly fixed: Preston (1998) showed that *Perilla frutescens* displayed stronger sectoriality of ^{14}C movement during reproductive than vegetative growth phases. In the clonal species Gechoma hederacea, regrowth following defoliation was significantly higher when leaf area removal was distributed between orthostichies than when all leaves were removed from a single orthostichy, indicating high sectoriality for this species (Price and Hutchings 1992). However, in an accompanying paper from the same laboratory, a nonsignificant trend of increased flow of ^{14}C between orthostichies was noted, suggesting some ability to over-

come vascular constraints following defoliation (Price et al. 1992).

While a number of studies have examined the effects of sectoriality on recovery from uniform or non-uniform defoliation events and the resulting distribution of ^{14}C, little information exists on the effect of defoliation on xylem translocation and on nutrient distribution. Furthermore, sectoriality studies to date have lacked a single theoretical framework for predicting the importance of sectoriality for uniform vs. non-uniform treatments. We present a hydraulic model for xylem sectoriality in basil (*Ocimum basilicum*), which we evaluated using split-root hydroponic basil with half of the root system receiving ^{15}N-labeled NO_3. We subjected plants to either uniform partial defoliation or asymmetrical partial defoliation on the same (orthostichous) or opposite side as the roots receiving label. Under the assumption that nitrogen distribution is a passive consequence of xylem sap movement, we predicted that crossover of locally supplied ^{15}N to the opposite side of the plant would only occur when the model predicted water crossover from the labeled side to the unlabeled side. We expected that this crossover would primarily occur for the orthostichous-side defoliation treatment (Fig. 2.1) and that any ^{15}N crossover in the other treatments would result from pre-existing biomass asymmetries in leaves or roots.

2.3 Model description

Similar to the model presented by Thorn and Orians (2011*a*), our sectoriality model adapts the Ohm's Law analogy for hydraulic conductance to simulate the rate of resource transfer between parallel xylem streams. The model simulates the whole plant xylem as two direct root-to-leaf pathways, connected to each other by a set of tangential resistors that represent the combined effects of indirect xylem pathways. Each direct pathway includes the resistance to vertical flow contributed by the roots ($r_{r1,2}$), the stem axial resistance ($r_{a1,2}$), and the leaves ($r_{l1,2}$) within this pathway. The overall stem axial resistance in each sector is modeled by n resistors each with resistance $r_{a1,2}/\mathrm{n}$, which are connected by

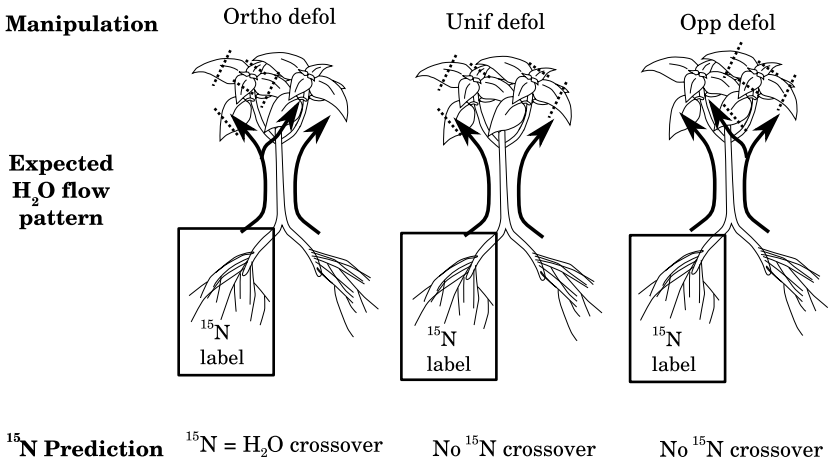

Figure 2.1: General predictions for how defoliation treatments (orthostichous to label = Ortho defol, uniform = Unif defol, opposite the label = Opp defol) will affect water flow between sectors and intersector crossover of the ^{15}N label applied as nitrate. Dotted lines on leaves indicate the cuts made to remove parts of leaves for each of the three treatments.

n + 1 tangential resistors each with resistance rt$\times$(n + 1), where rt is the overall tangential resistance. Flow within and between sectors is driven by differences in water potential between the roots ($\Psi_{r1,2}$) and the leaves ($\Psi_{l1,2}$) (Fig. 2.2).

Based on the unit pipe model, which relates xylem secondary growth to the leaf area supplied by that tissue (cited in Tyree and Ewers 1991) and the observation that xylem differentiation is regulated by the presence of leaves on that side of the plant (Wangermann 1967), we assumed that for a particular plant, the leaf and stem axial resistances for each sector i are inversely proportional to the estimated area of leaves in that sector (A_{li}) prior to defoliation:

$$r_{ai} = R_a A_{li} \tag{2.3.1}$$

$$r_{li} = R_l A_{li} \tag{2.3.2}$$

where R_a is the stem axial area resistivity (MPa d cm^2 mL^{-1}), which we estimated from hydraulic measurements on basil (see Materials and Methods), and R_l is the leaf area resistivity and was assumed to be one quarter of the whole plant axial resistance (Sack et al. 2003). The overall tangential resistance

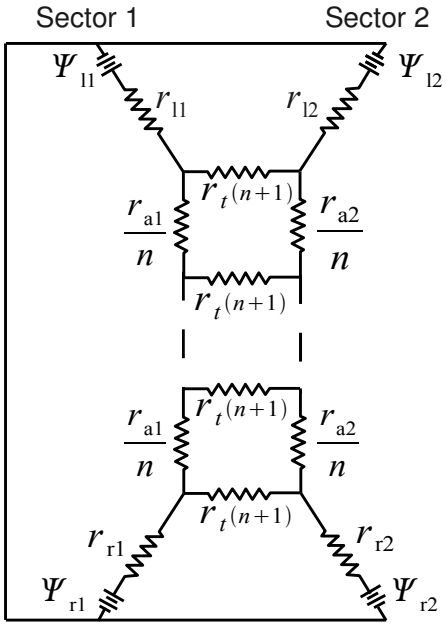

Figure 2.2: Diagram of Ohm's law model for hydraulic sectoriality in basil plants. The parameters of the circuit include water potentials for the leaves (Ψ_l) and roots(Ψ_r) of each sector (1 and 2), hydraulic resistances to flow through the leaves (r_l), along the main axis of the stem (r_a), and to flow from the soil into the roots (r_r) of each sector (1 and 2). The parameter r_t designates the tangential resistance to flow between the two hydraulic sectors of the plant. In the circuit, the stem is subdivided into n segments, and the resistance components for r_a and r_t for each component are scaled to represent just the contribution of that component (modified from Thorn and Orians 2011*a*).

r_t (MPa d ml^{-1}) is assumed uniform across plants was also estimated based on our based on empirical resistance measurements.

Root resistance for each sector is assumed to be inversely proportional to the lateral root biomass for that sector (W_{ri}):

$$r_{ri} = R_r W_{ri} \tag{2.3.3}$$

where R_r is the root mass resistivity assumed to equal 0.0015 MPa d g dry mass mL^{-1}, a value consistent with flows observed through excised basil roots when positive root pressures typical of herbaceous plants are assumed (see Supplemental Data from Thorn and Orians (2011*c*), or Appendix of Chapter 3, section 3.7) and toward the lower end of resistivities reported by Newman (1973) for herbaceous plants.

The internal root pressure for each sector ($\Psi_{r1,2}$) was assumed to be 0.1 MPa, a mid-range value for herbaceous plants (Taiz and Zeiger 2002). The hydraulic pressure for leaves was modeled as:

$$\Psi_{li} = \Psi_{pli} + \Psi_{oli} \tag{2.3.4}$$

where Ψ_{pli} is the pressure potential of mesophyll cells in sector i, and Ψ_{oli} is the osmotic potential of mesophyll cells in sector i. These water potentials are in turn modeled as a function of leaf water content, based on Thornley and Johnson (2000) models for plant water potential. Pressure potential is always positive and increases with water content above the turgor loss point:

$$\Psi_{pli} = max(0, \epsilon \times (\frac{c_{dw} W_{wli}}{W_{li}} - 1)) \tag{2.3.5}$$

where W_{wli} is the simulated mass of water in the leaves of a sector (Eq. 2.3.7), W_{li} is the dry mass of leaves in a sector, ϵ is the elastic modulus of leaf cell walls (assumed 1.0 MPa after Thornley, 1996), and c_{dw} is the ratio of leaf dry mass to leaf water content at $\Psi_{pli} = 0$ (assumed to be 0.15 based on the typical mass difference between fresh and dry mass for basil leaves). Osmotic potentials are

always negative, but become more positive with increasing leaf water content:

$$\Psi_{oli} = -K_o \times \frac{W_{li}}{W_{wli}} \tag{2.3.6}$$

where K_o is an osmotic parameter ordinarily dependent on temperature and mesophyll osmotic properties that we assume is constant at 1.83 MPa.

For each sector, W_{wli} is calculated as the steady state solution ($dW_{wli}/dt = 0$) to the equation:

$$\frac{dW_{wli}}{dt} = q_{li} - E_{ti} \tag{2.3.7}$$

where q_{li} is the flux of water into the leaves of sector i calculated by solving the our model circuit (Fig. 2.2) and E_{ti} is the total rate of evapotranspiration from leaves in the sector, assumed for modeling purposes to be constant on a per-area basis at 1.0 mL d^{-1} cm^{-2} based on typical water uptake rates observed for our hydroponic basil plants.

2.4 Materials and Methods

2.4.1 Plants and cultivation

To evaluate our hypotheses, basil (*Ocimum basilicum* var. Sweet Basil from Burpee, Warminsler, Pennsylvania, USA) was cultivated in a split-root hydroponic setup. As noted already, basil grows quickly and has opposite-leaf growth habit, an ideal trait in sectoriality studies because it permits intersector comparison of leaves or branches of the same age. Throughout cultivation and the experiments, all plants were grown in a greenhouse at Tufts University, Medford, Massachusetts, USA. Natural light was supplemented with 400-W sodium halide light to give a total of 16 h of light in each 24-h period.

For stem hydraulic measurements, seeds were sown between 8 October 2008 and 31 December 2008 and harvested on staggered dates between 4 April 2009 and 23 May 2009. For the ^{15}N experiment, seeds were sown between March and June 2009, and the experiment was performed in five time-staggered

blocks, with harvest dates between June and September 2009. Seeds were germinated in moist MetroMix potting soil with water supplied from below. Shortly after emergence of the first true leaves, seedlings were transplanted into individual pots containing 50% sand and 50% zeolite (ZeoPro zeolite) to facilitate later transfer to hydroponic solutions. Plants growing in the zeolite mixture were watered every 2 d and were fertilized twice weekly with 70 mL of a Hoagland solution: 603.0 μmol/L Ca(NO_3)2, 795.0 μmol/L KNO_3, 190.0 μmol/L KH2PO4, 270.0 μmol/L MgSO4, 0.09 μmol/L ZnSO4, 0.15 μmol/L CuSO4, 20.0 μmol/L CuSO4, 20.0 μmol/L H3BO3, 0.25 μmol/L Na2MoO4, and 40.5 μmol/L FeNa EDTA. After fifth-node leaves had emerged, plants were decapitated just above the fourth node. When lateral branches had emerged from the fourth node, all other leaves and branches were pruned from the main axis (Appendix, section 2.8 Fig. 2.7).

Between April and August, plants were transferred to split root hydroponics containers. Roots were rinsed to remove the sand-zeolite mixture, and the taproot was carefully cut down the center using a razor blade (Appendix, section 2.8 Fig. 2.7). This split was placed such that each half had direct vascular connections to one of the two branches emerging from node 4. This cut was extended upward to the height of the cotyledons. Any portions of the main root too narrow to divide were removed, and if the number of lateral roots on the two halves of the root system differed substantially after these manipulations, excess lateral roots were removed to equalize the two halves of the root system.

Each half of the root system was trained into one of a pair of 300 mL containers of hydroponic solution and supported using an attached stake. Hydroponic containers received a 50% dilution of the same nutrient solution used for plants grown in zeolite (see above), which was fully replaced once every 2 d. Once a day, deionized water was added to maintain constant solution volume. The volume of water added was recorded as a measure of water uptake. Air was supplied to each half of the root system by plastic tubing connected to a pressure pump (model UN035.1.2 STP, KNF Neuberger, Trenton, New Jersey, USA).

Each plant received air via a plastic tube (interior diameter = 1.6 mm), which in turn was attached to a 20-gauge hypodermic needle inserted into a short length of vacuum tubing connected to the pump. Air flow rates to each container were maintained at a minimum of 30 mL air/min.

2.4.2 Stem hydraulic measurements

Stem axial and tangential resistances were measured on three plants not subject to the defoliation treatments. The bases of branches and the two halves of the root system were wrapped in parafilm, plants were submerged in water, and a razor blade was used to remove roots and leafed portions of branches by cutting through the parafilm. Also under water, plastic tubing (internal diameter = 3.2 mm) was attached to each cut branch and each half of the root system, with the parafilm left in place as a seal. A zip-tie was used to secure each length of tubing in place. The plastic tubing attached to the branches had been previously filled with water, while the tubing attached to the roots contained 20 mmol/L KCl solution to simulate the osmotic properties of xylem sap (sensu Zwieniecki et al. 2003). Each of the four tubes was connected to a stop-cock to control inflow or outflow, so that 20 mmol/L KCl, pressurized to about 0.05 MPa could be forced through either half of the root system, while water was only permitted to flow out through one or the other of the branches (Fig. 2.3). Hydraulic resistances were calculated as the flow rate divided by the pressure applied. Tangential resistance (r_t; Fig. 2.2) was assumed to correspond to the total resistance to flow from half of the root system to the branch on the opposite side, minus the resistance to flow to the same-side branch. Leaf area specific resistivity for axial flow was determined by multiplying the resistance for each sector by the area of leaves from the outflow branch, as calculated from the leaf dry mass for each branch and specific leaf area 200 $cm^2\ g^{-1}$. The average stem axial resistivity (scaled by leaf area, R_a) was 2.2 $\pm$ 0.4 MPa d $cm^2\ mL^{-1}$. For modeling purposes, we used a stem axial resistivity value of 2 MPa d $cm^2\ mL^{-1}$. Tangential resistances were more variable, 0.013 $\pm$ 0.015 MPa d cm^2

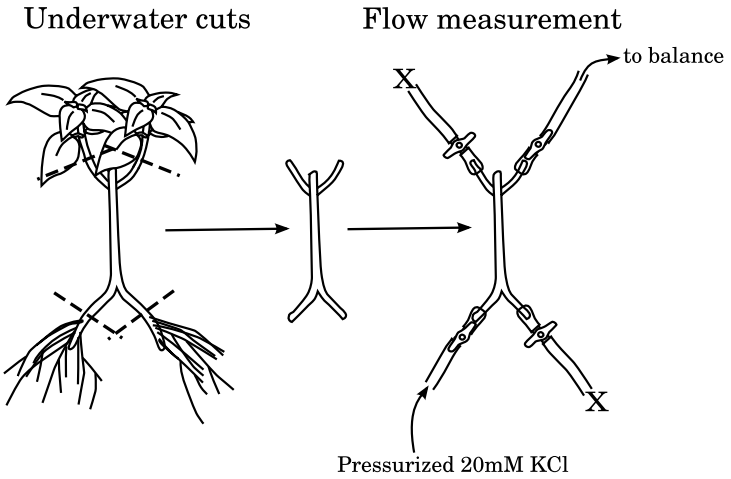

Figure 2.3: Diagram of setup for measurement of stem hydraulic properties in basil plants. After pruned nodes of the plant had healed, branches and root bases were cut underwater after wrapping each in parafilm. Tubing attached underwater permits measurement of flow of pressurized 20 mmol/L KCl from half of the cut root system to either the orthostichous or opposite root, while alternative flow routes are blocked (X) by closed stop-cocks.

mL^{-1} (mean $\pm$ SD), and for modeling purposes, we selected a mid-range value 0.01 for the tangential resistance (r_t). Based on axial resistance measurements, the leaf area resistivity was estimated as 0.6 MPa d cm^2 mL^{-1}.

2.4.3 Defoliation and ^{15}N treatments

A total of 29 plants ($\sim$6 per treatment date) were evenly divided into three defoliation treatment categories: orthostichous (N = 9), opposite (N = 10), or uniform (N = 10). For each treatment category, roughly one quarter of the leaf area was removed. For the orthostichous and opposite treatments, half the length of each leaf was removed from one branch selected at random; for the uniform treatment, half of the length of half of the leaves was removed from each branch, in as symmetrical a fashion as possible (Fig. 2.1). To achieve this, lengths of all leaf blades > 1.0 cm long were measured for all plants the day before the defoliation treatment. The following day, a razor blade was used to remove the distal portions of the appropriate leaves to a length one half of the total blade length.

After a 24-h recovery period, nutrient solutions were replaced for all plants, with one container for each plant receiving fertilizer solution equivalent to the ordinary 50% dilution Hoagland solution, but with the KNO_3 enriched to 10

atom% ^{15}N, while the other container received unlabeled solution. For the orthostichous treatment, the label was applied orthostichous to the defoliated branch, for the opposite treatment label was applied to roots opposite the defoliated branch, and for the uniform treatment label was applied to a container selected at random. After a 48-h pulse of the ^{15}N label, solutions in all containers were replaced with unlabeled nutrient solution. Four days later, all plants were harvested.

2.4.4 Measurement of total accumulation of ^{15}N label

Plants were separated by sector and tissue type into main stem, leaves, branches, lateral roots, and main roots, dried in an oven at 70°C, and weighed. For assessing ^{15}N content, samples were dried and ground and analyzed at the Stable Isotope Facility at UC Davis.

For all labeled plants and an unlabeled control plant, the mass % ^{15}N was calculated for nitrogen in roots, stems, branches, and leaves. For each tissue, the mass % ^{15}N was calculated as $(100 \times 15 \times \text{ atom\% } ^{15}N)/[(100 \times 15 + \text{ atom\% } ^{15}N \times (15 - 14)]$. Then the ^{15}N mass concentration of the controls was subtracted from the ^{15}N mass % for each tissue sample for labeled plants, and the resulting mass % for label only was multiplied by the total N content of each tissue to give the total mass accumulation of ^{15}N label in each tissue.

2.4.5 Leaf area and biomass estimates for simulations

To simulate transpiration rates (Eq. 2.3.7), the leaf areas before and after defoliation were estimated from total leaf blade lengths and the length proportion removed. Models for leaf area and specific leaf area were empirically determined using basil plants not included in this study that had been cultivated under the same split-root and pruning treatments. The area for each leaf before defoliation was estimated as 0.34 times the squared of the original blade length. The area removed by the defoliation treatment was estimated as (original area)$\times$[2.6$\times$(proportion leaf length removed)^2 - 1.7$\times$(proportion of length

removed)^3], where the proportion of leaf length removed is the length removed divided by the original length. Leaf area after defoliation was estimated as the area before defoliation minus the area removed. The specific leaf area was estimated as 200 cm^2 g^{-1}. Total leaf areas were calculated as the sum of estimated leaf areas for all leaves in a sector. Leaf dry mass prior to defoliation was estimated from leaf length measurements and the estimated specific leaf area.

2.4.6 Statistical analysis and other calculations

Water uptake is highly dependent on temperature and sunlight, which varied between blocks because of the time-staggering of treatment times between blocks and imperfect climate control in the greenhouse. Therefore, values for total water uptake and total leaf area for plants in each experiment were standardized to relative values by dividing the actual value for each individual by the maximum value among all plants treated on the same day.

In addition to simulating xylem intersector transport using our model, we also estimated the rate of intersector movement from the labeled side to the unlabeled side, using leaf dry mass distributions between the two branches and the rate of water uptake for the two halves of the root system. Using the assumption that transpiration is uniform across leaf tissues, we calculated that estimate as the percentage leaf biomass on the opposite side minus the percentage of total water uptake from the unlabeled container (sensu Thorn and Orians 2011*c*).

Two-way analyses of variance (ANOVAs) were used to test the effects of (1) treatment and root dry mass in the labeled container on total ^{15}N accumulation, (2) treatment and relative total leaf area on relative total water uptake (see above), and (3) sector and treatment on ^{15}N accumulation in the leaves of each sector of the plant. In particular, we tested whether there was a significant difference in slope depending on whether the crossover was positive (net movement toward the opposite side) or negative (net movement into the labeled sector). Tukey HSD post hoc analysis was used to assess significant

differences in the ANOVA for total leaf accumulation of ^{15}N.

Linear least squares regression models were generated for the relationships between actual and simulated proportion of water taken up from the labeled container and between the proportion ^{15}N accumulation on the opposite side of the plant and either the simulated or estimated proportions of xylem sap crossing from the labeled container to the opposite side leaves. Slopes generated with these regression models were compared with hypothesized slopes using t tests. Specifically, we tested the predictions (1) that the slope of the regression curve for simulated vs. actual water uptake distributions would be 1, (2) that the slope of the regression curve for ^{15}N on the opposite side vs. simulated or estimated sap crossover would be 1 when the simulated or estimated net flow was positive (from the labeled container to the opposite side of the plant), and (3) that the slope of the regression curve for ^{15}N on the opposite side vs. simulated or estimated sap crossover would be zero when simulated or estimated net flow was negative.

All analyses were performed using R software (http://www.r-project.org/).

2.5 Results

2.5.1 Evaluation of model for water uptake

Across all plants, total water uptake per plant was closely correlated with total estimated leaf area, both before and after the defoliation treatment, and was unaffected by treatment Table 2.1. However, the slope of this relationship was significantly lower than the predicted value of 1 (before defoliation: t = -2.361, df = 27, P = 0.026; after defoliation: t = -2.132, df = 27, P = 0.042). This result suggests that constant water uptake per unit leaf area is a reasonable, but not perfect, assumption for the model.

Using the empirically estimated tangential resistance of 0.01 MPa d/mL, the model closely predicted the water uptake distribution both before and after the defoliation treatments (Fig. 2.4), with the exception of three individuals with

Table 2.1: ANOVAs for significance treatment and relative leaf area effects on relative total water uptake per basil plant, before and after defoliation treatments. Relative leaf areas and relative total water uptakes were calculated on a per-block basis by dividing the actual value by the maximum value among all plants treated on the same day. Leaf areas ($A_{orig} - A_{removed}$) were estimated from original leaf lengths (L_{orig}) and length proportion removed ($P_{removed}$) as: $A_{orig} = 0.34 \times {L_{orig}}^2$ and $A_{removed} = A_{orig} \times (2.6 \times {P_{removed}}^2 - 1.7 \times {P_{removed}}^3)$ for each leaf.

Source of variation	df	F	P
Before defoliation treatments			
Treatment	2	1.4	0.261
Relative leaf area before defoliation	1	23.2	<0.001
Treatment × relative leaf area	2	1.2	0.315
Residuals	23		
After defoliation treatments			
Treatment	2	1.1	0.350
Relative leaf area after defoliation	1	19.9	<0.001
Treatment × relative leaf area	2	0.9	0.426
Residuals	23		

asymmetrical biomass, for which the predefoliation model predicted more extreme asymmetries in water uptake than were observed (Fig. 2.4A). When these asymmetrical plants were included in the analysis, the slope of this relationship was significantly lower than the predicted value of 1 (before defoliation: t = -3.542.6, df = 27, P = 0.001; after defoliation: t = -3.324, df = 27, P = 0.003), but was not significantly different from 1 when these plants were omitted from analysis (before: t = -0.122, df = 24, P = 0.904; after: t = -1.951, df = 24, P = 0.063).

2.5.2 ^{15}N uptake and distribution

Of the 4.2 mg ^{15}N added for each plant, the total amount taken up ranged from 0.02 mg to 0.15 mg. When the combined effects of treatment and root biomass on the labeled side on ^{15}N uptake were tested, there was—as expected—no treatment effect on total ^{15}N uptake ($F_{2,23}$ = 0.12, P = 0.89), and no significant interaction ($F_{2,23}$ = 0.06, P = 0.95). There was, however, a nonsignificant positive correlation between total ^{15}N uptake and the dry mass of roots in the labeled container ($F_{1,23}$ = 3.37, P = 0.08).

Analysis of sector by treatment effects on leaf ^{15}N showed that leaves orthostichous to the labeled roots had significantly higher ^{15}N content than leaves

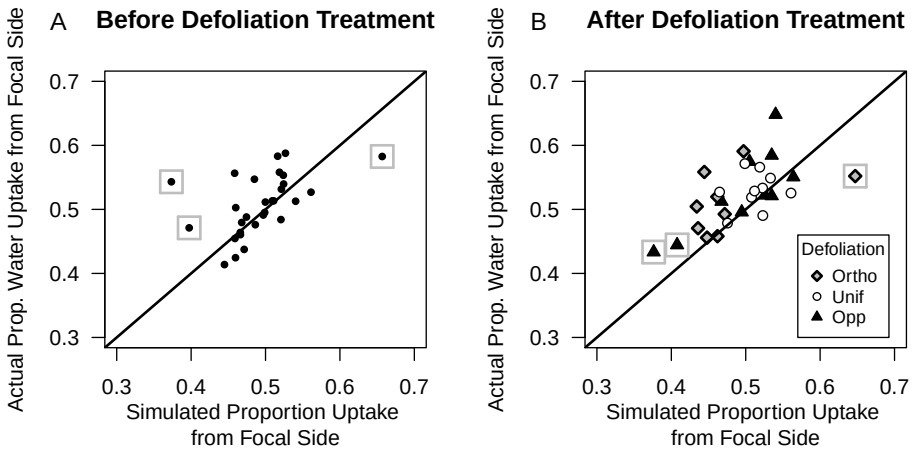

Figure 2.4: Simulated vs. actual water uptake distribution, as expressed by the proportion ("prop.") of water taken up from the focal (labeled) container before (A) and after (B) defoliation treatments of basil plants. In each plot, the curve shows the 1:1 predicted correspondence between actual and simulated values. The key indicates the symbols used for plants that had received different defoliation treatments in (B) (orthostichous to label = Ortho, uniform = Unif, opposite the label = Opp). Gray boxes indicate the individuals for which the model failed to predict water uptake distributions before defoliation treatments.

on the opposite side ($F_{1,52}$ = 45.66, P < 0.0001). There was no significant effect of treatment on ^{15}N content of leaves ($F_{2,52}$ = 0.80, P = 0.46), but there was a significant interaction between treatment and side ($F_{2,52}$ = 3.85, P = 0.028). This interaction was driven by a nonsignificant difference between the content of leaves in labeled and unlabeled sectors of plants receiving the orthostichous defoliation treatment (Fig. 2.5).

Qualitatively, the distribution of ^{15}N in the leaves of basil plants conformed with our prediction that it would be positively correlated with simulated (Fig. 2.6A) or estimated (Fig. 2.6B) rates of water crossover when these crossovers were from the labeled container to the opposite side leaves (positive crossover rates), but would be unrelated to crossover rates when net flow was from the opposite-side container to the labeled sector leaves (negative crossover rates) (Fig. 2.6A, B). The slope of the regression line for positive crossover rates was not significantly different from the hypothesized value of 1 for simulated water crossover (all plants: t = -1.574, df = 10, P = 0.147; asymmetrical plants excluded: t = -1.278, df = 9, P = 0.233) or estimated crossover (all plants: t = 0.015, df = 14, P =

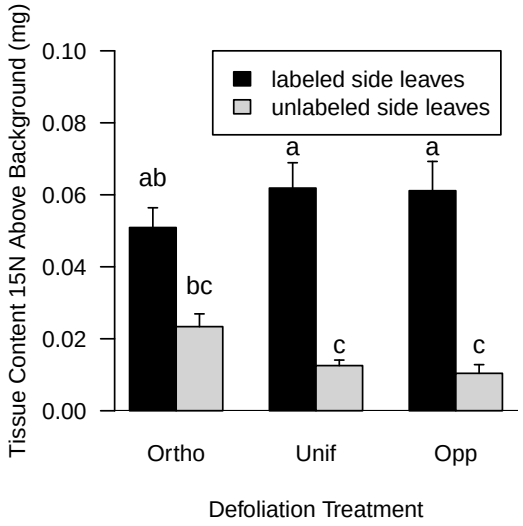

Figure 2.5: Leaf tissue content of ^{15}N label (above background content) as a function of defoliation treatment and side of plant relative to the side labeled. The x-axis labels indicate defoliation treatments (orthostichous to label = Ortho, uniform = Unif, opposite the label = Opp). Error bars indicate standard error. Letters above the bars indicate significant differences at alpha = 0.05 (Tukey HSD).

0.988; asymmetrical plants excluded: t = -0.079, df = 13, P = 0.939). The slope for negative crossover rates was significantly above the hypothesized value of 0 for simulated crossover rates (all plants: t = 2.920, df = 15, P = 0.011; asymmetrical plants excluded: t = 2.463, df = 13, P = 0.029) but not for estimated crossover (all plants: t = 1.343, df = 11, P = 0.206, asymmetrical plants excluded: t = 0.684, df = 9, P = 0.511). Interestingly, both simulated and estimated crossover underestimated crossover rates by about 10% (Fig. 2.6), suggesting some background level of random mixing independent of biomass distribution.

2.6 Discussion

Our results support the usefulness of our framework for modeling xylem sectoriality and the allocation of nitrate nitrogen newly acquired by the roots. We found that leaf area predicts water uptake and, more importantly, that patterns of defoliation have significant effects on nitrogen translocation between sectors. Thus asymmetrical defoliation is likely to influence the capacity of plants to compensate for lost leaf area. Next, we evaluate the model and then focus on

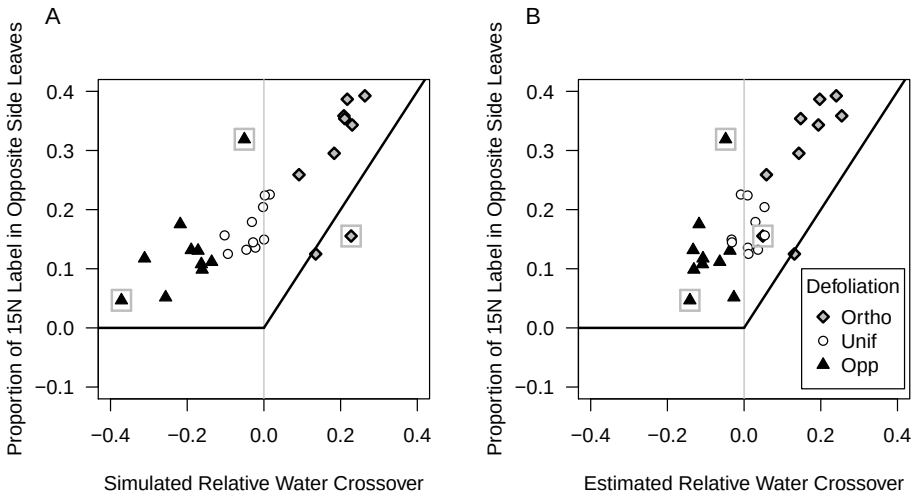

Figure 2.6: Proportion of leaf ^{15}N label accumulated in opposite-side leaves as a function of simulated (A) and estimated (B) proportions of water crossing from the labeled container to the leaves of the opposite side of basil plants. The solid curve is the predicted label distribution if ^{15}N label is passively carried by water movement (zero when water crossover is negative; equal to water crossover when water crossover is positive). The key indicates the symbols used for plants that had received different defoliation treatments (orthostichous to label = Ortho, uniform = Unif, opposite the label = Opp). Gray boxes indicate the individuals for which the model failed to predict water uptake distributions prior to defoliation treatments.

the ecological implications of our findings.

2.6.1 Evaluation of model

Total water uptake was consistent with the model assumption that transpiration scales with leaf area, and our hydraulic simulations provided good estimates for water uptake distribution both before and after our defoliation treatments. The predicted patterns of water uptake were less accurate for three individuals with pre-existing biomass asymmetries. This discrepancy might reflect limitations of our parameter approximations when asymmetries are stronger, but might also reflect dynamic changes to plant hydraulics to compensate for asymmetrical biomass, which are not captured by our model. Nonetheless, these three individuals did not substantially effect our overall findings.

Overall, there was a significant interaction between treatment and side for ^{15}N accumulation in leaves, driven by a more even distribution for the orthostichous defoliation treatment than for the other treatments, which supports our

general predictions as presented in Fig. 2.1. Furthermore, separating these values based on model predictions, water crossover rates for individual plants reveal that much of the variation within and among treatments is indeed explained by the model, although a closer fit was obtained by using estimated water crossover rates instead of simulated values.

Interestingly, the degree of ^{15}N crossover to opposite side leaves was generally higher than the quantitative predictions under our assumption that nutrients are passively carried by water and that crossover is unidirectional. Across all individuals, a crossover rate of ca. 10% above the predictions of the hydraulic model was observed. This discrepancy cannot be explained by parameter selection because it also occurred for estimated crossover rates and it was apparent even when the estimated net flow was from the unlabeled roots to the labeled sector. This result suggests that basil has a high level of potential integration, despite the strong sectoriality observed for the overall distribution of ^{15}N label. Several mechanisms may underlie this apparently random mixing. One hypothesis would be that specialized transfer cells may move solutes from one xylem stream to parallel vessels (Pate and Jeschke 1995), but the absence of any evidence for active adjustment with defoliation treatment does not support an active process. Perhaps a background level of mixing is actively maintained independently of short-term defoliation effects. Alternatively, microscale water potential differences among xylem vessels could result in bidirectional mixing within the xylem, not predicted by our macroscale model. Mixing may also result from temporal variation in light to the two halves of the plant, causing transient water potential differences opposing the prevailing gradient. Finally, it is also possible, since 4 d passed between isotope treatments and harvest, that some mixing may have resulted from redistribution of nutrients initially carried directly to the leaves. This possibility is supported by the fact that we generally observed some ^{15}N label in the opposite side roots (Appendix, section 2.8 Fig. 2.8), though not as much as in the leaves.

The predictive value of the model could be improved by fine-tuning the

parameter values used. In particular, tangential resistance and root resistance have been shown to play an important role in the dynamics of this style of model (Thorn and Orians 2011*c*). In general, tangential resistance is expected to increase with plant growth and suberization, but this parameter is more difficult to measure in smaller plants. Root resistance in herbaceous plants varies dynamically in a diurnal cycle and in response to environmental factors such as nutrient environment (e.g., Gloser et al. 2007). For the purposes of this paper, we have chosen to present outputs using our a priori best guesses of these parameter values, rather than tuning these values to provide the best fit for our empirical observations. We believe that this approach provides a more realistic picture of the predictive value of a model. Although our observations differed significantly from model projections, the qualitative similarity between empirical and theoretical patterns underlines the general utility of our model.

2.6.2 Implications for regrowth and defense following herbivory

Overall, our results suggest a strong potential in basil for nutrient allocation in the crown to be adjusted in response to stressors that adjust water flow, such as partial defoliation of the crown. The pattern of increased crossover was apparent even at the low defoliation levels of our experimental treatments, and the observed crossover was consistent with our model for water crossover rates following defoliation. A more extreme event such as total defoliation of half of the crown or high light on a single branch while the rest of the plant is in shade would be expected to result in even greater crossover. In the case of herbivory, the expected consequence is increased resource supply to the remaining leaves, enhancing compensatory photosynthesis and regrowth, analogous to the effects of photoassimilate translocation noted for Glechoma hederacea (Price and Hutchings 1992). On the other hand, for species in which high sectoriality limits hydraulic redistribution of resources between sectors, such as the desert plant Cryptantha flava (Salguero-Gómez and Casper 2011), drought tolerant shrubs (Schenk et al. 2008), and ring-porous trees (Zanne et al. 2006*b*), nutrient distri-

bution is unlikely to change. In such cases, regrowth after a defoliation event may be significantly slowed.

These results also have important implications for the distribution of defense compounds and signal molecules in response to a localized herbivory event. For a relatively integrated plant, such as basil appears to be, transport of signal molecules to the roots may provide a pathway through which attacked leaves can transcend ordinary vascular constraints, inducing chemical defense of leaves in separate integrated physiological units (Erb et al. 2009), especially in cases of extreme defoliation. For instance, in Nicotiana tobacum the signal molecule methyl jasmonate is transported by both xylem and phloem and has been shown to move from an attacked leaf to the roots, and from there, to mature leaves via the xylem (Thorpe et al. 2007). This pathway may work in conjunction with that compound's volatility (Thorpe et al. 2007) to permit translocation between orthostichies. In a plant similar to basil, some sectorial asymmetry within the crown would still be expected, as can be seen by our trend of sectored distribution of ^{15}N, even for the orthostichous defoliation treatment, but in plants that are more integrated still, such as the Betula seedlings examined by (Orians et al. 2004), the xylem transport could result in essentially uniform defense throughout the crown. In contrast, if high sectoriality completely prevents crossover of nutrients, induced defense compounds would tend to remain concentrated in the attacked sector, increasing the probability of future attack in other sectors, although potentially also decreasing the likelihood of complete defoliation: some leaves would have much higher concentrations of induced defenses than others, forcing herbivores to move continually within a plant (e.g., Paschold et al. 2007).

2.6.3 Relevance to induced nutrient redistribution

It should be emphasized that the results shown here reflect passive changes to water movement in the xylem, and should not be conflated with actively induced changes in resource allocation, which has been documented in a wide di-

versity of plant species (Babst et al. 2008, Gómez et al. 2010) (reviewed by Orians et al. 2011). The lack of evidence for active adjustment in this short-term study does not rule out the possibility of longer-term induced changes in nitrogen allocation in basil. Indeed, it has been shown that incremental manual defoliation of basil will increase the rate of leaf senescence, and hence nitrogen export, when nutrients are limiting (Roma, Thorn and Orians, unpublished data). This induced mobilization and subsequent recycling of nitrogen and other nutrients from the leaves is likely to result in further intersector crossover over a longer time frame, and deserves further attention.

2.6.4 Future directions

The quantitative approach used in this study provides a new perspective on sectoriality of nutrient transport, with general applicability for studies on xylem sectoriality. Our results support the usefulness of this model for understanding nitrogen distribution following a defoliation event, and similar methods can easily be applied to any process expected to change xylem water potential differences, such as patchy nutrients (Gloser et al. 2007) or light (Thorn and Orians 2011*a*). The availability of quantitative a priori expectations for nutrient distribution under passive flow provides a baseline to which observations can be compared. In the case of our present study, crossover rates higher than our predictions suggest mechanisms for mixing in the stem that would not otherwise be apparent. Future research should examine whether this mixing occurs in the xylem alone or whether it is related to transfer cell activity or xylem-phloem recycling.

2.7 Acknowledgements

The authors thank C. Roma for plant care and members of the Department of Biology for logistical support. The authors thank Rob Salguero-Gómez and an anonymous reviewer for comments on an earlier version of this manuscript. This work was supported by the Tufts Department of Biology, the Tufts Grad-

uate School of Arts and Sciences, NSF REU (grant DBI 1005082), and USDA National Institute of Food and Agriculture (Grant number 2007-35302-18351).

2.8 Appendix

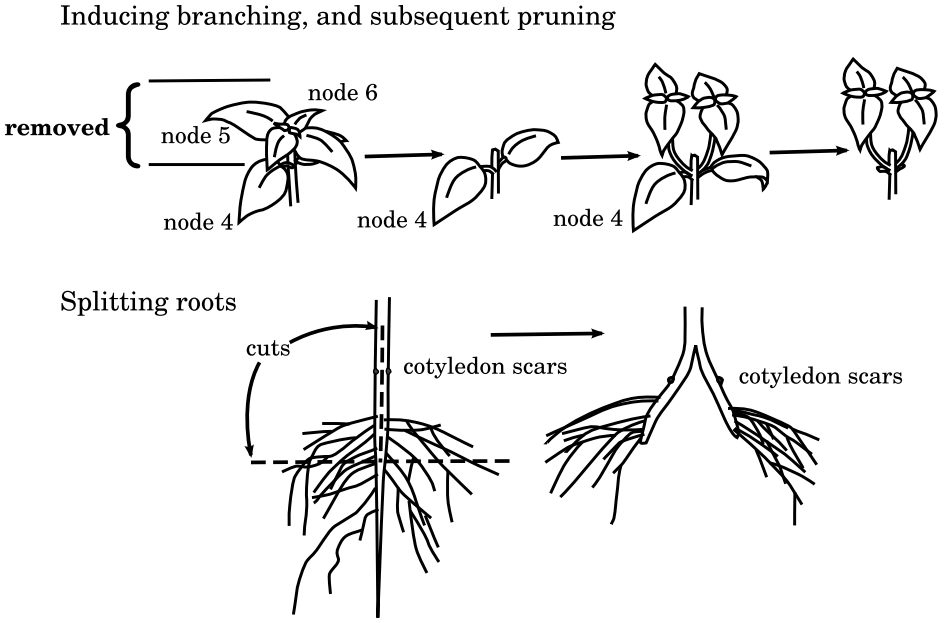

Figure 2.7: Diagram of protocols used for inducing branching and splitting roots for the split-root hydroponic treatments.

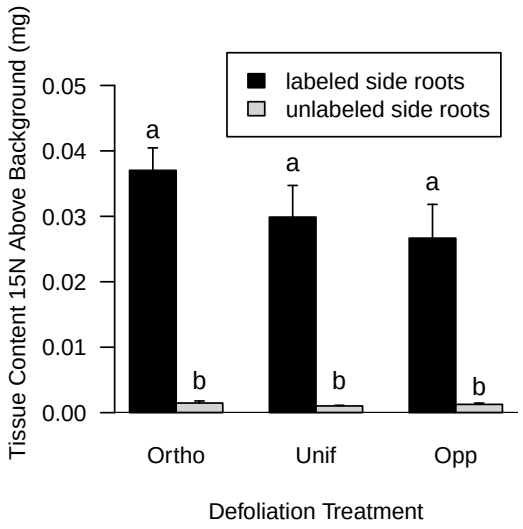

Figure 2.8: Root tissue content of ^{15}N label (above background content), as a function of defoliation treatment and side of plant relative to the side labeled. The x-axis labels indicate defoliation treatments (orthostichous to label = Ortho, uniform = Unif, opposite the label = Opp). Error bars indicate standard error. Letters above the bars indicate significant differences at the alpha = 0.05 level (TukeyHSD).

CHAPTER 3

Patchy nitrate promotes inter-sector flow and ^{15}N allocation in *Ocimum basilicum*: A model and an experiment

Authors: Alexandra M. Thorn and Colin M. Orians

Published: 2011 *Functional Plant Biology*, 38: 879–887

3.1 Abstract

Root conductance increases under high nitrate conditions. This plasticity might increase water and nutrient transport between parallel xylem pathways, but restrictions to lateral flow — called sectoriality — are expected to limit this crossover. We simulated the effects of a high nitrate patch on root conductance, water uptake, and inter-sector water transport, and then empirically tested whether a high nitrate patch affects water uptake and nitrogen distribution (applied ^{15}N as $^{14}NH_4{}^{15}NO_3$ to half the root system) within the crowns of split root hydroponic basil (*Ocimum basilicum* L.). Simulations showed that at low sectoriality, the proportion of water taken up in a patch scales with the relative change in root resistance, and that this fraction decreases with increasing tangential resistance. The effect of sectoriality decreased when a higher background root resistance was assumed. Empirically, water flow through excised basil roots was 1.4x higher in high nitrate than no nitrate solution. In split-root basil, a nitrate patch resulted in a marginally significant increase in the proportion of water taken up from the patch, and water uptake patterns significantly predicted the distribution of ^{15}N. Our results suggest that root conductance can mediate nitrogen allocation between sectors, a previously unexplored benefit.

3.2 Introduction

Plant responses to nutrient heterogeneity in the soil include proliferation of roots into nutrient patches, changes to the anatomy of newly formed roots, and physiological adjustments to increase the uptake rate for a nutrient (Robinson 1994, Hodge 2004, 2006). It has also been noted that at least some species can increase root conductance in response to the presence of high nitrate patches (Gloser et al. 2007, Gorska et al. 2008). The adaptive value of hydraulic responses to nutrient patches is not known, but researchers have suggested that this increased hydraulic conductance improves competition for nitrate ions, which are highly mobile and so easily carried by water flux toward the roots (Gloser et al. 2007, Gorska et al. 2008, Maurel et al. 2010). Other benefits may exist as well. If a high nutrient patch locally elevates hydraulic conductance, it could result in a pressure gradient between parallel xylem pathways, increasing movement of water and nutrients between them (Zwieniecki et al. 2003). Here, we examine the combined effect of root and stem hydraulics on water uptake by roots and evaluate the hypothesis that these hydraulic changes could benefit the plant by helping to overcome vascular constraints to nitrogen transport within the crown.

It is well-known that the transportation and distribution of resources within the plant is constrained by vascular anatomy (Watson and Casper 1984, Zanne et al. 2006*a*, Gloser et al. 2008). Vascular constraints—called sectoriality—affect xylem connections from roots to leaves as well as phloem connections from leaves to roots and other sinks, and species vary in their capacity to transport resources between sectors (Orians et al. 2004, 2005*b*, Zanne et al. 2006*b*, Ellmore et al. 2006). In the case of xylem transport, sap can move between parallel vessels in response to inter-sector hydraulic gradients, primarily at bordered pit fields. These pit fields vary among species in frequency and conductive properties (e.g., Ellmore et al. 2006, Hacke et al. 2006), resulting in differences in the resistance to flow between sectors, i.e. differences in tangential resistance. Since water transport in the xylem is driven by water potential gradi-

ents, inter-sector transport is expected to be minimal under uniform conditions, even for species with high anatomical integration (Ellmore et al. 2006, Zwieniecki et al. 2003). However, in patchy resource conditions, vascular constraints could limit growth by preventing allocation of resources from a high quality patch (one with relatively high light, nutrients, or water) to the entire plant (Gloser et al. 2008) unless there are factors that increase inter-sector transport. In the case of patchy water or light, environmental heterogeneity naturally favors flow between sectors (Orians and Jones 2001, Thorn and Orians 2011*a*). For example, through its direct effect on transpiration rates, patchy light is expected to result in lower water content — and therefore water potential — for some leaves relative to others and so increase inter-sector crossover (Thorn and Orians 2011*a*). In contrast, it is not known whether patchy nutrients increase inter-sector crossover. Zwieniecki et al. (2003) argue that the xylem conductivity changes associated with ion concentration will increase water supply to high nutrient sectors and thus facilitate nutrient transport between sectors. Similarly, the increased root conductance observed in some species (Gloser et al. 2007) should also generate a hydrostatic gradient that would increase the spread of nutrient rich xylem sap throughout the crown.

In order to examine the interactive effects of root hydraulics and tangential resistance on water uptake and nutrient allocation, we used two sectoriality models to evaluate patterns of water uptake under steady-state conditions. Then, to empirically evaluate how changes to root resistance influence nutrient allocation in an intact plant, we used split root hydroponic basil (*Ocimum basilicum* L.) to test the effects of patchy nitrate on water uptake and ^{15}N distribution in whole plants. We hypothesized that changes in the distribution of water uptake in split root plants would match model predictions, and that the distribution of ^{15}N would be correspondingly more uniform when the ^{15}N coincided with a high nutrient patch than when ^{15}N was locally supplied in a uniform nutrient environment (Fig. 3.1).

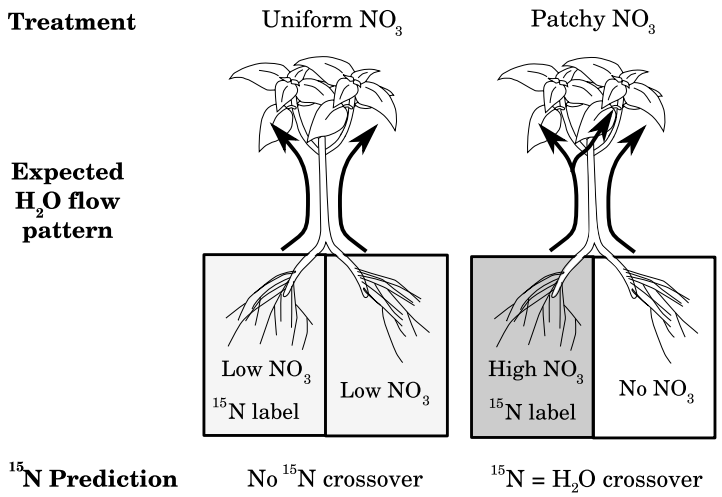

Figure 3.1: Diagram of qualitative predictions for how water and nutrient movement will be affected if roots in a nutrient patch have lower resistance than roots in the background nutrient environment.

3.3 Methods

3.3.1 Models

To simulate the effects of patchy nitrate on xylem hydraulics, we use two different Ohm's Law circuit models to simulate flow of resources within and between sectors (Fig. 3.2). The first model (Model 1) uses the same framework as Thorn and Orians (2011*a*), directly simulating the fact that flow between sectors is the consequence of numerous connections at different heights up the stem. To do this, the stem is simplified as two parallel axial pathways, and the various routes for tangential flow between sectors are simulated by a large number of resistors (N=100), each with resistance equal to $N \times r_t$, where r_t is the overall tangential resistance (Fig. 3.2A). The second model (Model 2) sacrifices some of the structural realism of Model 1 in favor of a simpler, less computationally intensive, circuit. Specifically, Model 2 assumes that axial resistance below the branch point is negligible, so that inter-sector pathways can be simulated as a single resistor with resistance r_t (Fig. 3.2B).

For both models, flow within and between sectors is driven by the root pressure (Ψ_r), which is assumed constant, and the leaf water potential for each sector ($\Psi_{l1,2}$), which varies as a function of the content of water in the leaves of that

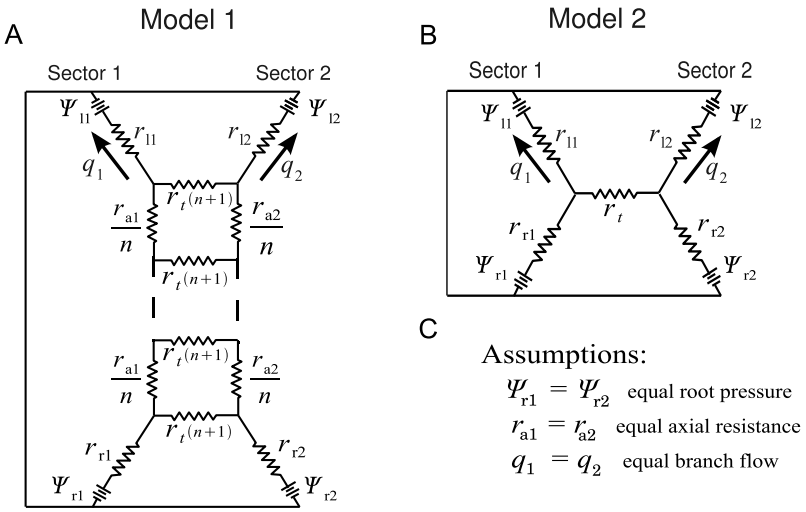

Figure 3.2: Circuits for Ohm's law models for hydraulic sectoriality. Model 1 includes n repeating units in the stem, incorporating both axial (r_a) and tangential (r_t) resistance (A). Model 2 is a simplified circuit representing the case in which r_a = 0 (B). We use the model to simulate water uptake by the two root sectors in response to localized changes in root resistance, under steady state conditions and otherwise uniform hydraulics (C).

sector. In particular, the water potential of the leaves of sector i ($\Psi_l i$) is the sum of the osmotic (Ψ_{oli}) and pressure (Ψ_{pli}) potentials for those leaves:

$$\Psi_{li} = \Psi_{pli} + \Psi_{oli} \tag{3.3.1}$$

Pressure potential is always positive, and increases with water content above the turgor loss point (sensu Thornley and Johnson 2000):

$$\Psi_{pli} = \max(0, \epsilon \times (\frac{c_{dw} W_{wld}}{W_{li}} - 1) \tag{3.3.2}$$

where W_{wli} is the dynamically modeled mass of water in the leaves of a sector, W_{li} is the dry weight of leaves in a sector, ϵ is the elastic modulus of leaf cell walls, and c_{dw} is the ratio of leaf dry weight to leaf water content at $\Psi_{pli} = 0$. Osmotic potentials are always negative, but become more positive with increasing leaf water content:

$$\Psi_{oli} = -K_o \times \frac{W_{li}}{W_{wli}} \tag{3.3.3}$$

where K_o is a parameter for the osmotic properties of the mesophyll cells.

The water content of leaves is dynamically modeled by:

$$\frac{dW_{wli}}{dt} = q_{li} - E_{ti} \tag{3.3.4}$$

where q_{li} is the flux of water into the leaves of sector i calculated by solving the our model circuit (Fig. 3.2A,B) and Eti is the total rate of transpiration from leaves in the sector, assumed for our purposes to scale uniformly with leaf area.

Flows through the complicated circuit used for Model 1 are determined by a large system of equations, which can be easily computed numerically, but for which the analytical solution is extremely complicated. Model 2 provides a more tractable system, with simple analytical solutions that can provide a more intuitive framework for quantifying expected flow. In particular, under steady state conditions of equal transpiration from the two halves of the crown (Fig. 3.2), the proportion of water uptake that is taken up by roots in sector 1 (P_{u1}) is given by the expression:

$$P_{u1} = \frac{2r_{r2} + r_t}{2(r_{r1} + r_{r2} + r_t)} \tag{3.3.5}$$

where r_{r1} and r_{r2} are the root resistances of sectors 1 and 2 respectively.

The same default parameter values were used for both models, based on estimates for basil (Table 3.1).

3.3.2 Simulations

We used the models to evaluate the potential effect of root resistance changes on water uptake patterns. To simulate the steady state sap fluxes for plants in asymmetrical nutrient environments, we varied the difference in hydraulic resistance between the two sectors, assuming resistance on the low nutrient side was elevated by a factor of 1.1, 1.25, 1.5, or 2.0. To understand the role of sectoriality in water uptake patterns we varied the tangential resistance from 0.0 to 0.1 MPa day mL^{-1} a broad range that includes our unpublished measurements of 0.01 MPa day mL^{-1} for mature basil plants. We also examined the importance

Table 3.1: Parameter values used in hydraulic model.

Symbol	Description	Default values	Units	Estimate based on
W_{li}	Dry mass of leaves of sector i	1.0	g	Our measurements in basil
ϵ	Elastic modulus of leaf cell walls	1.0	MPa	Thornley (1996)
c_{dw}	Ratio of leaf dry weight to leaf water content at $\Psi_{pli} = 0$	0.15	g biomass mL^{-1}	Comparing dry and fresh weights for basil leaves
K_o	Osmotic parameter	1.83	MPa	Thorn and Orians (2011*a*)
r_{ri}	Resistance to water uptake by roots of sector i	0.0015	MPa day mL^{-1}	Typical of herbaceous plants (Newman 1973)
r_a	Resistance to axial flow through stems of sector i	0.01	MPa day mL^{-1}	Unpublished basil measurements
r_t	Stem tangential resistance	0.01	MPa day mL^{-1}	Unpublished basil measurements
r_{li}	Resistance to axial flow through leaves of sector i	0.003	MPa day mL^{-1}	Typical ratios of leaf to axial resistance (Sack et al. 2003)
Ψ_{sri}	Soil-root water potential associated with sector i	0.1	MPa	Typical of herbaceous plants (Taiz and Zeiger 2002)

of root resistance relative to the rest of the plant by varying the high nutrient root resistance from 0 to 0.01 MPa day mL^{-1}, a range that includes published root resistances for herbaceous plants Newman (1973). For all simulations, we present output for the steady-state case, with equal flow into the two branches. We focus on the consequences for the proportion of total water uptake by roots in the nitrate patch, which will correlate with changes to water uptake for those roots, assuming that transpiration is unaffected. This variable directly determines the amount of water, and therefore nutrients, expected to cross to the opposite side of the plant (Fig. 3.1).

We compare the predictions of the two models, using output from the simulations described above, as well as additional runs of the model with the axial resistance varied between 0.0005 and 0.05 MPa day mL^{-1}.

3.3.3 Cultivation of plants for ^{15}N experiment

To evaluate the predictions of our model and assess the consequences for nitrate nitrogen allocation, we used basil (*Ocimum basilicum* var. Sweet Basil from Burpee, 30 Park Avenue, Warminsler PA 18974), an ideal species for sectoriality studies because it grows quickly and has opposite-leaf growth habit, permitting inter-sector comparison of leaves or branches of the same age.

Seeds were sown in January and February 2007 into moist MetroMix potting soil with water supplied from below. About one month after sowing, seedlings were transplanted into individual pots containing 50% sand and 50% zeolite (ZeoProTM). We watered plants every two days and added 70 mL of a Hoagland solution (603.0 μM $Ca(NO_3)_2$, 795.0 μM KNO_3, 190.0 μM KH_2PO_4, 270.0 μM $MgSO_4$, 0.09 μM $ZnSO_4$, 0.15 μM $CuSO_4$, 20.0 μM $CuSO_4$, 20.0 μM H_3BO_3, 0.25 μM Na_2MoO_4, and 40.5 μM FeNa EDTA) twice a week. Throughout cultivation and experiments, plants were grown in a greenhouse at Tufts University, Medford MA, USA. Natural light was supplemented with 400 W sodium halide light to give a total of 16 hours of light in each 24 hour period. For the root hydraulics experiment, unpruned plants were harvested and roots excised in June 2007 (see protocols below).

For the split root experiment, we took advantage of the known vascular anatomy of plants in the Lamiaceae, in which each branch or leaf is fed by two vascular traces, which connect to roots in the same orthostichy (Rinne and Langston 1960, Murphy and Watson 1996). Plants were decapitated just above the fourth node after fifth-node leaves had emerged. When lateral branches had emerged from the fourth node of decapitated plants, all other leaves and branches were removed from the main axis. On October 10, 2007, pruned plants were transferred to split root hydroponics containers. We rinsed the roots and carefully split the taproot down the center, such that each half of the root system was orthostichous to one of the two branches. Previous studies using dye tracers have confirmed that for basil plants in this type of split root setup, orthostichous roots and branches share direct xylem connections not shared by

structures on the opposite side of the plant (unpublished data). Parts of the main root too narrow to split were removed. Each half of the root system was trained into one of a pair of 250 mL uncapped Corning cell culture flasks containing hydroponic solution, and stabilized using a stake taped to one side of the flask pair. Hydroponic containers received a 50% dilution of the Hoagland solution described above. Air was supplied at a minimum rate of 30 mL air / minute to each half of the root system via plastic tubing (interior diameter = 1.6 mm). These plastic tubes were in turn attached to a 20-gauge hypodermic needle inserted into a short length of vacuum tubing connected to a pressure pump (Model UN035.1.2 STP, KNF Neuberger, Inc., Trenton NJ). Once a day, deionized water was added to each container to maintain constant solution volume, and the volume of water added was recorded as a measure of water uptake. Once every two days, just after the addition of the deionized water, the hydroponic solution was fully replaced for all containers.

Split root experimental treatments were applied on November 6, 2007 and plants were harvested between November 9 and 11, 2007.

3.3.4 Measuring nitrate effects on root hydraulics in basil

To prepare plants for root hydraulic measurements, the base of the root system was wrapped in parafilm and the root system was cut from the rest of the plant underwater, cutting through the parafilm. Water-filled tubing was then pushed over the cut base of the root system, and secured in place using a zip-tie. The root system was placed in a hydroponic container with a 50% dilution of either the complete (+N) Hoagland solution described above or of a no-nitrate (-N) Hoagland solution in which $CaCl_2$ and K_2SO_4 replaced $Ca(NO_3)_2$ and KNO_3, respectively. The hydroponic container was elevated 1 m above the height of an electronic balance, on which the outflow of water from the root system was weighed at 10 s intervals.

For each of 6 plants, changes in flow rates were measured both when roots were immersed in +N solution and transferred to -N solution and when roots

were immersed in -N solution and transferred to +N solution. A minimum of 60 minutes acclimation time was permitted for each nutrient environment. Measurements were made in the late morning (9AM-12PM) for three plants, and the mid afternoon (2PM-5PM) for the other three plants. As has been observed in other species (e.g. Gloser et al. 2007), there was clear evidence of diurnal variation in root conductance, with flow rates trending upward during the hours when measurements were taken. To control for this diurnal variation, measurements were recorded both for the transition from +N to -N solution, and from -N to +N solution, and analysis focused on short term changes. For each transition, flow rates were measured immediately before and 10 minutes after nutrient solutions were changed. After flow measurements, roots were dried in a 70^{circ}C oven for a minimum of 3 days and dried roots were weighed.

This protocol does not permit calculation of the absolute hydraulic resistance of roots, but it does show the relative short-term change in resistance with nitrate environment. The flow is driven by a combination of gravitational potential (0.01 MPa for one meter of elevation) and the osmotic potential of the roots xylem. Although we did not measure the xylem osmolarity, the literature suggests that it will only change modestly with nitrate supply (Gloser et al. 2007). To quantify the short-term effects of nitrate addition or removal on root conductance, we calculated the flow rate per unit dry mass for each plant in each of the nutrient environments. We used paired t-tests to compare the flow rates before and after nitrate addition, and before and after nitrate removal.

3.3.5 Patchy nutrient and ^{15}N treatments

To determine the effects of patchy nitrate supply on water uptake and crown allocation of ^{15}N, 13 split root hydroponic plants were divided into two treatment groups: a patchy nutrient treatment group (N=6) and a uniform nutrient treatment group (N=7) (Fig. 3.1). Starting on November 6, 2007, plants in the patchy nutrient treatment received 50% dilution +N solution in one container, with ^{15}N added as 2.0 to 2.5 mg $^{14}NH_4{}^{15}NO_3$ giving roughly 8 atom% ^{15}N for nitrate in

the +N container. The other container for patchy treatment plants received a 50% dilution of unlabeled Hoagland -N solution. Plants in the uniform nutrient treatment received a 50% dilution of a 50% N Hoagland solution created by mixing equal volumes of the +N and -N solutions. For the uniform nutrient treatments, one container also received the same amount of ^{15}N label that was added for the patchy treatment (giving $\sim$15 atom% ^{15}N for the labeled container, since the overall nitrate concentration is lower in these containers). For both treatments, the side of the plant receiving the ^{15}N label (and high nitrate for the patchy treatment) was randomized. After application of nutrient treatments, nutrients were not replenished prior to harvest, but water continued to be added to measure water uptake. Plants were harvested between November 9 and 11, 2007. Main roots, lateral roots, leaves, and branches for each sector were separated from the main stem, and all plant components were oven-dried and weighed. Each tissue type, except for labeled roots, were then ground in a ball mill and analyzed for ^{15}N content at the UC Davis Stable Isotope Facility.

3.3.6 Calculations — Estimated water crossover and actual ^{15}N distribution

The proportion of total water uptake crossing from the labeled container to opposite side leaves was estimated as the % of leaf biomass on the opposite side (assumed to equal the % of total transpiration) minus the % of total water taken up in the first day of the treatment by roots in the opposite side container. This value was then divided by the % of water uptake from the labeled container to give the estimated fraction of water from the labeled container that would flow into leaves on the opposite side of the plant. This value was our prediction for the proportion of ^{15}N crossing over to the opposite side of each plant.

We compared this prediction to the actual rate of crossover of ^{15}N label. For all experimental plants, as well as an unlabeled control, the mass % ^{15}N was calculated for nitrogen in roots, stems, branches, and leaves. For each sample the mass % ^{15}N was calculated as 100 $\times$ 15 $\times$ atom% ^{15}N)/(100$\times$15 + atom %

^{15}N $\times$ (15-14)). Then the mass % ^{15}N label was calculated as the mass % ^{15}N in each sample, minus the mass % ^{15}N in the control. The resulting value was multiplied by the total N content of each tissue (=tissue mass $\times$ sample mg N / sample mass) to give the total mass accumulation of ^{15}N label in each tissue. The percent of ^{15}N crossing over to the opposite side of the plant was calculated as the total mass of ^{15}N label in opposite-side leaves, divided by the total mass of ^{15}N label in all leaves of that plant.

We had hypothesized that ^{15}N crossover would be proportional to water crossover when there was a net flow of water from the labeled side to the opposite side, but would be unaffected by water crossover when the flow was in the opposite direction. To test this hypothesis, we divided the plants into two groups: those with a positive estimated water crossover and those with a negative water crossover. For each group, we used linear least squares regression to test for correlations between the percent ^{15}N crossing to the opposite side and the proportion of water crossing to the opposite side.

3.4 Results

3.4.1 Model output

Results from both models show that water uptake distribution should be affected by local changes to root hydraulics and that the change is sensitive to tangential resistance (Fig. 3.3). The maximum change in water uptake — and therefore in inter-sector flow — occurs at zero tangential resistance, with the proportion of water determined by the ratio of root resistances between the two halves of the plant. Thus, when resistance for the low nitrate roots is 2x that of the high nitrate roots, two thirds (=0.67) of the water is taken up in the high nitrate sector. With a 1.5x change in root resistance, three fifths (=0.60) of the water is taken up in the high nitrate sector, and with a 1.2x change in root resistance, six elevenths (=0.55) is taken up in the high nitrate sector.

The simulated proportion water taken up in the nitrate patch drops off with

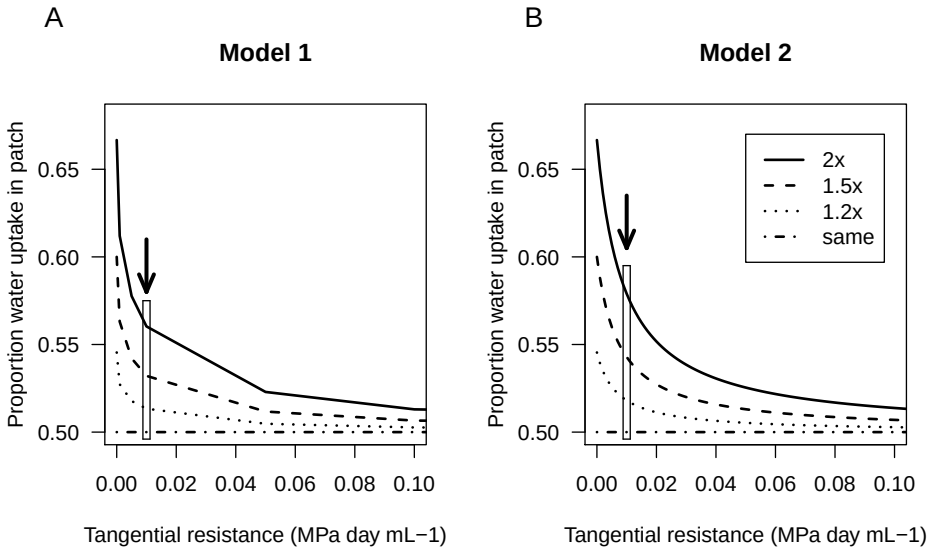

Figure 3.3: Simulated patterns of water uptake as a function of the hydraulic resistance to tangential flow, based on Model 1 (A) and Model 2 (B). Hydraulic resistance in roots in low nutrients was either multiplied by a factor of 2x, 1.5x, or 1.2x or was unchanged (same) relative to the high nutrient patch. For each model, an arrow and rectangle indicates the outputs for our default tangential resistance, as estimated for basil. Default values were used for all other parameters.

increasing tangential resistance, however. At our estimated tangential resistance for basil and a 2x change in root resistance, a 56% change in water uptake is expected in the high nitrate patch for Model 1 (boxed area of Fig. 3.3A), or about a 58% change for Model 2 (boxed area of Fig. 3.3B). Similar tangential resistance effects are observed with lower changes in root resistance with nutrient environment.

The simulated effects of tangential resistance decrease as root resistance is increased. Our models predict that as the root resistance increases, the proportion of water taken up on the high nitrate side will asymptotically approaches its theoretical maximum (Fig. 3.4). This result reflects the equation for steady-state water uptake distribution according to Model 2: as r_{r1} and r_{r2} get large, the effect of r_t diminishes (Eq. 3.3.5). Thus, at the relatively low root resistance estimated for tomato (Newman 1973), the proportion water taken up in the high nitrate patch is substantially below the theoretical maximum, and is noticeably higher for Model 2 (Fig. 3.4B) than for Model 1 (Fig. 3.4A). At root resistances measured for other herbaceous species (Newman 1973), the effects are closer

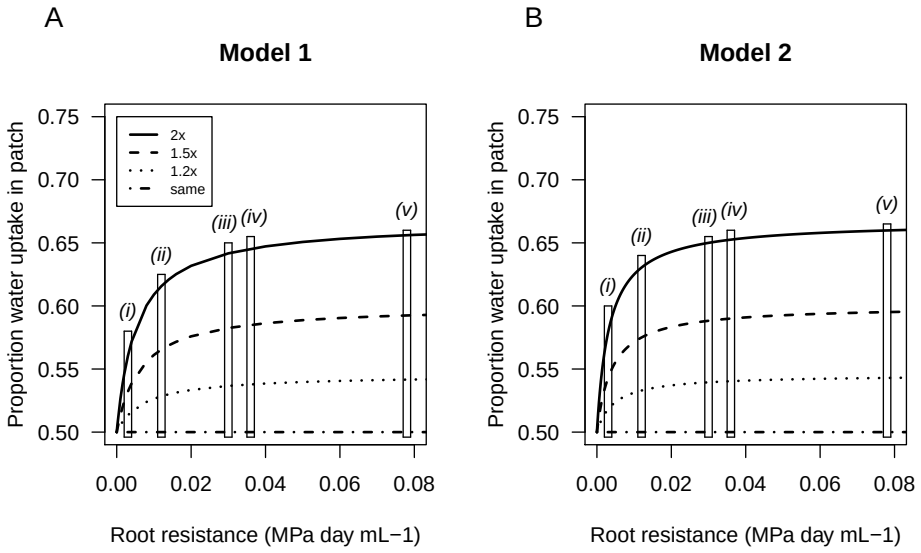

Figure 3.4: Simulated patterns of water uptake as a function of the root resistance in high nutrient conditions, based on Model 1 (A) and Model 2 (B). Hydraulic resistance in roots in low nutrients was either multiplied by a factor of 2x, 1.5x, or 1.2x or was unchanged (same) relative to the high nutrient patch. Simulated results for the herbaceous species in Newman (1973) are boxed and labeled with lower case Roman numearals: tomato (= 0.003 MPa day mL^{-1}, our default value) (i), maize (= 0.012 MPa day mL^{-1}) (ii), sunflower (=0.03 MPa day mL^{-1}) (iii), dwarf bean (=0.036 MPa day mL^{-1}) (iv), and broad bean (=0.078 MPa day mL^{-1}) (v). These values are based on Newman's (1973) measurement of root conductance per root volume, assuming of 5 cm^3 roots per sector. The value for tomato (i) was used as our default root resistance Default values were used for all other parameters.

to their theoretical maximum. In particular, an increase in root resistance from the value for tomato (0.0015 MPa day mL^{-1}) to the value for maize (0.012 MPa day mL^{-1}) or sunflower (0.030 MPa day mL^{-1}) results in a substantial increase in nutrient effects, while the higher root resistances observed for dwarf bean (0.036 MPa day mL^{-1}) and broad bean (0.079 MPa day mL^{-1}) are already close to the theoretical maximum for both models (Fig. 3.4A,B).

It should be noted that although our two models are qualitatively similar, they do not give identical output (Fig. 3.5). The similarity between the models was greatest when axial resistance was less than or equal to half of the tangential resistance. At higher ratio of axial resistance to tangential resistance, Model 2 predicts a larger proportion of water taken up in the high nutrient patch compared to Model 1 (Fig. 3.5). At our default values, the ratio was 1.0, resulting in moderate discrepancies between the two models.

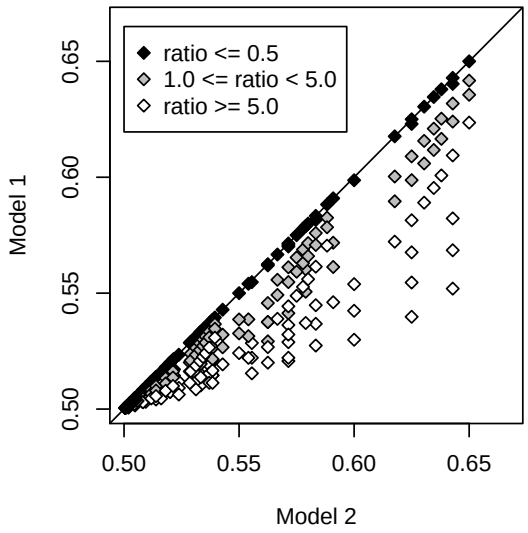

Figure 3.5: Relationship between outputs from the two models analyzed in this paper using the same parameters. The scatter of points here represents results when tangential resistance between 0.0005 and 0.1 MPa day mL^{-1}, when low root resistance is varied between 0 and 0.01 MPa day mL^{-1}, when the ratio between high and low root resistances is varied between 1.1 and 2.0, and when axial resistances varied between 0.0 and 0.05 Mpa day mL^{-1}. Otherwise, model defaults are used. Color indicates the ratio of axial resistance to tangential resistance, with ratios up to 0.5 shown in black, ratios from 1.0 to 5.0 shown in gray, and ratios above 5.0 shown in white.

3.4.2 Nitrate effects on excised roots

Water flow through excised basil roots that had acclimated >1 hour in -N solution was significantly lower than the same roots acclimated >1 hour in +N solution. This change in flow rates result was much faster when +N solution was replaced with -N solution than when -N was replaced with +N, as indicated by a significant (paired t-test, t=-2.81, df=4, $p<0.05$) change within 10 minutes for nitrate removal but over the time scale for nitrate addition (paired t-test, t=1.06, df=4, p=0.35). The average ratio of flow rates between the +N and -N treatments was 1.4 ± 0.3 (mean $\pm$ standard deviation) (see Appendix, section 3.7 Tables 3.2, 3.3).

3.4.3 Patchy nutrient and ^{15}N experiment

Application of the patchy nitrate treatment resulted in a slight and marginally significant trend of increased proportion of water uptake from the high nitrate (labeled) side of the root system (paired t-test, t=2.16; df=5; p=0.08) while no change in water uptake was observed for the uniform nutrient treatment (paired t-test, t=0.57; df=5; p=0.59) (Fig. 3.6).

There was no significant treatment effect on ^{15}N distribution (t test, t=-0.20; df=10.5; p=0.85), but as predicted by the model, the pattern of ^{15}N distribution in the leaves (as expressed by the percent ^{15}N above background that was found in the leaves of the unlabeled side of the plant) was positively related to the estimated percent when the estimates for percent water crossover (r^2=0.77; $p < 0.01$), and unrelated when estimated percent water crossover was negative ($r^2 < 0.01$; p=0.97) (Fig. 3.7). The ^{15}N distribution for individual plants varied as predicted from water uptake patterns, but with higher values for the calculated percent ^{15}N crossover than what would be predicted based on estimated water crossover.

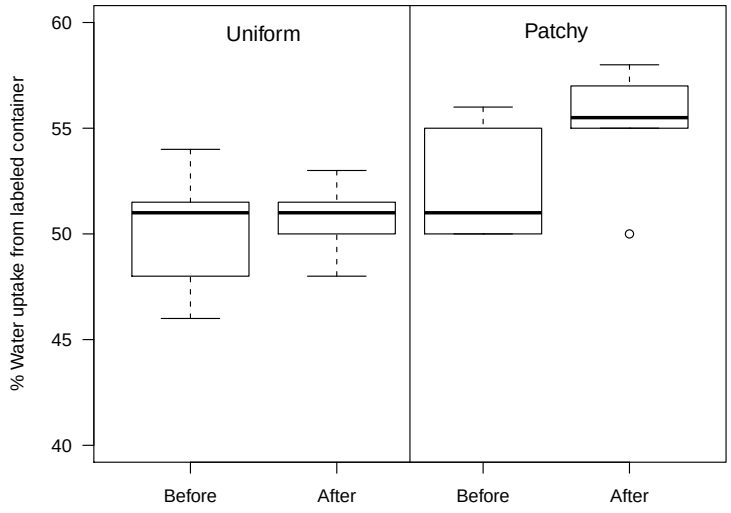

Figure 3.6: Average percent water uptake from the labeled container for plants with patchy (N=6) or uniform (N=7) nitrate supply, before and after beginning of nutrient treatments and labeling. No significant change was observed for the uniform treatment (paired t-test, t=-0.57; df=6; p=0.59). For the patchy nutrient treatment, a marginally significant increase was observed (paired t-test t=-2.16; df=5; p=0.08).

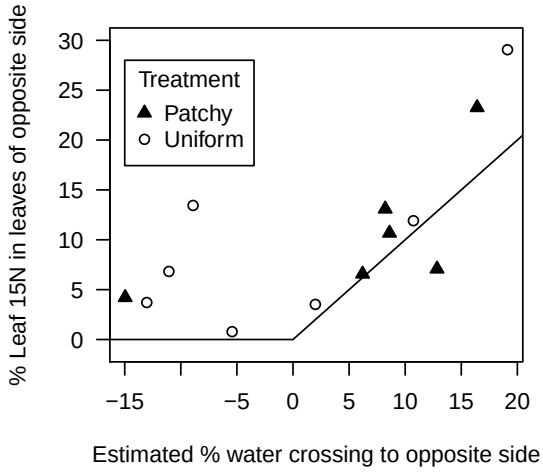

Figure 3.7: Percent of ^{15}N label accumulation in opposite branch leaves as a function of the estimated percent water crossing over to the opposite side in the first day after nutrient treatments and labeling were applied. Estimated % water crossing to the opposite side is calculated as (% leaf area on opposite side - % water uptake on opposite side) / (% water uptake from labeled side). The curve is the predicted distribution if ^{15}N label is passively carried by water movement (=% water crossover for water crossover > 0%, =0% for water crossover <0%). Solid triangles indicate plants receiving the patchy nitrate treatment (with all nitrate supplied to the labeled side of the plant). Empty circles indicate plants receiving the uniform nitrate treatment.

3.5 Discussion

Taken together, our modeling and empirical work demonstrate that xylem sectoriality can limit the effect of dynamically varied root resistance on water uptake patterns, and support the hypothesis that these changes in water uptake directly influence the internal distribution of nitrogen taken up in a nitrate patch.

Outputs from both of our models support the expectation that patterns of water uptake following a local change in root resistance should be constrained by stem tangential resistance in basil. However, the simulated effect of sectoriality also depends on the magnitude of the root resistance relative to the tangential resistance: when root resistance is higher, a small relative change produces a larger change in water uptake. Model 2 — which is much simpler and therefore less computationally intensive than Model 1 — provides similar outputs to Model 1, especially when the ratio of axial to tangential resistance is low. Under these conditions, Model 2 can be useful for general predictions about sectored water transport. Equation 3.3.5 provides an easy means of calculating expected patterns of water uptake, although it should be emphasized that this equation assumes symmetry of biomass distribution. When circumstances are less equal, such as when only a small portion of the root system is in the nutrient patch, these models would have to be modified to account for differences between the two sectors.

Results from the root conductance experiment suggest that, on average, the root conductance is 40% higher in a high nitrate environment than a no nitrate environment, i.e. that the resistance is 40% higher in the no nitrate environment. The simulations suggest that this relative change in root resistance should result in between 52% to 53% of water uptake in the nitrate patch when 50% of the root system receives nitrate. In actuality, the average proportion of water taken up in the nutrient patch was 56%. This difference is unsurprising given the difference in time scales between the two studies, one hour for the root conductance experiment versus several days for the patchy nutrient experiment, but could also be explained if the background root resistance in basil is higher

than Newman's (1973) value for root resistance in tomato, and more similar to his measurement for sunflower or bean (Newman 1973). Dynamic changes to stem sectoriality due to xylem hydrogel properties could also contribute to increased crossover not accounted for by our models (Zwieniecki et al. 2001).

We hypothesized that changes to root resistance would result in nitrogen crossover rates proportional to the resulting changes in the water uptake distribution. Our results support this hypothesis. We were able to detect a marginally significant change in water uptake by comparing water uptake before and after the nutrient treatments were applied. Since before and after comparisons could not be made for nitrogen allocation, we would not expect a significant treatment effect on ^{15}N distribution given these results, and indeed no treatment effect was observed. On the other hand, as predicted, the observed patterns of ^{15}N distribution were significantly correlated with our predictions based on water uptake patterns. This strongly suggests that any short-term adjustments to nitrate allocation in basil are mediated by xylem fluxes rather than, e.g. by activity of transfer cells (Pate and Jeschke 1995). These changes to xylem fluxes most likely result from the aggregated effects of root conductivity changes (Gloser et al. 2007) and stem xylem conductance changes due to hydrogel responses to ion concentrations (Zwieniecki et al. 2001).

The confirmation that nitrate from a patch follows xylem fluxes suggest a previously unexamined benefit of physiological changes to root conductance in response to nutrient heterogeneity. Previous studies have emphasized the role of these adjustments in increasing water flow through the soil toward roots in nutrient patches, thereby drawing mobile soil ions toward those roots, and increasing whole plant competitiveness (Gloser et al. 2007, Gorska et al. 2008, Maurel et al. 2010). We present the view that there could also be benefits for nutrient allocation within the plant. While the model outputs presented here only suggest a modest increase in nutrient crossover due root hydraulic changes, larger effects are predicted by a less symmetrical circuit, e.g. Thorn and Orians (2011*a*), suggesting a larger effect of root hydraulics on nutrient movement

when only a small portion of the root system experiences high nitrate conditions. Greater benefits are also expected when a patchy nutrient environment is combined with a patchy light environment (Thorn and Orians 2011*a*) or localized defoliation (Orians and Jones 2001). If, for example, most of the transpiration occurs in a portion of the crown in a canopy gap, then changes in root conductance will ensure that a higher proportion of xylem sap delivered to those leaves contains high nitrate content, maximizing photosynthesis and growth potential in the light patch. Conversely, the importance of increased movement of nitrate toward the roots through the soil may be of greater importance for plants in direct competition with one another. Future studies should evaluate the relative selective benefit of these factors through ecologically realistic competition experiments, e.g. Hodge et al. (1999).

In conclusion, we show that basil, like sunflower (Gloser et al. 2007) and tomato and cucumber (Gorska et al. 2008), adjusts root hydraulic properties in response to its nitrate environment. We confirm that there is also an elevated proportion of water taken up by roots in a nitate patch for split-root hydroponic basil. In addition, we show that the distribution of ^{15}N label applied in the nitrate patch can be explained by water uptake patterns. These observations indicate that the short-term crown distribution of nitrate nitrogen is determined by xylem fluxes. Thus, our research suggests an adaptive reason for nutrient-dependent changes in root hydraulics that has not previously been explored. Further research is needed to determine the relative role of root hydraulics and xylem hydrogel properties in influencing these fluxes. Other fruitful avenues for future research should include closer examination of the mechanisms for uptake changes and competition experiments to establish the fitness benefit of root hydraulic changes.

3.6 Acknowledgements

We would like to thank Matilda Singleton for plant care and assistance with the root conductance experiment. We thank NSF (Grant number DBI 0649190),

USDA National Institute of Food and Agriculture (Grant number 2007-35302-18351), and the Graduate School of Tufts University for providing funding this work. We thank the Tufts University Department of Biology for other financial and logistical support.

3.7 Appendix

Table 3.2: Raw data from root flow measurements. In all cases, measurements were taken for excised basil roots in an aerated Hoagland solution with (+N) or without (-N) nitrate. Roots in solution were elevated 1 meter above the balance used to monitor flow rates.

Minutes after start	Treatment	Plant 1 Flow rates (g/s) start=2:55PM	Plant 2 Flow rates (g/s) start=8:59AM	Plant 3 Flow rates (g/s) start=12:20PM
Starting with +N				
50	+N	0.000230	0.000264	0.000258
60	+N	0.000234	0.000454	0.000477
70	-N	0.000157	0.000388	0.000252
110	-N	0.000155	0.000495	0.000271
120	-N	0.000167	0.000532	0.000286
130	+N	0.000184	0.000556	0.000240
170	+N	No data	0.000627	0.000240

Minutes after start	Treatment	Plant 4 Flow rates (g/s) start=2:30PM	Plant 5 Flow rates (g/s) start=9:38AM	Plant 6 Flow rates (g/s) start=8:55AM
Starting with -N				
50	-N	0.000074	0.000080	0.000173
60	-N	0.000082	0.000089	0.000189
70	+N	0.000103	0.000112	0.000234
110	+N	0.000152	0.000141	0.000293
120	+N	0.000149	0.000154	0.000307
130	-N	0.000121	0.000125	0.000270
170	-N	0.000114	0.000120	0.000252

Table 3.3: Flow rate data summarized.

	Transition	Plant 1	Plant 2	Plant 3
Flow (g/s)	Starting at -N	0.000167	0.000532	0.000286
Flow (g/s)	Ending at +N (10 min. later)	0.000184	0.000556	0.000240
	change	0.000016	0.000024	-0.000046

	Transition	Plant 1	Plant 2	Plant 3
Flow (g/s)	Starting at +N	0.000234	0.000454	0.000477
Flow (g/s)	Ending at -N (10 min. later)	0.000157	0.000388	0.000252
	change	-0.000077	-0.000066	-0.000225
Root dry weight (g)		0.7194	0.6103	0.668
Flow / mass (g water/s/g DW)	Starting at -N	0.000233	0.000872	0.000428
Flow / mass (g water/s/g DW)	Ending at +N (10 min. later)	0.000255	0.000911	0.000359
	ratio (+N/-N)	1.096616	1.045113	0.839161
Flow / mass (g water/s/g DW)	Starting at +N	0.000326	0.000744	0.000714
Flow / mass (g water/s/g DW)	Ending at -N (10 min. later)	0.000218	0.000636	0.000377
	ratio (+N/-N)	1.491510	1.170103	1.892857

	Transition	Plant 4	Plant 5	Plant 6
Flow (g/s)	Starting at -N	0.000082	0.000089	0.000189
Flow (g/s)	Ending at +N (10 min. later)	0.000103	0.000112	0.000234
	change	0.000022	0.000024	0.000045

	Transition	Plant 4	Plant 5	Plant 6

Table 3.3: (continued)

Flow (g/s)	Starting at +N	0.000149	0.000154	0.000307
Flow (g/s)	Ending at -N (10 min. later)	0.000121	0.000125	0.000270
	change	-0.000028	-0.000029	-0.000037
Root dry weight (g)		1.598	0.259	0.7752
Flow / mass (g water/s/g DW)	Starting at -N	0.000051	0.000342	0.000244
Flow / mass (g water/s/g DW)	Ending at +N (10 min. later)	0.000065	0.000432	0.000302
	ratio (+N/-N)	1.267853	0.790179	0.807692
Flow / mass (g water/s/g DW)	Starting at +N	0.000093	0.000593	0.000396
Flow / mass (g water/s/g DW)	Ending at -N (10 min. later)	0.000076	0.000483	0.000348
	ratio (+N/-N)	1.226679	1.227696	1.137037

Summary:	Transition	Mean	Standard deviation
Flow (g/s)	Starting at -N	0.000224	0.000168
Flow (g/s)	Ending at +N (10 min. later)	0.000238	0.000166
	change	0.000014	0.000031
Flow (g/s)	Starting at +N	0.000296	0.000144
Flow (g/s)	Ending at -N (10 min. later)	0.000219	0.000104
	change	-0.000077	0.000075
Root dry weight (g)		0.771650	0.443888

Table 3.3: (continued)

Flow / mass (g water/s/g DW)	Starting at -N	0.000361	0.000280
Flow / mass (g water/s/g DW)	Ending at +N (10 min. later)	0.000387	0.000285
	ratio (+N/-N)	0.974435	0.192909
Flow / mass (g water/s/g DW)	Starting at +N	0.000478	0.000252
Flow / mass (g water/s/g DW)	Ending at -N (10 min. later)	0.000356	0.000196
	ratio (+N/-N)	1.357647	0.290603

CHAPTER 4

Modeling the influence of differential sectoriality on the photosynthetic responses of understory saplings to patchy light and water availability

Authors: Alexandra M. Thorn and Colin M. Orians

Published: 2011 *Trees—Structure and Function*, 25(5):833-845

4.1 Abstract

Exploitation of patchy light is a key determinant of plant performance in the forest understory. While many adaptive traits are known, the role of stem vasculature in understory photosynthesis is not established. Sectoriality—the degree of vascular constraint to long distance transport—has been hypothesized to limit growth in heterogeneous light. We simulated the photosynthetic potential of sectored and integrated plants in patchy light, as a function of soil water potential (patchy or uniform). We used hydraulic parameters typical of temperate woody species in an Ohm's law model including a tangential resistance parameter, and simulated cavitation by varying axial resistance of leaves, leaves and roots, or the whole plant. Our results suggest that differential sectoriality will not affect photosynthesis when water is plentiful, but can constrain stomatal conductance at more negative soil water potentials, especially when only a small portion of the crown receives light. This effect is strongest just below the turgor loss point, and depends on axial resistance and soil water heterogeneity. Increased resistance in high light leaves decreases photosynthesis regardless of sectoriality. However, when resistance is increased for leaves and roots or the

whole plant, photosynthesis decreases more for sectored than for integrated plants. Moreover, the simulations suggest that sectoriality can further depress photosynthesis when water availability is asymmetrical. These results might explain why integrated species, such as *Betula lenta*, *B. alleghaniensis*, and *Acer saccharum* thrive in the forest understory and grow rapidly into canopy gaps, while sectored species, such as *Quercus rubra*, do not.

4.2 Introduction

As sessile organisms, plants experience unique challenges in resource acquisition, especially in highly patchy environments. Young trees in the forest understory experience particular extremes in resource heterogeneity: these plants must be able to photosynthesize at baseline light levels 5-10% of full sunlight, while maintaining the ability to efficiently exploit infrequent high light patches with intensities similar to full sunlight. Plants growing along the edges of forest gaps experience similar extremes. Transient light patches may strike individual branch for as little as seconds to hours at a time, but often represent the majority of photosynthetically active radiation that understory plants receive in a day (reviewed by Knapp 1992, Singsaas et al. 2000). In shade-adapted plants, many physiological and anatomical leaf traits have been documented to increase plant performance when light comes as infrequent patches (e.g. Pearcy et al. 1997, Sack et al. 2003), but less is known about adaptive responses to light heterogeneity at the whole plant level. Specifically, is the ability to exploit high light patches dependent upon the unimpeded transport of water and nutrients to that part of the crown? It has been shown that hydraulic conductivity can constrain photosynthesis in water-limited conditions (e.g. Jones et al. 2010), but the role of whole plant hydraulics in patchy conditions has received less attention. In this context, vascular sectoriality—the degree to which long distance resource transport is constrained to specific pathways between root and shoots—could pose an important limitation on photosynthetic potential and ultimately on growth (sensu Gloser et al. 2008). Indeed, in a principal component analy-

sis of 18 temperate woody species, Zanne et al. (2006*b*) noted a strong negative correlation between sectoriality and shade tolerance, which the authors hypothesized to reflect the benefits of low sectoriality under variable light conditions. We might also expect that under dry soil conditions, the ability to use the entire root system to supply water to high light leaves would extend the conditions in which leaves can effectively exploit light patches.

Sectoriality is known to vary considerably among woody species (Greenidge 1955, Kozlowski and Winget 1963, Orians et al. 2004, 2005*b*, Ellmore et al. 2006, Gloser et al. 2008). Members of the ring porous genus *Quercus* display high sectoriality compared to the members of the diffuse porous genus *Acer*, while *Betula* species have lower sectoriality still (Orians et al. 2004, Ellmore et al. 2006, Gloser et al. 2008). "Double saw cut" experiments demonstrate one aspect of the physiological impact of this variation. In these experiments, overlapping horizontal saw cuts are used to sever xylem vessels at different heights up the trunk, forcing any water flow through the trunk to occur along indirect pathways (Tyree and Zimmerman 2002). Integrated species—those with low sectoriality—are able to maintain normal crown functioning with a much smaller distance between cuts than can high sectoriality species. For instance, *Betula occidentalis* was shown to maintain normal stem conductance with overlapping saw cuts as little as 1 cm apart through a 1 cm diameter portion of the main axis (Sperry et al. 1993). In contrast, leaves of *Acer pseudoplatanus* saplings quickly wilted when overlapping cuts were less than a critical distance of 2 cm apart (Mackay and Weatherly 1973). Even more extreme vascular changes cuts are observed in *Quercus rubra*, in which individual earlywood vessels can range from 1 to 10 m in length, resulting in vascular restriction over axial distances of many meters from a single saw cut (Tyree and Zimmerman 2002). Thus, saw cut experiments show that integrated species can tolerate and recover from greater extremes of physical damage than can sectored species, but the effect of sectoriality on responses to milder stressors such as patchy light and water is not known.

Here, we present a modeling framework to examine the potential role of xylem sectoriality in limiting photosynthesis by understory trees. We simulate plant hydraulics using an Ohm's law analogy circuit, modified to introduce a parameter to describe the stem tangential resistance to flow between sectors. Combining this framework with published models for photosynthesis, we simulate the effects of soil water limitation on photosynthetic potential, for patchy light conditions and varied levels of sectoriality. This approach contrasts with more detailed xylem network models (e.g. Loepfe et al. 2007), in that we vary a single sectoriality parameter to capture overall patterns in tangential hydraulic resistance, without delving into anatomical details, such as the degree to which these patterns depend on vessel-to-vessel lateral connections and the presence of "cross-grained" vessels (Tyree and Zimmerman 2002, Orians et al. 2004, Nadezhdina 2010). Our purpose is to establish general expectations for the relationship between sectoriality and photosynthesis, to inform future empirical research.

4.3 Materials and methods

4.3.1 Model overview

We model photosynthesis in patchy light conditions by combining published models for stomatal conductance, carbon assimilation, and transpiration with a novel construct for modeling xylem sectoriality. To simulate sectoriality, we simplify the vasculature of a plant as divided into two sets of parallel pathways ("sectors"), each comprising the xylem vessels directly feeding a portion of the crown. These sectors may correspond to two equal halves of the plant (Fig. 4.1A), but can also be used to designate asymmetrical portions of the plant, e.g. one sector corresponding to a small portion of the crown receiving direct sunlight while the other sector corresponds to shaded portions of the crown (Fig. 4.1B). Leaf water status, dynamically determined by the balance of transpiration and water supply to the leaves of each sector, is the basis for water

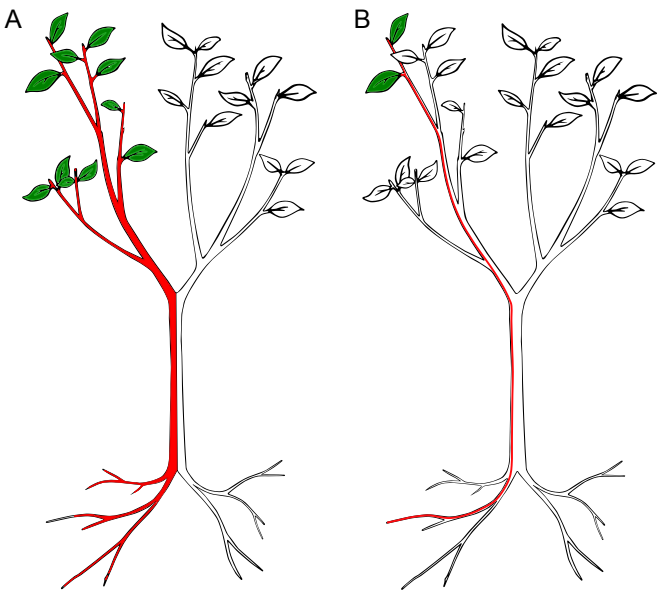

Figure 4.1: Diagram of portions of idealized tree considered in our simulation models. In each tree, the leaves exposed to a high light patch and the associated vasculature are shown in color. Integrated plants possess the ability to use uncolored, as well as colored stem tissue to supply water to leaves in high light. Highly sectored plants depend primarily on the colored stem tissue for water supply. For modeling purposes, we simulate the proportion of leaf area in high light relative to the rest of the plant by adjusting the relative resistance of stem, leaf, and roots for each of two "sectors", where the two sectors correspond to the portion of biomass in each of the two possible light environments. We simulate plants where equal portions of the leaf biomass are in high versus low light (A), and plants where one-tenth as much biomass is in high light relative to low light (B). We hypothesize that leaves in smaller light patches will benefit more from integration than leaves in light patches shared by a larger portion of the crown.

potential gradients within and between sectors. These gradients are simulated using the Ohm's law analogy for plant hydraulics (Fig. 4.2; Tyree and Ewers 1991). In these models, the hydraulic resistance within a sector is inversely proportional to the biomass of leaves in that sector, and the hydraulic resistance to flow between sectors is manipulated as a parameter characterizing xylem sectoriality. Parameters for all components of the model are summarized in Table 4.1 and additional variables are defined in Table 4.2. In the next two subsections, we present the equations used to model the relationships among water status, water potential, transpiration, and photosynthesis. We then describe the simulations tested.

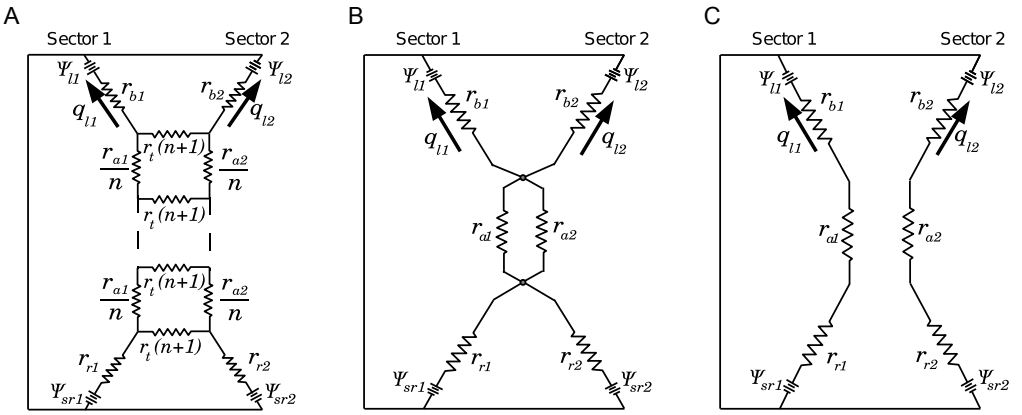

Figure 4.2: Circuit model for hydraulic flow at varied levels of sectoriality. We model sectored flow through the plant using the circuit in A, where sectoriality increases with the value of the sectoriality parameter r_t. For each sector (1 or 2), the hydraulic resistances (r) and water potential sources (Ψ) are shown for different plant components (l leaves, b branches and leaves, a stem axis, r roots, and sr soil-root). The stem is axially divided into n repeating segments by $n+1$ tangential resistors. Only the bottom and top segments are shown, with the intervening segments indicated by dashed lines. The stem axial resistance for each sector i is subdivided into n equal resistors each with $1/n$ of the overall axial resistance, and the sectors are connected by $n+1$ resistors each with resistance $r_t(n+1)$. The arrows designate the hydraulic flux (q) into the leaves of each sector. When the parameter r_t is equal to zero, the model is equivalent to the circuit depicted in B. As r_t approaches infinity, the circuit approaches C.

Table 4.1: Standard parameter values used in sectoriality model with citation and/or rationale.

Symbol	Description	Default value(s)	Units	Derived from
Plant parameters				
W_{li}	Dry mass of leaves of sector i (equation 4.3.2)	variable	g	N/A
a_{ls}	Specific leaf area (equations 4.3.5, 4.3.7, 4.3.8)	0.02	$m^2\ g^{-1}$	Estimated from temperate tree traits (Sack et al. 2003)
ϵ	Elastic modulus of leaf cell walls (equation 4.3.2)	5	MPa	Typical value for temperate trees (Sack et al. 2003)
c_{dw}	Ratio of leaf dry weight to leaf water content at $_{pli} = 0$ (equation 4.3.2)	0.75	g biomass g^{-1} water	Estimated from temperate tree traits (Sack et al. 2003)

Table 4.1: (continued)

Symbol	Description	Default value(s)	Units	Derived from
C_s	Concentration of osmotically active molecules in leaf cytoplasm	7.5×10^{-4}	mol g^{-1} biomass	Estimated from temperate tree traits (Sack et al. 2003)
$g_{b,C}$	Boundary layer conductance to CO2 (equations 4.3.4, 4.3.8, 4.3.9)	2763	m day^{-1}	Thornley and Johnson (2000)
$r_{C\theta}$	Parameter determining how stomatal conductance changes with leaf water status (equation 4.3.4)	0.29	day m^{-1}	Thornley and Johnson (2000)
σ_C	Carbon fixation constant (equation 4.3.5)	5.4	g C m^{-2} day^{-1}	Modified from Yang and Midmore (2005)
s	Relates saturating water vapor to air temperature (equation 4.3.7)	1.01	g m^{-3} degrees K^{-1}	Thornley and Johnson (2000)
ϕ	Solar energy available for evaporation (equation 4.3.7)	3.456 x 10^7	MPa g day^{-1} m^{-2}	Thornley and Johnson (2000)
L_H	Latent heat of vaporization of water (equation 4.3.7)	2450	MPa	Thornley and Johnson (2000)
γ	psychrometric parameter (equation 4.3.7)	0.495	g degrees K^{-1} m^{-3}	Thornley and Johnson (2000)
$\Delta\rho_v$	water vapor deficit of the atmosphere (equation 4.3.7)	7.5	g m^{-3}	Thornley and Johnson (2000)
$g_{b,w}$	Boundary layer conductance to water (equations 4.3.7, 4.3.9)	4320	m day^{-1}	Thornley and Johnson (2000); equation 4.3.10
R_u	Resistance to water uptake by roots (Fig. 4.2)	variable	MPa day g^{-1} water	See text

Table 4.1: (continued)

Symbol	Description	Default value(s)	Units	Derived from
R_a	Resistance to axial flow through stems (Fig. 4.2)	variable	MPa day g^{-1} water	See text
R_b	Resistance to axial flow through branches and leaves (Fig. 4.2)	variable	MPa day g^{-1} water	See text
Physical Constants and Environmental Parameters				
R	The gas constant (equation 4.3.3)	8.3144	MPa g degrees K^{-1} mol^{-1}	N/A
T	Temperature (equation 4.3.3)	293	degrees K	N/A
C_o	Concentration of carbon dioxide in the atmosphere (equation 4.3.3)	0.76	g m^{-3}	Calculated for standard conditions, assuming 385 ppm CO2 in the atmosphere (Tans 2009)
L_i	Relative measure of photon flux density striking leaves of sector i (equation 4.3.5)	variable	Unitless	Yang and Midmore (2005)
Ψ_{sri}	Soil-root water potential associated with sector i (equation 4.3.1)	variable	MPa	N/A

Table 4.2: Symbols and units for dynamic variables.

Symbol	Description	Units
q_{li}	Hydraulic flux into leaves of sector i (Fig. 4.1)	g water day^{-1}
Ψ_{li}	Water potential of the leaves of sector i (equation 4.3.1)	MPa
Ψ_{pli}	Pressure component of water potential of leaves of sector i (equation 4.3.2)	MPa
Ψ_{oli}	Osmotic component of water potential of leaves of sector i (equation 4.3.3)	MPa
W_{wli}	Mass of water in leaves of sector i (equations 4.3.2, 4.3.3, 4.3.10)	g
$g_{si,c}$	stomatal conductance to carbon dioxide (equation 4.3.4)	m day^{-1}
U_{Cpi}	Potential carbon fixation for leaves of sector i (equation 4.3.5)	g carbon day^{-1}
θ_{wli}	Relative leaf water content for leaves of sector i as mass fraction of saturating leaf water content (equation 4.3.6)	Unitless
U_{Ci}	Actual carbon fixation rate by leaves of sector i, incorporating leaf water content into stomatal conductance (equation 4.3.8)	g C day^{-1}

4.3.2 Sectoriality model and hydraulic parameters

To simulate the effects of sectoriality on leaf water supply and the resulting effects on photosynthesis, we use the Ohm's law analogy to simulate hydraulic flow through a pair of parallel pathways ("sectors") running axially through a plant. The leaves and roots of each sector are independent, but the stem vasculature is interconnected. Specifically, the stem axial pathway is divided into n identical segments by the presence of $n+1$ tangential resistors which constrain flow between the two sectors (Fig. 4.2). The resistance of each tangential resistor scales with a tangential resistance parameter r_t and with the number of resistors included in the model (Fig. 4.2A). When the value of r_t is zero, the plant is considered to be perfectly integrated, and the two axial pathways through the stem function as a pair of resistors in parallel (Fig. 4.2B). As the parameter r_t approaches infinity, the plant approaches perfect sectoriality (Fig. 4.2C). We assume that all hydraulic resistances and soil water potentials are constant, while the leaf water potentials vary dynamically as a function of leaf water content for each sector i. Water content increases with the flux (q_{li}) of water into the leaves sector i, and decreases with transpiration from those leaves (E_{li}). We simulate photosynthesis over time, using Kirchoff's voltage laws to calculate the flux of

water into the leaves of each sector i (q_{li}).

In both models, the flow of water vertically in each sector of the plant is constrained by the hydraulic resistances to flow through leaves and branches (r_b), along the main stem axis (r_a), and through the roots (r_r). In general, r_b is assumed to be 25% of the whole plant resistance, with the assumption that leaves present the primary resistance in the branches (Sack et al. 2003), and r_r is assumed to be 60% of whole plant resistance while the r_a is the remaining 15% (based on data from Nardini and Salleo 2000). Water flow within and between sectors is driven by two sources of water potential in each sector i: the leaf water potential (Ψ_{li})—calculated from the leaf water content (Eqs. 4.3.1–4.3.3) and the water potential difference between the soil and roots (Ψ_{sri})—a parameter representing the additive effects the soil matric potential and the difference in osmotic potential between the soil and the root xylem. The leaf water potential for sector i (Ψ_{li}) is calculated as the sum of the osmotic (Ψ_{oli}) and pressure potentials (Ψ_{pli}) of mesophyll tissue, with the assumption that gravitational potential will not significantly affect flow:

$$\Psi_{li} = \Psi_{pli} + \Psi_{oli} \tag{4.3.1}$$

Models for pressure and osmotic potentials are adapted from Thornley and Johnson's (2000) models for plant water potential as a function of whole plant water status. Leaf pressure potentials are always positive and are calculated by a linear function of leaf water content (W_{wli}):

$$\Psi_{pli} = max(0, \epsilon \times (\frac{c_{dw} W_{wli}}{W_{li}} - 1)) \tag{4.3.2}$$

where W_{li} is the dry weights of leaves in sector i, ϵ is the elastic modulus of leaf cell walls, and c_{dw} is the ratio of leaf dry weight to leaf water content at Ψ_{pli} = 0. Osmotic potentials are a non-linear function of leaf water content:

$$\Psi_{oli} = \frac{-RTC_s W_{li}}{W_{wli}} \tag{4.3.3}$$

where R is the gas constant, T is the absolute temperature, and C_s is the concentration of osmotically active molecules in the cytoplasm leaf cells expressed in moles per unit dry weight.

4.3.3 Transpiration, photosynthesis, and leaf water status

Photosynthetic responses to light patches depend on stomatal conductance, which, in turn, depends on a variety of internal and external factors, including leaf water status. Following models presented by Thornley and Johnson (2000), we model stomatal conductance as a function of light conditions and water status, photosynthesis and transpiration as a function of stomatal conductance, and dynamically model leaf water status as determined by transpiration and leaf flux. Since our interest is in vascular architecture, and not the detailed dynamics of stomatal physiology, we chose to model stomatal closure as a simple function of leaf hydration. More detailed stomatal models including vapor pressure deficits and other environmental parameters (e.g. Collatz et al. 1991) are beyond the scope of this paper, but would be expected to yield qualitatively similar results.

We assume that stomatal pores adjust in size to meet the carbon demands of photosynthesis, but that their maximum size is constrained by leaf water status. We model stomatal conductance to carbon dioxide (g_{Ci}) per leaf area in sector i as the minimum two possible models: a model based on potential carbon fixation rates (U_{Cpi}) and a model based on leaf relative water content (θ_{wli}) (both adapted from Thornley and Johnson 2000):

$$g_{si,C} = min\left(\frac{1}{\frac{C_a}{U_{Cpi}} - \frac{1}{g_{b,C}}}, \frac{1}{r_{C\theta} \times (1 - \theta_{wli})}\right) \tag{4.3.4}$$

where C_a is the CO_2 concentration in the atmosphere, $g_{b,C}$ the boundary layer conductance to CO_2, and $r_{C\theta}$ is a measure of how the stomatal resistance changes as the stomatal pores close. U_{Cpi} per unit leaf biomass is assumed for simplicity to increase linearly with leaf specific area (a_{ls}), W_{li}, and relative light intensity on leaves (L_i):

$$U_{Cpi} = a_{ls} \times W_{li} \times L_i \times \sigma_C \tag{4.3.5}$$

where σ_C is the carbon fixation constant.

The relative water content of the leaves of sector i (θ_{wli}) is defined as the ratio of water content of those leaves (W_{wli}) to the leaf water content at full turgor ($W_{wli;\Psi=0}$):

$$\theta_{wli} = \frac{W_{wli}}{W_{wli;\Psi=0}} \tag{4.3.6}$$

Note that $W_{wli;\Psi=0}$ is computed by setting Ψ_{li} to 0 and solving Eqs. 4.3.1–4.3.3 for W_{wli} as described in Thornley and Johnson (2000).

Stomatal conductance (determined in Eq. 4.3.4) is used to compute the transpiration rate (E_{ti}):

$$E_{ti} = \frac{a_{ls} \times W_{li} \times (s\phi + L_H \gamma g_{b,w} \Delta\rho_v)}{L_H(s + \gamma(1 + \frac{g_{b,w}}{g_{si,w}})} \tag{4.3.7}$$

where s is a parameter relating the saturating water vapor content of the air to temperature, ϕ the solar energy available for evaporation, L_H the latent heat of vaporization of water, γ a psychrometric parameter, $\Delta\rho_v$ the water vapor deficit of the atmosphere, $g_{b,w}$ the boundary layer conductance to water vapor, and $g_{si,w}$ is the stomatal conductance to water of the leaves of sector i.

Similarly, since we assume that stomatal conductance either adjusts to maximize photosynthesis or—when water is limiting—constrains photosynthesis, stomatal conductance can be used to calculate the carbon assimilation rate (U_{Ci}) (Thornley and Johnson 2000):

$$U_{Ci} = \frac{a_{ls} \times W_{li} \times C_a}{g_{si,C} + g_{b,C}} \tag{4.3.8}$$

It should be noted that for the purposes of the model, the stomatal and boundary conductance to water vapor is assumed to relate to the stomatal conductance of CO_2 by the ratio of the molecular masses for the two molecules (Thorn-

ley and Johnson 2000):

$$g_{si,w} = g_{si,C}(\frac{\mu_C}{\mu_w})^{1/2} \tag{4.3.9}$$

$$g_{b,w} = g_{b,C}(\frac{\mu_C}{\mu_w})^{1/2} \tag{4.3.10}$$

where μ_C and μ_w are, respectively, the molecular masses of CO_2 and of water.

Finally, for each sector, W_{wli} varies dynamically, with rate of change expressed as:

$$\frac{dW_{wli}}{dt} = q_{li} - E_{ti} \tag{4.3.11}$$

4.3.4 Simulations

To assess the importance of sectoriality as a constraint to photosynthesis, we consider patchy light scenarios, and the photosynthetic potential of the leaves exposed to high light conditions. For integrated plants we simulate the photosynthetic potential of high light leaves when half of the tree is exposed to high light (i.e. with the two sectors of equal size and resistance), and when just a small portion of the crown is in high light. In the latter scenario, we treat the high light leaves and associated vasculature as one sector, and the remainder of the plant as a second sector, with ten times as much leaf biomass and one tenth of the hydraulic resistance for branches, stems, and roots (Fig. 4.1). Light patches (high light conditions; $L_i = 1.0$) represent ten times the light intensity of the baseline low light conditions ($L_i = 0.1$). We first examine changes that occur immediately following an increase in light availability, and then focus on the simulated effects of sectoriality on steadystate photosynthesis that occurs after 1 h of patchy light at a range of soil water potentials. To examine the potential consequence of increased resistance due to droughtinduced embolisms, we simulated three different embolism scenarios, where in each case embolism in a tissue was simulated as increased resistance in that tissue (either 2× or 10×

the default resistance). The scenarios were (1) increased resistance in only the leaves in the high light branch, (2) increased resistance in all leaves, as well as in the roots, and (3) increased resistance axial resistance throughout the entire plant. Finally, we simulated the effects of non-uniform water supply, with soil water potential 0.1 or 0.5 MPa more positive for the shaded portion of the plant than for the high light sector.

4.4 Results

According to our model, when leaves are first exposed to a light patch, transpiration (Fig. 4.3A) and photosynthesis (Fig. 4.3C) are unaffected by sectoriality, but when soil water potential is low transpiration outpaces hydraulic flux into leaves and leaf water content is drawn down (Fig. 4.3B) resulting in lower rates of photosynthesis (Fig. 4.3C). This effect is stronger for sectored than for integrated plants. As leaf water content goes down, leaf water potential becomes more negative, and flux into the leaf increases, while transpiration decreases (Fig. 4.3A), until (after approximately 3600 s = 1 h) a steady state is reached with lower leaf water content and photosynthesis for sectored than integrated plants (Fig. 4.3B, C).

At more positive soil water potentials, water never limits photosynthesis, and so no sectoriality effects are observed, while at strongly negative water potentials, water constrains photosynthesis for integrated as well as sectored plants (Fig. 4.4). When half of the crown experiences high light, the strongest benefit of integration—with a theoretical maximum photosynthesis 5% higher for integrated than sectored plants—are observed just as leaves are beginning to lose turgor (-1.5 MPa at a whole plant hydraulic resistance of 4.0 MPa day g^{-1} m^{-2}; Fig. 4.4A). The potential effect is stronger when only a small portion of the crown experiences high light—photosynthesis 6% higher for perfectly integrated plants (Fig. 4.4B).

When resistance is elevated only for the leaves on the high light portion of the plant, sectoriality effects decreased for large light patches, and slightly in-

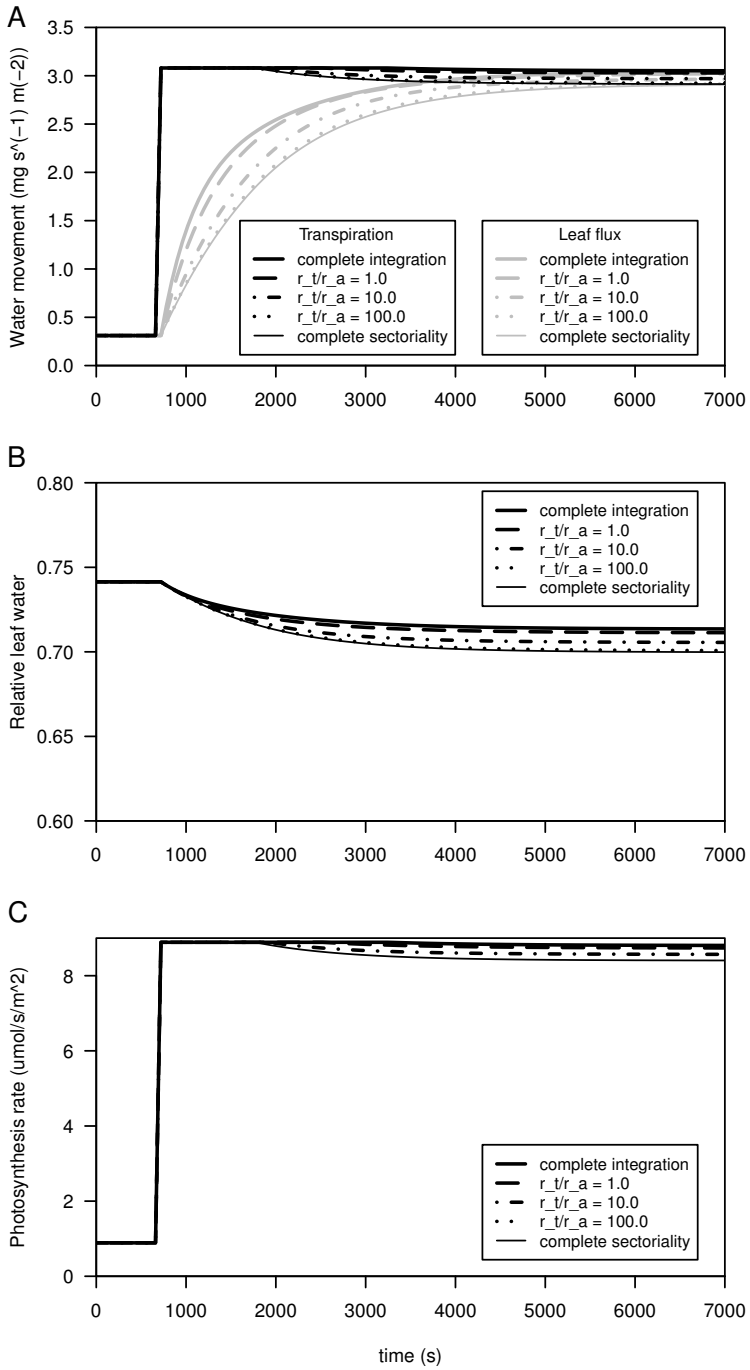

Figure 4.3: Simulated changes in transpiration, leaf flux, relative leaf water, and photosynthesis rates in response to a light patch illuminating half of the crown. Dynamic changes in transpiration and leaf flux (A), relative leaf water (B), and photosynthesis are shown for plants with different tangential resistance parameters (indicated by the ratio of tangential to axial resistance) (C). Transpiration is shown in black lines, and leaf flux in gray lines. The simulated plant is exposed to uniform low light until time = 720 s, when the focal portion of the crown receives high light. Soil water potential is assumed to be uniformly -1.5 MPa, just slightly more negative than the point at which water begins to limit photosynthesis in high light. Whole plant axial resistance is 4.0 MPa day g^{-1} m^{-2}.

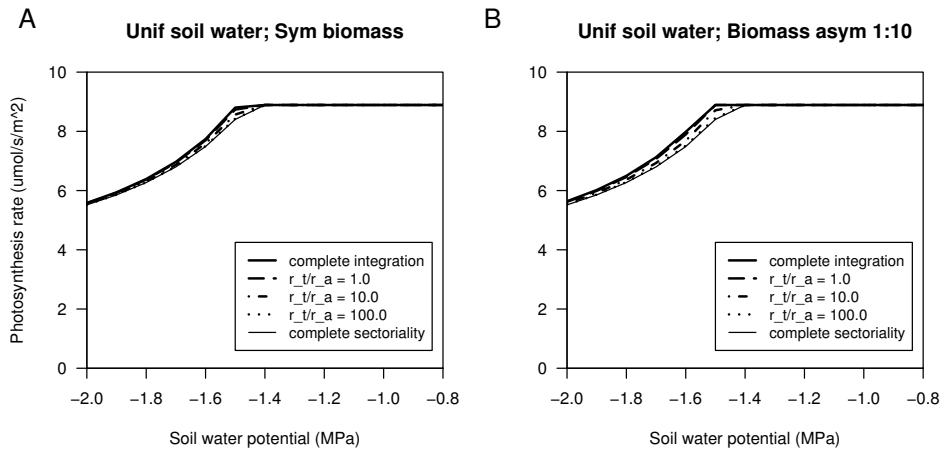

Figure 4.4: Simulated photosynthesis in leaves of high light branches, as a function of uniform soil water potential, at different levels of sectoriality. Steady-state photosynthesis rates are shown on a per area basis when half of the plant is simulated to be in high light (A), and one branch is in high light while the rest of the plant (ten times the biomass of the sector receiving high light) receives low light (B). Soil water potential is maintained uniformly at the levels shown on the xaxis. Whole plant hydraulic resistance is assumed to be 4.0 MPa day g^{-1} m^{-2}.

creased for small light patches (see Appendix, section 4.7 Fig. 4.8). However, when resistance is elevated for the leaves and roots of the entire plant, sectoriality becomes a much more important constraint (Fig. 4.5). When leaf and root hydraulic resistance is increased by a factor of two and half of the crown receives high light, the effect of sectoriality is only slightly different from the baseline resistance (Fig. 4.5A), but when only a small portion of the crown is illuminated, the potential photosynthetic benefit of integration increases to about 20% at -1.5 MPa (Fig. 4.5B). When leaf and root resistance increased by a factor of ten, the photosynthetic rate for integrated plants is just over 20% higher than for sectored plants at -0.95 MPa when half the crown is in high light (Fig. 4.5C) and this difference increases to 50% at -1.2 MPa when only a fraction of the crown is illuminated (Fig. 4.5D). Similar outputs, but with greater sectoriality effects, are observed when the resistance of the main axis is increased as well (see Appendix, section 4.7 Fig. 4.9).

Even at baseline levels of whole plant axial resistance, the effects of sectoriality increase dramatically when soil water is assumed to be non-uniform (Fig. 4.6). If the roots directly feeding the shaded portion of the crown experience water potentials 0.1 MPa more positive than the roots directly connected

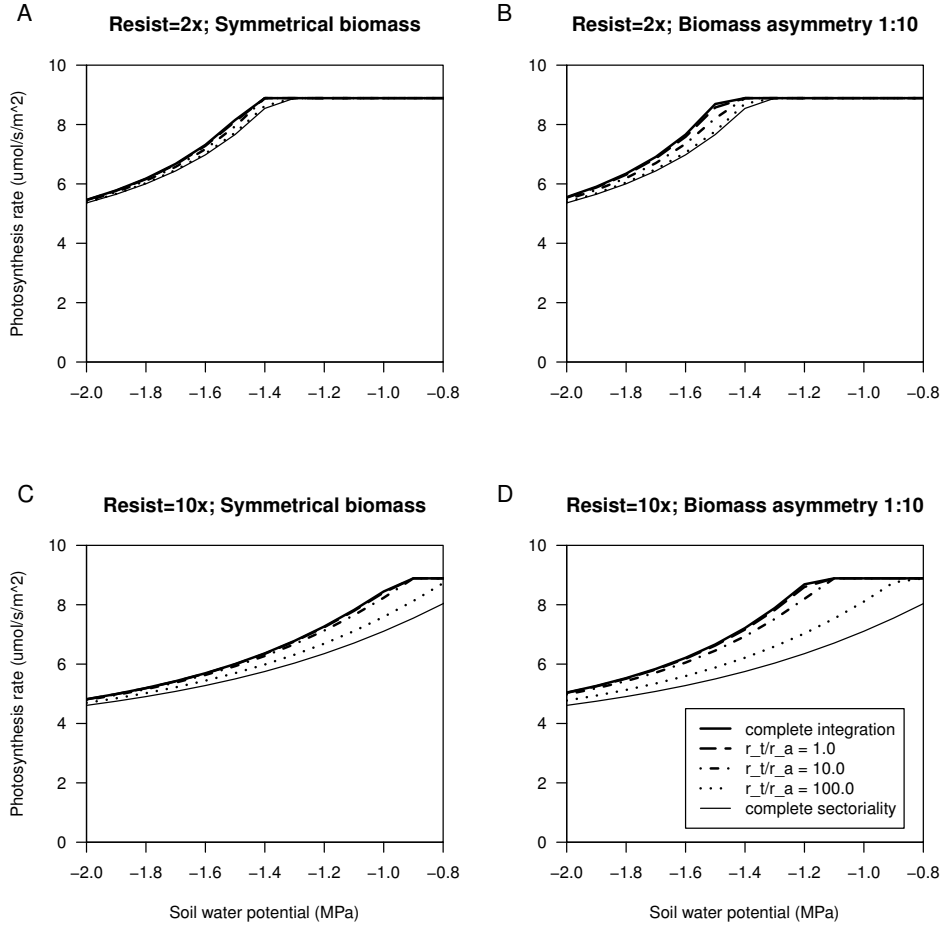

Figure 4.5: Simulated photosynthesis in leaves of high light sector, as a function of uniform soil water potential for uniformly elevated leaf and root resistance. Steady-state photosynthesis rates are shown on a per area basis for plants with different sectoriality levels and with leaf and root resistances elevated to either 2 times (A, B) or 10 times (C, D) their default resistances of 1.0 MPa day g^{-1} m^{-2} for leaves and 2.2 MPa day g^{-1} m^{-2} for roots. For each resistance, output is shown where half of the crown is in high light and the rest of crown is in low light (A, C) and where a small portion of the crown is in high light, while the rest of the crown (ten times the leaf biomass) is in low light (B, D). Simulated sectoriality is indicated by the ratio of tangential to axial resistance. Soil water potential is assumed to be uniform.

to the high light portion of the crown (which would occur when higher transpiration rates in the high light patch reduces water availability in that sector of the plant), the potential benefit of integration is 10% when half the crown is in high light (-1.6 MPa for the high light sector; Fig. 4.6A) and 19% when the high light sector represents one tenth the leaf area of the low light sector (-1.6 MPa for the high light sector; Fig. 4.6B). With a more extreme gradient of 0.5 MPa between the roots of high and low light sectors, the potential benefit is greater still: 30% when half the crown is in high light (-1.8 MPa for the high light sector; Fig. 4.6C) and 56% when the high light sector represents one tenth the biomass of the low light sector (-2.0 MPa; Fig. 4.6D).

4.5 Discussion

Our model output supports the hypothesis that xylem sectoriality could constrain photosynthesis in patchy light conditions, but suggests that under uniform water supply these effects would be slight—at least for temperate trees with no loss of stem conductance (Fig. 4.4). Under these conditions, the influence of sectoriality was somewhat stronger when a small portion of the crown is illuminated (Fig. 4.4B) than when half of the crown is in high light (Fig. 4.4A). Thus, the effects of sectoriality on photosynthesis are expected to be strongest when only a small portion of the crown is illuminated at any time, supporting the idea that integration is adaptive for trees growing in strongly shaded conditions, hypothesized by Zanne et al. (2006*b*).

The small effect of sectoriality depicted in Fig. 4.4 results from a low overall plant resistance, such that leaf water potential closely tracks root potential. As a result, when root water potential is uniform, there is never a substantial hydraulic gradient between sectors (sensu Zwieniecki et al. 2003). We selected hydraulic resistance values from the literature, but it should be noted that these values for hydraulic resistance represent well-hydrated plants (Sack et al. 2003, Ellmore et al. 2006). At low water potentials, cavitation is common (Hacke et al. 2006). Published vulnerability curves show substantial cavitation in the -1.0 to

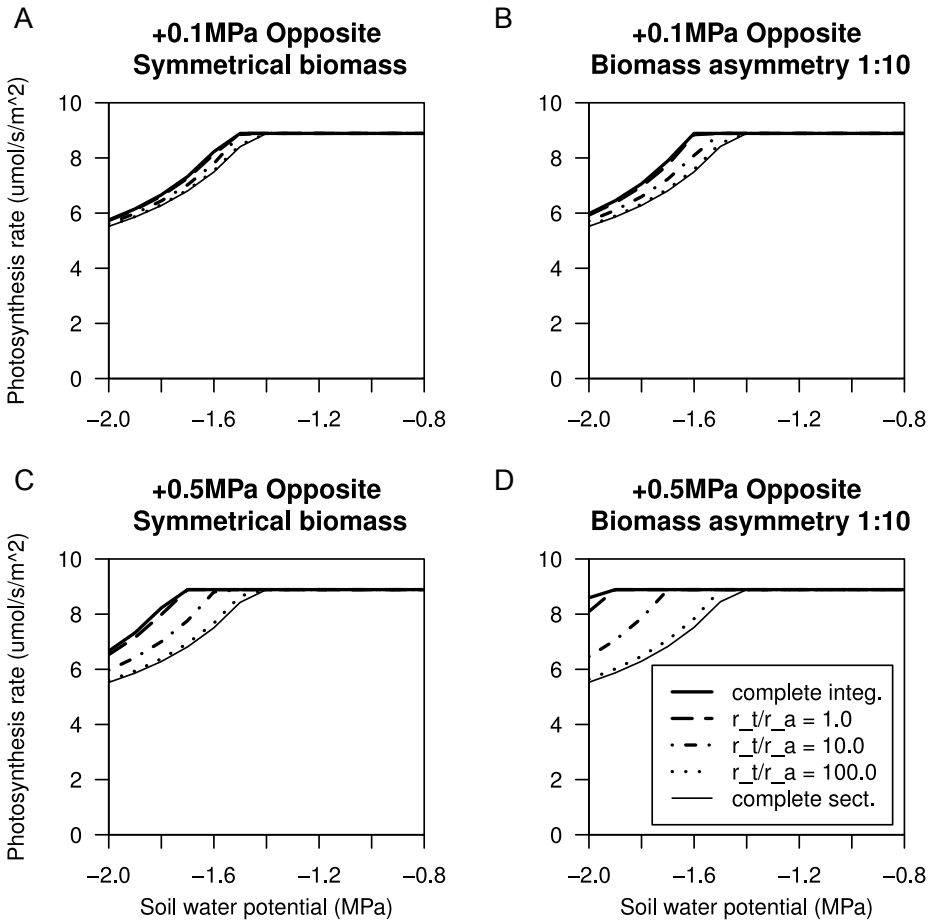

Figure 4.6: Simulated photosynthesis in leaves of high light sector as a function of soil water potential for the high light sector when water potential is more positive on the opposite side of the plant. Outputs are shown for simulations where the opposite sector water potential is 0.1 MPa higher than the high light sector (A, B), and where soil water potential for the opposite side is 0.5 MPa higher than for the high light sector (C, D). Graphs on the left (A, C) represent plants where half of the crown is high light, while graphs on the right (B, D) represent plants with one branch is in high light while the rest of the plant (ten times the biomass of the high light sector) receives low light. The whole plant hydraulic resistance is assumed to be 4.0 MPa day g^{-1} m^{-2}.

-2.0 MPa range for non-desert species. For example: Betula occidentalis shows dramatic percent loss conductance at -1 MPa, reaching 50% loss by -1.5 MPa; *Acer negundo* shows steady loss of conductance at negative pressures, with 50% loss at -2.5 MPa; and *Populus tremuloides* shows substantial cavitation at -2.0 MP, with 50% loss by -2.5 MPa (Hacke et al. 2001). Ring porous species show steeper vulnerability curves but maintain conductivity at much lower water potentials. As an example of ring porous species, *Q. gambelii* experiences a 50% loss around -0.5 MPa, but has mean cavitation pressures around -4.0 MPa, and similar curves were observed for other species of *Quercus* (Hacke et al. 2006).

Thus, since sectoriality was only found to affect photosynthesis at low soil water potential, it is important to consider how sectoriality changes when the axial resistance of leaves, roots, and/or the main stem axis is increased. Leaves and roots tend to be particularly sensitive to embolism. In most trees, the greatest xylem tension—and thus greatest embolism risk—is in the leaves; but for a given xylem tension, roots are generally most vulnerable to embolism (cited in Choat et al. 2007). Our model outputs suggest that embolism only in the leaves exposed to high light will increase sensitivity to soil drying, but will not substantially increase the effects of sectoriality. When a large portion of the crown is illuminated, the sectoriality effects are (if anything) diminished, while a very slight increase in sectoriality effects may occur when a smaller portion of the crown is affected (see Appendix, section 4.7 Fig. 4.8). These outputs reflect the fact that with the strongest resistance in the leaves, the ability to use parallel stem and root transport pathways will not dramatically increase water supply to the leaves. In contrast, increasing overall resistance by a factor of two or more throughout the crown and roots (Fig. 4.5) or in the whole plant (see Appendix, section 4.7 Fig. 4.9) dramatically increases sectoriality effects. These increases to whole plant resistance result in a greater water potential drop between soil and leaves and a stronger gradient between sectors.

The idea that cavitation could increase the benefits of integration is an interesting one for several reasons. First of all, it underlines the importance of

a variety of biotic and abiotic factors in determining the ecological role of sectoriality. Inter-species comparisons in sectoriality have generally focused on a single metric, such as anatomical traits (Ellmore et al. 2006), dye movement (Kozlowski and Winget 1963, Orians et al. 2004), isotope movement (Postlethwait and Rogers 1958, Orians et al. 2004) (reviewed by Watson and Casper 1984), or hydraulic resistance to tangential flow (Ellmore et al. 2006, Zanne et al. 2006*b*, Orians et al. 2005*b*). Our results further suggest that the degree of xylem crossover could depend on water status, cavitation susceptibility, and inherent axial resistances. In addition, leaf traits also affect the relationship between leaf water status and leaf water potential (Sack et al. 2003), and so are expected to influence the formation of hydraulic gradients between sectors. These considerations suggest probable differences between the "realized sectoriality" as observed by the movement of water and nutrients through the xylem and the "intrinsic sectoriality" as determined by xylem anatomy. This distinction between realized and intrinsic sectoriality is not generally emphasized in papers examining the ecological significance of inter-species differences in sectoriality (e.g. Zanne et al. 2006*b*) but has been alluded to certain papers, e.g. in the changes in sectoriality of source-sink dynamics with ontogeny (Preston 1998). Our output suggests that while sectoriality correlates with embolism resistance, embolism formation may also result in lower "realized sectoriality" in light limited conditions.

Secondly, there are fascinating questions to be addressed regarding the interactions between sectoriality and drought tolerance. A common hypothesis to explain the existence of high sectoriality species is that sectoriality helps prevent the spread of runaway embolism (Orians et al. 2004), and this idea is consistent with empirical studies showing a correlation between sectoriality and drought tolerance (Zanne et al. 2006*b*, Schenk et al. 2008). Variation in sectoriality among desert and chaparral shrubs shows a strong positive correlation between drought tolerance and sectoriality (Schenk et al. 2008). Zanne et al. (2006*b*) showed the same pattern for temperate trees, but none of the species

examined in that study were characterized as both drought tolerant and shade tolerant. We know of no studies that have specifically examined the relationship between sectoriality and drought tolerance in understory or shade-tolerant species. Nonetheless, indirect support for the hypothesis that integration is beneficial in understory species in dry conditions can be gleaned from the literature (Zanne et al. 2010). We took species described by Zanne et al. (2010) and separated them by shade and drought tolerance (classifications from Niinemets and Vallaraes 2006). As predicted, the shade-tolerant species with the highest drought tolerance indices showed among the lowest vessel areas and higher vessel numbers (Fig. 4.7). Interestingly, the opposite trend was seen for shade-intolerant species (data not shown). For a given vessel area fraction, higher vessel number implies higher vessel surface area, more opportunities for vessel-to-vessel contact, and potentially higher integration (Zanne et al. 2010). Based on our model output and these published data, we suggest that exploration of sectoriality traits in shade-tolerant species from different moisture environments would be a fruitful line of future research.

The above observations depend on the assumption that soil water potential is uniform. When water supply is patchy—due to heterogeneity of soil conditions, topography, throughfall, or hydraulic activity of either the focal plant or its neighbors (Stark 1994)—the simulated effects of sectoriality become more pronounced. In these conditions, hydraulic gradients in the soil drive intersector flow in the plant. When strong gradients in soil water correlate with light availability, such as would be expected if evapotranspiration under long-term light heterogeneity depletes soil water for roots in the high light sector, sectoriality becomes much more costly (Fig. 4.6). This situation may be most frequent when one side of the plant consistently receives high light, such as at a forest edge. Other sources of water heterogeneity may or may not correlate with light conditions. Hydraulic lift by neighboring trees can result in significant water potential gradients, which could result in more positive water potentials closer to a large neighbor, where shade may also be greater. Gradi-

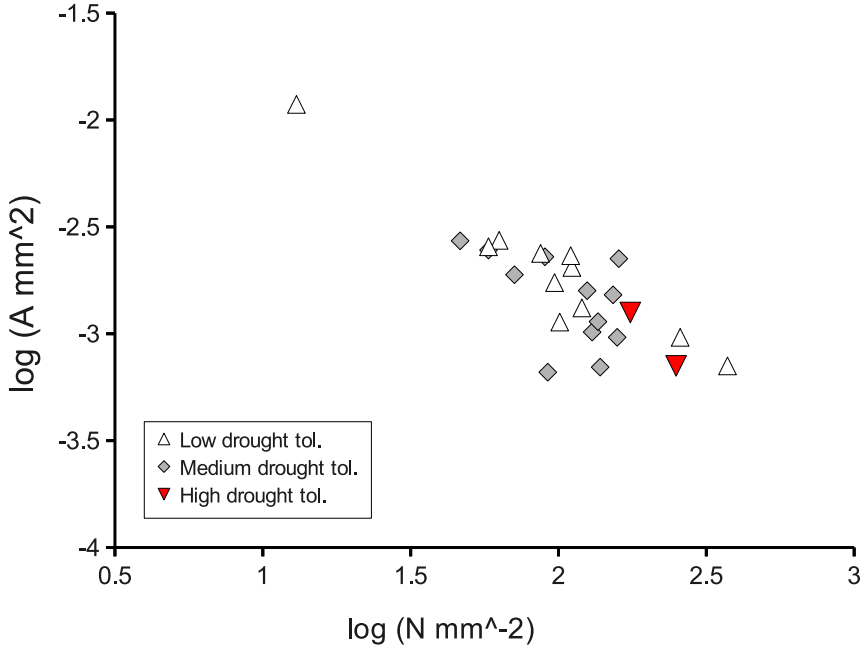

Figure 4.7: Log-log plot of area per vessel (A mm^2) versus vessel number (N vessels per mm^2) for shade-tolerant species of different drought tolerances. Data for vessel areas and densities are taken from the supplemental data for Zanne et al. (2010). Ecological classifications are derived from Niinemets and Vallaraes (2006), where high tolerance is defined as an index>3.5, and low tolerance is defined as an index<2.5. Species included are: low drought-tolerance species *Camellia japonica*, *Cleyera japonica*, *Cornus alternifolia*, *Cornus nuttalli*, *Diospyros virginiana*, *Fagus sylvatica*, *Ilex decidua*, *Nyssa ogeche*, *N. sylvatica*, *Prunus laurocerasus*, and *Viburnum dilatatum*; medium drought tolerance species *Aucuba japonica*, *Carpinus betulus*, *Cornus florida*, *Cornus racemosa*, *Corylus avellana*, *Eurya japonica*, *Ilex aquifolium*, *Ilex cassine*, *Ilex opaca*, *Illicium anisatum*, *Ligustrum lucidum*, and *Magnolia grandiflora*; and high drought tolerance species *Buxus sempervirens* and *Sorbus domestica*.

ents of 1.0 MPa have been documented between 0.5 and 5 m distance from the trunk of Acer saccharum, with more positive water potentials close to the trunk as a result of hydraulic lift (Dawson 1993 cited in Caldwell et al. 1998). On the other hand, decreases in soil water due to transpiration from neighboring trees would result in the opposite gradient, while rain throughfall is expected to be highest under canopy gaps where light is also higher (e.g. Breshears et al. 1997). When the soil water gradient is such that water content is higher for roots directly connected to high light branches, integration is expected to be costly, since it will tend to result in hydraulic redistribution toward the low light sector. Thus—depending on site characteristics— light heterogeneity may be positively or negatively related to water heterogeneity, or there may be no relationship. Data light and water heterogeneity at scales relevant to individual plants may provide important insights into the suitability of a particular site for high- versus low-sectoriality understory plants.

4.5.1 Implications for species-specific sectoriality

In addition to providing general predictions for the qualitative effect of sectoriality on photosynthesis, our model also sets up a quantitative framework for comparing sectoriality between different species. Our output suggests that photosynthesis is only sensitive to sectoriality when the overall tangential resistance is between 1 and 100 times the stem axial resistance, with the greatest variation between 1 and 10 times axial resistance. This result illuminates the relationship between previously documented variation in interspecies sectoriality and the probable ecological relevance of this sectoriality. For instance, we estimate from published data that 1 cm diameter stems of *Acer* and *Betula* have an r_t between 0.2 and 1 times the axial resistance (Sperry et al. 1993) and (data from Ellmore et al. 2006). In contrast, excised stem segments of the same diameter for Quercus rubra showed tangential resistance 30 times the stem axial resistance (Ellmore et al. 2006). This suggests that variation in sectoriality among relatively integrated diffuse-porous species (*Acer* and *Betula*) would be

more biologically meaningful than among highly sectored ringporous species (such as *Quercus*).

Our model output therefore supports the hypothesis that vascular integration helps integrated species such as *Betula alleghaniensis* and *Acer saccharum* thrive in the forest understory and grow rapidly in response to gaps, while sectored species such as *Quercus rubra* do not (Kobe et al. 1995)(cited in Nowacki and Abrams 1997). Furthermore, our model output suggests that *Betula* and *Acer saplings* will continue to display some integration as trunk diameter, and therefore tangential resistance, increases. Small differences in sectoriality may have a large effect on the ability of these species to exploit patches as they increase in size. A. saccharum often spends 20 or more years growing in shaded conditions (Canham 1985), and *B. alleghaniensis* is documented to commonly achieve stem diameters of 18 cm before gap openings permit rapid increases in growth (Webster and Jensen 2007). Therefore, these species may experience substantial selection for decreased sectoriality in the understory.

In contrast, our model suggests that 1 cm diameter *Q. rubra* already experience nearly complete sectoriality, which would only increase with diameter. A small change in the level of connection among parallel vessels would be unlikely to change this fact, reducing the likelihood sufficient phenotypic variation for natural selection on the sectoriality in *Q. rubra* and closely related species. Indeed, dye injection experiments have shown that in both bur oak (*Q. macrocarpa* Michx.) and white oak (*Q. alba* L.), the width of the streak produced by dye movement through the transpiration stream was nearly constant with height (Kozlowski and Winget 1963). On the other hand, the same study documented a gradually widening dye streak for northern pin oak (*Q. ellipsoidalis* Hill), suggesting some hydraulic integration for this species. The high sectoriality for oak might be explained by the particular vulnerability of ring porous species to freezing-induced embolism (Davis et al. 1999) or to the large space between individual xylem vessels that is distinct to oaks (Ellmore et al. 2006). The relative simplicity of our model provides a useful framework for

thinking about sectoriality that may be extended for a variety of applications. In particular, by characterizing sectoriality in terms of the parameters r_t and r_a, our model suggests a new approach for comparing sectoriality across species and across size classes. There is promising potential for adapting the model to predict species- specific allometric changes in sectoriality. For instance, r_a is expected to increase with tree height, and with circumferential path traveled (i.e. with diameter), but to decrease with sapwood thickness and with sapwood cross-sectional area. These general relationships may be combined with existing allometric models (e.g. West et al. 1999) to generate predictions for how sectoriality will change with growth. The model might also be used to scale the results of hydraulic experiments on stem segments (e.g. Zanne et al. 2006*b*, Ellmore et al. 2006) to predict whole plant level in order to predict responses to defoliation, vascular damage, or light heterogeneity.

Some limitations may exist in generalizing the model across size classes, however, particularly for very large trees. In large trees, sectoriality has been shown to depend not only on intervessel pitting (Orians et al. 2004, Ellmore et al. 2006) but also on "cross-grained" drift of vessels with height up the tree (Tyree and Zimmerman 2002, Kitin et al. 2004). While intervessel pitting constrains flow between sectors in the presence of a hydraulic gradient, as is represented by our model, cross-grained drift is expected to result in tangential spread of resources independent of such a gradient (Nadezhdina 2010). Empirical work will be required to determine the applicability of the model in trees displaying substantial drift, and it should be noted that the frequency of drift in younger trees has not been established. It may be that the most realistic approach to modeling sectoriality across size classes would combine our Ohm's law approach with xylem network topology models (Steppe et al. 2004) or modeling wood as an anisotropic solid (Schulte and Costa 2010), such as that presented by Steppe et al. (2004).

4.5.2 Conclusions

The model in this paper presents a novel framework for quantifying sectoriality, used here to predict the relationship between xylem sectoriality and photosynthesis for trees in the forest understory or along forest/gap edges. Simulation outputs suggest that under baseline hydraulic and environmental conditions, sectoriality should present only a modest constraint to photosynthesis, but that when xylem resistance is increased or water supply is non-uniform, this pattern can change dramatically. These predictions may be particularly valuable for understanding changes in species composition with climate change, especially with changes in precipitation. In moist regions, tree species may not previously have experienced selection based on vascular restrictions, but as drought becomes more frequent this could change. Previous research has emphasized the role of sectoriality in preventing the spread of embolisms (Schenk et al. 2008), but our results suggest that for understory trees experiencing drought, selection may be more complicated than previously recognized.

Our model provides a quantitative means of relating hydraulic properties of excised stems to expected whole plant functionality in vivo, and may help establish a relationship between the "realized sectoriality" as observed through transport patterns and the "intrinsic sectoriality" as characterized by xylem anatomy. Combined with allometric models for changes in hydraulics with stem diameter, our modeling framework can be used to generate specific biological predictions from hydraulic data. The development of allometric models for xylem sectoriality would be particularly useful in relating data from different types of studies, such as comparing experiments using 1 cm diameter stems (e.g. Zanne et al. 2006*b*, Orians et al. 2004) to patterns of resource or dye movement in larger trees (e.g. Greenidge 1955, Kozlowski and Winget 1963). Our model could also be easily extended to include stem water storage, through the inclusion of capacitors in our circuit model, to examine the role of transport of stored water between sectors in more dynamic responses to heterogeneity.

To our knowledge, the model presented here represents the first functional

model to describe the potential consequences of woody plant sectoriality. Our approach provides important insights into short-term hydraulic dynamics in response to patchy light. Future modeling efforts should examine the theoretical influence of vessel topology relative to inter-vessel pitting, in order to improve theoretical comparisons of sectoriality between species, and should include allometric scaling relationships to relate models for sectoriality of different sized saplings. In sum, our model presents a promising framework for making specific predictions about plant responses to heterogeneity. With adjustments to scale allometrically and to better adapt idiosyncracies of vessel anatomy, this framework can be adapted for tight partnership with empirical studies on species-specific responses to environmental heterogeneity.

4.6 Acknowledgments

We would like to thank the Tufts University Department of Biology for financial and logistical support, Dr. Lawren Sack for advice on the modeling of leaf hydraulics, Dr. Amy Zanne for assistance relating the literature on vessel anatomy to sectoriality, and Dr. George Ellmore and Dr. Nathan Phillips for their comments on previous drafts.

4.7 Appendix

When resistance is elevated only for the leaves on the high light portion of the plant, sectoriality effects decreased for large light patches, and slightly increased for small light patches, to (Fig. 4.8). When whole plant hydraulic resistance is increased to 8.0 MPa day g^{-1} m^{-2} (equivalent to 50% loss of conductance from baseline), the maximum potential benefit of integration is 7% when half the crown is in high light (Fig. 4.9A) and 14% when a small portion of the crown is in high light (Fig. 4.9B). At a hydraulic resistance of 40.0 MPa g^{-1} m^{-2} (90% loss of conductance), the maximum benefit is 22% at -0.9MPa when half the crown is in high light (Fig. 4.9C) and 40% at -1.1MPa for a small portion of the crown illuminated (Fig. 4.9D).

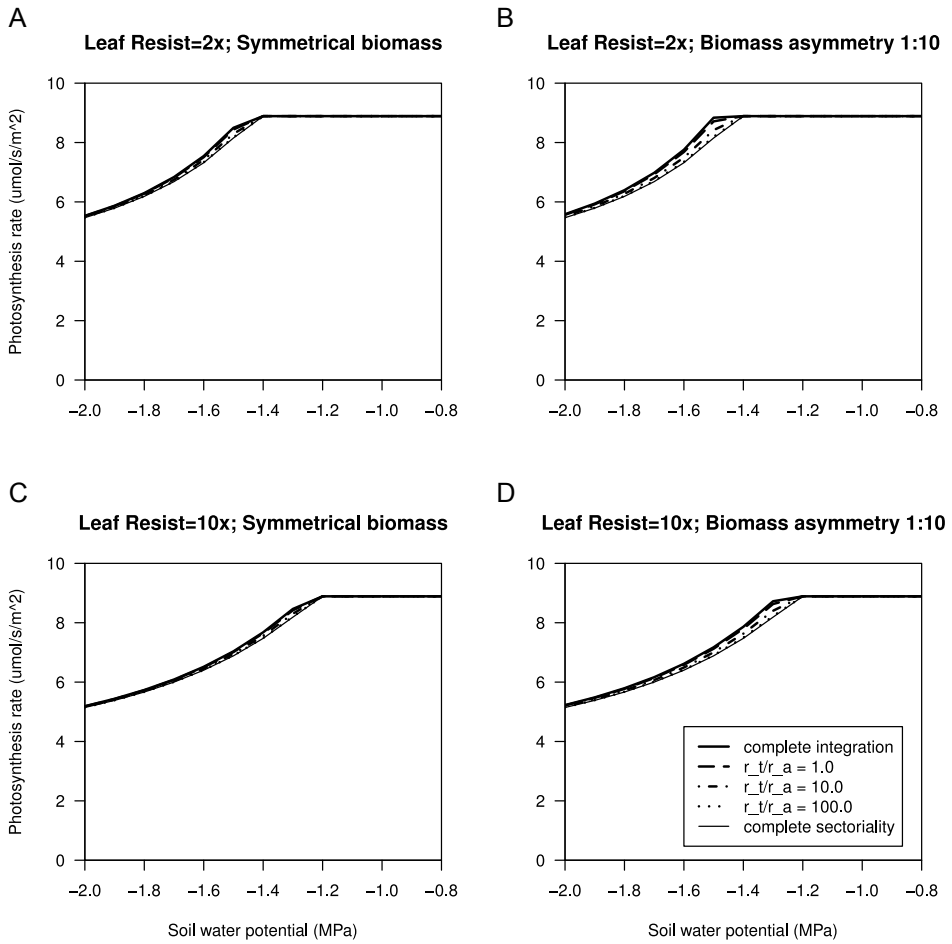

Figure 4.8: Simulated photosynthesis in leaves of high light branches as a function of soil water potential, with leaf resistance elevated for the portion of the crown in high light. Steady-state photosynthesis rates are shown on a per area basis for plants with different sectoriality levels and with leaf resistance elevated to either 2 times (A, B) or 10 times (C, D) the default leaf resistances of 1.0 MPa day g^{-1} m^{-2}. For each resistance, output is shown where half of the crown is in high light and the rest of crown is in low light (A, C) and where a small portion of the crown is in high light, while the rest of the crown (ten times the leaf biomass) is in low light (B, D). Simulated sectoriality is indicated by the ratio of tangential to axial resistance. Soil water potential is assumed to be uniform.

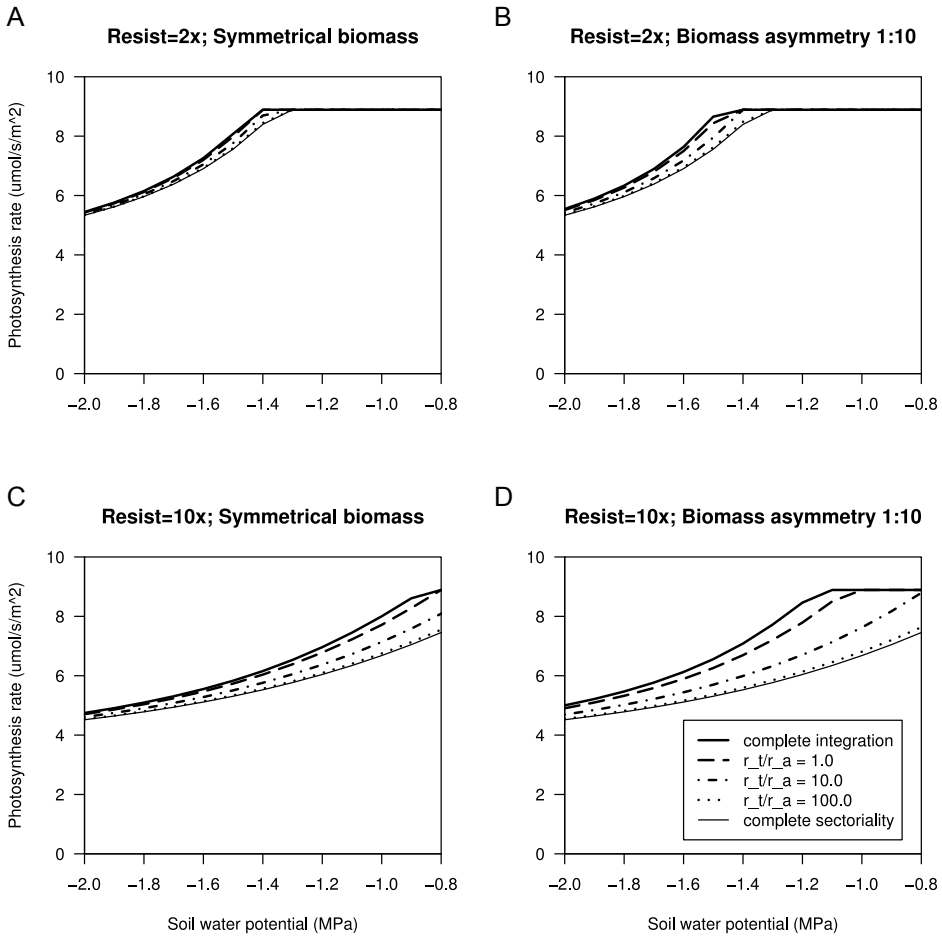

Figure 4.9: Simulated photosynthesis in leaves of high light sector as a function of uniform soil water potential for elevated axial resistance, for plants with different levels of sectoriality. Steady-state photosynthesis rates are shown on a per area basis for plants with a whole plant axial resistance of where either either 8.0 MPa day g^{-1} m^{-2} (A, B) or 20.0 MPa day g^{-1} m^{-2} (C, D). For each axial resistance, output is shown where half of the crown is in high light and the rest of crown is in low light (A, C) and where a small portion of the crown is in high light, while the rest of the crown (ten times the leaf biomass) is in low light (B, D). Simulated sectoriality is indicated by the ratio of tangential to axial resistance. Soil water potential is assumed to be uniform.

CHAPTER 5

Do stem inclination and branch asymmetry play different roles in canopy displacement for trees of different wood types?: An observational analysis of understory trees

Authors: Alexandra M. Thorn, Eliza McFarland, and Colin M. Orians

5.1 Abstract

Under patchy light, trees change crown morphology to increase leaf placement in high light patches. Plastic responses affecting leaf and overall crown placement include changes to stem inclination, driven by phototropism at the meristems, and correlative inhibition, whereby branches in high light experience increased growth and branches in low light experience decreased growth. Vascular constraints to long distance transport, are expected to limit correlative inhibition of branch growth, since resource competition with a tree is only possible between branches fed by the same vacular pathways stream. Based on the assumption that correlative inhibition drives branch asymmetry in understory trees, we hypothesized that—when controlling for light environment—branch asymmetry would be greater for diffuse porous species, which tend to have higher vascular integration, compared to ring porous species, which tend to have more sectored vasculature. We further predicted that ring porous species would make up for limitations in correlative inhibition by using displaying higher stem inclination than diffuse porous species for a given light environment. To test these hypothesis, we measured stem inclination, branch asymmetry, and overall canopy displacement of understory trees in seven taxa

(*Acer*, *Betula*, *Carya*, *Ostrya*, *Pinus*, *Sassafras*, and *Quercus*) growing near canopy gaps. We found that stem inclination was greater for ring porous species than for diffuse porous species or pine, but we found no difference in branch asymmetry between ring and diffuse porous species, although ring porous species showed significantly greater asymmetry than pine. Canopy displacement was primarily predicted by stem lean, with some additional variation explained by distance from the center of the gap. These results did not support our hypothesis: branch asymmetry did not differ between ring porous and diffuse porous species, even when light environment and spatial distribution were included in the model. The lack of an effect of wood type on branch asymmetry might indicate an important role for within-sector growth feedbacks between roots and leaves, or it might be explained by other inter-species differences not considered here. However, since our study was strictly observational, our results should be regarded as preliminary. Under controlled light conditions, a relationship between branch asymmetry and wood type may yet be uncovered.

5.2 Introduction

Forest trees display numerous strategies for increasing light interception and photosynthesis under patchy light conditions. One response that has received particular attention in forest research is crown displacement through phototropic processes. Crown displacement has been used to understand competition between individual trees (Muth and Bazzaz 2003, Getzin and Wiegand 2007, Seidel et al. 2011), phototropic responses of trees growing on slopes (Getzin and Wiegand 2007, Lang et al. 2010), and responses of understory trees to canopy gaps or openness gradients (Muth and Bazzaz 2003, Schamp et al. 2007). Common metrics of asymmetrical growth include the horizontal displacement of a tree's canopy from the base of its trunk (Lang et al. 2010, Seidel et al. 2011) and the inclination angle of the trunk, the "stem inclination" (King 2001, Schamp et al. 2007, Lang et al. 2010). It has also been occasionally noted (e.g. Lang et al. 2010) that canopy displacement is affected by correlative inhibition of

branch growth—whereby high light branches grow disproportionately faster, and low light branches disproportionately slowly when conditions are patchy than when conditions are uniform (Stoll and Schmid 1998, Takenaka 2000, Sprugel 2002). Unfortunately, correlative inhibition studies in trees have generally focused on single species, usually gymnosperms (e.g. Stoll and Schmid 1998, Takenaka 2000). Furthermore, we know of no studies examining the relationship between correlative inhibition and stem inclination in determining overall canopy displacement. Here, to evaluate the prediction (explained below) that correlative inhibition—and therefore greater branch asymmetry—will be more important in species with high vascular integration, we examine the relationship among stem inclination, branch asymmetry, and crown displacement in seven understory species with differing wood properties.

Trunk inclination and branch correlative inhibition are constrained by different traits. Phototropic stem inclination is constrained by the mechanical properties of stems and roots, as shown by the increased tendency for leaning trees near canopy gaps to fall in the direction of gaps (Young and Hubbell 1991). Correlative inhibition, in contrast, is expected to be affected by patterns of sectoriality, the degree to which resources can be moved between parallel xylem and phloem pathways (Watson and Casper 1984). More specifically, correlative inhibition should be maximal in vascularly intergrated species because of increased competition among branches for resources. In sectored species, branches are expected to compete less. Since water and nutrient allocation in the crown is constrained by xylem sectoriality (Orians et al. 2004), especially under dry conditions (Thorn and Orians 2011*a*), we expect vasculature to have large effects on patterns of branch growth. Moreover, long distance signalling depends on the existence of pathways for communication between different parts of the plant and might further promote relative growth differences between light and shade in more integrated species.

Xylem sectoriality in particular has been shown to vary dramatically among temperate hardwood species (Orians et al. 2004, 2005*b*, Ellmore et al. 2006, Zanne

et al. 2006*b*), and a principal component analysis of 18 such species showed an inverse relationship between sectoriality and shade tolerance (Zanne et al. 2006*b*). One possible reason for the inverse relationship between sectoriality and shade tolerance might be that correlative inhibition allows understory trees with low sectoriality to better exploit light patches. If true, this hypothesis would predict a stronger correlative inhibition response by integrated trees growing in the understory, while sectored trees would rely on stem inclination to respond to light gradients. Thus, canopy displacement in sectored species would be expected to depend primarily on stem inclination, while canopy displacement in integrated species might also depend on branch asymmetry (Fig. 5.1).

To evaluate our hypothesis that stem inclination would be more important for light foraging in sectored species, and that branch asymmetry would be more important in integrated species, we measured crown morphological traits of seven species in the forest understory of the Middlesex Fells Reservation (Melrose, MA). The seven species included three ring porous species (generally high sectoriality), three diffuse porous species (generally integrated), and one gymnosperm. We assessed the relative importance of wood type, light environment, and proximity to canopy gaps created by major trail junctions in predicting stem inclination, branch asymmetry, and overall canopy displacement.

5.3 Materials and Methods

5.3.1 Study design

We measured stem inclination, branch asymmetry, and overall crown displacement in understory trees of three ring porous species, three diffuse porous species, and one gymnosperm. To evaluate our hypothesis that stem inclination and branch asymmetry as responses to light gradients would differ depending on sectoriality, and therefore would play different roles in overall crown placement for trees of different wood types, we also measured the spatial dis-

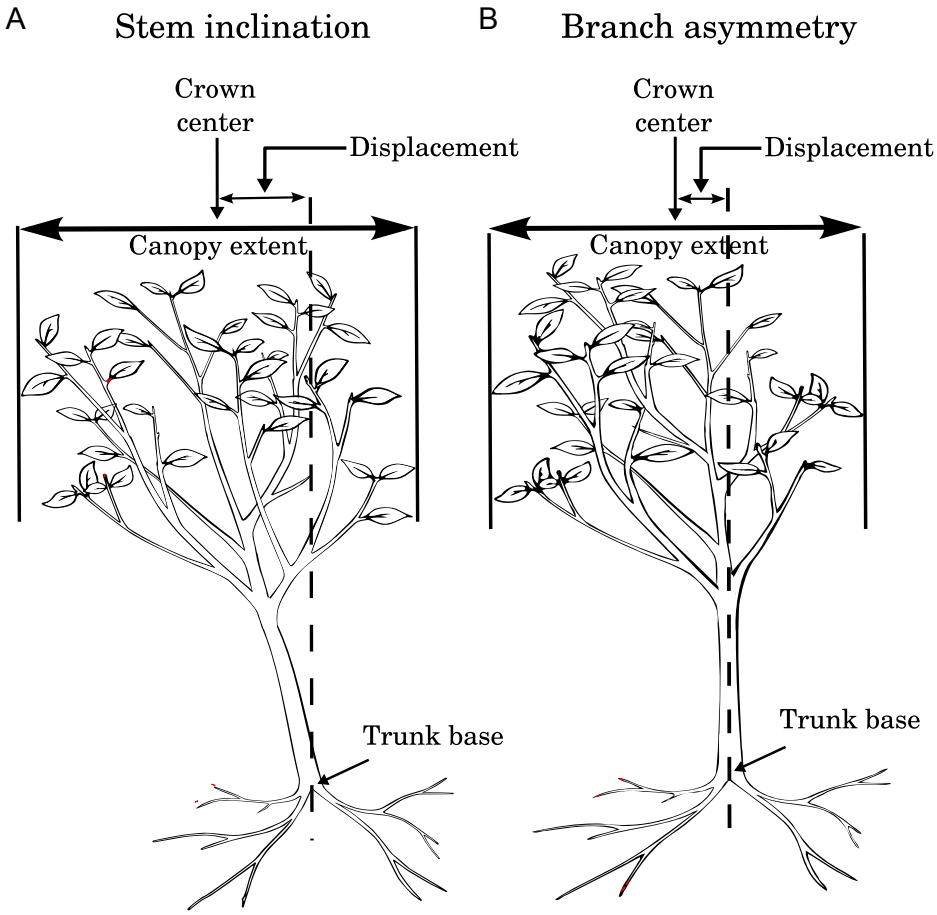

Figure 5.1: Diagram of two mechanisms for crown displacement relative to the location of the trunk base: stem inclination (A) and patterns of branching from the primary axis (B). We hypothesized that stem inclination would be more important for sectored species, and branch asymmetry would be more important for integrated species.

tribution of trees relative to a canopy gap and the spatial variation in hours of sunlight across each study site. We generated linear models for the combined effects of wood type, light levels, light gradients, and location relative to gaps, and the interaction of wood type with each of the other variables in predicting stem inclination and branch asymmetry, and then generated AICc scores for all submodels in order to assess the relative likelihood of all submodels. We then generated a linear model for the combined effects of branch asymmetry, stem inclination, wood type, and the light and spatial variables on overall crown displacement and generated AICc scores to assess the relative likelihood of all submodels. We performed further statistical analysis on the most parsimonious model for each of the three morphology traits.

5.3.2 Study site

We conducted our research at the Middlesex Fells Reservation (N 42° 27′ W 71° 07′) in Melrose, MA. The Reservation is a 1042 ha wooded park, surrounded by developed urban land, primarily residential. The park dates back to 1935, and the wooded areas have been maintained since, along with trails groomed for foot traffic (Middlesex Fells Reservation). We selected four sites (20m x 20m), each centered on a three-way trail junction (Site 1 = +42° 25′ 58.91", -71° 6′ 24.71"; Site 2 = +42° 25′ 53.34", -71° 7′ 12.16"; Site 3 = +42° 26′ 6.04", -71° 6′ 27.08"; Site 4 = +42° 26′ 10.19", -71° 6′ 31.54"), with a substantial light gradient between the center of the trail junction and the surrounding woods. The trails forming these junctions ranged in width from about 5 to 10 meters, and trail surfaces included bare soil, gravel, and turf.

5.3.3 Species

Across the four sites, dominant broad-leaf taxa were hickory (*Carya* sp.), oak (*Quercus* sp.), sassafras (*Sassafras albidum*), black birch (*Betula lenta*), hop hornbeam (*Ostrya virginiana*), and sugar maple (*Acer saccharum*). White pine (*Pinus strobus*) was also a dominant species, and although its sectoriality relative to

Table 5.1: Dominant tree taxa, and number of understory trees measured in each taxon.

Taxa	Wood type	Sectoriality	Sources for sectoriality data	# measured
Carya sp.	Ring porous	Sectored	Orians, unpublished data	13
Quercus sp.	Ring porous	Sectored	Ellmore et al. 2006, Orians et al. 2005	22
Sassafras albidum	Ring porous	Sectored	Zanne et al. 2006	11
Acer saccharum	Diffuse porous	Moderate	Ellmore et al. 2006, Orians et al. 2004, Orians et al. 2005	11
Betula lenta	Diffuse porous	Integrated	Orians et al. 2004	20
Ostrya virginiana	Diffuse porous	Integrated	Orians, unpublished data	19
Pinus strobus	Pine	Unknown	N/A	7

the broadleaf species is not well characterized, it was included in our analysis as a species known to have upright growth habit, with a radial arrangement of branches, suggesting a strong dependence on branch placement for crown asymmetry, similar to our hypothesized growth pattern for integrated species. Of the broadleaf species, the ring porous taxa (*Carya*, *Quercus*, and *Sassafras*) were considered sectored, and the diffuse porous taxa (*Acer*, *Betula*, and *Ostrya*) were considered integrated. Within the diffuse porous taxa present, *Acer* has been shown to be more sectored than *Betula* and *Ostrya* — both members of the Betulaceae (Table 5.1).

5.3.4 Plots

At each site, we used GPS to determine the latitude and longitude of the center of the trail junction. We then created a 20 x 20 meter plot by measuring 10 meters from this point in each of the four cardinal directions. String was used to mark the boundaries of each plot, which was then subdivided into a 5 x 5 grid of cells 4 meters on a side. We recorded the diameter at breast height (DBH) for all trees in each plot with DBH greater than 1.0 cm. These individuals were classified to the genus or species level, and the location of each trunk was mapped within each grid cell. Our analysis focused on small subcanopy trees (1cm-3cm DBH) that were members of the 7 dominant taxa (Table 5.1).

5.3.5 Canopy extent analysis

For all trees in the study, we measured the canopy extent using the methods described by Young and Hubbell (1991), Muth and Bazzaz (2002). Canopy extents in each of the cardinal and subcardinal directions were measured from the trunk center. For tall trees, a densitometer was used to determine where the canopy ended. These eight extent measurements defined the vertices of an octagonal polygon approximating the canopy shape. When no canopy extended in a particular direction, the trunk center was used as the vertex for that direction.

The north-south and east-west locations of each trunk relative to the plot center were determined from our plot maps (see previous section), and from these the canopy vertices were also calculated. These coordinates were used to generate canopy maps in and QuantumGIS 1.4.0 (http://www.qgis.org) and ArcGIS 9.1. For each tree, a point file was created with the coordinates of canopy vertices arranged in clockwise order and converted into a polygon using the QuantumGIS POINTS2ONE extension. These polygons were exported as shapefiles for analysis in ArcGIS. In ArcGIS, the center of mass for the crown of each sub-canopy tree was calculated using the using the Feature to Point function. The distance and compass direction (ϕ_{disp}) from each trunk to that tree's canopy center of mass were also determined.

To control for tree size, we calculated the relative crown displacement (R_{disp}) as the distance from the trunk center to the crown centroid (m), divided by the height of the tree. Displacement was determined relative to tree height, not relative to canopy width, in order to more easily relate the displacement to the degree of stem inclination. The compass direction of crown displacement (ϕ_{disp}) was determined from the coordinates of the canopy center relative to the base of the trunk for each tree.

5.3.6 Canopy morphology measurements and analyses

The direction and magnitude of stem inclination were determined from photographs of the breast-height trunk of each small subcanopy tree, together with a plumb-bob attached to a 1-meter length of rope. Each trunk was photographed from two perpendicular directions (north or south and east or west). ImageJ was used to analyze the angle between the trunk and the plumb-bob in the two compass directions, and from these angles the direction (in degrees from magnetic north) and angle (in degrees from vertical) of lean were determined.

To characterize the directional distribution of branch biomass growing from the main axis, the compass direction ($\phi_{branchi}$) of each branch i was measured at the base for all branches between ground level and 2.2 m of height. In some trees, the main axis bent to a fully horizontal angle within the 2.2 m range. For these individuals, branch angles were only measured for branches below the point where the trunk became horizontal. As a proxy for biomass of individual branches, the basal diameter of each branch was also measured.

5.3.7 Canopy morphology measurements and calculations

The angle of stem inclination relative to vertical (θ_{lean}) and compass direction of stem inclination (ϕ_{lean}) were determined from north-south and east-west photographs of the trunk at breast-height next to the plumb-bob. Distances between the trunk and the plumb-bob at the top and bottom of the string were determined using ImageJ (http://rsb.info.nih.gov/ij/). From these distances and the length of the plumb-bob, θ_{lean} and ϕ_{lean} were determined using trigonometry (see Fig. 5.2).

For each tree, basal areas for each branch i ($A_{branchi}$) were calculated from branch basal diameters as: $\pi \times$ (basal diameter / 2)^2. We used circular statistics to calculate the area-scaled mean branch direction ($\overline{\phi}_{branch}$):

$$\sin(\overline{\phi}_{branch}) = \frac{\Sigma(A_{branchi} \times \sin(\phi_{branchi}))}{\Sigma(A_{branchi})} \tag{5.3.1}$$

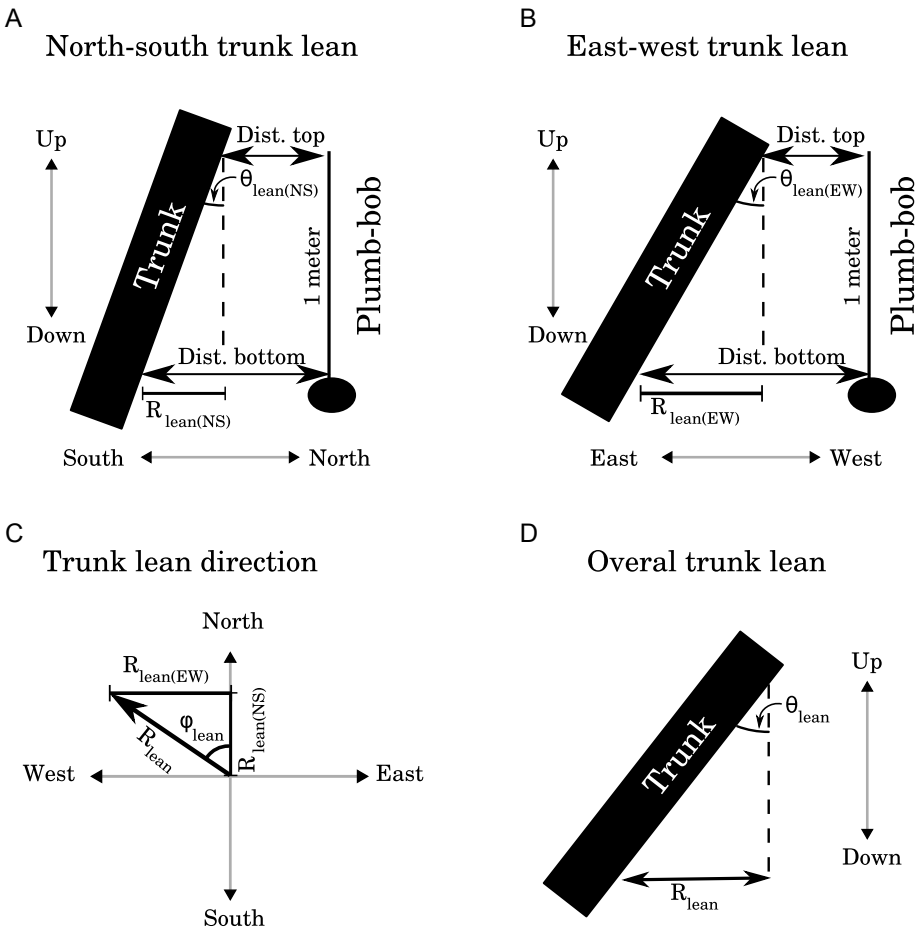

Figure 5.2: Schematic for determining stem inclination parameters. The top two diagrams diagrams show how the north-south (A) and east-west (B) components of the stem inclination angle ($\theta_{lean(NS)}$ north-south and $\theta_{lean(EW)}$ east-west) and relative lean distance ($R_{lean(NS)}$ north-south and $R_{lean(EW)}$ east-west) are determined from the top (Dist. top) and bottom (Dist. bottom) distances between the trunk and the plumb bob. The bottom two diagrams show how these values are used to determine the overall distance (R_{lean}) and direction (ϕ_{lean}) of stem inclination (C) and the overall angle of stem inclination (θ_{lean}) (D).

$$\cos(\overline{\phi}_{branch}) = \frac{\Sigma(A_{branchi} \times \cos(\phi_{branchi}))}{\Sigma(A_{branchi})} \tag{5.3.2}$$

$$\overline{\phi}_{branch} = \arctan(\frac{\sin(\overline{\phi}_{branch})}{\cos(\overline{\phi}_{branch})}) \tag{5.3.3}$$

with $\overline{\phi}_{branch}$ corrected to match quadrants (northward versus southward and eastward versus westward) indicated by the signs of $\sin(\overline{\phi}_{branch})$ and $\cos(\overline{\phi}_{branch})$.

Then the basal area was determined for all branches within $\pm 90^{\circ}$ of the area-scaled mean direction. The branch asymmetry was then calculated as the total basal areas for all branches within $\pm 90^{\circ}$ of the area scaled mean branch angle, divided by the total area for all branches.

5.3.8 Light levels maps

To assess general variation in light environment within and among plots, a Solar Pathfinder (Solar Pathfinder, 3953 Marsh Creek Road Linden, TN) was used to determine the path of the sun on the longest day of the year (June 21st), and what portion of this path is obstructed by tree canopies or other obstacles. From these measurements, the number of hours of full or partial direct sunlight were determined at the center of each of the 25 2m x 2m grid cells in each plot.

5.3.9 Light levels analysis

To determine spatial patterns of light variation through each plot, the solar pathfinder measurements for hours of full or partial sunlight determined were added as an attribute to a GIS point file defining the locations where solar pathfinder readings were taken. These points were used to interpolate light levels for each plot using splines. Splines interpolation was used because it captures the possibility that points measured may not represent the full range of values in the plot. In particular, the light levels between two high light points are assumed to be slightly higher than the measured points if the adjacent points have lower light levels. This property is important because we were

primarily interested in gradients, not absolute light levels. In a few cases, interpolation gave very slightly negative estimates for the number of hours of light per day. This artefact is not expected to affect the overall patterns observed, but to avoid having negative values for absolute light levels, we use relative scores (interpolated light level / (maximum interpolated light level - minimum interpolated light level)) in our analysis. The resulting 2 m resolution raster coverage estimated spatial variation in light levels across the plot.

The magnitude (G_{light}) and compass direction (ϕ_{light}) of the light gradients were determined from the resulting raster surface for light levels. The ArcGIS Slope tool was used to measure the gradient magnitude (% change in number of hours or number of canopies per meter), and the ArcGIS Aspect tool was used to determine the compass direction of this gradient. Point sampling was then used to determine the magnitude and slope of the estimated light gradient at trunk location for each of the small subcanopy trees.

To test the relationship between light levels and spatial relationship to the trails, we calculated AICc scores for all possible submodels of a linear model combining the effects of plot (PLOT), distance from plot center (D_{center}), and the distance from trail edge (D_{trail}) on the interpolated light level at the locations each tree included in the study. We then used AICc scores to assess the relative likelihood of the submodels. ANOVA and Tukey HSD post hoc analysis were used to assess the degree to which light levels varied across understory taxa.

5.3.10 Analysis of effects on crown morphology

We used likelihood analysis to assess the effects of wood type, light environment, and spatial data on each of the three crown morphology traits measured: 1) the horizontal component of stem inclination (R_{lean}), 2) the asymmetry of branch area distribution (R_{branch}), and 3) the relative canopy displacement (R_{disp}). Each of these response variables has an associated direction: ϕ_{lean} for R_{lean}, ϕ_{branch} for R_{branch}, and ϕ_{disp} for R_{disp}. The effects of predictive values with a direction, such as the distance to the center of the gap and the light gradient

can be understood in terms of their direction relative to the direction of the response variable of interest ($\phi_{focal} = \phi_{lean}$, ϕ_{branch}, or ϕ_{disp}, depending on which response variable is being modeled), as well as in terms of their overall magnitude. To incorporate these two possible effects into the model, we included the cosine of the angle of these variables and the response variable of interest as possible predictive variables in addition to the total magnitude.

In all, the full model for R_{lean} and R_{branch} included wood type (W = diffuse porous, ring porous, or pine) and 7 variables relating to location and light environment. Light variables included the relative light level (H_{light}), the light gradient scaled for canopy width (G_{light}), and the component of the scaled light gradient that was parallel to the response variable of the model ($G_{lightparallel} = G_{light} \times \cos(\phi_{light} - \phi_{focal})$. Spatial variables included the distance to the center of the canopy gap (D_{center}), the distance to the edge of the trail (D_{trail}), and the cosine of the angle between the direction of the response variable and the directions to center of the gap ($P_{center} = \cos(\phi_{center} - \phi_{focal})$) and to the edge of the trail ($P_{trail} = \cos(\phi_{trail} - \phi_{focal})$). Since we expected crown morphology to respond to environmental variables differently depending on wood type, we also included the interaction of W with each of these 7 variables in the full models for stem inclination and branch lean.

In the model for canopy displacement (R_{disp}), we included wood type and the 7 location and light variables, as well as R_{lean} and R_{branch} as possible predictive variables. We also included terms for interaction between wood type and R_{lean} and R_{branch}, but did not include interactions between wood type and the other 7 variables.

For each likelihood analysis, we report the results for all models with delta AICc < 2 of the model with the lowest AICc score, as well as the results for the overall model, the individual components of the most parsimonious model, and the null model (Intercept only). Then, for the most parsimonious model in each case, we present graphical relationships between the predictive variables and response variables. Where the selected model included a categorical pre-

dictive variable, we used ANOVA and Tukey HSD post hoc analysis to investigate which categories differed for the response variable. Where the selected model included continous variables, and scatterplots with best fit lines are used to show the overall effect. In cases where two continuous variables predicted the response variable, we first present the relationship between the predictive and response variables with the highest r-squared value, and then show the residuals of that relationship plotted against the second predictive variable.

All statistical analyses were performed using R (http://www.r-project.org/).

5.4 Results

5.4.1 Species distributions

The four plots varied considerably in species represented. Site 1 included canopy species *A. saccharum*, *O. virginiana*, and *Quercus* sp. and understory species *A. saccharum*, *Carya* sp. and *O. virginiana*; Site 2 included canopy species *Carya* sp., *O. virginiana*, *P. strobus*, and *Quercus* sp., and understory species *Carya* sp., *O. virginiana*, and *Quercus* sp.; Site 3 included canopy species *B. lenta*, *P. strobus*, *Quercus* sp., and *Tsuga canadensis*, and understory species *B. lenta*, *Quercus* sp., *P. strobus*, and *S. albidum*; and Site 4 included canopy species *B. lenta*, *P. strobus*, and *Quercus* sp., and understory species *B. lenta*, *P. strobus*, and *Quercus* sp. The locations of understory trees are shown in Fig. 5.3.

5.4.2 Tree heights and frequency of horizantal stems

The 103 trees included in the study ranged in height from 0.6 m to 5.0 m, with a median height of 2.4 m. The median heights were similar across species: 2.7 m for *A. saccharum*, 2.6 for *B. lenta*, 2.6 m for *O. virginiana* sp., 1.4 m for *Carya* sp., 2.3 for *Quercus* sp., 2.2 for *S. albidum*, and 2.8 m *P. strobus*.

Since we were only able to measure branch distributions to a height of 2.2 meters, it is important to note that 61 of the 103 species were taller than 2.2 meters in height, including 7 out of 11 *A. saccharum*, 16 out of 20 *B. lenta*, 14 out

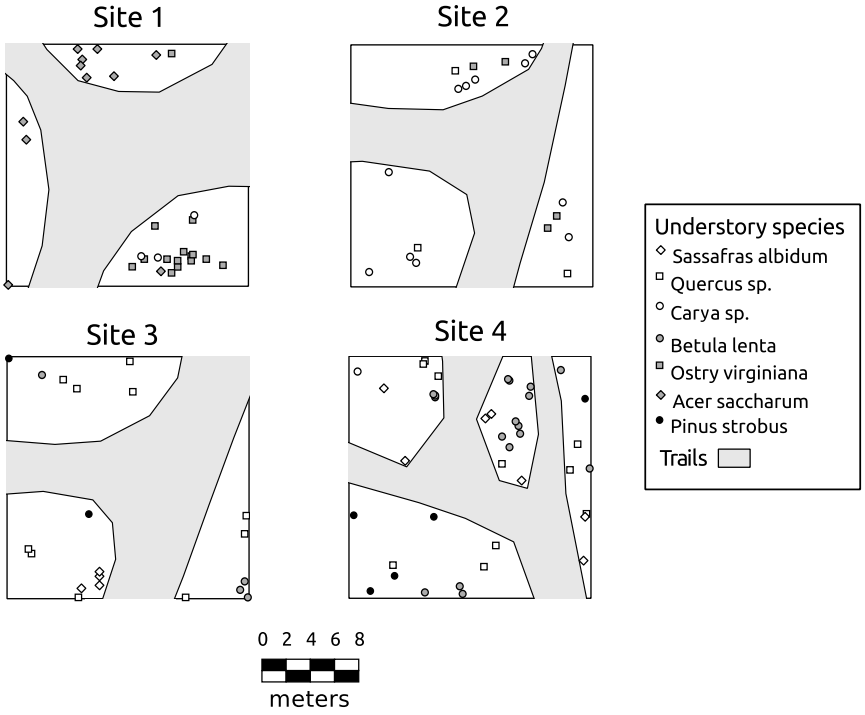

Figure 5.3: Maps of the locations of trails and understory tree species (1cm < DBH < 3cm) on the four plots we examined.

of 19 *O. virginiana*, 3 out of 13 *Carya* sp., 11 out of 22 *Quercus* sp., 5 out of 11 *S. albidum*, and 5 out of 7 *P. strobus*.

In addition, in 20 of the trees measured, the main axis bowed to horizontal, and we did not measure branch distribution above this point. Trees with horizontal main axes included 2 *A. saccharum*, 2 *B. lenta*, 2 *O. virginiana*, 7 *Carya* sp., 6 *Quercus* sp., and 1 *S. albidum*. Only 8 of the trees with horizonal main axes were above 2.2 meters in height.

5.4.3 Spatial light variation

There was substantial variation in light levels within and between plots. The best spatial model for light variation included the distance from the center of the plot and variation among plots (Table 5.2). Together, these two variables explained ∼50% of the variation in light levels. Plots 1 and 2 had significantly less direct light reaching the understory than Plots 3 and 4 had (Fig. 5.4A). As expected, across plots, the highest light levels were closest to the center of the

Table 5.2: AICc and regression analysis for models of light levels within and between plots. Results are shown for all submodels with ΔAICc < 2 for a full model for light levels including plot (PLOT), distance from the center of plot (D_{center}), and distance from the edge of the trail (D_{trail}), as well as the individual predictive values for the most parsimonious model and the intercept only.

Light levels model	AICc	ΔAICc	r^2
*$H_{light} = \text{PLOT} + D_{center}$	272.0	0.0	0.52
$H_{light} = \text{PLOT} + D_{center} + D_{trail}$ = FULL MODEL	274.0	2.0	0.51
$H_{light} = \text{PLOT}$	286.7	14.7	0.44
$H_{light} = D_{center}$	333.5	61.5	0.11
INTERCEPT ONLY	344.5	72.5	0.0

* Model selected for graphical analysis based on parsimony and AICc scores.

plot (Fig. 5.4B).

Light levels were similar across wood types, with the exception that the diffuse porous species *A. saccharum* (which was only present at Site 1) was found at significantly lower light levels that the other species (Fig. 5.5).

5.4.4 Crown displacement, asymmetry, and morphology

Based on likelihood analysis using AICc scores (Table 5.3), the most parsimonious model for stem inclination with ΔAICc < 2 only included the categorical variable for wood type. The effect of wood type was driven by a higher stem inclination for the sectored ring porous taxa than for pine or the integrated diffuse porous taxa (Fig. 5.6).

The most parsimonious model for branch asymmetry included only wood type (Table 5.3). This effect was due to a significantly higher branch asymmetry for ring porous species than for pine (Fig. 5.7). There was no difference in branch asymmetry between ring and diffuse porous species.

According to likelihood analysis, the overall relative canopy displacement depended primarily on stem inclination, with secondary effects due to distance from the center of the plot (Table 5.4). Relative displacement was positively correlated with stem inclination (Fig. 5.8A), and when the variation due to the horizontal component of stem inclination was removed, the overall displacement was inversely related to distance from the center of the plot (Fig. 5.8B).

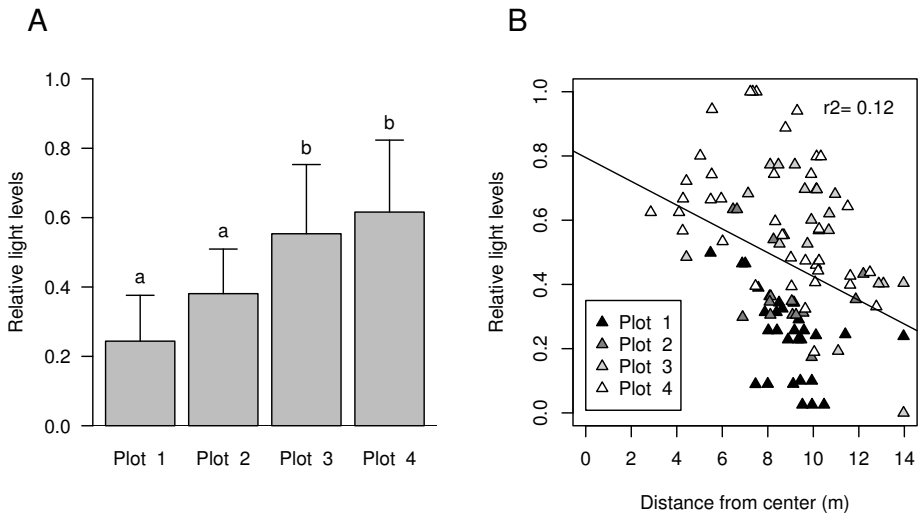

Figure 5.4: Variation in light levels among and within plots. Light levels for each tree trunk location were estimated from a splines interpolated surface generated from hours of full and partial direct sunlight per day measured at 25 locations per plot. According to these estimates, plots differed significantly in light levels, with significantly lower light levels for Plots 1 and 2 than for Plots 3 and 4 (A). There was also a significant negative correlation between light levels and distance from the plot centers, indicating a significant light gradient associated with distance from the trail junction on which each plot was centered (B). In the graph of light levels versus plots, the error bars indicate standard deviations, and letters above error bars indicate significant differences at the alpha=0.05 level, as calculated by Tukey HSD post hoc analysis.

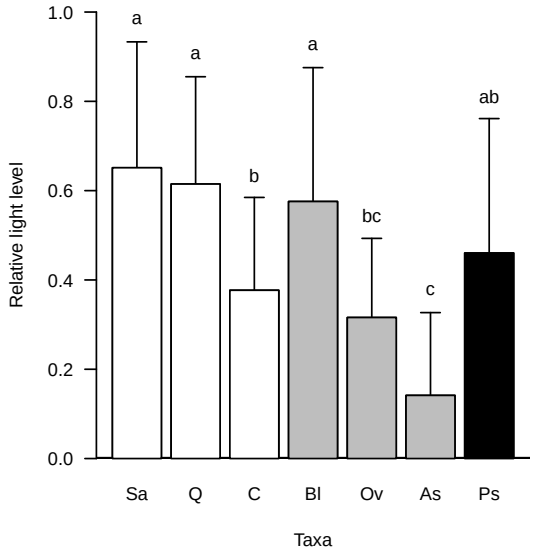

Figure 5.5: Relative light levels associated with understory tree species, pooled across sites. Bar colors correspond to wood type: ring porous species in white, diffuse porous species in gray, and pine in black. Taxon abbreviations are as follows: Sa = *Sassafras albidum*, Q = *Quercus* sp., C = *Carya* sp., Bl = *Betula lenta*, Ov = *Ostrya virginiana*, As = *Acer saccharum*, Ps = *Pinus strobus*. Error bars indicate standard deviation, and letters above error bars indicate significant differences at the alpha=0.05 level, as calculated by Tukey HSD post hoc analysis.

Table 5.3: AICc and regression analysis of models for stem inclination ($R_{lean} = sin\theta_{lean}$) and the branch asymmetry (R_{branch}). The full models included the wood type (W), the light level (H_{light}), the relative light gradient (G_{light}), parallel component of relative light gradient ($G_{lightparallel}$, distance to center of plot (D_{center}), the parallel component of the direction to center of plot (P_{center}), distance to trail edge (D_{trail}), and the parallel component of the direction to the trail edge ($P_{trail} = cos(trail - \phi_{focal})$). The full models also included the interaction of W with each other term.

Trunk lean model	AICc	ΔAICc	r^2
*$R_{lean} = W$	-120.0	0.0	0.19
$R_{lean} = H_{light} + W + H_{light} \times W$	-119.9	0.1	0.24
$R_{lean} = P_{center} + W$	-118.5	1.5	0.20
$R_{lean} = G_{light} + W$	-118.4	1.6	0.19
$R_{lean} = P_{trail} + W$	-118.2	1.8	0.19
$R_{lean} = H_{light} + P_{center} + W + H_{light} \times W$	-118.1	1.9	0.24
INTERCEPT ONLY	-102.6	17.4	0.00
FULL MODEL	-82.5	37.5	0.32

Crown asymmetry model	AICc	ΔAICc	r^2
*$R_{branch} = W$	-66.3	0.0	0.09
$R_{branch} = G_{lightparallel} + W$	-66.3	0.0	0.12
$R_{branch} = P_{center} + W$	-65.8	0.5	0.11
$R_{branch} = H_{light} + W$	-64.9	1.4	0.10
$R_{branch} = H_{light} + G_{lightparallel} + W$	-64.6	1.7	0.13
$R_{branch} = P_{center} + G_{lightparallel} + W$	-64.5	1.8	0.12
$R_{branch} = G_{lightparallel} + W + G_{lightparallel} \times W$	-64.5	1.9	0.15
$R_{branch} = H_{light} + P_{center} + W$	-64.4	2.0	0.12
INTERCEPT ONLY	-63.8	2.5	0.00
FULL MODEL	-8.3	58.0	0.26

* Models selected for graphical analysis based on parsimony and AICc scores.

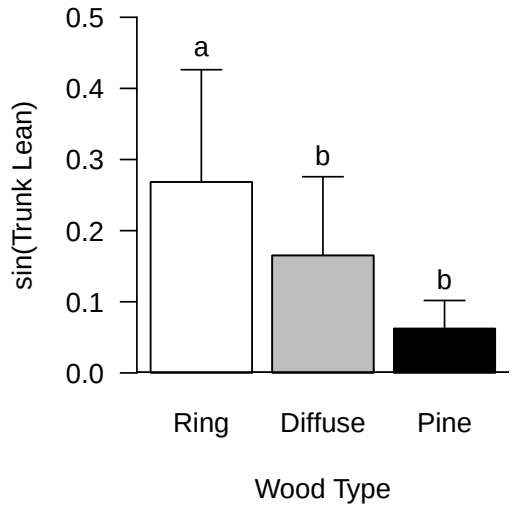

Figure 5.6: Horizontal component of stem inclination as a function of wood type ("Ring"=ring porous, "Diffuse"=diffuse porous, "Pine"=*P. strobus*). Error bars indicate standard deviation, and letters above error bars indicate significant differences at the alpha=0.05 level, as calculated by Tukey HSD post hoc analysis.

Figure 5.7: Branch asymmetry as a function of wood type ("Ring"=ring porous, "Diffuse"=diffuse porous, "Pine"=*P. strobus*). Branch area symmetry is calculated as the fraction of total branch basal area that is within 90 degrees in either direction of the area mean branch direction. Error bars indicate standard deviation, and letters above error bars indicate significant differences at the alpha=0.05 level, as calculated by Tukey HSD post hoc analysis.

Table 5.4: AICc and regression analysis of model the model for overall crown displacement (R_{disp}). The full model includes the wood type (W), the light level (H_{light}), the relative light gradient (G_{light}), parallel component of relative light gradient ($G_{lightparallel}$, distance to center of plot (D_{center}), the parallel component of the direction to center of plot (P_{center}), distance to trail edge (D_{trail}), and the parallel component of the direction to the trail edge ($P_{trail} = cos(\phi_{trail} - \phi_{focal})$), the horizontal component of stem inclination (R_{lean}) and its component parallel to the displacement ($R_{leanparallel}$), and branch asymmetry (R_{branch}) and its component parallel to the displacement ($R_{branchparallel}$). The full model also includes the interaction of W with R_{lean}, $R_{leanparallel}$, R_{branch} and $R_{branchparallel}$.

Relative canopy displacement model	AICc	Δ AICc	r^2
*$R_{disp} = D_{center} + R_{lean}$	-82.9	0.0	0.27
$R_{disp} = D_{center} + P_{trail} + R_{lean}$	-82.7	0.3	0.28
$R_{disp} = D_{center} + P_{center} + R_{lean}$	-81.9	1.0	0.28
$R_{disp} = D_{center} + P_{center} + P_{trail} + R_{lean}$	-81.6	1.3	0.29
$R_{disp} = D_{center} + D_{trail} + R_{lean}$	-81.3	1.7	0.27
$R_{disp} = D_{center} + G_{lightparallel} + R_{lean}$	-81.2	1.7	0.27
$R_{disp} = D_{center} + G_{light} + R_{lean}$	-81.1	1.9	0.27
$R_{disp} = R_{lean}$	-79.5	3.4	0.23
$R_{disp} = D_{center}$	-58.3	24.6	0.05
$R_{disp} =$ INTERCEPT ONLY	-55.1	27.8	0.00
FULL MODEL	-43.7	39.2	0.41

* Model selected for graphical analysis based on parsimony and AICc scores.

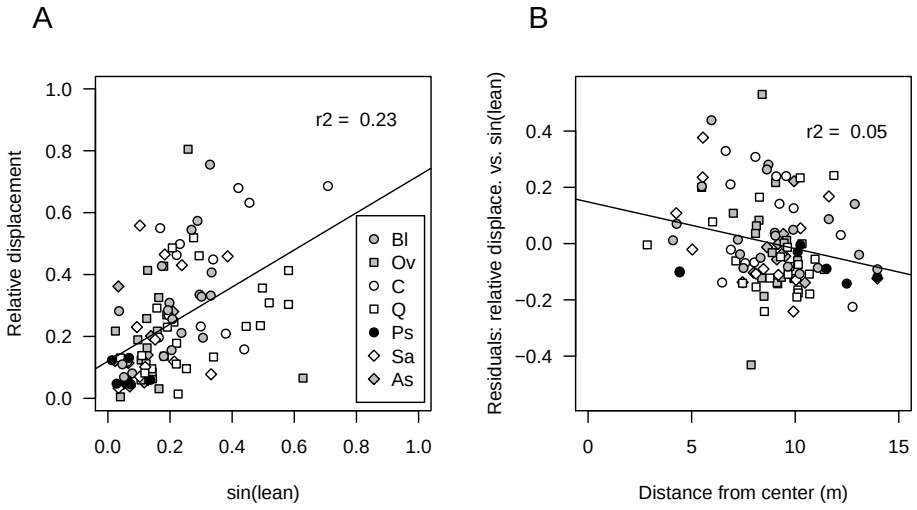

Figure 5.8: Relative displacement as a function of the sine of stem inclination (A), and resulting residuals as a function of distance from the center of the plot (B). Taxon abbreviations in the legend are as follows: Sa = *Sassafras albidum*, Q = *Quercus* sp., C = *Carya* sp., Bl = *Betula lenta*, Ov = *Ostrya virginiana*, As = *Acer saccharum*, Ps = *Pinus strobus*. Ring porous species are shown in white, diffuse porous species in gray, and pine in black. Regression shows that lean angle is the primary driver of crown displacement (A), but the plot of residuals versus distance from the center shows that the lean-based model tended to underestimate the crown displacement closer to the gap and to overestimate displacement further from the gap (B).

5.5 Discussion

Based on the expectation that sectoriality should constrain correlative inhibition of branch growth, we had hypothesized that understory ring porous species (generally highly sectored) would display higher stem inclination toward areas of high light, while diffuse porous species (generally more integrated) would tend to produce asymmetrical branch growth due to correlative inhibition in a partially shaded environment. While we did find that stem inclination was higher for ring porous than for diffuse porous species, there was no difference in branch asymmetry between ring and diffuse porous species. Instead, the only detectable pattern in branch asymmetry was that ring porous species showed higher asymmetry than pine. Also contrary to our expectations, branch asymmetry had no effect on overall crown displacement. Thus, our data did not support our predictions.

Stem inclination was the major predictor of overall canopy displacement, with additional variation correlated with distance from the gap. Most likely, this additional variation is due to bowing of the trunk above the point we measured (e.g. as measured by King 2001, Schamp et al. 2007), although differences in branch growth not detected by our branch asymmetry metric may also have contributed. Interestingly, total stem inclination was a better predictor of canopy asymmetry than was the component of stem inclination in the same direction as canopy asymmetry, suggesting morphological factors not included in our models affected the direction and magnitude of canopy displacement. For instance, bowing of the main axis occurring above the height we measured may not always be in the same compass direction as the inclination of the lower portion of the trunk. Furthermore, 61 out of the 103 trees were taller than the 2.2 meter height to which we were able to measure branch distribution, and effects of branch distribution above that height could not be included in the model. In addition, 20 trees (only 8 of which were above 2.2 meters in height) had main axes that became horizontal, and branches above this point were also not included. Curvature in measured branches could also result in a contribu-

tion to crown placement not correlated with their direction of emergence from the trunk. Finally, asymmetries in secondary branching off of the branches we measured could have contributed to overall crown displacement. More detailed assessment of crown morphology would be valuable in understanding the relative importance of these possible factors. Such analysis would be facilitated by the use of laser scanning technology, similar to that employed by Seidel et al. (2011).

Leaving aside the possible role of the morphological traits outlined above, there are many possible interpretations for the unexpected results of our study. The difference in stem inclination between ring- and diffuse-porous species does not appear to be explained by our hypothesis that stem inclination in ring-porous species would make up for their limitations in correlative inhibition, since no differences in branch assymmetry were detected. Other explanations for this difference are required. One possibility is that the difference in stem inclination between ring porous and diffuse porous species reflects interspecies differences in wood tensile strength and other biomechanical traits constraining the ability to maintain growth with an inclined stem (Anten and Schieving 2010, Collet et al. 2011).

Alternatively, the inter-species difference might have partly been due to environmental variation not captured by our model. In particular, it is possible that there are non-linear interactions of light level with light gradient in producing stem inclination. Notably, it has been shown that bowed stems can be a response to absolute light level, as well as a phototropic response to light levels (King 2001). In a study including 11 deciduous angiosperms, 1 evergreen angiosperm, and 2 evergreen gymnosperms, King (2001) observed a strong tendency for deciduous species to bow their trunks to near horizontal growth habit in shaded conditions, a pattern presumed to maximize light capture by placing all of the leaves in the same plane. Furthermore, a study on the two decidous species *Fagus sylvatica* and *Acer pseudoplatanus* demonstrated a clear tendency in both species to straighten their stems toward upright growth when canopy

openings appeared (Collet et al. 2011). These two pieces of evidence suggest that, in some situations, stem inclination can be very high at low light gradients and that it could decrease in the presence of a canopy opening that increases both the light availability and the light gradient.

The lack of differences in branch asymmetry between ring porous and diffuse porous species is also extremely thought provoking. One interpretation is that correlative inhibition is not very important in determining branch asymmetry for understory trees in these taxa. Branch asymmetry can exist without correlative inhibition, simply by virtue of the higher carbon fixation by and therefore carbohydrate availability to branches in high light. Sectoriality may even enhance the asymmetry by confining carbon transport to orthostichous roots, which in turn increase the supply of water and nutrients to the branches in the high light. If sectoriality plays a role in increasing branch asymmetry, then the lack of a difference between ring porous and diffuse porous species may actually be taken as evidence for correlative inhibition in diffuse porous species. This question would best be addressed by measuring the exact light environment of each branch, and comparing growth and survival between shaded branches on trees experiencing patchy light and branches of trees experiencing similar levels of uniform shade, as has been measured in *Litsea acuminata* (Bl.) (Takenaka 2000).

It is not surprising that ring porous and diffuse porous species showed higher branch asymmetry than *P. strobus*. The low number of branches on the angiosperm species compared to pines alone is likely to produce some asymmetry, just by chance. Furthermore, gymnosperms are are known for radial growth habit (King 2001), and a correlative inhibition study on the related species *P. silvestris* failed to find evidence of correlative inhibition (Stoll and Schmid 1998).

Overall, our results do not support our hypothesis that sectoriality would constrain correlative inhibition in the branches and so affect light foraging strategies of understory plants. These results should be taken as preliminary however, given that our study was strictly observational and did not examine growth

over time. Future research is needed. Our results are strongly suggestive of other morphological factors contributing to overall crown placement in understory plants, suggesting a number of hypotheses worth future study. In particular, a more complete model for crown displacement should include curvature of stems and branches, as well as asymmetry of secondary branches as well as the branches emerging directly from the main axis.

CHAPTER 6

Modeling sectored resource allocation in patchy soils: A new perspective on root precision with implications for nutrient foraging by plants

Authors: Alexandra M. Thorn and Colin M. Orians

6.1 Abstract

1. Despite years of research, causes of interspecific differences in root proliferation in nutrient-rich patches are not fully understood. We hypothesize that the restriction of long distance resource transport to specific vascular pathways, called sectoriality, would influence the strength of root proliferation in a nitrogen patch.

2. To theoretically assess the prediction that higher sectoriality will tend to decrease plant growth when nitrogen is patchy and root proliferation into nitrogen patches, we constructed a bottom-up simulation model for plant growth. This model combines a modular model for growth of different tissue types with an Ohm's law model for sectored xylem and phloem transport. The full model predicts patterns of passive resource allocation and growth in a plant divided into two sectors exposed to different nutrient environments.

3. We simulated root and whole plant growth responses for plants with high and low sectoriality for xylem and for phloem, combined in a two way factorial setup. Growth was simulated under two soil heterogeneity scenarios. We first examined growth patterns when one sector was exposed to ten times the nitrogen concentration of the other sector over a 60 day simulated growth

period, a common treatment used in empirical studies. Then we simulated root and whole plant growth when, after an initial 30 days of simulated unchanging nitrogen heterogeneity, the nutrient environment was changed such that the previously high nitrogen sector receives low nitrogen and vice versa. Following this change in nutrient environment, we simulated growth for an additional 30 days.

4. We found interactive effects of xylem and phloem sectoriality in predicting both overall plant growth and the percent of root biomass produced in the high nitrogen sector (root "precision"). Plants integrated for both xylem and phloem showed the highest growth in all scenarios, followed by plants integrated for xylem but sectored for phloem. Root "precision" was highest when plants were integrated for both xylem and phloem and was lowest when plants were integrated for xylem but not for phloem. In the temporally variable nutrient scenario, growth patterns following the change in nitrogen distribution were affected by overall biomass allocation due to the initial nutrient treatment. The overall effect was a reduction in phloem sectoriality effects on total biomass accumulation, while xylem sectoriality still constrained growth.

5. Model outputs underline the importance of sectoriality as a predictor or covariate in studies of local root proliferation. We present possible strategies for inclusion of sectoriality in root foraging experiments.

6.2 Introduction

Extensive research has explored plant responses to nutrient heterogeneity and the ecological importance of such responses, such as the "precision" of root proliferation into nutrient patches (Robinson 1994, Hodge 2004, 2009). These studies have revealed substantial interspecific variation in the ability of plants to proliferate roots in nutrient patches, and have shown that these differences can affect ecological factors such as plant-plant competition (Hodge et al. 1999) and plant-microbe interactions (Hodge 2006). No general rule has been established, however, to explain why some species respond differently from others

(Hodge 2009).

Hypotheses proposed to explain interspecific differences in root proliferation have included: 1) a "precision-scale" tradeoff between investment in local proliferation (high precision) in subordinate species versus large extensive root systems (high scale) in dominant species (Campbell et al. 1991); 2) that intrinsic growth rates produce greater local root proliferation (Fransen et al. 1999); and 3) that species differences depend on phylogenetic or architectural constraints (Kembel and Cahill 2005). Until the last decade, the precision-scale tradeoff hypothesis has been the best-known of these hyptheses, but a recent meta-analysis by Kembel et al. (2008) found no correlation between root precision and scale, spurring renewed interest in the causes of root precision (e.g. Hodge 2009, McNickle and Cahill 2009, Shemesh et al. 2010). We suggest that differences among species in sectoriality (=vascular constraints in resource transport) could contribute to differences in root proliferation (Watson and Casper 1984, Murphy and Watson 1996, Bledsoe and Orians 2006, Gloser et al. 2008), unrelated to differences in adaptive foraging traits.

Sectoriality refers to the degree to which transport of carbon, nutrients, water, and signal molecules within a plant is constrained by vascular pathways (Orians and Jones 2001). In particular, leaves and roots located directly above one another along the main axis of a plant—i.e. structures in the same orthostichy—tend to be fed by the same vascular conduits (Watson and Casper 1984). In a highly sectored plant, resource transport primarily occurs among orthostichous leaves and roots (those in the same orthostichy), while less sectored species are able to make use of indirect pathways as well. In the short term, high sectoriality of phloem pathways is expected to limit carbon supply to specific roots by restricting the portion of the crown that supplies carbon to roots in a nutrient patch (Murphy and Watson 1996, Bledsoe and Orians 2006). For instance, Bledsoe and Orians (2006) demonstrated that, in a sectored plant, carbon from one sector tends not to accumulate in roots of the opposite sector even when the "opposite" roots are the only source of nutrients and therefore

display higher growth rates and sink strength. Moreover, high sectoriality in xylem transport limits nutrient delivery to specific parts of the crown and generates aboveground heterogeneity in plant traits (Orians et al. 2002, Zanne et al. 2006*a*, Gloser et al. 2008). Xylem and phloem sectoriality are commonly hypothesized to be correlated (e.g. Bledsoe and Orians 2006), an assumption grounded in the observation that xylem and phloem traces both develop from procambium tissue, and tend to co-occur in the same vascular bundles (Scarpella and Meijer 2004). This assumption does not necessarily always apply, however. While the role of lateral pit fields connecting parallel xylem vessels is well documented (e.g. Kitin et al. 2004), and it is not clear whether lateral sieve areas in the phloem sieve tubes (Esau 1969) would play a similar role in tangential transport. Furthmore, in woody plants, xylem and phloem are spatially separated, with xylem vessels distributed through the growth rings (Tyree and Zimmerman 2002), while phloem is restricted to the inner bark (Taiz and Zeiger 2002).

The importance of inter-species variation in sectoriality has generally been overlooked in the root foraging literature (but see van Vuuren et al. 2003, Gloser et al. 2008), despite an increased interest in other architectural constraints in shaping root proliferation patterns (Kembel and Cahill 2005). When vascular constraints are acknowledged at all, they are often treated as absolute, with authors assuming complete vascular independence between orthostichies (e.g. McNickle and Cahill 2009). This perspective—closely related to the unit-pipe model for tree architecture—is often more realistic than the assumption of complete vascular integration, but in reality most vascular plants are neither perfectly sectored nor perfectly integrated. Furthermore, sectoriality is not a static trait. Phloem sectoriality has been shown to change with developmental stage in *Perilla frutescens* (Preston 1998), and xylem sectoriality has been shown to change with size in *Cryptantha flava* (Salguero-Gómez and Casper 2011). Moreover, recent work by our lab suggests a high potential for inter-sector crossover of xylem sap in *Ocimum basilicum*, a species that otherwise shows strong sectoriality (Thorn and Orians 2011*b*,*c*).

Sectoriality—like "root precision"—varies dramatically among species (Watson and Casper 1984, Hutchings and Bradbury 1986, Orians et al. 2004, 2005*b*, Zanne et al. 2006*b*), and is also correlated with the ecological distribution of species (Zanne et al. 2006*b*, Schenk et al. 2008). Given the variability in sectoriality and its clear influence on plant responses to patchy resources, we argue that a sectoriality-based framework is needed to interpret inter-species variation in root precision. Without specific predictions for how passive resource allocation will affect growth patterns when accounting for sectoriality, it is difficult to determine what component of root precision is actually explained by adaptive strategies for root placement. One model by Yang and Midmore (2005) took an important step in this direction, accounting for branch and root vascular growth in response to heterogeneous resource concentration within the plant, but this model did not include the sectoriality of long distance transport. Some sectoriality models have been developed in the clonal plant literature, comparing the theoretical performance of "splitter" (or "fragmented") species, in which ramets respond individually to their local environments, versus to "integrated" species, in which resources acquired by one ramet may be used uniformly throughout the genet (Oborny et al. 2001, Golubski et al. 2008). A few of these models have explicitly simulated transport between parent and daughter ramets (Caraco and Kelly 1991), but we know of no previous efforts to incorporate sectoriality into a model for growth precision or foraging in single-stemmed non-clonal plants.

Here, we assess the theoretical effect of sectoriality on plant growth in a patchy nitrogen environment, using a bottom-up model for allocation and growth. We examine simulated patterns of root allocation and overall plant growth in a patchy nitrogen environment, for plants with high and low sectoriality for both xylem and phloem, with xylem and phloem sectoriality combined in a two-way factorial setup. We simulated growth in two patchy nitrogen scenarios: 1) a static nutrient scenario in which the roots of one sector receive high nitrogen over a 60 day simulation period (similar to many empirical studies of

root precision), while the roots of the other sector receive low nitrogen over the same time frame; and 2) a temporally variable nutrient scenario similar to one of the treatments from Jansen et al. (2006). In our temporally variable nutrient scenario, the static nutrient scenario is applied for the first 30 days of the simulation, after which the nitrogen distribution was reversed, with the initially low nitrogen sector now receiving high nitrogen, and vice versa. We expected that sectoriality—especially phloem sectoriality—would constrain both whole plant growth and the relative biomass allocation to roots in the nitrogen patch, and that the effect of sectoriality on growth would increase in the temporally variable scenario, because of the need in that scenario to rapidly respond to changes in resource distribution between sectors.

6.3 Materials and Methods

6.3.1 Model overview

Our model uses a bottom-up approach, subdividing the plant into two sectors, and each sector into physiological modules as shown in Fig. 6.1A. The general structure of each module is similar, with some variation by tissue type. In particular, leaf and fine root modules are handled differently than branch, stem, and coarse root modules. Carbon fixation rates are determined by leaf biomass and local light intensity (here light is assumed constant), and nitrogen acquisition rates are determined by fine root biomass and local nitrogen availability. In each module, nitrogen and carbon are allocated toward new tissue production at rates determined by internal concentrations of available nitrogen and carbon. Carbon is also expended for nitrogen uptake, and for maintenance metabolism at a rate determined by local dry weight. Plant modules are indexed by sector (j) and by module (i) within each sector (Fig. 6.1B). In each time step, xylem transport of nitrogen from roots to the various modules is assumed to occur instantaneously (sensu Dewar 1993), while phloem transport is handled in a discrete fashion, with phloem carbon pools explicitly modeled for each mod-

Table 6.1: State variables defined for each plant component (leaves, branches, stem segments 1-5, coarse roots, and fine roots) of each sector (sectors 1 & 2), and other variables used in model

Symbol	Description	Units
$W_{dwi,j}$	Dry weight of module i in sector j (eqn 6.3.1)	g
$W_{Ci,j}$	Mass of labile carbon outside phloem of module i in sector j (eqn 6.3.2, 6.3.3)	g
$W_{Ni,j}$	Mass of labile nitrogen outside xylem of module i in sector j(eqn 6.3.4, 6.3.5)	g
$W_{pCi,j}$	Mass of labile carbon inside phloem of module i in sector j(eqn 6.3.6, 6.3.7)	g
$W_{w1,j}$ (leaves only)	Mass of water in leaves (module 1) of sector j (eqn 6.3.8)	g

ule.

In our model, patterns of long distance transport for both phloem and xylem are determined using an Ohm's law circuit (Fig. 6.2), similar to the xylem sectoriality model from Thorn and Orians (2011*a*). Carbon transport between modules occurs via phloem, and nitrogen and water transport through the plant occur via xylem. The phloem and xylem axial resistance for each module scale with module dry weight, while tangential resistance is assumed fixed. State variable definitions are summarized in Table 6.1, and parameters and non-state variables are summarized in the Appendix (section 6.6, Tables 6.3, 6.4).

Dynamic equations

Four state variables exist for each module i in sector j: the module dry weight ($W_{dwi,j}$), the mass of available carbon ($W_{Ci,j}$), the mass of available nitrogen ($W_{Ni,j}$), and the mass of carbon in the phloem of that module ($W_{pCi,j}$). In the case of leaves (module 1 of each sector j), there is a fifth state variable $W_{w1,j}$, which tracks the leaf water content.

Biomass ($W_{dwi,j}$) for each module i in sector j is assumed to increase at a relative growth rate determined by Michaelis-Menten kinetics, with locally available carbon and nitrogen acting as substrates (as in Thornley and Johnson 2000). Thus, relative growth rate is proportional to both the mass concentration of carbon ($[C]_{i,j} = W_{Ci,j}/W_{dwi,j}$) and the mass concentration of nitrogen

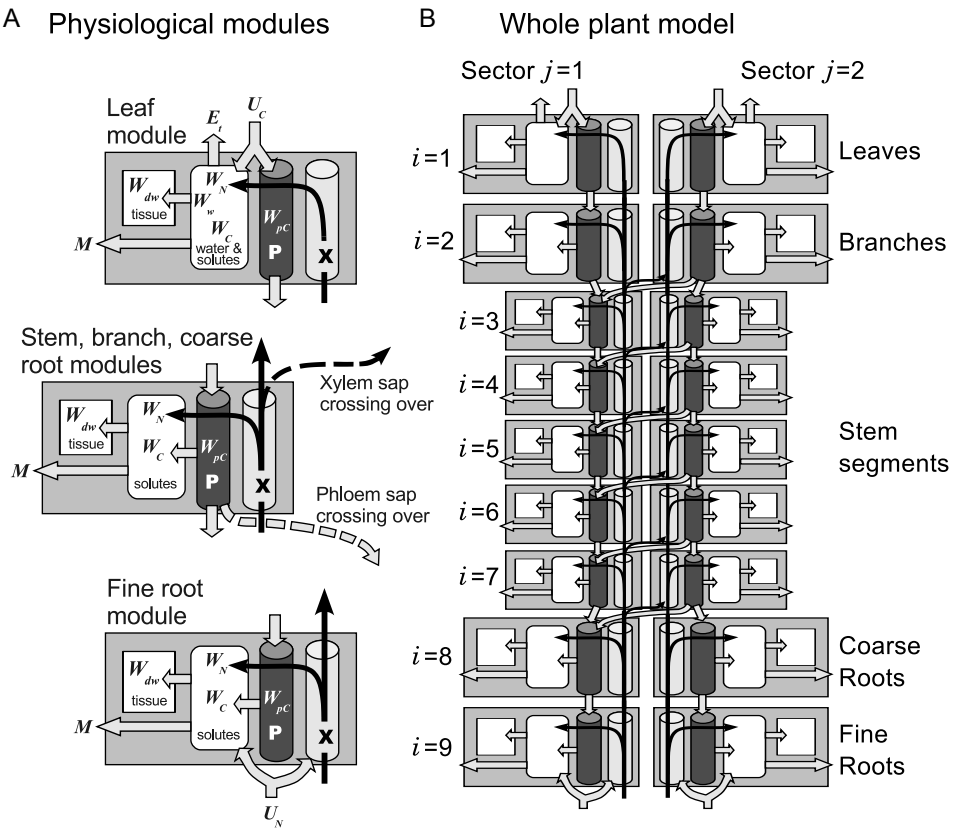

Figure 6.1: Diagrams of example physiological modules for leaves, stems, and roots (A) and the whole plant transport model (B). In each module (A), carbon in the phloem (P) and nitrogen arriving via the xylem (X) are allocated to local availables pools of carbon (W_C) and nitrogen (W_N). These pools are depleted by conversion into functional dry weight (W_{dw}), and available carbon pools are further depleted by metabolic processes (M). Carbon fixation occurs in the leaves at rate U_C, and nitrogen uptake occurs in the fine roots at rate U_N. Of these acquired resources, a fixed proportion remains locally, while the rest is allocated to the phloem or xylem, respectively. In the case of the leaf module, the water content (W_w) is also modeled, depleted by evapotranspiration (E_t), and replenished by xylem flow into the leaves. Long black arrows designate xylem transport, reflecting the model assumption that water and nitrogen from the roots are translocated instantaneously to the various parts of the plant, in proportions determined by simulated xylem flows. The shorter gray arrows reflect processes that only occur once per time step, including the movement of carbon between the phloem carbon pools (W_{pC}) for each module. In the whole plant model (B), the modules are indexed from $i = 1$ to $i = 9$ within a sector, and the sectors are indexed $j = 1$ and $j = 2$. In the diagram depicted, xylem flow is from sector 1 to sector 2 at each node, and phloem flow is from sector 2 to sector 1 at each node, but all directional combinations are possible in the model, depending on simulated flow processes.

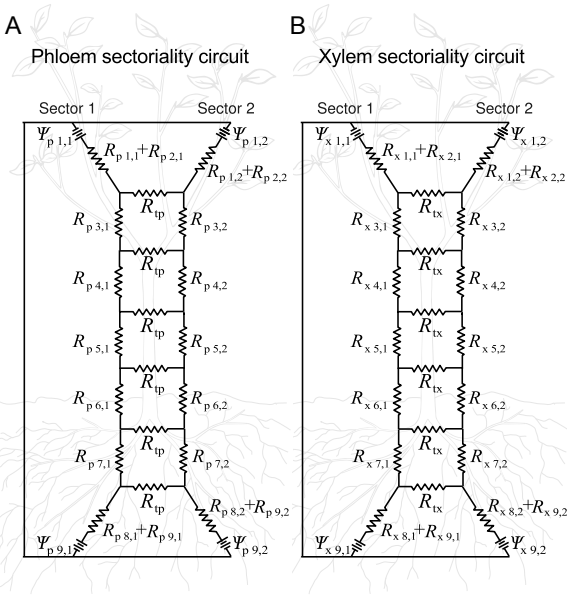

Figure 6.2: Ohm's law circuits for sectoriality of phloem (A) and xylem (B) transport within and between sectors. Xylem water potentials ($\Psi_{pi,j}$, $\Psi_{xi,j}$) and resistances ($R_{xi,j}$,$R_{xi,j}$) in each diagram represent the values associated with module i in sector j. For graphical simplicity, the resistances for modules 1 and 2 (leaves and branches) within each sector, and the resistances for modules 8 and 9 (coarse and fine roots) are combined into a single resistor. The tangential resistance parameter is given by R_{tp} for phloem and R_{tx} for xylem.

($[N]_{i,j} = W_{Ni,j}/W_{dwi,j}$) within that module:

$$\frac{1}{W_{dwi,j}} \times \frac{dW_{dwi,j}}{dt} = k_G \times [C]_{i,j} \times [N]_{i,j} \tag{6.3.1}$$

where k_G is a constant.

The mass of available carbon ($W_{Ci,j}$) in most modules i of sector j changes according to:

$$\frac{dW_{Ci,j}}{dt} = I_{Ci,j} - M_{i,j} - G_{Ci,j} \tag{6.3.2}$$

where $I_{Ci,j}$ is the rate of phloem unloading in that module, $M_{i,j}$ is rate of carbon loss to metabolism by that module, and $G_{Ci,j}$ is the rate of carbon incorporation into new functional biomass. In the case of the leaf module (module 1) for each sector j, the available carbon ($W_{C1,j}$) changes according to the equation:

$$\frac{dW_{C1,j}}{dt} = U_{C1,j} - \alpha_{1,j} - G_{C1,j} \tag{6.3.3}$$

where $U_{C1,j}$ is the net rate of carbon fixation by those leaves, $\alpha_{1,j}$ is the rate of carbon unloading from those leaves, and $G_{C1,j}$, again, is the rate of carbon incorporation into functional biomass.

The mass of available nitrogen ($W_{Ni,j}$) in most modules i of sector j changes according to the equation:

$$\frac{dW_{Ni,j}}{dt} = I_{Ni,j} - G_{Ni,j} \tag{6.3.4}$$

where $I_{Ni,j}$ is the rate of nitrogen delivery from the xylem into that module and $G_{Ni,j}$ is the rate of nitrogen incorporation into new functional biomass. In the case of the fine root module (module 9) of each sector j, the available nitrogen ($W_{N9,j}$) changes with:

$$\frac{dW_{N9,j}}{dt} = U_{N9,j} - \lambda_{9,j} - G_{N9,j} \tag{6.3.5}$$

where $U_{N9,j}$ is the rate of nitrogen uptake by that module, $\lambda_{9,j}$ is the rate of nitrogen export from that fine root module, and $G_{N9,j}$ is the rate of nitrogen incorporation into new functional fine root biomass.

The mass of carbon in the phloem ($W_{pCi,j}$) of each module i in sector j changes according to:

$$\frac{dW_{pCi,j}}{dt} = I_{Ci,j} - I_{pCi,j} - e_{pCi,j} \tag{6.3.6}$$

where $I_{pCi,j}$ is the rate of carbon unloading from the phloem into that module, $I_{pCi,j}$ is the rate of phloem carbon import from nearby modules, and $e_{pCi,j}$ is the rate of phloem carbon export into nearby modules. In the case of the leaf module (module 1) of sector j, the phloem carbon ($W_{pC1,j}$) changes according to:

$$\frac{dW_{pC1,j}}{dt} = \alpha_{1,j} - e_{pC1,j} \tag{6.3.7}$$

where $\alpha_{1,j}$ is the rate of carbon loading by the leaves of that module, and $e_{pC1,j}$ is the rate of phloem carbon export to the branch modules.

Also, for the leaf module (module 1) of each sector j, the water content ($W_{w1,j}$) changes according to:

$$\frac{dW_{w1,j}}{dt} = q_{x1,j} - E_{t1,j} \tag{6.3.8}$$

where $q_{x1,j}$ is the xylem flux of water into that leaf module, determined by solving the circuits shown in Fig. 6.2, and $E_{t1,j}$ is the rate of evapotranspiration for that module.

The details of the mathematical models for all non-state variables mentioned in this section, as well as the xylem and phloem hydraulic parameters shown in Fig. 6.2, are provided in the Appendix (section 6.6, eqns 6.6.1–6.6.27).

6.3.2 Simulations

We simulated the factorial effects of xylem and phloem sectoriality on overall growth and aboveground and belowground biomass distributions over a 60 day growth period for plants in two different patchy nitrogen scenarios.

Sectoriality was varied by setting the value of the xylem tangential resistance (R_{tx}) and phloem tangential resistance (R_{tp}) to 0.0 or 10.0 MPa day mL^{-}1 in all factorial combinations. Tangential resistances of 0.0 corresponded to high integration scenarios, and tangential resistances of 10.0 MPa day mL^{-}1 had been previously shown to result in nearly complete sectoriality. Thus, we simulated the most extreme scenarios for sectoriality of xylem and phloem. Plants with intermediate sectoriality are expected to fall between these extremes.

All nutrient scenarios began with a five day period of low nitrogen availability (U_N = 0.05 g N g^{-1} dw day^{-1}), after which half of the root system received high nitrogen (U_N = 0.50 g N g^{-1} dw day^{-1}) while the other half still received low nitrogen. Starting values for state variables (Table 6.1) were established in an initial run of the model with uniform low nitrogen until the relative values of all state variables stabilized. These stable values were scaled to a small plant size as starting values for the model (Table 6.2).

Our first nutrient scenario assumed a static nutrient environment, with the

Table 6.2: Starting values for all state variables, selected based on stable relative values when nitrogen is uniformly low

Module #	Plant component (sectors 1 & 2)	W_{dw} (mg)	W_C (mg)	W_N (μg)	W_{pC} (μg)	W_w (mg)
1	Leaves	0.245	0.064	0.112	2.30	0.2
2	Branches	0.111	0.078	0.172	0.80	–
3	Stem segment 1	0.023	0.013	0.005	0.16	–
4	Stem segment 2	0.025	0.010	0.006	0.16	–
5	Stem segment 3	0.026	0.008	0.010	0.16	–
6	Stem segment 4	0.027	0.006	0.016	0.16	–
7	Stem segment 5	0.029	0.003	0.032	0.16	–
8	Coarse roots	0.126	0.003	2.500	0.52	–
9	Fine roots	0.387	0.014	2.030	0.79	–

asymmetrical nitrogen treatment continued throughout the 60 day simulation period, with high nitrogen availability in 1 and at low nitrogen in sector 2. This type of temporally static heterogeneity scenario is very common in the root foraging literature, but more dynamic nitrogen availability may be expected in many natural ecosystems. Static nitrogen distributions might also decrease the growth-limiting effects of sectoriality, since constraints that keep resources inside a sector that will reliably continue to experience a high quality environment could be advantageous. We therefore also considered a temporally variable nutrient scenario. In our temporally variable scenario, after 30 days of growth in the static asymmetric nitrogen environment, the nutrient environment of the two sectors reversed, such that the formerly low nitrogen sector now received high nitrogen, and vice versa. The goal of this scenario was to evaluate the effects of the most extreme possible temporal variation in spatial nutrient distribution, and thus the situation in which temporal variation would be expected to have the largest effect.

6.4 Results

6.4.1 Static patchy nitrogen environment

To understand patterns of root growth in sectored plants, it is important to first examine the patterns of growth in the leaves, the sources of carbon required for root growth. We found that simulated growth and root distribution in the static

nutrient scenario depended upon both phloem and xylem sectoriality. In all scenarios, sectoriality had no effect on the growth rate of leaves orthostichous to roots in the high nitrogen patch (Fig. 6.3A). The sharp spike observed in growth of those leaves immediately following the appearance of the nitrogen patch may or may not be physiologically realistic, depending on the precise manner in which nitrogen affects growth rates, whether the plant is able to up-regulate photosynthesis, and whether stored carbon can be mobilized for proliferation. The growth rate of non-orthostichous leaves was greatest when xylem was integrated and highly constrained with xylem was sectored (Fig. 6.3B). There was only a tiny effect of phloem sectoriality on the growth rate of these leaves. This pattern reflects nitrogen limitation and the availability of high nitrogen sap to these leaves when the xylem is integrated and not when the xylem is sectored.

Root growth rate in the high nitrogen patch was greatest when both xylem and phloem were integrated (Fig. 6.3C). In this case, tthe fine roots of the high nitrogen sector—the strongest carbon sinks— are able to use both halves of the crown as carbon sources. When xylem, phloem, or both are sectored, however, the growth of the fine roots in the high nitrogen patch is limited by carbon supply from leaves in the same sector. [Note: When the nitrogen patch first appeared, the roots in the nitrogen patch actually experience a temporary decrease in growth, regardless of sectoriality scenario (Fig. 6.3C). This pattern reflects the facts that our model is strictly passive and that root growth is assumed to use carbon left over after nitrogen uptake (which is metabolically costly). The growth of these roots soon increases again due to the increased leaf growth and thus carbon supply.]

The roots in the low nitrogen patch experience the highest growth rate when xylem is integrated but phloem is sectored (Fig. 6.3D). In this situation, leaves in both sectors benefit from the nitrogen patch and the sectored phloem transport ensures that all the carbon remains in the low nitrogen sector.

As expected, the highest simulated proportion of roots in the high nitrogen patch (a common measure of "root precision") was for plants integrated for

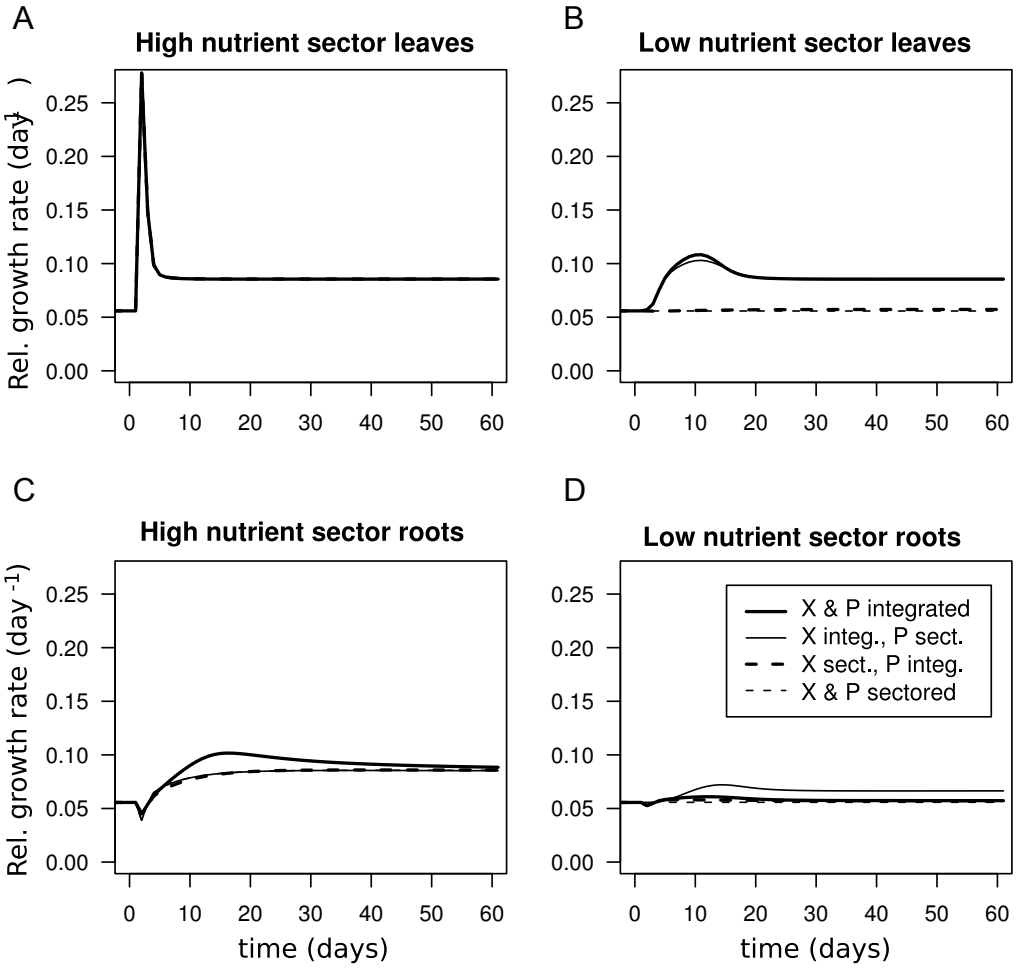

Figure 6.3: Simulated temporal variation in relative growth rates for leaves (A,B) and fine roots (C,D) of each sector for plants receiving high nitrogen (10x) in one sector and low nitrogen (1x) in the other sector throughout the simulation period. Results for the high nitrogen sector are shown on the left (A,C), and results for the low nitrogen sector are shown on the right (B,D). In (A), the all scenarios showed the same growth pattern, so all of the lines overlap. Relative growth rates were calculated as the change in biomass per time, divided by the biomass at the start of that time interval. Outputs are shown for four combinations of xylem and phloem sectoriality: xylem and phloem both integrated ($r_{tx} = 0$, $r_{tp} = 0$), designated "X & P integrated"; xylem integrated and phloem sectored ($r_{tx} = 0$, $r_{tp} = 10$), designated "X integ., P sect."; xylem sectored and phloem integrated ($r_{tx} = 10$, $r_{tp} = 0$), designated "X sect., P integ."; and both xylem and phloem sectored ($r_{tx} = 10$, $r_{tp} = 10$), designated "X & P sectored". In each case, integrated xylem is indicated by solid lines and sectored xylem by broken lines, and integrated phloem is indicated by heavy lines and sectored phloem by light lines.

both xylem and phloem (Fig. 6.4A). However, when both were sectored, precision was intermediate. The lowest "precision" was for plants integrated for xylem and sectored for phloem (Fig. 6.4A). This pattern reflects the fact that when xylem is integrated the growth of leaves in both sectors is promoted but sectored phloem constrains carbon transport from the low nitrogen sector to the roots in the high nitrogen patch: recall that the low nitrogen roots experience enhanced growth compared to the other scenarios (Fig. 6.3D).

The patterns of total biomass accumulation did not match the accumulated relative root allocation into the patch. At the end of 60 days simulated growth, total biomass accumulation was highest for plants integrated for both xylem and phloem, low when both were sectored (Fig. 6.4B). Interestingly, for both root allocation and total plant growth, there was an interactive effect of xylem and phloem sectoriality on long-term biomass accumulation. In both cases, when xylem was integrated the response (growth or root precision) was higher when phloem was integrated than when phloem was sectored. However, when xylem was sectored, little or no effect of phloem sectoriality was observed.

6.4.2 Temporally varied nutrient environment

As found at 60 days (see above), after 30 days of asymmetrical nutrient conditions, the highest root biomass on the high nitrogen sector was for plants with both xylem and phloem integrated (Fig. 6.5A), and the highest root biomass on the low nitrogen side was for plants with integrated xylem and sectored phloem (Fig. 6.5B). Following the change in nitrogen distribution, growth of the roots in the side initially receiving high nitrogen was highest when xylem was integrated and phloem was sectored (Fig. 6.5A), once again due to the carbon trapped in that sector. This scenario also provided the highest growth rate for roots in the new nitrogen patch (Fig. 6.5B). In this case, the high growth under integrated xylem and sectored phloem reflects the combination of initially higher biomass in that sector and combined with the lack of carbon competition between the roots in the new patch and the initially much higher root biomass

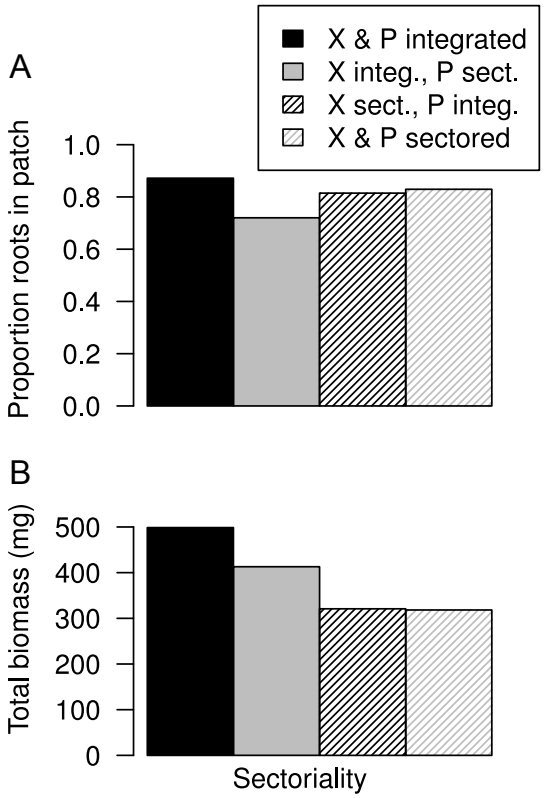

Figure 6.4: Simulated proportion fine roots in the high nitrogen patch (A) and total plant biomass (B) after 60 days of simulation time for plants receiving high nitrogen (10x) in one sector and low nitrogen (1x) in the other sector throughout the simulation period. Simulated values are shown for four combinations of xylem and phloem sectoriality: xylem and phloem both integrated ($r_{tx} = 0$, $r_{tp} = 0$), designated "X & P integrated"; xylem integrated and phloem sectored ($r_{tx} = 0$, $r_{tp} = 10$), designated "X integ., P sect."; xylem sectored and phloem integrated ($r_{tx} = 10$, $r_{tp} = 0$), designated "X sect., P integ."; and both xylem and phloem sectored ($r_{tx} = 10$, $r_{tp} = 10$), designated "X & P sectored."

in the opposite sector.

The overall result is an increase in whole plant biomass accumulation for plants with integrated xylem and sectored phloem, reducing the difference in growth between these simulated plants and those integrated for both xylem and phloem (Fig. 6.5C).

6.5 Discussion

We present a novel framework for modeling plant responses to heterogeneity, which we use to demonstrate the probable roles of xylem and phloem sectoriality in shaping asymmetrical growth and total biomass accumulation under patchy nutrient conditions. Our model output suggests that both xylem and phloem sectoriality can limit carbon supply needed for proliferation in a nitrogen patch, and that both can limit whole plant growth in these conditions. This pattern is consistent with findings suggesting that more sectored species display less response to nitrogen patches (e.g. Gloser et al. 2008) and with the general expectation that sectoriality will be disadvantageous where resources are patchy (Watson and Casper 1984). The difference between simulated effects of sectoriality on total plant growth and root "precision" may also shed light on the observation—in a meta-analysis by Kembel and Cahill (2005)—that root proliferation responses did not predict whole plant responses to heterogeneity.

The role of xylem sectoriality in growth patterns reflected its importance in determining whether all of, or only part of, the crown received the benefit of high nitrogen availability. This pattern was true whether the location of the nitrogen patch was static or variable. In contrast, phloem sectoriality, which limited growth in the static nutrient scenario, was much less important when the location of the nitrogen patch changed. In the temporally variable nutrient scenario, phloem integration actually imposed a cost by producing a less balanced root system, and by permitting increased root growth in the initial patch, at cost of root growth elsewhere. In addition to the insights this pattern provides about the role of vascular sectoriality, this result also underlines the

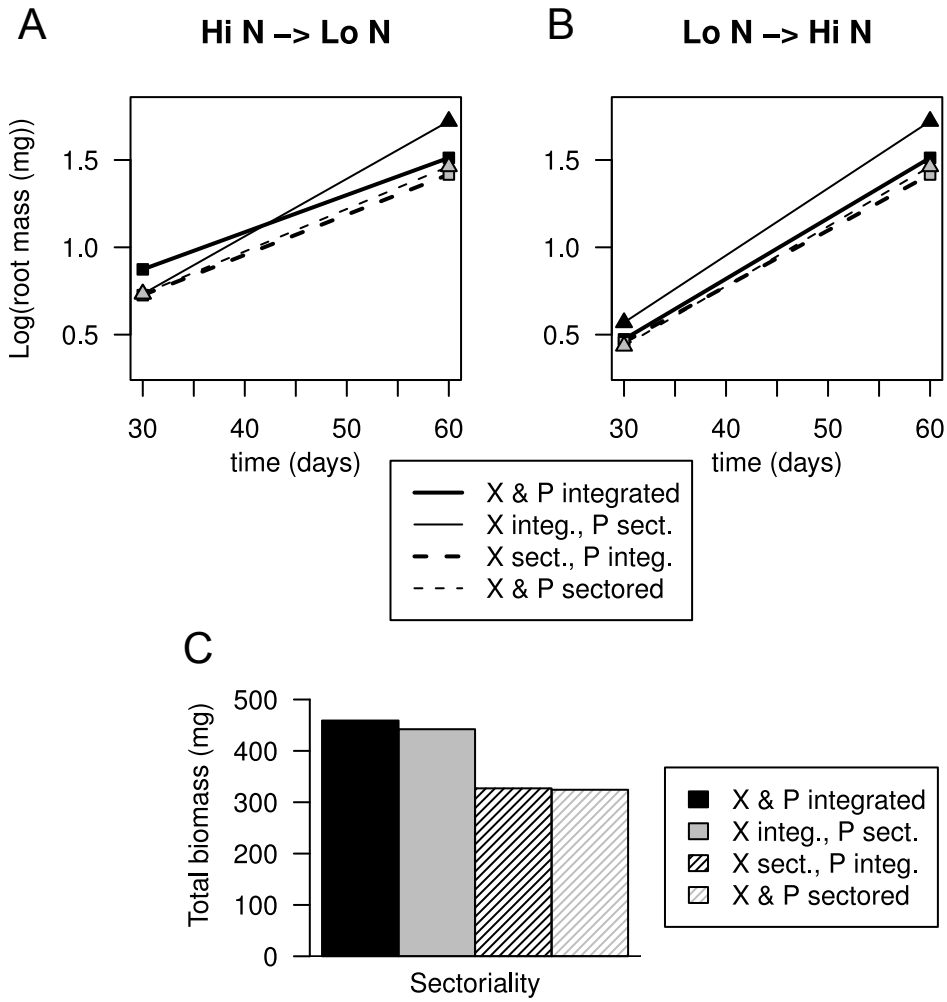

Figure 6.5: Log_{10}(simulated root biomasses) for 30 days (just before the change in nitrogen distribution) and 60 days for the side receiving high nitrogen first and low nitrogen second (A) and for the side receiving low nitrogen first and high nitrogen second (B), and the total plant biomass following the total 60 days of simulation (C). Simulated values are shown for all factorial combinations of xylem and phloem sectoriality: xylem and phloem both integrated($r_{tangx} = 0$, $r_{tangp} = 0$), phloem integrated and xylem sectored ($r_{tangx} = 10$, $r_{tangp} = 0$), phloem sectored and xylem integrated ($r_{tangx} = 0$, $r_{tangp} = 10$), and xylem and phloem both sectored ($r_{tangx} = 10$, $r_{tangp} = 10$). In the line graphs, integrated xylem is indicated by solid lines and sectored xylem by broken lines, and integrated phloem is indicated by heavy lines and sectored phloem by light lines. In the bar graph, integrated phloem is indicated by solid bars and sectored phloem by striped bars, and integrated xylem is indicated by black and sectored xylem by gray.

importance of understanding growth plasticity in terms of the predictability of future environments: in conditions of temporal variability, high plasticity is costly.

The creation of a tool for predicting how sectoriality will affect growth in patchy nutrient conditions is timely, given the recent meta-analysis by Kembel et al. (2008) demonstrating a correlation between root "precision" and a variety of other traits associated with a "fast" life history strategy, traits favoring rapid growth and reproduction. Sectoriality also appears to be related to life history strategies: high sectoriality is more often associated with long-lived slow-growing species, where it may help protect against spread of embolism and disease at expense of growth potential. For example, among trees, slow-growing oaks display higher hydraulic sectoriality than maples, which in turn display higher sectoriality than fast growing, short-lived birches (Orians et al. 2004, 2005*b*, Zanne et al. 2006*b*, Ellmore et al. 2006). Thus, it is likely that part of the life history correlation observed by Kembel et al. (2008) might be explained by sectoriality itself. The modeling framework presented here can be used to establish expected sectoriality traits when all other factors are held constant, helping not only to reveal not only the degree to which sectoriality influences growth, but also enabling experimenters to control for sectoriality in order to uncover other mechanisms affecting patterns of growth.

6.5.1 Value of our bottom-up approach

The bottom-up approach presented here reflects the well-established decentralization of plant growth and plasticity. Plant adaptive behaviors are best understood as the growth and signaling of partially autonomous subunits responding to both their local environments and information received from the rest of the plant (de Kroon et al. 2005). Decentralized processes have been used in previous theoretical studies on root-shoot allocation patterns (Dewar 1993), allocation of material to roots or shoots in high quality patches (Yang and Midmore 2005), and to illuminate the role of signal molecules in responses to het-

erogeneity (Yang and Midmore 2009), but we know of no theoretical efforts to simultaneously incorporate sectoriality and source-sink dynamics into a modular approach to understanding responses to heterogeneity.

In the simulations presented here, we emphasize passive processes, as driven by Michaelis-Menten growth kinetics. While this focus is unlikely to capture all processes regulating root growth, this simplified focus can help to stimulate specific experiments to evaluate the importance of passive sectorial processes, just as the passive root-shoot allocation model by Dewar (1993) paved the way for subsequent empirical examination of the relative importance of optimality as opposed to ontogeny in predicting root:shoot allocation patterns (e.g. McConnaughay and Coleman 1999).

At the same time, the bottom-up modeling framework presented here can be easily adapted to include other processes, enabling a broader tool set for addressing questions relating to root:shoot allocation in a patchy environment, as posed by Hutchings and John (2004). For instance, the model presented here could be modified to include factors such as activity of signal hormones (e.g. Pearce et al. 2001, Holton et al. 2007), root age (e.g. Volder et al. 2005), spatial heterogeneity in root morphology (reviewed in Hodge 2004), and mobilization of stored resources in response to environmental cues. Finally, explicit modeling of nitrogen conversion between chemical forms with different transport properties could be used to situations where newly acquired inorganic nitrogen is processed into biologically useful forms in the leaves (see citations in Andrews et al. 2006), requiring more stages of long-distance transport before it can be incorporated into new tissue.

6.5.2 Interaction of xylem and phloem sectoriality

The separate effects of xylem and phloem sectoriality simulated here also point to important areas for future sectoriality research, particularly regarding phloem sectoriality. A great deal is known about the relative xylem sectorialities of different species, including quantitative indices for comparing hydraulic sectori-

ality (e.g. Orians et al. 2005*b*, Zanne et al. 2006*b*, Schenk et al. 2008). Less is known about the details of phloem sectoriality. Comparisons of phloem sectoriality between species have been more general, with most phloem sectoriality studies focusing on a single species, making inter-species comparisons difficult (e.g. Murphy and Watson 1996, Preston 1998, Bledsoe and Orians 2006). It has been noted that xylem and phloem traces tend to co-occur (Scarpella and Meijer 2004), suggesting that xylem and phloem sectoriality will be correlated, but this hypothesized correlation has not to our knowledge been tested. Our findings suggest that phloem integration would provide the strongest growth benefit in a patchy nutrient environment when xylem is also integrated, so quantitative measurement of phloem sectoriality in species known to exhibit xylem integration may be particularly valuable in understanding root growth patterns in a patchy nutrient environment.

Furthermore, due to the lack of detailed knowledge of the processes underlying phloem inter-sector transport, we have assumed here that phloem inter-sector transport—like xylem inter-sector transport—is driven by pressure gradients. This assumption may or may not capture actual patterns of carbon movement between sectors. It is generally accepted that vessel pits connecting parallel xylem vessels play a key role in tangential xylem transport (Kitin et al. 2004, Ellmore et al. 2006, e.g.), but less is known about tangential transport in the phloem. Lateral sieve areas connecting parallel sieve tubes are known to exist in angiosperms (Esau 1969), but it is not clear whether they play a role in inter-sector transport. Other likely mechanisms for inter-sector transport in the phloem include leakage of material from sieve tubes taken up by neighboring sieve tubes (Thorpe et al. 2005), or activity of transfer cells (Pate and Jeschke 1995). While these processes may similarly favor transport from high carbon sectors to metabolically active low carbon sectors, the dynamics may differ from our simulations here. Closer evaluation of these mechanisms may provide a more sophisticated framework for modeling phloem sectoriality.

6.5.3 Implications for experimental design

One limitation to the idea of including sectoriality as a covariate in root foraging studies is the absence of sectoriality literature on most species. Even when sectoriality data exist, changes in sectoriality with life stage are not always known. Fortunately, our modeling framework suggests some simple modifications to root foraging studies could provide a preliminary measure of sectoriality for species in which the trait has not been measured.

Our assumption that each sector receives a distinct nutrient environment closely resembles the experimental design of many root foraging studies. A common setup is to divide pots into quadrants supplied with different concentrations of fertilizer solution (e.g. Campbell et al. 1991). While it is improbable that these quadrants contain exclusively the roots of any single sector, there is likely to be some correlation between plant sectors and pot quadrants due to the fact that roots on the same side of the plant are generally fed by the same set of vascular bundles (Watson and Casper 1984). This type of inter-sector asymmetry also exists in many other experimental designs. Methods used to create patchy nutrient environments have included: training one or two lateral roots into a different container from the rest of the roots system (e.g. van Vuuren et al. 2003, Gloser et al. 2008); introduction of a soil core with added organic matter, and comparing proliferation within the core to proliferation in a control core, sometimes on the opposite side of the plant (e.g. Bliss et al. 2002, Lamb et al. 2004); or vertically splitting the tap root with a razor to provide two equal halves of the root system which are then trained into separate containers (e.g. Guo et al. 2007).

In all of these cases, evidence for sectoriality or integration could easily be obtained by simultaneously examining leaves for heterogeneous growth or chemistry corresponding to asymmetry of nutrient supply (e.g. Orians et al. 2002, Gloser et al. 2008). Comparison of these asymmetries to the predictions of modular models like ours could help relate quantitative measures of heterogeneity to the expected heterogeneity for particularly levels of xylem and

phloem sectoriality. The use of minirhizotrons to measure temporal dynamics in the spatial distribution of roots (e.g. McNickle and Cahill 2009, Dupuy et al. 2010) may provide a particularly powerful framework for assessing sectoriality, when combined with ongoing measurements of leaf growth.

6.5.4 Conclusions

The modular model presented here for the effects of xylem and phloem sectoriality provides important insights into the interplay of sectoriality, water potential gradients, and source-sink dynamics in predicting growth patterns in a patchy nitrogen environment. The simulation output here suggests that xylem and phloem sectoriality will have an interacting effect on both whole plant growth and root allocation in the presence of a nitrogen patch, especially when patches have sufficient duration to affect biomass distribution. While we have emphasized nitrogen heterogeneity, the same model could be used to examine heterogeneity of other nutrients with only very minor modifications.

The model could also easily be extended to include a variety of known plastic responses to environmental heterogeneity, any of which could influence resource allocation, growth, and inter-sector hydraulics. For example the inclusion of root plasticity (see discussion above), changes to leaf anatomy and physiology with light and nutrient status (Meziane and Shipley 1999, Sack et al. 2003), changes in nitrogen:carbon balance with nutrient status (Van Arendonk et al. 1998, De Groot et al. 2002, Shipley et al. 2005), and plasticity of phloem loading and unloading (Chiou and Bush 1998, Roitsch 1999, Babst et al. 2005) could all provide greater realism in future variations on our model. The same framework could also be used to examine plant growth responses to other forms of heterogeneity, such as patchy light (Campbell et al. 1991), and localized herbivore attack (Orians 2005, Thorn and Orians 2011*b*).

Overall, the modular approach presented here fills an important gap in the theoretical literature, reflecting the long-standing view that plants are best understood as partially independent subunits. In addition to the results pre-

sented here, this approach has a high potential generalizability to other questions about plant responses to environmental heterogeneity.

6.6 Appendix

6.6.1 Model details

Growth allocation

For simplicity, we assume that the fractions of functional dry weight as carbon (f_C) and as nitrogen (f_N) are constant (after Dewar 1993, Thornley and Johnson 2000), such that the rates of conversion of available carbon and of available nitrogen in module i of sector j ($G_{Ci,j}$ and $G_{Ni,j}$ respectively) to new dry weight are:

$$G_{Ci,j} = f_C \times \frac{dW_{dwi,j}}{dt} \tag{6.6.1}$$

$$G_{Ni,j} = f_N \times \frac{dW_{dwi,j}}{dt} \tag{6.6.2}$$

Metabolism

Meanwhile, available carbon is also expended for metabolic processes, which we again model following growth models from Thornley and Johnson (2000). For leaves, branches, stems, and coarse roots, the only simulated metabolic cost is maintenance metabolism, which is assumed to occur at a fixed rate m_m per unit dry weight. Thus, the metabolic rate ($M_{i,j}$ for most modules i in sector j are calculated as:

$$M_{i,j} = m_m \times W_{dwi,j} \tag{6.6.3}$$

However, in the case of fine roots, we also model metabolic cost m_{uN} associated with the rate of nitrogen uptake in each root module (module 9) in sector j ($U_{N9,j}$). Thus, for fine root modules (module 9) in each sector j, the overall metabolism is given by:

$$M_{9,j} = m_m \times W_{dw9,j} + m_{uN} \times U_{N9,j} \tag{6.6.4}$$

Carbon fixation, nitrogen uptake, and transpiration

We use models similar to Dewar (1993) for carbon fixation, nitrogen uptake, and transpiration. Thus, we assume that within each sector j the rate of carbon fixation ($U_{C1,j}$) by the leaf module (module 1) scales with the dry weight of that leaf module:

$$U_{C1,j} = \sigma_{Cj} \times W_{dw1,j} \tag{6.6.5}$$

where σ_{Cj} is the photosynthesis rate for that sector. For the purposes of simulations in this paper, we assume that σ_{Cj} is a constant, i.e., there is no difference in photosynthetic environment between sectors.

We assume that the nitrogen uptake rate ($U_{N9,j}$) for the fine root module (module 9) of sector j scales with biomass for that root module:

$$U_{N9,j} = \sigma_{Nj} \times W_{dw9,j} \tag{6.6.6}$$

where σ_{Nj} is a variable parameter defining the rate of nitrogen uptake for sector j, which we assume reflects variation in soil nitrogen availability. For our purposes, we assume that nitrogen uptake is either high or low, varying by sector and by time, with the high rate of uptake $10\times$ the low rate of uptake.

Finally, we assume that transpiration ($E_{t1,j}$) per leaf module (module 1) in sector j scales with carbon fixation for that module:

$$E_{t1,j} = E_{rt} \times U_{C1,j} \tag{6.6.7}$$

where E_{rt} relates evapotranspiration to carbon uptake.

Carbon loading and nitrogen export

For simplicity, we assume that the rate of carbon loading ($\alpha_{1,j}$) by the leaf module (module 1) of each sector j is a fixed fraction (f_{lC}) of the carbon fixed by that module:

$$\alpha_{1,j} = f_{lC} \times U_{C1,j} \tag{6.6.8}$$

and that the rate of nitrogen ($\lambda_{9,j}$) export from the fine root module (module 9) of sector j a fixed fraction (f_{eN}) of nitrogen taken up by that module:

$$\lambda_{9,j} = f_{eN} \times U_{N9,j} \tag{6.6.9}$$

In the model, the exported carbon and nitrogen enter the phloem and xylem streams respectively, and subsequent allocation depends on whole plant transport dynamics. The remaining carbon in leaves and nitrogen in fine roots is assumed to be allocated directly to the local pool of available carbon ($W_{C1,j}$) in that leaf module, and pool of available nitrogen ($W_{N9,j}$) in that fine root module. It should be noted in the case of nitrogen, the validity of the assumption that newly acquired resources remain local depends on a variety of factors, such as the chemical form of the source material (Cambui et al. 2011).

Phloem transport and carbon unloading

Translocation of carbon in the phloem depends on phloem sap flux carbon concentration. For our purposes, rates of sap flux through any module are assumed to depend on the solution to the Ohm's law circuit model for phloem sectoriality Fig. 6.2A. Since we are most interested in the relations between root sinks and leaf sources, we make the simplifying assumption that flow rates through the whole circuit are determined by phloem pressure due to the phloem content of osmotically active molecules at these endpoints.

We model the phloem pressure potentials ($\Psi_{pi,j}$) of the leaf ($i = 1$) and fine root ($i = 9$) modules of each sector j as equal to the osmotic potential:

$$\Psi_{pi,j} = k_{\Psi p}[C]_{pi,j} \tag{6.6.10}$$

where $k_{\Psi p}$ is a parameter relating the mass per volume concentration of carbon in the phloem ($[C]_{pi,j}$) to the osmotic potential of the phloem. The mass per

volume carbon in the phloem sap ($[C]_{pi,j}$) of module i in sector j is calculated as:

$$[C]_{pi,j} = \frac{W_{pCi,j}}{V_{pi,j}} \tag{6.6.11}$$

where $W_{pCi,j}$ is the mass of available carbon in the phloem of that module, and $V_{pi,j}$ is the total lumen volume of phloem in that module. Phloem lumen volume is assumed to be a fixed proportion of the module volume, which in turn scales with module dry mass:

$$V_{pi,j} = \frac{f_p \times W_{dwi,j}}{\rho_{dw}} \tag{6.6.12}$$

where f_p is the volume fractions as phloem lumen, and ρ_{dw} is the dry mass density per unit module volume.

The rates of axial phloem sap flow ($q_{pi,j}$) through each module i in sector j are calculated by solving the Ohm's law circuit for phloem sectoriality Fig. 6.2 with water potentials as calculated above, and with the axial resistances Rpi, j calculated as:

$$R_{pi,j} = \frac{r_p}{W_{dwi,j}} \tag{6.6.13}$$

where and r_p relates phloem resistance to the inverse of the dry weight ($W_{dwi,j}$).

With the exception of leaf phloem, the pool of carbon (W_pCi, j) in the phloem of each module i in sector j increases with inflows from the phloem of upstream modules—generally the module $(i-1)$ just above in the same sector j and sometimes (if there is net tangential flow into sector j just above module i) also from module $(i-1)$ of the opposite sector, j'. The pool of phloem carbon in each module also decreases with outflow into downstream modules. Thus, when the phloem tangential flow above module i is toward sector j, the phloem carbon import rate ($I_{pCi,j}$) into each branch, stem segment, and root modules i in sector j is calculated as:

$$I_{pCi,j} = e_{p(i-1),j} + e_{pC(i-1),j'} \times \frac{q_{tp((i-1),j')\rightarrow(i,j)}}{q_{pi,j'} + q_{tp((i-1),j')\rightarrow(i,j)}} \tag{6.6.14}$$

where $e_{pC(i-1),j}$ is the rate of phloem carbon export out of module $(i-1)$ of sector j and $e_{pC(i-1),j'}$ is the rate of phloem carbon export from module $(i-1)$ of sector j', as calculated in eqn 6.6.16 below. Phloem sap flow rates in eqn 6.6.14 are designated as follows: $q_{tp((i-1),j')\rightarrow(i,j)}$ is the rate of tangential phloem sap flow above module i from sector j' to sector j, and $q_{pi,j'}$ is the rate of phloem sap flow through module i of sector j'. On the other hand, when phloem tangential flow above module i is away from sector j, the phloem carbon export from module i of sector j is given by:

$$I_{pCi,j} = e_{pC(i-1),j} \times \frac{q_{pi,j}}{q_{pi,j} + q_{tp((i-1),j)\rightarrow(i,j')}} \tag{6.6.15}$$

where $q_{pi,j}$ is the carbon sap flow rate through module i of sector j and $q_{tp((i-1),j)\rightarrow(i,j')}$ is the rate of phloem tangential flow from sector j to sector j', above module i.

For each module i of sector j the rate of phloem carbon export ($e_{pCi,j}$) is calculated as:

$$e_{pCi,j} = q_{pi,j} \times [C]_{pi,j} \tag{6.6.16}$$

For simplicity, we assume that carbon unloading in the fine root modules (module 9 of each sector j) is the major driver of source-sink dynamics. Based on unloading zone model for carbon transport rates from Thompson and Holbrook (2003), we model the rate of carbon unloading into fine root available pools of each sector j as:

$$I_{C9,j} = k_{uC} \times \frac{[C]_{p9,j}}{[C]_{9,j}} \tag{6.6.17}$$

where k_{uC} is a parameter for the rate of unloading. In contrast, for each vascular tissue (branches, stem segments, and coarse roots) module i in sector j, we assume that incorporation of phloem carbon into available pools $I_{Ci,j}$ scales with the rate of phloem carbon transport through the phloem of that module—the combination of phloem carbon concentration and phloem sap flow rates—i.e., with $e_{pCi,j}$:

$$I_{Ci,j} = f_{pCi,j} \times e_{pCi,j} \tag{6.6.18}$$

where $f_{pCi,j}$ is a constant of carbon unloading for each module i in sector j. The parameter $f_{pCi,j}$ is assumed to equal 0.3 for branches and coarse roots, and to equal 0.06 for stem segments (which are assumed to each represent one fifth of the overall stem). Combined with the our assumed rates of nitrogen delivery to vascular tissues below (eqn 6.6.25), this assumption produces similar growth patterns to the assumption by Yang and Midmore (2005) that vascular cross-sectional area increases according to the flux of carbon and nitrogen through that tissue.

Xylem long distance transport and nitrogen delivery

Xylem transport of water and nutrients is determined by tension in the water column, ultimately driven by water deficits due to evapotranspiration. For our purposes, we assume that all transpiration occurs from the leaves, and we do not include the capacitance of individual modules. We further assume that the water delivered to non-leaf modules for growth purposes is negligible, so that all water taken up by the roots contributes directly to water balance in the leaves, which in turn is depleted by evapotranspiration.

Since we are not specifically focused on drought conditions, we assume that the water is plentiful, and therefore that the water potential ($\Psi_{x9,j}$) of the root module (module 9) for each sector j is continuously equal to 0. As in Thorn and Orians (2011*a*), water potential ($\Psi_{x1,j}$) for the leaf module (module 1) of each sector j is determined from the combined influence of leaf water content on leaf osmotic and pressure potentials. Thus, leaf module water potentials are calculated as:

$$\Psi_{x1,j} = \Psi_{xo1,j} + \Psi_{xp1,j} \tag{6.6.19}$$

where the osmotic ($\Psi_{xo1,j}$) and pressure ($\Psi_{xp1,j}$) potentials for the module are

calculated from the water content of that leaf module ($W_{w1,j}$) and its dry weight (Thorn and Orians 2011*a*). Thus, the osmotic potential is given by:

$$\Psi_{xo1,j} = \frac{-R \times T \times C_s \times W_{dw1,j}}{W_{w1,j}} \tag{6.6.20}$$

where R is the gas constant, T is the absolute tempature, and C_s a parameter for the osmotic content of the cytoplasm of leaf cells. The pressure potential ($\Psi_{xp1,j}$) is calculated as:

$$\Psi_{xp1,j} = max(0, \epsilon(\frac{c_{dw} \times W_{w1,j}}{W_{dw1,j}} - 1)) \tag{6.6.21}$$

where ϵ is the elastic modulus of leaf cell walls and c_{dw} defines the leaf water content when the pressure is zero.

As with phloem transport, there is a xylem resistance associated with each module. The xylem resistance ($R_{xi,j}$) for module each i in sector j are calculated as:

$$R_{xi,j} = \frac{r_x}{W_{dwi,j}} \tag{6.6.22}$$

where r_x relates the xylem resistance to the inverse of the dry weight ($W_{dwi,j}$) for the module i of sector j.

In contrast to carbon movement through the phloem, where the phloem of each module acts as a distinct pool, exporting (eqn 6.6.16) and importing carbon in each time step, we assume that nitrogen transport through the xylem is effectively instantaneous. Nevertheless, we also assume that nitrogen is delivered to each module as the sap ascends, resulting in only part of the nitrogen being delivered to the leaves. The model for nitrogen delivery through the plant is calculated in a similar fashion to the movement of carbon between phloem modules. For all modules above the fine roots, the rate of nitrogen flow into the module from that module is equal to the nitrogen flowing out of the module below, plus or minus any tangential nitrogen flow. Thus, when tangential flow below the module is into sector j, the nitrogen flow ($I_{xNi,j}$) into the xylem of

module i in sector j is:

$$I_{xNi,j} = e_{xN(i+1),j} + e_{xN(i+1),j'} \times \frac{q_{tx(i,j')\rightarrow(i,j)}}{q_{xi,j'} + q_{tx(i,j')\rightarrow(i,j)}} \tag{6.6.23}$$

where $e_{xN(i+1),j}$ is the rate of xylem nitrogen flow out of module $(i+1)$ of sector j and $e_{xN(i+1),j'}$ is the rate of nitrogen flow out of module $(i+1)$ of the opposite side sector (sector j'), as calculated in eqn 6.6.27 below. Xylem sap flow rates in eqn 6.6.23 are designated as follows: $q_{tx(i,j')\rightarrow(i,j)}$ is the rate of tangential xylem sap flow below module i from sector j' to sector j, and $q_{xi,j'}$ is the rate of xylem sap flow through module i of sector j'. On the other hand, when tangential flow below module i is out of sector j, the nitrogen flow into module i of sector j is given by:

$$I_{xNi,j} = e_{xN(i+1),j} \times \frac{q_{xi,j}}{q_{xi,j} + q_{tx(i,j)\rightarrow(i,j')}} \tag{6.6.24}$$

where $q_{xi,j}$ is the xylem sap flow rate through module i of sector j and $q_{tx(i,j)\rightarrow(i,j')}$ is the rate of tangential flow from sector j to sector j', below module i.

The rate of nitrogen delivery ($I_{Ni,j}$) from the xylem to the available nitrogen pools of each module i in sector j for coarse roots, stem segements, and branches is calculated:

$$I_{Ni,j} = f_{xNi,j} \times I_{xNi,j} \tag{6.6.25}$$

where $f_{xNi,j}$ is a constant of nitrogen delivery for each module i in sector j. The parameter $f_{pCi,j}$ is assumed to equal 0.3 for branches and coarse roots, and to equal 0.06 for stem segments (which are assumed to each represent one fifth of the overall stem). Combined with our model for carbon unloading in vascular tissues vascular tissues in eqn 6.6.18), this nitrogen delivery model produces similar growth patterns to the assumption by Yang and Midmore (2005) that vascular cross-sectional area increases according to the flux of carbon and nitrogen through that tissue.

For the leaf module (module 1) of each sector i, whatever nitrogen remain-

ing in the xylem stream is delivered directly into the available nitrogen pools at rate ($I_{N1,j}$):

$$I_{N1,j} = I_{xN1,j} \tag{6.6.26}$$

Finally, for coarse roots, stem segments, and branches, the the rate of xylem nitrogen flow out of module i of sector j ($e_{xNi,j}$) is calculated:

$$e_{xNi,j} = I_{xNi,j} - I_{Ni,j} \tag{6.6.27}$$

Table 6.3: Default parameter values with citation and/or rationale

Symbol	Description	Default value(s)	Units	Derived from
k_G	Growth parameter (eqn 6.3.1)	500.0	day^{-1}	Dewar (1993)
f_C	Tissue fraction C (eqn 6.6.1)	0.45	g C g^{-1} dw	Dewar (1993)
f_N	Tissue fraction N (eqn 6.6.2)	0.03	g N g^{-1} dw	Dewar (1993)
m_m	Maintenance metabolism (eqn 6.6.3, 6.6.4)	0.015	g C g^{-1} dw day^{-1}	Thornley and Johnson (2000) eq. 11.2
m_{uN}	Metabolic cost of N uptake (eqn 6.6.4)	0.5	g C g^{-1} N	Thornley and Johnson (2000) eq. 16.14
σ_{Cj}	Carbon fixation rate for sector j (eqn 6.6.5)	0.2	g C g^{-1} dw day^{-1}	Modified from Dewar (1993)
σ_{Nj}	Nitrogen uptake rate for sector j (eqn 6.6.6)	0.05, 0.005	g N g^{-1} dw day^{-1}	Modified from Dewar (1993)
E_{rt}	Evapotranspiration ratio (eqn 6.6.7)	750.0	g water g^{-1} C	Taiz and Zeiger (2002)
f_{lC}	Fraction fixed C loaded into phloem (eqn 6.6.8)	0.8	unitless	balanced allocation
f_{eN}	Fraction new N exported from roots (eqn 6.6.9)	0.6	unitless	balanced allocation
$k_{\Psi p}$	Relates phloem osmotic potential to phloem mass carbon content (eqn 6.6.10)	17.2	unitless	Assumes C as sucrose
f_p	Module volume fraction as phloem lumen (eqn 6.6.12)	0.05	unitless	personal observation
ρ_{dw}	Module dry weight per wet volume (eqn 6.6.12)	0.1	g dw mL^{-1}	personal observation

Table 6.3: (continued)

Symbol	Description	Default value(s)	Units	Derived from
r_p	Phloem biomass resistance to axial flow (eqn 6.6.13)	0.002	MPa day g dw mL^{-1}	Assumed slightly higher than xylem resistance
R_{tp}	Resistance to tangential flow for phloem (Fig. 6.2A)	0, 10	MPa day mL^{-1}	extreme values
k_{uC}	Fine roots carbon unloading parameter (eqn 6.6.17)	0.04	g C day^{-1}	balanced allocation
$f_{pCi,j}$	Constant of carbon unloading rate for each module i in sector j (eqn 6.6.18)	0.3, 0.06	unitless	balanced allocation
C_s	Parameter for osmotic activity of leaf cell cytoplasm (eqn 6.6.20)	0.00075	mol g^{-1} dw	Thorn and Orians (2011*a*)
T	Absolute temperature (eqn 6.6.20)	298	K	i.e., 25 °C
R	Gas constant (eqn 6.6.20)	8.3144	MPa g K^{-1} mol^{-1}	n/a
ϵ	Elastic modulus of leaf cell walls (eqn 6.6.21)	5.0	MPa	Thorn and Orians (2011*a*)
c_{dw}	Parameter for leaf water content at $\Psi_{xp} = 0$ (eqn 6.6.21)	0.75	g dw g^{-1} water	Thorn and Orians (2011*a*)
r_x	Xylem biomass resistance to axial flow (eqn 6.6.22)	0.001	MPa day g dw mL^{-1}	FILL IN
R_{tx}	Resistance to tangential flow for xylem (Fig. 6.2B)	0, 10	MPa day mL^{-1}	extreme values
$f_{xNi,j}$	Constant of nitrogen delivery for each module i in sector j (eqn 6.6.25)	0.3, 0.06	unitless	balanced allocation

Table 6.4: Non-state variables used in model

Symbol	Description	Units
$[C]_{i,j}$	Mass concentration available carbon in module i of sector j (eqn 6.3.1)	g C g^{-1} dw
$[N]_{i,j}$	Mass concentration available nitrogen in module i of sector j (eqn 6.3.1)	g C g^{-1} dw
$G_{Ci,j}$	Rate of available carbon conversion to dry weight in module i of sector j (eqn 6.6.1)	g C day^{-1}
$G_{Ni,j}$	Rate of available nitrogen conversion to dry weight in module i of sector j (eqn 6.6.2)	g N day^{-1}
$M_{i,j}$	Metabolic rate in module i of sector j (eqn 6.6.3, 6.6.4)	g C day^{-1}
$U_{C1,j}$	Carbon fixation rate in leaf module (module 1) of sector j (eqn 6.6.5)	g C day^{-1}
$U_{N9,j}$	Nitrogen uptake rate in fine root module (module 9) of sector j (eqn 6.6.6)	g N day^{-1}
$E_{t1,j}$	Rate of transpiration from leaf module (module 1) of sector j (eqn 6.6.7)	g water day^{-1}
$\alpha_{1,j}$	Rate of carbon loading in leaf module (module 1) of sector j (eqn 6.6.8)	g C day^{-1}
$\lambda_{9,j}$	Rate of nitrogen export from root module (module 9) of each sector j (eq 6.6.9)	g N day^{-1}
$\Psi_{pi,j}$	Phloem water potential for leaf and fine root modules (modules 1 and 9) of sector j (Fig. 6.2A, eqn 6.6.10)	MPa
$[C]_{pi,j}$	Phloem carbon concentration for module i in sector j (eqn 6.6.11)	g C mL^{-1}
$V_{pi,j}$	Lumen volume of phloem for module i in sector j (eqn 6.6.12)	mL
$R_{pi,j}$	Phloem axial resistance for module i in sector j (eqn 6.6.13)	MPa day mL^{-1}
$I_{pCi,j}$	Rate of phloem carbon import into module i in sector j (eqn 6.6.14, 6.6.15)	g C day^{-1}
$q_{pi,j}$	Rate of phloem axial sap flow through module i in sector j (eqn 6.6.14, 6.6.15, derived from Fig. 6.2A)	mL day^{-1}

Table 6.4: (continued)

Symbol	Description	Units
$q_{tp(i,j)\rightarrow(i,j')}$	Rate of phloem tangential sap flow from sector j to the opposite sector j' just below module i (eqn 6.6.14, 6.6.15, derived from Fig. 6.2B)	mL day^{-1}
$e_{pCi,j}$	Rate of phloem carbon export from module i in sector j (eqn 6.6.16)	g C day^{-1}
$I_{Ci,j}$	Rate of carbon unloading the phloem in module i in sector j into available pools of that module (eqn 6.6.17, 6.6.18)	g C day^{-1}
$\Psi_{xi,j}$	Xylem water potential for leaf and fine root modules (modules 1 and 9) of sector j (Fig. 6.2B, eqn 6.6.19)	MPa
$\Psi_{xo1,j}$	Xylem osmotic potential for leaf module (module 1) of sector j (eqn 6.6.20)	MPa
$\Psi_{xp1,j}$	Xylem pressure potential for leaf module (module 1) of sector j (eqn 6.6.21)	MPa
$R_{xi,j}$	Xylem axial resistance for module i in sector j (eqn 6.6.22)	MPa day mL^{-1}
$I_{xNi,j}$	Rate of nitrogen arrival in the xylem of module i in sector j (eqn 6.6.23, 6.6.24)	g N day^{-1}
$q_{xi,j}$	Rate of xylem axial sap flow through module i in sector j (eqn 6.6.23, 6.6.24, derived from Fig. 6.2B)	mL day^{-1}
$q_{tx(i,j)\rightarrow(i,j')}$	Rate of xylem tangential sap flow from sector j to the opposite sector j' just below module i (eqn 6.6.23, 6.6.24, derived from Fig. 6.2B)	mL day^{-1}
$e_{xNi,j}$	Rate of xylem nitrogen export from module i in sector j (eqn 6.6.27)	g N day^{-1}
$I_{Ni,j}$	Rate of nitrogen delivery to the available pools of module i in sector j (eqn 6.6.25, 6.6.26)	g N day^{-1}

CHAPTER 7

Conclusions and Future Directions

In this dissertation I have presented several lines of evidence for the interrelationship between local and whole plant responses to environmental heterogeneity, as mediated by sectoriality. Here, I summarize findings from previous chapters, tie together the major conclusions, and suggest several lines of future research drawing on my findings.

Chapters 2-6 present theoretical and empirical studies on five distinct aspects of how sectored resource transport is affected by environmental heterogeneity, and how sectoriality, in turn, constrains plant responses to heterogeneity. Chapter 2 shows how partial defoliation can affect sectored nitrogen allocation in basil. Chapter 3 shows how changes to root hydraulics in basil can also affect nitrogen allocation in basil, as well as how water uptake by the roots is theoretically affected by xylem sectoriality. Chapter 4 uses a theoretical approach to examine how xylem sectoriality in understory trees is likely to affect photosynthesis in a patchy light environment. Chapter 5 examines crown morphology of understory trees to test the hypothesis that sectoriality will affect patterns of branch growth in response to a light gradient. Finally, Chapter 6 uses a theoretical approach to show the probable interaction of xylem and phloem sectoriality in shaping whole plant growth in a patchy nitrate environment. Taken together, these studies demonstrate that plant responses to environmental heterogeneity are best understood through an integrative view of whole plant physiology and morphology.

Central to these studies is the underlying assumption that inter-sector trans-

port is driven by the same water pressure gradients that drive vertical resource transport. To model this understanding, I have extended the Ohm's law analogy used for vertical transport in plants (Tyree and Ewers 1991) to include lateral (tangential) transport as well. This modeling framework provides a predictive tool relating vascular traits to quantitative predictions for how resources will be distributed (Chapters 2-4), and what patterns of growth are expected to result (Chapter 6). Chapter 5 builds on the conclusions of Chapter 4 by examining the hypothesis that sectoriality effects overall growth patterns as well as photosynthesis of understory trees, an alternative explanation for the inverse relationship between sectoriality and shade tolerance observed by Zanne et al. (2006*b*). In the next section, I summarize the ways in which this theoretical framework has guided the research presented in Chapters 2-6, and the insights that have resulted.

7.1 Ohm's law model for sectoriality: Applications and insights

Chapters 2 and 3 play the dual role of providing preliminary validation for the modeling framework while using the model to understand nutrient allocation in patchy conditions. These two chapters demonstrate the model's usefulness in predicting variation between individual basil plants in the inter-sector movement of nitrate nitrogen, a result that is probably generalizable to other herbaceous plants with similar vascular architecture. Chapter 2 shows that the patterns of nitrate movement correspond to transpiration-driven predictions in partially defoliated plants. Chapter 3 shows that a similar relationship between water uptake and nitrate distribution occurs when hydraulic differences are instead induced by changes in root hydraulics due to a nitrogen patch. It should be noted, however, that not all of the inter-sector movement of nitrogen in Chapters 2 and 3 was explained by the model. Thus, these first two data chapters show that the model explains much, but not all, of the inter-sector movement, and raises the question of what mechanisms drives the background

movement of nitrogen between sectors. Is it driven by random mixing in the xylem, by active transport processes, or by some combination of the two? Does the mixing occur in the xylem alone, or is phloem transport also involved? Finally, with a quantitative measure of the unexplained crossover compared with the quantity predicted by the model, it is possible for researchers to estimate the biological significance of this crossover—which may be more important for some research questions than for others.

The theoretical examination of sectoriality and root hydraulics in Chapter 3 also provides important insights into how patterns of water uptake in the roots are likely to be affected by stem vascular architecture. Smaller relative changes in root conductance are expected to produce a larger effect when baseline root conductance is large compared to stem axial resistance. Thus, plasticity of root hydraulics is an area where whole plant architecture must be understood in order to understand tissue level processes. In addition to the implications for resource allocation within the plant, this conclusion is also relevant to the hypothesis that increased root conductance in a nitrate patch helps to draw nitrate ions toward the root (e.g., Gloser et al. 2007). Thus Chapter 3 may inform future research on the adaptive significance of changes in root conductance. On the other hand, the results presented in Chapter 3 assume uniform transpiration by the leaves as well as unchanging stem hydraulics. The consequences of root hydraulics might be different in situations where, e.g., the availability of nitrogen affects leaf transpiration (Polley et al. 1999) perhaps on a sectoral basis, or if changes in ion concentration change the hydrogel properties of the xylem (Zwieniecki et al. 2003).

Chapter 4 builds further on the relationship between water flow in one tissue and the whole plant hydraulics. This theoretical study addresses the question: will sectoriality constrain water supply to photosynthesizing leaves when other parts of the same plant are in shade? It appears that the answer to this question depends on soil water availability, as well as the stem resistance to axial flow, which can increase dynamically with embolism and cavitation or

with mechanical damage. The model suggests that, at least for temperate hardwoods, sectoriality should not affect transpiration and photosynthesis as long as water supply is plentiful and xylem hydraulics are not disrupted. At lower water availability or higher stem axial resistance, sectoriality becomes more important. This theoretical result suggests a situation in which hydraulic integration might improve tolerance of drought conditions. This idea contrasts with the prevailing understanding that high sectoriality is a drought tolerance trait. More research is needed to elucidate the relationship between sectoriality and drought tolerance, but preliminary examination of xylem anatomy data provide tantalizing support: anatomical data from Zanne et al. (2010) suggests that hydraulic integration may indeed be positively related to drought tolerance among shade-tolerant woody species (Chapter 4, Fig. 4.7). Here, results from a theoretical study addressing one question provide an unexpected hypothesis about the role of sectoriality in understory species.

The results from Chapter 4 also leave open the question—previously raised by the analysis by Zanne et al. (2006*b*)—of why it is that temperate woody species adapted to the forest understory tend to be more hydraulically integrated than those adapted for more exposed sites. Chapter 4 suggests photosynthetic differences will only exist under dry conditions, but what selective pressures exist when water is plentiful? The observational study in Chapter 5 hypothesizes that sectoriality might constrain understory growth by reducing correlative inhibition of branch growth as a light-foraging strategy. Specifically, we examined the relationship between branch asymmetry and wood type for species growing at sites with a prevailing light gradient. We predicted that branch asymmetry would contribute more to crown placement for diffuse porous species (which tend to be hydraulically integrated) compared to ring porous species (which tend to be more sectored), and expected that sectored species would rely more on stem inclination to place their crowns in areas of high light. Contrary to our predictions, we found no evidence of differences in branch asymmetry between ring porous trees and diffuse porous trees, al-

though both displayed significantly higher branch asymmetry than white pine, and ring porous species displayed higher stem inclination than diffuse porous species. One possible interpretation of the unexpected result for branch asymmetry is that within-sector feedbacks between root growth orthostichous to high light branches and branch growth orthostichous to roots in high quality branches is sufficient to drive branch asymmetry in sectored species at the same level as correlative inhibition in integrated species. On the other hand, the lack of a difference between ring porous and diffuse porous species may indicate that other differences between species—e.g. in intrinsic growth rates, and tissue plasticity—and differences in environmental context among individuals—e.g. in overall light levels, prevailing light gradients, and soil characteristics—create enough variation in branch asymmetry to swamp any sectoriality effects. Manipulative studies would help in elucidating what factors underly branch asymmetry in different species.

Finally, in Chapter 6 we present a modular modeling framework using Ohm's law models to tie together the effects of xylem and phloem sectoriality on whole plant growth and root allocation in a patchy nitrogen environment. Our simulation outputs suggest an important role for both xylem and phloem sectoriality, especially when nitrogen patches are very long-lived. This result suggests that studies examining root allocation as a possible "nutrient foraging" strategy should also consider sectoriality as a related trait. In addition to the immediate implications for root foraging studies, the model presented in Chapter 6 provides a new and flexible framework for modeling plant responses to heterogeneity that reflects the established view that plant plasticity is best understood as the level of partially independent modules (de Kroon et al. 2005). The same model could easily be modified to simulate the long-term effects of light heterogeneity, partial defoliation, or of changes to tissue conductance, similar to the short term models presented in Chapters 2 and 3.

7.2 Implications

The studies presented in previous chapters strongly suggest that sectoriality is a necessary consideration in understanding plant plasticity. These studies also show that for a given plant, the effect of its vascular sectoriality on overall growth depends on environmental context. The modeling framework presented demonstrates separate roles of environmental heterogeneity (Chapters 2-4 and 6), tangential resistance (Chapters 2-4 and 6), axial resistance (Chapters 3 and 4), and water availability (Chapter 4), as well as separate effects of xylem and phloem sectoriality (Chapter 6). Both short term (Chapters 2-4) and long term (Chapters 5 and 6) effects are considered. At the same time, the lack of evidence for sectoriality effects on branch asymmetry in Chapter 5 reemphasizes the biological reality that sectoriality is not a trait that varies in isolation. Other differences between species must be understood to predict how vascular architecture will affect whole plant growth.

Thus, the whole plant emphasis of my modeling approaches has far-reaching uses in future research. Theoretical and empirical evidence presented in this dissertation shows a two-way relationship between vascular architecture and plant responses to environmental heterogeneity at a variety of scales, from the tissue level to the whole plant level, and from temporal scales from minutes to an entire growing season. The observations compiled here demonstrate the usefulness of my theoretical approach, but these studies only represent a first step in applying this approach to understanding plant responses to environmental heterogeneity. Future research could extend the applications of this model in countless directions.

The research presented here raises key questions for future research. I have shown that partial defoliation can affect nitrogen allocation (Chapter 2), but what are the implications for regrowth following an herbivore attack? Furthermore, it is not known whether the same patterns would be observed if transpiration was affected by shading rather than defoliation. Water uptake changes due to a nitrate patch also affect nitrogen allocation (Chapter 3), but to what de-

gree are these water uptake changes due to root hydraulics changes compared to stem hydrogel properties (Zwieniecki et al. 2003)? Hydraulic integration appears to be beneficial for understory plants in water limited conditions (Chapter 4), and no evidence was found of sectoriality effects on correlative inhibition for understory trees (Chapter 5), but what other factors contribute to the higher occurrence of hydraulic integration in understory trees observed by Zanne et al. (2006*b*)? I present theoretical evidence suggesting an interactive effect of xylem and phloem on whole plant growth and nutrient allocation (Chapter 6), but we do not know the exact processes regulating phloem sectoriality. Would the theoretical effects be different if new knowledge about phloem sectoriality is added to the model? How would the growth patterns be changed if specific models for growth upregulation in a patch were substituted for the Michaelis-Menten model used in Chapter 6? Moreover, throughout this dissertation, the modeling efforts have focused on the effects of heterogeneity when diurnal effects are ignored. How do the predictions change when diurnal changes in evapotranspiration, root conductance, and metabolic activities are included?

In addition to stimulating questions for future research, the studies presented here also provide new theoretical tools for understanding sectoriality. In particular, the Ohm's law circuits I have used to simulate sectored processes can provide a useful complement to future empirical studies addressing these questions. These circuits can be modified to include changes in conductance to different parts of the plant—e.g. to include changes to xylem sectoriality with nutrient availability due to hydrogel properties (Zwieniecki et al. 2003)—or the effects of dynamic changes in water storage through the inclusion of capacitors in the circuit (Tyree and Ewers 1991). Furthermore, while passive processes are emphasized in the chapters of this dissertation, the same framework can be modified to include active adjustments, especially when the circuit is incorporated into a modular allocation model as in Chapter 6. Inclusion of local upregulation of specific processes, such as the production and distribution of hormones through the plant can further elucidate theoretical benefit of plastic

responses with hypothesized growth benefits. Also, with species-specific parameterization, the modeling framework can also be used to quantitatively predict the effects on allocation and growth, a tool with potential broad-reaching applications for hypothesis testing.

Finally, the general applicability of these models across vascular plants may be particularly useful for understanding dynamics of species in non-ancestral environments. Thus there may be timely applications in the areas of climate change biology and invasion biology. Local patterns of precipitation and temperature are expected to change in the century ahead, in some cases dramatically (IPCC Intergovernmental Panel on Climate Change). At the same time that freezing-induced embolism is expected to generally decrease in frequency, drought-induced embolisms are expected to become more common in some areas and seasons, while flooding becomes more common in others. Meanwhile global warming is expected to expand the ranges of numerous herbivores and pathogens (Dale et al. 2001). Synergistic interactions, e.g. between embolism and and leaf chewing herbivore activity, or between diseases transmitted through the vascular system and flooding-induced root anoxia—which decreases root conductance and increases the benefits of vascular integration (Zanne et al. 2006*b*)—will undoubtedly have unanticipatable detrimental effects on numerous species. Flexible physiological models like the sectoriality models presented here will be helpful in analyzing the impacts on particular species, speeding diagnosis and improving the ability to develop management regimes to preserve ecosystems as well as individual species.

CHAPTER 8

Appendix

The following sections display code for the plant growth model used in Chapter 6. The same code can be easily modified to simulate xylem transport, as was modeled in Chapters 2-4. Section 8.1 presents code for all object classes used in the model, most importantly the object classes to define plants and plant modules. Section 8.2 presents the code that does the work of solving circuit models based on plant traits in PLANT objects. Section 8.3 shows code to calculate leaf water potential, stomatal conductance, and transpiration physics. Section 8.4 presents example code for setting up and running a set of simulations.

All code is written in the programming language Python (version 2.6.6). Required packages are listed in headers of each file.

Code presented in these sections was formatted for easier viewing using the syntax hilighter PYGMENTS. Colors indicate symbols with special meanings. For example, numerical values (integers and floats) are shown in gray. The names of functions in function definitions, as well as imported packages are shown in blue. Strings and function descriptions are shown in red. Other important keywords in the Python language are shown in green. Finally, comments (each line preceded by the symbol '#'), is shown in blue-gray and is italicized to make it distinct from the actual code. These comments provide documentation of what various portions of the code are meant to do.

8.1 Plant modules and other programming classes

This code defines classes for all of the objects used in the model. Classes include: VAR, which creates objects with a dictionary-like structure, PLANT, which defines the properties of plant objects, and classes for the constituent parts of a plant object. Each PLANT object is made up of two SECTOR objects. Each SECTOR object is made up of a collection of SEGMENT objects, the modules in the model. Segment subclasses include FINEROOTS, COARSEROOTS, STEM, BRANCH, and LEAF. When incorporated into a python file titled "PlantDataStructures.py" together with files containing the code in subsequent section, these class definitions can be imported for local use.

```
# imports a standard package to makes arithmetic behave more intuitively
from __future__ import division #prevent horrible integer division
# imports python standard package "numpy" for handling matrices
from numpy import *
# imports file with various functions for computing leaf water potential,
#  stomatal conductance, and evaporation physics
import leafprops
# imports file with functions for generating and solving electrical circuits
import PlantCircuits

# Convenient data structure, used in circuit definitions
class Var:
  def __init__(self,sectnum,value,varname):
    self.list = value * ones(sectnum)
    self.name = varname

class Plant:
  perfectMixing = False
  left = None
  right = None
  dt = 1.0/24.0/60.0  #dt in units of days (1/24=1hr)
  time = 0.0
  k_tangx = 0.01
  k_tangp = 0.01
  phloemTangFlows=None
  xylemTangFlows=None
  wholePlantN = None
  wholePlantC = None
  wholePlantBiomass = None
  changeWholePlantN = None
  changeWholePlantC = None
  changeWholePlantBiomass = None
  wholePlantRGR = None
  wholePlantNUptake = None
  wholePlantCFix = None
```

```
wholePlantCResp = None
version = None
printinterval = 1.0 #days
outfile=None
printtime=None

def __init__(self,version=3,stemsegments=5):
  """Creates plant with specified biomass distributions,
            including lists of stem segments for each sector."""
  self.version=version
  self.left = Sector(version,stemsegments)
  self.right = Sector(version,stemsegments)
  self.tangresistx = self.k_tangx * (stemsegments + 1)
  self.tangresistp = self.k_tangp * (stemsegments + 1)
  self.update_derived()

def update_derived(self):
  """Makes sure all derived variables reflect current state of plant."""
  self.left.update_derived()
  self.right.update_derived()

  self.left.fineroot.calcNrNEW(self.time)
  self.right.fineroot.calcNrNEW(self.time)

  self.calcXylemFlows()
  self.calcPhloemFlows()
  self.calcPhloemCTransport()
  self.calcWholePlantNAndChange()
  self.calcWholePlantCAndChange()
  self.calcWholePlantBiomassAndChange()
  self.calcWholePlantCFix()
  self.calcWholePlantNUptake()
  self.calcWholePlantCResp()

  #Tangential resistance calculated
  self.tangresistx = self.k_tangx * (len(self.left.stemlist) + 1)
  self.tangresistp = self.k_tangp * (len(self.left.stemlist) + 1)

def grow(self,growthtime):
  """Grows plants for one time step."""
  endtime = self.time + growthtime
  while self.time < endtime:
    self.step()

def step(self):
  """Everything that needs to happen in each time step."""
  self.update_derived() #Makes sure everything is consistent first
  self.calcPlantCFix() #Calculate photosynthesis for each leaf,
                            #calculate C export
  self.calcPlantNUptake() #Calculate root N uptake for each
               #fine root system, update root N, calculate N export
  self.calcVascularGrowthAndXylemN() #From N uptake, phloem C,
               # Start from roots;
               # Calculates growth (C,N uptake) & N supply to next segment;
               # Works way to to top, then determine N supply to each leaf;
```

```
                # Takes care of growth, N allocation.

    self.left.fineroot.calcGrowthRateAlloc()
    self.left.fineroot.calcRGR()
    self.right.fineroot.calcGrowthRateAlloc()
    self.right.fineroot.calcRGR()
    self.left.leaf.calcGrowthRateAlloc()
    self.left.leaf.calcRGR()
    self.right.leaf.calcGrowthRateAlloc()
    self.right.leaf.calcRGR()

    self.updateStateVariables()
    if self.outfile != None: #If there's an outfile defined, print state.
      if self.time >= self.printtime:
        self.printfileline()
        self.printtime=self.printtime+self.printinterval

  def outputBiomass(self,filename="BiomassDistrib.csv"):
    """Outputs biomass file formatted for R "pyramid" graphing module."""
    f=open(filename,'w')
    f.write("Left, Right, ID \n")
    for j in range(0,len(self.left.sectorSegList)):
      i = len(self.left.sectorSegList)-1-j
      f.write(str(self.left.sectorSegList[i].biomass)+", "+
          str(self.right.sectorSegList[i].biomass)+", "+
          self.right.sectorSegList[i].ID+"\n")
    f.close()

  def closeOutfile(self):
    """Closes current outfile for plant."""
    self.outfile.close()

  def setOutfile(self,filename="Out.csv",type='w',printinterval=1.0):
    """Assigns new outfile for plant."""
    self.printinterval=printinterval
    self.printtime=self.time+self.printinterval
    self.outfile=open(filename,type) #type defaults to 'w'=write
    if type=='w':
      f=self.outfile
      f.write("time"+" ,")
      f.write("k_tangx"+" ,")
      f.write("k_tangp"+" ,")
      f.write("LeafWaterLeft"+" ,")
      f.write("LeafWaterRight"+" ,")
      f.write("NrLeft"+" ,")
      f.write("NrRight"+" ,")
      f.write("LsLeft"+" ,")
      f.write("LsRight"+" ,")
      f.write("Psi_pRootLeft"+" ,")
      f.write("Psi_pRootRight"+" ,")
      f.write("Psi_pLeafLeft"+" ,")
      f.write("Psi_pLeafRight"+" ,")
      f.write("Psi_xRootLeft"+" ,")
      f.write("Psi_xRootRight"+" ,")
      f.write("Psi_xLeafLeft"+" ,")
```

```
    f.write("Psi_xLeafRight"+" ,")
    for var in ["biomass","WN","WC","phloemC","RGR"]:
      for side in ["Left","Right"]:
        for segment in self.left.sectorSegList:
          f.write(var+side+segment.ID+" ,")
    f.write("wholePlantRGR"+" ,")
    f.write("wholePlantBiomass"+" ,")
    f.write("wholePlantN"+" ,")
    f.write("wholePlantC"+" ,")
    f.write("\n")

def printfileline(self):
  """Add one line to csv file, capturing plant's current state."""
  f=self.outfile
  f.write(str(self.time)+" ,")
  f.write(str(self.k_tangx)+" ,")
  f.write(str(self.k_tangp)+" ,")
  f.write(str(self.left.leaf.Wwater)+" ,")
  f.write(str(self.right.leaf.Wwater)+" ,")
  f.write(str(self.left.fineroot.NrNEW)+" ,")
  f.write(str(self.right.fineroot.NrNEW)+" ,")
  f.write(str(self.left.leaf.Ls)+" ,")
  f.write(str(self.right.leaf.Ls)+" ,")
  f.write(str(self.left.fineroot.Psi_p)+" ,")
  f.write(str(self.right.fineroot.Psi_p)+" ,")
  f.write(str(self.left.leaf.Psi_p)+" ,")
  f.write(str(self.right.leaf.Psi_p)+" ,")
  f.write(str(self.left.fineroot.Psi_x)+" ,")
  f.write(str(self.right.fineroot.Psi_x)+" ,")
  f.write(str(self.left.leaf.Psi_x)+" ,")
  f.write(str(self.right.leaf.Psi_x)+" ,")
  for sector in [self.left.sectorSegList,self.right.sectorSegList]:
    for segment in sector:
      f.write(str(segment.biomass)+" ,")
  for sector in [self.left.sectorSegList,self.right.sectorSegList]:
    for segment in sector:
      f.write(str(segment.WN)+" ,")
  for sector in [self.left.sectorSegList,self.right.sectorSegList]:
    for segment in sector:
      f.write(str(segment.WC)+" ,")
  for sector in [self.left.sectorSegList,self.right.sectorSegList]:
    for segment in sector:
      f.write(str(segment.phloemC)+" ,")
  for sector in [self.left.sectorSegList,self.right.sectorSegList]:
    for segment in sector:
      f.write(str(segment.RGR)+" ,")
  f.write(str(self.wholePlantRGR)+" ,")
  f.write(str(self.wholePlantBiomass)+" ,")
  f.write(str(self.wholePlantN)+" ,")
  f.write(str(self.wholePlantC)+" ,")
  f.write("\n")

def outputState(self,filename="PlantState.csv"):
  """Outputs single file with current state of plant."""
  f=open(filename,'w')
```

```
    f.write("time"+" ,")
    f.write("LeafWaterLeft"+" ,")
    f.write("LeafWaterRight"+" ,")
    f.write("NrLeft"+" ,")
    f.write("NrRight"+" ,")
    f.write("LsLeft"+" ,")
    f.write("LsRight"+" ,")
    for var in ["biomass","WN","WC","phloemC"]:
      for side in ["Left","Right"]:
        for segment in self.left.sectorSegList:
          f.write(var+side+segment.ID+" ,")
    f.write("\n")
    f.write(str(self.time)+" ,")
    f.write(str(self.left.leaf.Wwater)+" ,")
    f.write(str(self.right.leaf.Wwater)+" ,")
    f.write(str(self.left.fineroot.NrNEW)+" ,")
    f.write(str(self.right.fineroot.NrNEW)+" ,")
    f.write(str(self.left.leaf.Ls)+" ,")
    f.write(str(self.right.leaf.Ls)+" ,")
    for sector in [self.left.sectorSegList,self.right.sectorSegList]:
      for segment in sector:
        f.write(str(segment.biomass)+" ,")
    for sector in [self.left.sectorSegList,self.right.sectorSegList]:
      for segment in sector:
        f.write(str(segment.WN)+" ,")
    for sector in [self.left.sectorSegList,self.right.sectorSegList]:
      for segment in sector:
        f.write(str(segment.WC)+" ,")
    for sector in [self.left.sectorSegList,self.right.sectorSegList]:
      for segment in sector:
        f.write(str(segment.phloemC)+" ,")
    f.write("\n")

  def updateStateVariables(self):
    #Updates all values that increment in a time step:
    #Biomass for each segment
    #Phloem C for each segment
    #N for roots and leaves
    #C for roots and leaves
    #Water for leaves
    for sector in [self.left.sectorSegList, self.right.sectorSegList]:
      for i in range(0,len(sector)):
        sector[i].biomass = sector[i].biomass + sector[i].growthRate * self.dt
        if i == 0: # if leaves
          sector[i].Wwater = (sector[i].Wwater + (sector[i].xylemFlow -
                                                  sector[i].transp) * self.dt)
          assert sector[i].Wwater >=0.0, ("Wwater["+str(i)+"] = "+
                str(sector[i].Wwater)+
               " went negative.  State variables should not be negative.")
          sector[i].WN = (sector[i].WN + (sector[i].NImportRate -
                                          sector[i].NGrowthAllocRate) * self.dt)
          sector[i].WC = (sector[i].WC + (sector[i].CFix -
               sector[i].LoadingRate - sector[i].CGrowthAllocRate) * self.dt)
                  # metabolic term not needed for leaves
                        # since CFix = net photosynthesis
```

```
        sector[i].phloemC = (sector[i].phloemC +
                (sector[i].CImportRate - sector[i].CExportRate) * self.dt)

      elif i == len(sector) - 1: # if fine roots
        sector[i].WN = (sector[i].WN + (sector[i].NImportRate -
          sector[i].NExportRate - sector[i].NGrowthAllocRate) * self.dt)
        sector[i].WC = (sector[i].WC + (sector[i].UnloadingRate -
               sector[i].CGrowthAllocRate - sector[i].metabolism -
               sector[i].CcostNImportRate) * self.dt)
        sector[i].phloemC = (sector[i].phloemC + (sector[i].CImportRate -
              sector[i].CExportRate - sector[i].UnloadingRate) * self.dt)
      else: #Branches, stems, coarse roots
        sector[i].phloemC = (sector[i].phloemC + (sector[i].CImportRate -
               sector[i].CExportRate - sector[i].UnloadingRate) * self.dt)
             # works for everything except leaves and fine roots
        sector[i].WN =  (sector[i].WN + (sector[i].localNAllocRate -
               sector[i].NGrowthAllocRate) * self.dt)
        sector[i].WC = (sector[i].WC + (sector[i].UnloadingRate -
              sector[i].CGrowthAllocRate - sector[i].metabolism) * self.dt)
    assert sector[i].biomass >=0.0, ("biomass["+str(i)+"] = "+
             str(sector[i].biomass)+
             " went negative.  State variables should not be negative.")
    assert sector[i].WN >=0.0, ("WN["+str(i)+"] = "+
             str(sector[i].WN)+
             " went negative.  State variables should not be negative.")
    assert sector[i].WC >=0.0, ("WC["+str(i)+"] = "+
             str(sector[i].WC)+
             " went negative.  State variables should not be negative.")
    assert sector[i].phloemC >=0.0, ("phloemC["+str(i)+"] = "+
             str(sector[i].phloemC)+
             " went negative.  State variables should not be negative.")
  self.time=self.time+self.dt

def calcWholePlantNAndChange(self):
  newWholePlantN = 0.0
  for sector in [self.left.sectorSegList, self.right.sectorSegList]:
    for i in range(0,len(sector)):
      newWholePlantN = newWholePlantN + sector[i].WN
      newWholePlantN = (newWholePlantN +
                        sector[i].biomass * sector[i].tissueFractionN)
  if self.wholePlantN != None:
    self.changeWholePlantN = newWholePlantN - self.wholePlantN
  self.wholePlantN = newWholePlantN

def calcWholePlantCAndChange(self):
  newWholePlantC = 0.0
  for sector in [self.left.sectorSegList, self.right.sectorSegList]:
    for i in range(0,len(sector)):
      newWholePlantC = newWholePlantC + sector[i].WC
      newWholePlantC = newWholePlantC + sector[i].phloemC
      newWholePlantC = (newWholePlantC +
                        sector[i].biomass * sector[i].tissueFractionC)
  if self.wholePlantC != None:
    self.changeWholePlantC = newWholePlantC - self.wholePlantC
  self.wholePlantC = newWholePlantC
```

```
def calcWholePlantBiomassAndChange(self):
  newWholePlantBiomass = 0.0
  for sector in [self.left.sectorSegList, self.right.sectorSegList]:
    for i in range(0,len(sector)):
      newWholePlantBiomass = newWholePlantBiomass + sector[i].biomass
  if self.wholePlantBiomass != None:
    self.changeWholePlantBiomass = (newWholePlantBiomass -
                                            self.wholePlantBiomass)
    self.wholePlantRGR = (self.changeWholePlantBiomass/
                                      self.wholePlantBiomass/self.dt)
  self.wholePlantBiomass = newWholePlantBiomass

def calcWholePlantCFix(self):
  self.wholePlantCFix = ((self.left.leaf.CFix + self.right.leaf.CFix) *
                                                                  self.dt)

def calcWholePlantNUptake(self):
  self.wholePlantNUptake = ((self.left.fineroot.NImportRate +
                             self.right.fineroot.NImportRate) * self.dt)

def calcWholePlantCResp(self):
  newWholePlantCResp = 0.0
  for sector in [self.left.sectorSegList, self.right.sectorSegList]:
    for i in range(0,len(sector)):
      newWholePlantCResp = (newWholePlantCResp +
                                        sector[i].metabolism * self.dt)
    newWholePlantCResp = (newWholePlantCResp +
                      sector[len(sector)-1].CcostNImportRate * self.dt)
    newWholePlantCResp = newWholePlantCResp - sector[0].metabolism * self.dt
  self.wholePlantCResp = newWholePlantCResp

def calcPlantCFix(self):
  self.left.calcCFixAndTransp()
  self.right.calcCFixAndTransp()

def calcPlantNUptake(self):
  self.left.calcNImportRate()
  self.right.calcNImportRate()

def calcPhloemCTransport(self):
  self.left.leaf.calcCExportRate()
  self.right.leaf.calcCExportRate()
  self.left.branch.calcCExportRate()
  self.right.branch.calcCExportRate()
  self.left.coarseroot.calcCExportRate()
  self.right.coarseroot.calcCExportRate()
  self.left.fineroot.calcCExportRate()
  self.right.fineroot.calcCExportRate()
  self.left.fineroot.calcUnloadingRate()
  self.right.fineroot.calcUnloadingRate()
  stemsegnum=len(self.left.stemlist)
  for i in range(0,stemsegnum):
    self.left.stemlist[i].calcCExportRate()
    self.right.stemlist[i].calcCExportRate()
```

```
self.left.branch.calcUnloadingRate()
self.right.branch.calcUnloadingRate()
self.left.coarseroot.calcUnloadingRate()
self.right.coarseroot.calcUnloadingRate()
stemsegnum=len(self.left.stemlist)
for i in range(0,stemsegnum):
  self.left.stemlist[i].calcUnloadingRate()
  self.right.stemlist[i].calcUnloadingRate()

plantsegsleft=self.left.sectorSegList
          #NOTE DIFFERENCE FROM XYLEM TRANPORT FUNCTION
plantsegsright=self.right.sectorSegList
plantsegnum = len(plantsegsleft)

if self.perfectMixing==True:
  for i in range(0,plantsegnum):
    #LEFT
    if plantsegsleft[i].phloemFlow < 0.0:
     #Usual case - Phloem flows are ordinarily downward
      if i == 0: #i.e. if these are leaves
        plantsegsleft[i].CImportRate = plantsegsleft[i].LoadingRate
      elif i == 1 or i == len(plantsegsleft) - 1:
                                        # if branches or fine roots
        plantsegsleft[i].CImportRate = plantsegsleft[i-1].CExportRate
      elif i == len(plantsegsleft) - 2: # if coarse roots
        if plantsegsright[i].phloemFlow < 0.0: # if right side also down
          totalCImport=(plantsegsleft[i-1].CExportRate +
                                       plantsegsright[i-1].CExportRate)
          propLeft = (plantsegsleft[i].phloemFlow /
           (plantsegsleft[i].phloemFlow + plantsegsright[i].phloemFlow))
          plantsegsleft[i].CImportRate = totalCImport * propLeft
        else: # if right side up or zero
          if plantsegsleft[i-1].phloemFlow < 0.0:
            # if above is down, add together
            totalCImportFromAbove = (plantsegsleft[i-1].CExportRate +
                                       plantsegsright[i-1].CExportRate)
            plantsegsleft[i].CImportRate = (totalCImportFromAbove +
                                        plantsegsright[i].CExportRate)
          else:
            # if above is up, subtract
            propCCrossingOver = (abs(plantsegsleft[i].phloemFlow)/
                                   (abs(plantsegsleft[i].phloemFlow) +
                                 abs(plantsegsleft[i-1].phloemFlow +
                                 plantsegsright[i-1].phloemFlow)))
            plantsegsleft[i].CImportRate = (propCCrossingOver *
                                        plantsegsright[i].CExportRate)
      elif i == 2: # if first segment of stems
        # if both branches flow downward, just take appropriate proportion
        if (plantsegsleft[i-1].phloemFlow < 0.0
                    and plantsegsright[i-1].phloemFlow < 0.0):
          totalCImport=(plantsegsleft[i-1].CExportRate +
                                       plantsegsright[i-1].CExportRate)
          propLeft = (plantsegsleft[i].phloemFlow /
            (plantsegsleft[i].phloemFlow + plantsegsright[i].phloemFlow))
          plantsegsleft[i].CImportRate = totalCImport * propLeft
```

```
      elif (plantsegsleft[i-1].phloemFlow > 0.0
                  and plantsegsright[i-1].phloemFlow < 0.0):
        # if left side up and right side down take from one that
              #is flowing down, minus amount flowing up
        propDown = (abs(plantsegsleft[i].phloemFlow) /
                  (abs(plantsegsleft[i].phloemFlow) +
                     abs(plantsegsleft[i-1].phloemFlow)))
        plantsegsleft[i].CImportRate = (plantsegsright[i-1].CExportRate *
                                        propDown)

      elif (plantsegsleft[i-1].phloemFlow < 0.0
                  and plantsegsright[i-1].phloemFlow > 0.0):
        # if right side up and left side down take from one that
               #is flowing down, minus amount flowing up
        propDown = (abs(plantsegsleft[i].phloemFlow) /
                  (abs(plantsegsleft[i].phloemFlow) +
                     abs(plantsegsright[i-1].phloemFlow)))
        plantsegsleft[i].CImportRate = (plantsegsleft[i-1].CExportRate *
                                        propDown)

      else:
        assert "Something wrong with phloemFlows."

    else: # if other stems
      totalCImport=(plantsegsleft[i-1].CExportRate +
                                plantsegsright[i-1].CExportRate)
      propLeft = (plantsegsleft[i].phloemFlow /
                 (plantsegsleft[i].phloemFlow +
                                     plantsegsright[i].phloemFlow))
      plantsegsleft[i].CImportRate = totalCImport * propLeft

  else: # if phloem flow is upward
    if i == 0: # if leaves
      plantsegsleft[i].CImportRate = (plantsegsleft[i].LoadingRate +
                                      plantsegsleft[i+1].CExportRate)
    elif i == len(plantsegsleft)-1: # if fine roots
      plantsegsleft[i].CImportRate = 0.0 # flow is out of roots
    elif i == len(plantsegsleft)-2: # if coarse roots
      plantsegsleft[i].CImportRate = plantsegsleft[i+1].CExportRate
    elif i == 1: # if branches check whether opposite side is up or down
      if plantsegsright[i].phloemFlow > 0.0: # if right side also up
        totalCImport=(plantsegsleft[i+1].CExportRate +
                              plantsegsright[i+1].CExportRate)
        propLeft = (plantsegsleft[i].phloemFlow /
          (plantsegsleft[i].phloemFlow + plantsegsright[i].phloemFlow))
        plantsegsleft[i].CImportRate = totalCImport * propLeft
      else: # if right side down or zero
        if plantsegsleft[i+1].phloemFlow > 0.0:
          # if below is up, add together
          totalCImportFromBelow = (plantsegsleft[i+1].CExportRate +
                                       plantsegsright[i+1].CExportRate)
          plantsegsleft[i].CImportRate = (totalCImportFromBelow +
                                       plantsegsright[i].CExportRate)
        else:
          # if below is down, subtract
```

```
        if ((abs(plantsegsleft[i].phloemFlow) +
             abs(plantsegsleft[i+1].phloemFlow +
               plantsegsright[i+1].phloemFlow)) == 0.0):
          propCCrossingOver=0.0
        else:
          propCCrossingOver = (abs(plantsegsleft[i].phloemFlow)/
                               (abs(plantsegsleft[i].phloemFlow) +
                                  abs(plantsegsleft[i+1].phloemFlow +
                                  plantsegsright[i+1].phloemFlow)))
        plantsegsleft[i].CImportRate = (propCCrossingOver *
                                        plantsegsright[i].CExportRate)
    elif i== len(plantsegsleft)-3:
        # if last stem segment, check whether coarse roots match
      if (plantsegsleft[i+1].phloemFlow > 0.0
                          and plantsegsright[i+1].phloemFlow > 0.0):
        # if both roots flow upward, just take appropriate proportion
        totalCImport= (plantsegsleft[i-1].CExportRate +
                                       plantsegsright[i-1].CExportRate)
        propLeft = (plantsegsleft[i].phloemFlow /
         (plantsegsleft[i].phloemFlow + plantsegsright[i].phloemFlow))
        plantsegsleft[i].CImportRate = totalCImport * propLeft
      elif (plantsegsleft[i+1].phloemFlow < 0.0
                          and plantsegsright[i+1].phloemFlow > 0.0):
            # if left side down and right side up take from one
                #that is flowing up, minus amount flowing down
        propUp = (abs(plantsegsleft[i].phloemFlow) /
                    (abs(plantsegsleft[i].phloemFlow) +
                      abs(plantsegsleft[i+1].phloemFlow)))
        plantsegsleft[i].CImportRate = (plantsegsright[i+1].CExportRate *
                                        propDown)

      elif (plantsegsleft[i+1].phloemFlow > 0.0
                          and plantsegsright[i+1].phloemFlow < 0.0):
           # if right side down and left side up take from one that
                  # is flowing up, minus amount flowing down
        propDown = (abs(plantsegsleft[i].phloemFlow) /
                     (abs(plantsegsleft[i].phloemFlow) +
                        abs(plantsegsright[i+1].phloemFlow)))
        plantsegsleft[i].CImportRate = (plantsegsleft[i+1].CExportRate *
                                        propDown)

      else:
        assert "Something is not right in the state of phloemFlows."
    else: # if stems
      totalCImport = (plantsegsleft[i+1].CExportRate +
                                      plantsegsright[i+1].CExportRate)
      if ((abs(plantsegsleft[i].phloemFlow) +
                abs(plantsegsleft[i+1].phloemFlow +
                   plantsegsright[i+1].phloemFlow)) == 0.0):
        propLeft=0.0
      else:
        propLeft = (plantsegsleft[i].phloemFlow /
                        (plantsegsleft[i].phloemFlow +
                             plantsegsright[i].phloemFlow))
      plantsegsleft[i].CImportRate = totalCImport * propLeft
```

```
#RIGHT
if plantsegsright[i].phloemFlow < 0.0:
 #Usual case - Phloem flows are ordinarily downward
  if i == 0: #i.e. if these are leaves
    plantsegsright[i].CImportRate = plantsegsright[i].LoadingRate
  elif i == 1 or i == len(plantsegsleft) - 1:
   # if branches / fine roots
    plantsegsright[i].CImportRate = plantsegsright[i-1].CExportRate
  elif i == len(plantsegsright) - 2: # if coarse roots
    if plantsegsleft[i].phloemFlow < 0.0: # if left side also down
      totalCImport=(plantsegsright[i-1].CExportRate +
                                      plantsegsleft[i-1].CExportRate)
      propRight = (plantsegsright[i].phloemFlow /
                     (plantsegsright[i].phloemFlow +
                         plantsegsleft[i].phloemFlow))
      plantsegsright[i].CImportRate = totalCImport * propRight
    else: # if left side up or zero
      if plantsegsright[i-1].phloemFlow < 0.0:
        # if above is down, add together
        totalCImportFromAbove = (plantsegsleft[i-1].CExportRate +
                                      plantsegsright[i-1].CExportRate)
        plantsegsright[i].CImportRate = (totalCImportFromAbove +
                                         plantsegsleft[i].CExportRate)
      else:
        # if above is up, subtract
        propCCrossingOver = (abs(plantsegsright[i].phloemFlow)/
                              (abs(plantsegsright[i].phloemFlow) +
                                abs(plantsegsright[i-1].phloemFlow +
                                  plantsegsleft[i-1].phloemFlow)))
        plantsegsright[i].CImportRate = (propCCrossingOver *
                                       plantsegsleft[i].CExportRate)
  elif i == 2: # if first segment of stems
    # if both branches flow downward, just take appropriate proportion
    if (plantsegsright[i-1].phloemFlow < 0.0 and
                              plantsegsleft[i-1].phloemFlow < 0.0):
      totalCImport=(plantsegsleft[i-1].CExportRate +
                                    plantsegsright[i-1].CExportRate)
      propRight = (plantsegsright[i].phloemFlow /
                      (plantsegsright[i].phloemFlow +
                           plantsegsleft[i].phloemFlow))
      plantsegsright[i].CImportRate = totalCImport * propRight
    elif (plantsegsright[i-1].phloemFlow > 0.0 and
                           plantsegsleft[i-1].phloemFlow < 0.0):
      # if right side up and left side down take from one that
          #is flowing down, minus amount flowing up
      propDown = (abs(plantsegsright[i].phloemFlow) /
                    (abs(plantsegsright[i].phloemFlow) +
                       abs(plantsegsright[i-1].phloemFlow)))
      plantsegsright[i].CImportRate = (plantsegsleft[i-1].CExportRate *
                                           propDown)

    elif (plantsegsright[i-1].phloemFlow < 0.0
                         and plantsegsleft[i-1].phloemFlow > 0.0):
      # if left side up and right side down take from one that
```

```
            #is flowing down, minus amount flowing up
        propDown = (abs(plantsegsright[i].phloemFlow) /
                    (abs(plantsegsright[i].phloemFlow) +
                       abs(plantsegsleft[i-1].phloemFlow)))
        plantsegsright[i].CImportRate = (plantsegsright[i-1].CExportRate
                                                              * propDown)

      else:
        assert "Something is wrong with phloemFlows."

    else: # if other stems
      totalCImport=(plantsegsright[i-1].CExportRate +
                                    plantsegsleft[i-1].CExportRate)
      propRight = (plantsegsleft[i].phloemFlow /
                   (plantsegsright[i].phloemFlow +
                      plantsegsleft[i].phloemFlow))
      plantsegsright[i].CImportRate = totalCImport * propRight

  else: # if phloem flow is upward
    if i == 0: # if leaves
      plantsegsright[i].CImportRate = (plantsegsright[i].LoadingRate +
                                       plantsegsright[i+1].CExportRate)
    elif i == len(plantsegsright)-1: # if fine roots
      plantsegsright[i].CImportRate = 0.0 # flow is out of roots
    elif i == len(plantsegsright)-2: # if coarse roots
      plantsegsright[i].CImportRate = plantsegsright[i+1].CExportRate
    elif i == 1: # if branches check whether opposite side is up or down
      if plantsegsleft[i].phloemFlow > 0.0: # if left side also up
        totalCImport=(plantsegsright[i+1].CExportRate +
                                      plantsegsleft[i+1].CExportRate)
        propRight = (plantsegsright[i].phloemFlow /
                     (plantsegsright[i].phloemFlow +
                       plantsegsleft[i].phloemFlow))
        plantsegsright[i].CImportRate = totalCImport * propRight
      else: # if left side down or zero
        if plantsegsright[i+1].phloemFlow > 0.0:
          # if below is up, add together
          totalCImportFromBelow = (plantsegsright[i+1].CExportRate +
                                       plantsegsleft[i+1].CExportRate)
          plantsegsright[i].CImportRate = (totalCImportFromBelow +
                                       plantsegsleft[i].CExportRate)
        else:
          # if below is down, subtract
          if ((abs(plantsegsleft[i].phloemFlow) +
                 abs(plantsegsleft[i+1].phloemFlow +
                   plantsegsright[i+1].phloemFlow)) == 0.0):
            propCCrossingOver=0.0
          else:
            propCCrossingOver = (abs(plantsegsright[i].phloemFlow)/
                                 (abs(plantsegsright[i].phloemFlow) +
                                    abs(plantsegsright[i+1].phloemFlow +
                                    plantsegsleft[i+1].phloemFlow)))
          plantsegsright[i].CImportRate = (propCCrossingOver *
                                       plantsegsleft[i].CExportRate)
    elif i==len(plantsegsright)-3:
```

```
            # if last stem segment, check whether coarse roots match
          if (plantsegsright[i+1].phloemFlow > 0.0
                            and plantsegsleft[i+1].phloemFlow > 0.0):
            # if both roots flow upward, just take appropriate proportion
            totalCImport=(plantsegsright[i-1].CExportRate +
                                        plantsegsleft[i-1].CExportRate)
            propRight = (plantsegsright[i].phloemFlow /
                          (plantsegsright[i].phloemFlow +
                            plantsegsleft[i].phloemFlow))
            plantsegsright[i].CImportRate = totalCImport * propRight
          elif (plantsegsright[i+1].phloemFlow < 0.0 and
                  plantsegsleft[i+1].phloemFlow > 0.0):
             # if right side down and left side up take from one that
                #is flowing up, minus amount flowing down
            propUp = (abs(plantsegsright[i].phloemFlow) /
                        (abs(plantsegsright[i].phloemFlow) +
                          abs(plantsegsleft[i+1].phloemFlow)))
            plantsegsright[i].CImportRate = (plantsegsleft[i+1].CExportRate
                                                          * propDown)

          elif (plantsegsright[i+1].phloemFlow > 0.0
                            and plantsegsleft[i+1].phloemFlow < 0.0):
             # if left side down and right side up take from one that
                 #is flowing up, minus amount flowing down
            propDown = (abs(plantsegsright[i].phloemFlow) /
                          (abs(plantsegsright[i].phloemFlow) +
                             abs(plantsegsleft[i+1].phloemFlow)))
            plantsegsright[i].CImportRate = (plantsegsright[i+1].CExportRate
                                        * propDown)

          else:
            assert "Something is not right in the state of phloemFlows."
        else: # if stems
          totalCImport = (plantsegsright[i+1].CExportRate +
                                        plantsegsleft[i+1].CExportRate)
          if ((abs(plantsegsright[i].phloemFlow) +
                 abs(plantsegsleft[i+1].phloemFlow +
                    plantsegsright[i+1].phloemFlow)) == 0.0):
            propRight=0.0
          else:
            propRight = (plantsegsright[i].phloemFlow /
                          (plantsegsright[i].phloemFlow +
                             plantsegsleft[i].phloemFlow))
          plantsegsright[i].CImportRate = totalCImport * propRight

    else: #if self.perfectMixing==FALSE:
      #This creates a list of tangential carbon transfer rates,
           #with pos for L to R, neg for R to L
      tangCarbonList=[]
      for i in range(0,len(self.phloemTangFlows)):
        if self.phloemTangFlows[i] == 0.0:
          tangCarbonList.append(0.0)
        elif self.phloemTangFlows[i] > 0.0:
         #Assuming positive is left to right; may need to change
          if plantsegsleft[1+i].phloemFlow < 0.0:
```

```
      # If positive contribution from above
       if plantsegsleft[2+i].phloemFlow > 0.0:
        # if positive contribution from below
         tangCarbonList.append(plantsegsleft[1+i].CExportRate+
                               plantsegsleft[2+i].CExportRate)
       else: # if negative contribution from below
         propLToRCross = (abs(self.phloemTangFlows[i]/
                               plantsegsleft[1+i].phloemFlow))
         tangCarbonList.append(propLToRCross *
                               plantsegsleft[1+i].CExportRate)
     else:
      # if negative contribution from above,
         #and positive from below (can't have negative for both)
       propLToRCross = (abs(self.phloemTangFlows[i]/
                               plantsegsleft[2+i].phloemFlow))
       tangCarbonList.append(propLToRCross *
                               plantsegsleft[2+i].CExportRate)
   else:
    #If flow is in other direction; Assuming positive is left to right;
    if plantsegsright[1+i].phloemFlow < 0.0:
     # If positive contribution from above
      if plantsegsright[2+i].phloemFlow > 0.0:
       # if positive contribution from below
        tangCarbonList.append(-(plantsegsright[1+i].CExportRate+
                              plantsegsright[2+i].CExportRate))
      else: # if negative contribution from below
        propLToRCross = abs(self.phloemTangFlows[i]/
                            plantsegsright[1+i].phloemFlow)
          #CHECK
        tangCarbonList.append(-propLToRCross *
                               plantsegsright[1+i].CExportRate)
     else:
      # if negative contribution from above,
       #and positive from below (can't have negative for both)
       propLToRCross = (abs(self.phloemTangFlows[i]/
                               plantsegsright[2+i].phloemFlow))
       tangCarbonList.append(-propLToRCross *
                               plantsegsright[2+i].CExportRate)

for i in range(0,plantsegnum):

  #LEFT SIDE
  if plantsegsleft[i].phloemFlow < 0.0:
   #Usual case - Phloem flows are ordinarily downward
    if i == 0: #i.e. if these are leaves
      plantsegsleft[i].CImportRate = plantsegsleft[i].LoadingRate
    else: # if not leaves
      if plantsegsleft[i].phloemFlow == plantsegsleft[i-1].phloemFlow:
       # if no crossover
        plantsegsleft[i].CImportRate = plantsegsleft[i-1].CExportRate
      elif plantsegsleft[i-1].phloemFlow < 0.0: #Flowing in
        plantsegsleft[i].CImportRate = (plantsegsleft[i-1].CExportRate -
          tangCarbonList[i-2])
            #tangCarbon + or - and "+" means left to right
      elif plantsegsleft[i-1].phloemFlow > 0.0: #Flowing out
```

```
      propTangToFocal = (abs(plantsegsleft[i].phloemFlow) /
                                      abs(self.phloemTangFlows[i-2]))
      plantsegsleft[i].CImportRate = (propTangToFocal *
                                          (-tangCarbonList[i-2]))
else: # if phloem flow is upward
  if i == 0:
    plantsegsleft[i].CImportRate = (plantsegsleft[i].LoadingRate +
                                     plantsegsleft[i+1].CExportRate)
  elif i == len(plantsegsleft)-1:
    plantsegsleft[i].CImportRate = 0.0 # flow is out of roots
  else:
    if plantsegsleft[i].phloemFlow == plantsegsleft[i+1].phloemFlow:
      plantsegsleft[i].CImportRate = plantsegsleft[i+1].CExportRate
    elif plantsegsleft[i+1].phloemFlow > 0.0: #Flowing in
      plantsegsleft[i].CImportRate = (plantsegsleft[i+1].CExportRate -
                                        tangCarbonList[i-1])
                                           #tangCarbon + or -
    elif plantsegsleft[i+1].phloemFlow < 0.0: #Flowing out
      propTangToFocal = (abs(plantsegsleft[i].phloemFlow) /
                             abs(self.phloemTangFlows[i-1]))
      plantsegsleft[i].CImportRate = (propTangToFocal *
                             (-tangCarbonList[i-1]))

#RIGHT SIDE
if plantsegsright[i].phloemFlow < 0.0:
 #Usual case - Phloem flows are ordinarily downward
  if i == 0: #i.e. if these are leaves
    plantsegsright[i].CImportRate = plantsegsright[i].LoadingRate
  else: # if not leaves
    if plantsegsright[i].phloemFlow == plantsegsright[i-1].phloemFlow:
     # if no crossover
      plantsegsright[i].CImportRate = plantsegsright[i-1].CExportRate
    elif plantsegsright[i-1].phloemFlow < 0.0: #Flowing in
      plantsegsright[i].CImportRate = (plantsegsright[i-1].CExportRate
                    + tangCarbonList[i-2]) #tangCarbon + or -
    elif plantsegsright[i-1].phloemFlow > 0.0: #Flowing out
      propTangToFocal = (abs(plantsegsright[i].phloemFlow) /
                                    abs(self.phloemTangFlows[i-2]))
      plantsegsright[i].CImportRate = (propTangToFocal *
                                     (tangCarbonList[i-2]))
else: # if phloem flow is upward
  if i == 0:
    plantsegsright[i].CImportRate = (plantsegsright[i].LoadingRate +
                                     plantsegsright[i+1].CExportRate)
  elif i == len(plantsegsright)-1:
    plantsegsright[i].CImportRate = 0.0 # flow is out of roots
  else:
    if plantsegsright[i].phloemFlow == plantsegsright[i+1].phloemFlow:
      plantsegsright[i].CImportRate = plantsegsright[i+1].CExportRate
    elif plantsegsright[i+1].phloemFlow > 0.0: #Flowing in
      plantsegsright[i].CImportRate = (plantsegsright[i+1].CExportRate
                          + tangCarbonList[i-1]) #tangCarbon + or -
    elif plantsegsright[i+1].phloemFlow < 0.0: #Flowing out
      propTangToFocal = (abs(plantsegsright[i].phloemFlow) /
                                    abs(self.phloemTangFlows[i-1]))
```

```
            plantsegsright[i].CImportRate = (propTangToFocal *
                                                (tangCarbonList[i-1]))

    assert plantsegsleft[i].CImportRate >=0.0, ("Import rate = "+
                              str(plantsegsleft[i].CImportRate)+
                              " Negative import rate on left illogical.")
    assert plantsegsright[i].CImportRate >=0.0, ("Negative import rate"+
                                                  " on right illogical.")



def calcVascularGrowthAndXylemN(self):
  #Pseudocode:
      #For fineroots, coarseroots, stem segments, branches
              # ...calculate N export from N import
              #
  self.left.fineroot.calcNExportRate()
  self.right.fineroot.calcNExportRate()
  self.left.coarseroot.calcGrowthNExport(self.left.fineroot.NExportRate)
  self.right.coarseroot.calcGrowthNExport(self.right.fineroot.NExportRate)
  NExportLeft=self.left.coarseroot.NExportRate
  NExportRight=self.right.coarseroot.NExportRate
  XylemFlowLeft=self.left.coarseroot.xylemFlow
  XylemFlowRight=self.right.coarseroot.xylemFlow
  stemsegnum=len(self.left.stemlist)
  for i in range(0,stemsegnum): #Note higher values are closer to bottom
    index = stemsegnum - 1 - i

    if self.perfectMixing == False:
      LToRCross = XylemFlowLeft - self.left.stemlist[index].xylemFlow
      if LToRCross > 0: # if crossover is from left to right
        propCrossover = LToRCross / XylemFlowLeft
        NImportLeft = NExportLeft * (1.0 - propCrossover)
        NImportRight = NExportRight + NExportLeft * propCrossover
      else: # if crossover is from right to left or 0
        propCrossover = -LToRCross / XylemFlowRight
        NImportRight = NExportRight * (1.0 - propCrossover)
        NImportLeft = NExportLeft + NExportRight * propCrossover
    else: #if self.perfectMixing==True:
      totalNImport=NExportLeft + NExportRight
      propNLeft=XylemFlowLeft/(XylemFlowLeft+XylemFlowRight)
      NImportLeft = totalNImport * propNLeft
      NImportRight = totalNImport * (1.0 - propNLeft)


    self.left.stemlist[index].calcGrowthNExport(NImportLeft)
    self.right.stemlist[index].calcGrowthNExport(NImportRight)

    NExportLeft=self.left.stemlist[index].NExportRate
    NExportRight=self.right.stemlist[index].NExportRate
    XylemFlowLeft=self.left.stemlist[index].xylemFlow
    XylemFlowRight=self.right.stemlist[index].xylemFlow

  if self.perfectMixing == False:
    LToRCross = XylemFlowLeft - self.left.branch.xylemFlow
```

```
    if LToRCross > 0: # if crossover is from left to right
      propCrossover = LToRCross / XylemFlowLeft
      NImportLeft = NExportLeft * (1.0 - propCrossover)
      NImportRight = NExportRight + NExportLeft * propCrossover
    else: # if crossover is from right to left or 0
      propCrossover = -LToRCross / XylemFlowRight
      NImportRight = NExportRight * (1.0 - propCrossover)
      NImportLeft = NExportLeft + NExportRight * propCrossover

  else: #if self.perfectMixing==True:
    totalImport=NExportLeft + NExportRight
    propLeft=XylemFlowLeft/(XylemFlowLeft+XylemFlowRight)
    NImportLeft = totalImport * propLeft
    NImportRight = totalImport * (1.0 - propLeft)

  self.left.branch.calcGrowthNExport(NImportLeft)
  self.right.branch.calcGrowthNExport(NImportRight)

  self.left.leaf.NImportRate = self.left.branch.NExportRate
  self.right.leaf.NImportRate = self.right.branch.NExportRate

#CALCULATE XYLEM FLOWS 1
def calcXylemFlows(self):
  """Uses circuit to calculate xylem flow through each component"""
  leftstemlistResist = []
  rightstemlistResist = []
  for i in range(0,len(self.left.stemlist)):
    leftstemlistResist.append(self.left.stemlist[i].xylemResist)
    rightstemlistResist.append(self.right.stemlist[i].xylemResist)
  flows=PlantCircuits.Flows(self.left.fineroot.Psi_x,
                  self.right.fineroot.Psi_x,
                  self.left.leaf.Psi_x, self.right.leaf.Psi_x,
                  self.left.fineroot.xylemResist +
                        self.left.coarseroot.xylemResist,
                  self.right.fineroot.xylemResist +
                        self.right.coarseroot.xylemResist,
                  self.left.leaf.xylemResist + self.left.branch.xylemResist,
                  self.right.leaf.xylemResist + self.right.branch.xylemResist,
                  leftstemlistResist, rightstemlistResist,
                  self.tangresistx, len(leftstemlistResist))
  self.left.setXylemFlows(flows[0])
  self.right.setXylemFlows(flows[1])
  self.xylemTangFlows=(-flows[2]).flatten().tolist()[0]
     #Hack fix for suboptimal data structure: Need to take first element
        #because comes back with a one element list of lists
  self.xylemTangFlows.reverse()

def calcPhloemFlows(self):
  """Uses circuit to calculate phloem flow through each component"""
  leftstemlistResist = []
  rightstemlistResist = []
  for i in range(0,len(self.left.stemlist)):
    leftstemlistResist.append(self.left.stemlist[i].phloemResist)
    rightstemlistResist.append(self.right.stemlist[i].phloemResist)
```

```
    flows=PlantCircuits.Flows(self.left.fineroot.Psi_p,
                    self.right.fineroot.Psi_p,
                    self.left.leaf.Psi_p, self.right.leaf.Psi_p,
                    self.left.fineroot.phloemResist +
                         self.left.coarseroot.phloemResist,
                    self.right.fineroot.phloemResist +
                         self.right.coarseroot.phloemResist,
                    self.left.leaf.phloemResist +
                         self.left.branch.phloemResist,
                    self.right.leaf.phloemResist +
                         self.right.branch.phloemResist,
                    leftstemlistResist, rightstemlistResist,
                    self.tangresistp, len(leftstemlistResist))
    #NOTE: "flows" is a sequence of matrices, although I refer to them
            #here as arrays
    self.left.setPhloemFlows(flows[0])
    self.right.setPhloemFlows(flows[1])
    self.phloemTangFlows=(-flows[2]).flatten().tolist()[0]
       #Hack fix for suboptimal data structure: Need to take first element
            #because comes back with a one element list of lists
    self.phloemTangFlows.reverse()


class Sector:
  sectorSegList = None
  version=None
  def __init__(self,version,stemsegments):
    self.version=version
    self.leaf=Leaf(version=version)
    self.branch=Branch(version=version)
    self.stemlist=[]
    for i in range (0, stemsegments):
      s = Stemsegment(version=version,index=i)
      s.biomass=s.biomass/stemsegments
      s.WC=s.WC/stemsegments
      s.WN=s.WN/stemsegments
      s.phloemC = s.phloemC/stemsegments
      s.k_resistx=s.k_resistx/stemsegments
      s.k_resistp=s.k_resistp/stemsegments
      s.length=s.length/stemsegments
      self.stemlist.append(s)
    #NOTE: "flows" is a sequence of matrices, although I refer to them
          #here as arrays
    self.coarseroot=Coarseroots(version=version)
    self.fineroot=Fineroots(version=version)
    self.update_derived()
    self.createSectorSegList()

  def update_derived(self):
    self.leaf.update_derived()
    self.branch.update_derived()
    self.coarseroot.update_derived()
    self.fineroot.update_derived()
    for seg in self.stemlist:
      seg.update_derived()
```

```
  def createSectorSegList(self):
    self.sectorSegList = ([self.leaf,self.branch]+
                          self.stemlist+
                          [self.coarseroot,self.fineroot])

  def calcCFixAndTransp(self):
    self.leaf.calcCFixAndTransp()

  def calcNImportRate(self):
    self.fineroot.calcNImportRate()

  def setXylemFlows(self,flowArray):
    stemsegments=len(self.stemlist)
    self.leaf.xylemFlow = float(flowArray[1+stemsegments])
    self.branch.xylemFlow = float(flowArray[1+stemsegments])
    for i in range (0, stemsegments):
      self.stemlist[i].xylemFlow=float(flowArray[stemsegments-i])
    self.coarseroot.xylemFlow = float(flowArray[0])
    self.fineroot.xylemFlow = float(flowArray[0])
    #NOTE: "flowArray"s are matrices, although I refer to them here as arrays
    # In the above code, "float" is used to extract values as floats
    #  rather than as matrices

  def setPhloemFlows(self,flowArray):
    stemsegments=len(self.stemlist)
    self.leaf.phloemFlow = float(flowArray[1+stemsegments])
    self.branch.phloemFlow = float(flowArray[1+stemsegments])
    for i in range (0, stemsegments):
      self.stemlist[i].phloemFlow=float(flowArray[stemsegments-i])
    self.coarseroot.phloemFlow = float(flowArray[0])
    self.fineroot.phloemFlow = float(flowArray[0])

class Segment:
  """Defines general segment object, parent to Leaf,
                          Branch, Coarseroots, Fineroots """
  ID = "None"
  biomass = 1.0
  length = 0.1 # meters
  WC = 0.01
  WN = 0.01
  phloemC = 0.1
  segmentVol = None # calculate as biomass / dry mass density
  phloemVol = None # calculate as segment vol * phloemVolRatio
  xylemVol = None # calculate as segment vol * xylemVolRatio
  dryMassDensity = 0.1 # g DW / ml wet volume
  xylemVolRatio = 0.05
  phloemVolRatio = 0.05
  k_resistx = 0.001
  k_resistp = 0.002
  k_Grw = 500.0 # 500 is value in Dewar
  m_C = 0.015
       # THIS VALUE USED BY Yang and Midmore FOR THRESHOLD NEEDED FOR
         #FUNCTION... DIFFERENT FROM MAINT METAB. COST
  tissueFractionN=0.03
```

```
tissueFractionC=0.45

xylemFlow = None
phloemFlow = None

NImportRate = None # Needs to be computed at plant level,
                     #except for fine roots
xylemNSapConc = None
xylemN = None # Computed as xylemVol * NImportRate / xylemFlow =
                                          #xylemVol * instantaneous conc.
NExportRate = None # Calculated as import rate - N allocated to growth
RGR = None # In order to check growth rates

localNAllocRate = None
NAllocRatePerLength = 3.0
CAllocRatePerLength = 3.0

phloemCSapConc = None
UnloadingRate = None

metabolism = None

growthRate = None
NGrowthAllocRate = None
CGrowthAllocRate = None

CExportRate = None
I = 0.04

concLabC = None
concLabN = None
concPhloemC = None # Computed as phloem C / biomass

def update_derived(self):
  self.calcXylemResistance()
  self.calcPhloemResistance()
  self.calcConcLabC()
  self.calcConcLabN()
  self.calcSegmentVol()
  self.calcPhloemVol()
  self.calcXylemVol()
  self.calcPhloemCSapConc()
  self.calcMetabolism()
  self.calcConcPhloemC()

def calcUnloadingRate(self): #Will apply to Branches, Stems, Coarseroots
  # biomass * const * sap conc / (labile conc * tissue density)
  self.UnloadingRate = (self.CExportRate * self.CAllocRatePerLength *
                                                          self.length)

def calcMetabolism(self):
  self.metabolism = self.biomass * self.m_C

def calcCExportRate(self):
  self.CExportRate=self.phloemCSapConc * abs(self.phloemFlow)
```

```
def calcPhloemCSapConc(self):
  self.phloemCSapConc = self.phloemC / self.phloemVol

def calcRGR(self):
  self.RGR = self.growthRate / self.biomass

def calcGrowthNExport(self, rateNimport):
  self.NImportRate = rateNimport
  self.calcConcXylemN() #Not actually needed
  self.calcLocalNAllocRate()
  self.calcNExportRate()

  #Growth; not related to N export in this version, but included
                              #for consistency with previous versions
  self.calcGrowthRateAlloc()
        # scales with product of concPhloemC and concXylemN ;
           #may need to play some with order of operations

def calcLocalNAllocRate(self):
  self.localNAllocRate = (self.NImportRate * self.NAllocRatePerLength *
                                                              self.length)

def calcNExportRate(self):
  self.NExportRate = self.NImportRate - self.localNAllocRate

def calcGrowthRateAlloc(self):
  #Michaelis-Menten
  self.growthRate = (self.biomass * (self.concLabC- self.m_C) *
                                          self.concLabN * self.k_Grw)
  self.calcNGrowthAllocRate()
  self.calcCGrowthAllocRate()

def calcNGrowthAllocRate(self):
  self.NGrowthAllocRate = self.growthRate * self.tissueFractionN

def calcCGrowthAllocRate(self):
  self.CGrowthAllocRate = self.growthRate * self.tissueFractionC

def calcPhloemVol(self):
  self.phloemVol = self.segmentVol * self.phloemVolRatio

def calcXylemVol(self):
  self.xylemVol = self.segmentVol * self.xylemVolRatio

def calcSegmentVol(self):
  self.segmentVol = self.biomass / self.dryMassDensity

def calcConcPhloemC(self):
  """Calculates concentration of carbon"""
  self.concPhloemC = self.phloemC / self.biomass

def calcConcXylemN(self):
  """Calculates concentration of carbon"""
  self.xylemNSapConc = self.NImportRate / self.xylemFlow
```

```
    self.xylemN = self.xylemNSapConc * self.xylemVol
    self.concXylemN = self.xylemN / self.biomass

  def calcConcLabC(self):
    """Calculates concentration of carbon"""
    self.concLabC = self.WC / self.biomass

  def calcConcLabN(self):
    """Calculates concentration of nitrogen"""
    self.concLabN = self.WN / self.biomass

  def calcXylemResistance(self):
    """Calculates xylem axial resistance for component"""
    self.xylemResist = self.k_resistx / self.biomass

  def calcPhloemResistance(self):
    """Calculates Phloem axial resistance for component"""
    self.phloemResist =  self.k_resistp / self.biomass

class Coarseroots(Segment):
  """Defines coarseroots object"""
  def __init__ (self,version=3):
    self.ID="coarse roots"
    self.version=version
    self.update_derived()

class Branch(Segment):
  """Defines branch object"""
  def __init__ (self,version=3):
    self.ID="branches"
    self.version=version
    self.update_derived()

class Stemsegment(Segment):
  """Defines segment of stem"""
  def __init__ (self,version=3,index=0):
    self.ID="stem seg "+str(index+1)
    self.version=version
    self.update_derived()

class ActiveBiomass(Segment):
  biomass = 1.0
  length = 0.1 # meters
  k_Psip = 2.478*1000/144 #Osmotic parameter
  """Creates activebiomass object, i.e. leaves or fine roots"""

  def update_derived(self):
    Segment.update_derived(self)
        # calls parental class's update_derived function
    self.calcPhloemWaterPotl()

  def calcGrowthRateAlloc(self):
    #Michaelis-Menten from old model
    self.growthRate = (self.biomass * (self.concLabC-self.m_C) *
                                            self.concLabN * self.k_Grw)
```

```
    self.calcNGrowthAllocRate()
    self.calcCGrowthAllocRate()

  def calcPhloemWaterPotl(self):
    """Calculates phloem water potential based on carbon in phloem...
                          For now only meaningful for leaves and roots."""
    self.Psi_p = self.k_Psip * self.phloemCSapConc
            #Note that k_Psip needs to incorporate mol glucose / g C

class Leaf(ActiveBiomass):
  """Creates leaf object"""
  Ls = 1.0  #Light environment parameter
  sigma_Cs = 0.1
  k_Cl = 0.1
  Wwater = 8.0
  CExportFraction = 0.8
  Psi_x=None
  Psi_pressx=None
  Psi_osmox=None
  boundaryConductH2O = 0.05 * 60.0 * 60.0 * 24.0
          # For calculating leaf properties; not currently needed
  transpWater = None #leafProps[0]
  stomatalConductH2OWater = None #leafProps[2]
  stomatalConductCO2Water = None #leafProps[3]
  relLeafWater = None #leafProps[4]
  transp = None
  transpRatio = 750.0
      # 750 g H2O / gC = 500 mol H2O / mol C =
                        # typical transp ratio for C3 plants T&Z p.99
  NExportRate = 0 # WARNING: This value should never change
  CFix = None
  LoadingRate = None
  rigidMod=5.0
  WlMin=0.000001

  def __init__ (self,version):
    self.ID="leaves"
    self.version=version
    self.update_derived()

  def update_derived(self):
    ActiveBiomass.update_derived(self)
              # calls parental class's update_derived function
    self.calcXylemWaterPotl()
    self.calcCFixAndTransp()
    self.calcLoadingRate()

  def calcArea(self):
    self.area = self.biomass * self.a_ls

  def calcLoadingRate(self):
    self.LoadingRate = self.CFix * self.CExportFraction

  def calcCFixAndTransp(self):
    self.calcCFix()
```

```
    self.calcTranspiration()

  def calcTranspiration(self):
    self.transp = self.transpRatio * self.CFix
                  #transpRatio = g H2O lost per g C fixed

  def calcCFix(self):
    """Old model for photosynthesis if determined by light function"""
    self.CFix = self.biomass * self.Ls * self.sigma_Cs

  def calcXylemWaterPotl(self):
    """Calculates water potential using leafprops file...
                            For now only meaningful for leaves."""
    leafProps = leafprops.computeLeafProps(curWaterCont=self.Wwater,
                        leafDryWeight=self.biomass,
                        boundaryConductH2O=self.boundaryConductH2O,
                        WlMin=self.WlMin,
                        rigidMod=self.rigidMod)

    #THIS STUFF IS ESSENTIAL, especially Psi_x
    self.Psi_x=leafProps[1]
    self.Psi_pressx=leafProps[5]
    self.Psi_osmox=leafProps[6]

    #THIS STUFF NOT NEEDED IN GROWTH MODEL (DISSERTATION CHAPTER 6)
    self.transpWater = leafProps[0]
    self.stomatalConductH2OWater = leafProps[2]
    self.stomatalConductCO2Water = leafProps[3]
    self.relLeafWater = leafProps[4]


class Fineroots(ActiveBiomass):
  """Create fineroots object """
  Nr = 0.02 #Nutrient environment parameter
  NrNEW = 0.5 #Nutrient environment parameter
  NrNEW_High = 0.5
  NrNEW_Low = 0.05
  NrNEW_Mode = "Steady"
  altinterval = 5.0
  alttime = 5.0
  Psi_x=0.0
  NImportRate = None
  CcostNImportRate = None
  k_mNImport = 0.5
  NExportRate = None
  NExportFraction = 0.6
  sigma_NrNEW = 0.1

  def __init__ (self,version):
    self.ID="fine roots"
    self.version=version
    self.update_derived()

  def update_derived(self):
    self.calcNImportRate()
```

```
      #calculates N uptake and carbon cost of that uptake
  self.calcNExportRate()
  ActiveBiomass.update_derived(self)
      # calls parental class's update_derived function

def calcUnloadingRate(self): #Will apply to fineroots only
  # biomass * const * sap conc / (labile conc * tissue density)
  self.UnloadingRate = (self.biomass * self.I * self.phloemCSapConc /
                              (self.concLabC * self.dryMassDensity))

def calcNrNEW(self,time):
  if self.NrNEW_Mode=="Steady":
    self.NrNEW = self.NrNEW
  elif self.NrNEW_Mode=="Alternate":
    if time > self.alttime:
      if self.NrNEW < (self.NrNEW_Low + self.NrNEW_High)/2:
        self.NrNEW = self.NrNEW_High
      else:
        self.NrNEW = self.NrNEW_Low
      self.alttime = self.alttime+self.altinterval
  elif self.NrNEW_Mode=="Sinusoid":
    if time > self.alttime:
      if self.NrNEW < (self.NrNEW_Low + self.NrNEW_High)/2:
        self.NrNEW = ((self.NrNEW_High - self.NrNEW_Low) *
           (1.0 + cos((time-self.alttime)*pi/self.altinterval))/2 +
                                                    self.NrNEW_Low)
      else:
        self.NrNEW = ((self.NrNEW_High - self.NrNEW_Low) *
              (1.0 - cos((time-self.alttime)*pi/self.altinterval))/2 +
                                                    self.NrNEW_Low)
  else:
    assert "Undefined N uptake mode."

def calcNExportRate(self):
  self.NExportRate = self.NImportRate * self.NExportFraction

def calcCExportRate(self):
  if self.phloemFlow < 0.0: # Downward
    self.CExportRate = 0.0
  else: # Upward
    self.CExportRate = self.phloemCSapConc * self.phloemFlow
                                            # g/ml * ml/day = g/day


def calcNImportRate(self):
  """Calculates N uptake rate... essentially is root biomass x constant """
  self.NImportRate=self.biomass * self.NrNEW * self.sigma_NrNEW
  self.CcostNImportRate = self.k_mNImport * self.NImportRate
  #NOTE: Yang and Midmore (2005) use a more complicated
                #function with negative feedbacks
```

8.2 Ohm's law circuit definitions

This code does the work of generating and solving electrical circuits for sectored plants at each time step. When incorporated into a python file titled "PlantCircuits.py" together with files containing the code in other sections, these functions can be imported for local use.

```
# Imports standard python package "numpy" which handles matrices
from numpy import *
import PlantDataStructures

# NOTE: All circuits in this file represent two-sector plants.
   # The variable "sectnum" is always set to 2.  In principle it
   # would be possible to generate more complicated circuits, but
   #that remains to be implemented.
#
# Plants and plant modules defined in the file PlantDataStructures
   #also assume two-sector plants.

# Top-level function for defining circuit and calculating sap flows
   # through each component.
def Flows(vr1,vr2,vl1,vl2,rr1,rr2,rl1,rl2,raxlist1,raxlist2,rtan,loopnum):
            """Define intersector flows for 2 sector plant."""
            print "vr1=",vr1,"vr2=",vr2,"vl1=",vl1,"vl2=",vl2
            sectnum=2
            IA=CircuitSolveVariedAxial(vr1,vr2,vl1,vl2,rr1,rr2,rl1,
                                       rl2,raxlist1,raxlist2,rtan,loopnum)
            for itemI in IA:
              for itemJ in itemI:
                assert ((not isnan(itemJ)) & (not isinf(itemJ))), "Inf. flows."
            print str(IA)
            print "length IA", str(len(IA))

            flows1=IA[0,0]-IA[1:loopnum+3,0]
            flows2=IA[1:loopnum+3,0]
            tangFlows=IA[1:loopnum+2]-IA[2:loopnum+3]
            print "length flows1", str(len(flows1))

            return flows1, flows2, tangFlows


def CircuitSolveVariedAxial(vr1,vr2,vl1,vl2,rr1,rr2,rl1,rl2,
                                      raxlist1,raxlist2,rtan,loopnum):
            """Calculate flow rates for 2 sector plant."""

            #creates matrix templates
            idsectA=identity(loopnum+3)
            idplusA=concatenate((idsectA[1:loopnum+3],idsectA[0:1]))
            idminusA=concatenate((idsectA[loopnum+2:loopnum+3],
                                        idsectA[0:loopnum+2]))
```

```
            plantlist1downward=concatenate(([rl1],raxlist1,[rr1],[0.0]))
            plantlist2downward=concatenate(([rl2],raxlist2,[rr2],[0.0]))
            plantlist1upward=list(plantlist1downward)
            plantlist1upward.reverse()
            plantlist2upward=list(plantlist2downward)
            plantlist2upward.reverse()

            RA=-rtan*(idplusA + idminusA) + (2*rtan+array(plantlist1upward)+
                                    array(plantlist2upward))*(idsectA)
            RA[loopnum+2,loopnum+2]= rtan + rl1 + rl2
            RA[1,1] = rtan + rr1 + rr2
            RA[0:loopnum+3,0], RA[0,0:loopnum+3] = (-array(plantlist1upward),
                                                    -array(plantlist1upward))
                                              #accounts for side of circuit

            RA[0,0]=sum(raxlist1)+rl1+rr1 #side of circuit

            RAmatrix=matrix(RA)
            EB=zeros((loopnum+3,1))*0.0
            #Assume positive Psi for roots, negative Psi for leaves
                #(with respect to upward flow) outside loop is on left
                #and loop currents are always counterclockwise
            EB[0,0]=vr1-vl1
            EB[1,0]=vr2-vr1
            EB[loopnum+2,0]=vl1-vl2
            EBmatrix=matrix(EB)
            print EBmatrix

            IAmatrix=(RAmatrix**(-1))*EBmatrix
            return IAmatrix


def SectorSelf((rootstem,stemleaf)):
   """Returns matrix characterizing flow within a sector."""
   mat = matrix(zeros((3,3)))
   if stemleaf>=0.0:
     mat[1,0]=stemleaf
     mat[0,0]=1.0
   else:
     mat[0,1]=1.0
   if rootstem>=0.0:
     mat[2,1]=1.0
   else:
     mat[1,2]=-rootstem
     mat[2,2]=1.0
   return mat

def SectorNext(tangplus):
   """Returns matrix characterizing flow to next sector over."""
   return matrix([[0.0,0.0,0.0],\
                  [0.0,max(tangplus,0.0),0.0],\
                  [0.0,0.0,0.0]])

def positives(list):
  """Returns list with positive elements,
```

```
                    replacing other elements with zeros. """
  return map(max,zip(zeros(len(list)),list))

def netflows(list1,list2,list3):
  return map(sum,(map(positives,zip(list1,list2,list3))))

class CircuitError(Exception):
  def __init__(self,value):
    self.value=value
  def __str__(self):
    return repr(self.value)

def listrotateplusN(tup,n):
  list2=list(tup)
  listlen=len(list2)
  return list2[listlen-n:listlen]+list2[0:listlen-n]

def diagonal(listlist):
  for i in range(0,len(listlist)):
    listlist[i]=listrotateplusN(listlist[i],i)
  return listlist

def MatrixCondense(mat,unitsize,fromunit,tounit):
  newmatsize=len(mat)/unitsize
  newmat=zeros((newmatsize,newmatsize))
  for i in range(0,newmatsize):
    for j in range(0,newmatsize):
      newmat[i,j]=mat[unitsize*i+fromunit, unitsize*j+tounit]
  return newmat
```

8.3 Models for leaf hydraulics

This code includes functions for calculating leaf water potential, stomatal conductance, and transpiration physics. When incorporated into a python file titled "leafprops.py", these functions can be imported for local use.

```
# Import standard python package for calculating square roots, etc.
import math

def quadPos(a, b, c):
    """Choose only positive, real root of quadratic solution."""

    discriminant = b*b-4*a*c
    assert discriminant >= 0, "Can't have complex roots for this quadratic."

    root1 = (-b + math.sqrt(discriminant))/(2*a)
    root2 = (-b - math.sqrt(discriminant))/(2*a)
    minRoot = min(root1, root2)
    maxRoot = max(root1, root2)

    assert minRoot <= 0, "Can't have two positive roots."
    assert maxRoot >= 0, "Can't have two non-positive roots."
    return maxRoot

if __name__ == "__main__":
    assert quadPos(1, -1, -2) == 2.0

def transp(stomWaterConduct,
                    Wl,
                    satDenseDeltaByTemp = 1.01, # change in saturating
                               #water vapor density with
                               #temperature (s)
                               # units = g / K^(-1) m(-3)
                               # = 0.00101 (kg K^(-1) m(-3))
                               #(constant for T=20C)
                    nrg4Evap = 400.0 * 60.0 * 60.0 * 24.0,
                               # units = MPa g / (day m^2)
                               #      =  W / m^2 / (60 * 60 * 24 s/day)
                               #energy available for evaporation (phi_N)
                    enthalpyBoil = 2450.0, # (MPa) = J kg^(-1) / 1000
                                  #(const at 20C) latent heat of
                                  #vaporization of water (lambda)
                    psychro = 0.495, #  g / (K m^3) =
                                  #0.000495 (kg K^(-1) m(-3))
                                  #(constant for T=20C)
                                  #psychrometric parameter (gamma)
                    boundaryConductH2O = 0.05 * 60.0 * 60.0 * 24.0,
                         # m/day = 0.05 (m/s)
                         #boundary layer conductance for
                         #water vapor (g_a)
                    vaporDenseDef = 7.5,
                         # g/(m^3) units= 0.0075 (kg m(-3))
```

```
                        #vapor density  deficit (Delta rho_va)
                        #(assumes T=20C and h_r = 0.57)
                    WlMin=0.000001
            ):
     if Wl <= WlMin:
       return 0.0
     else:
       return (satDenseDeltaByTemp * nrg4Evap + enthalpyBoil *
                     psychro * boundaryConductH2O *
                     vaporDenseDef) / (enthalpyBoil *
                     (satDenseDeltaByTemp + psychro *
                     (1 + boundaryConductH2O / stomWaterConduct)))


def presPotlFun(curWaterCont,
                structDryWeight,
                rigidMod=1.0, #MPa
                strToWaterMassRatio=0.15
                        #structure to water ratio unstretched
                ):
    """Returns pressure potential given non-zero dry weight"""
    return max(0.0, rigidMod *
            (strToWaterMassRatio * curWaterCont / structDryWeight - 1) )


def computeLeafProps(curWaterCont, # current water content (Q_pl)
                     leafDryWeight, # dry weight of leaf (W)
                     fracCellWall = 0.87393,
                      # from W_G : W_S :: 0.4 : 0.0577 -- W_G / (W_G + W_S)
                     curTempC = 20, # current temperature in Celsius (T)
                     avgMolMassOsmoStorageMatter = 20,
                            # mean molecular mass of soluble
                               #dry storage matter (mu)
                     r_s_min = 0.00000000001,
                             # day/m used in stomatal resistance
                     r_s_theta = 25000.0 / (60 * 60 * 24),
                             # day/m= 25000.0 s/m
                             # used in stomatal resistance
                     rigidMod = 1.0,
                          # MPa rigidity modulus (units of Pa) (epsilon)
                     satDenseDeltaByTemp = 1.01, # change in saturating
                                                 #water vapor density with
                                                 #temperature (s)
                                                 # units = g / K^(-1) m(-3)
                                                 # = 0.00101 (kg K^(-1) m(-3))
                                                 #(constant for T=20C)
                     nrg4Evap = 400.0 * 60.0 * 60.0 * 24.0,
                               # units = MPa g / (day m^2)
                               #      =  W / m^2 / (60 * 60 * 24 s/day)
                               #energy available for evaporation (phi_N)
                     enthalpyBoil = 2450.0, # (MPa) = J kg^(-1) / 1000
                                    #(const at 20C) latent heat of
                                    #vaporization of water (lambda)
                     psychro = 0.495, #  g / (K m^3) =
                                                 #0.000495 (kg K^(-1) m(-3))
```

```
                                #(constant for T=20C) psychrometric
                                                #parameter (gamma)
                    boundaryConductH2O = 0.05 * 60.0 * 60.0 * 24.0,
                                #m/day = 0.05 (m/s)
                                #boundary layer conductance for
                                        #water vapor (g_a)
                    vaporDenseDef = 7.5, # g/(m^3) units= 0.0075 (kg m(-3))
                                #vapor density  deficit (Delta rho_va)
                                #(assumes T=20C and h_r = 0.57)
                                #[for reference: (17.3 (saturating) -
                                        # 1.20 (dry) at T=20C)]
                    densityWater = 1000000.0, # density of liquid water
                       # g/(m^3) = (1000 g/kg * 1000 kg / m^(-3)) (rho_w)
                    solublePerStorage = 1.0,
                     # (f_0) = fraction of W_S that is soluble (default=1)
                    strToWaterMassRatio = 0.15, # kg structure / kg water
                    WlMin=0.000001
                    ):
"""Compute transpiration and water potential given current water content,
        non-zero dry weight of the leaf, and optional constants."""

gasConstant = 8.314         # g MPa / (mol * K) = 8314 J / (kgmol * K)
                                # gas constant (R)

curTempK = curTempC + 273.15;

# Dry weight of cell wall (W_G)
structDryWeight = leafDryWeight * fracCellWall

# Dry weight of cell contents, etc. (W_S)
storageDryWeight = leafDryWeight - structDryWeight

# pressure potential (Psi_P) -- eq 15.16g on 444
presPotl = presPotlFun(rigidMod=rigidMod,
                       strToWaterMassRatio=strToWaterMassRatio,
                       curWaterCont=curWaterCont,
                       structDryWeight=structDryWeight)

# osmotic potential (Psi_O) -- eq 15.16i on 444
if leafDryWeight<=WlMin:
  osmoPotl = 0.0
      #Supplies arbitrary finite value to ensure non-infinite Psi
else:
  osmoPotl = -(gasConstant * curTempK * solublePerStorage *
       storageDryWeight) / (avgMolMassOsmoStorageMatter * curWaterCont)

# Water content of leaf when leaf water potential is 0 -- eq 15.17a on 445
# a.k.a. Q_pl when solved with Psi_pl=0
satWaterCont = quadPos(rigidMod * strToWaterMassRatio /
                                            (structDryWeight),
                       - rigidMod,
                       - gasConstant * curTempK * solublePerStorage *
                          storageDryWeight / avgMolMassOsmoStorageMatter)

# plant relative water content (theta_pl) -- eq 15.15f on 443
```

```
    plRelWaterCont = curWaterCont / satWaterCont

    # stomatal resistance (r_s) -- 15.21d on 448
    stomResist = r_s_min + r_s_theta * (max(0.0,1.0 - plRelWaterCont))
    stomCO2Conduct = 1.0 / stomResist

    # stomatal conductance for water vapor (g_c (c = "canopy") or
         #g_s,h20 (s = "stomatal")) -- eq 15.22b on 449
    molMass_CO2 = 44.0 # molar mass of CO2 (mu_CO2)
    molMass_H20 = 18.0 # molar mass of H20 (mu_H20)
    stomWaterConduct = stomCO2Conduct * math.sqrt(molMass_CO2 / molMass_H20)

    # transpiration rate from canopy (E) -- eq 14.4k on 408
    transpRate = transp(stomWaterConduct=stomWaterConduct,
                        satDenseDeltaByTemp=satDenseDeltaByTemp,
                        nrg4Evap=nrg4Evap,
                        enthalpyBoil=enthalpyBoil,
                        psychro=psychro,
                        boundaryConductH2O=boundaryConductH2O,
                        vaporDenseDef=vaporDenseDef,
                        Wl=leafDryWeight,
                        WlMin=WlMin)

    # leaf water potential (Psi_pl)
    leafWaterPotl = presPotl + osmoPotl

    return (transpRate, leafWaterPotl , stomWaterConduct, stomCO2Conduct,
                      plRelWaterCont,presPotl,osmoPotl)
        # Units: transpRate g / (day m^2); Psi in MPa; stomCond m/day

if __name__ == "__main__":
    print computeLeafProps(10.0, 1.0)
```

8.4 Setting up and running simulation

The code below is an example command sequence for simulating plant growth under a time varied nutrient scenario. The assigned value "Alternate" for the variable NRNEW_MODE sets up a scenario where nitrogen availability alternates between high and low levels for each half of the root system. The code first generates a collection of plants for factorial scenarios of: high and low tangential resistance for xylem and for phloem, and patches with duration of either 15 days or 30 days. These plants are created and added to the list of plants by the nested for-loop. After this definition, the simulation is then run for 5 days without a nutrient patch, and then for 60 days with a nutrient patch. The location of the patch changes at intervals defined by the variable ALTINTERVAL.

```
# Imports file defining plant module, sector, and whole plant data structures
from PlantDataStructures import *

# Function to make plant "Plant" grow for "time" days, and then output
#  its biomass distribution to the file "outfile1".  "outfile1" will be
#  formatted for graphical output using the R "pyramid" package.
def growOutput(Plant,time,outfile1):
  Plant.grow(time)
  Plant.outputBiomass(outfile1)

#Variable specifying how nutrient patterns change
NrNEW_Mode = "Alternate"
#Creates an empty list to be flled with plant objects
plants=[]
#These for-loops cycle through alternative values for tangential resistance
# parameter for xylem (k_tangx), tangential resistance parameter for phloem
# (k_tangp), and the duration of the nutrient patches, measured in days
# (altinterval).
#Note that 0.0 for tangential resistance parameters means perfect integration,
# and 10.0 represents high sectoriality.
for k_tangx in [0.0,10.0]:
  for k_tangp in [0.0,10.0]:
    for altinterval in [15.0,30.0]:
      #create a plant object, p, using version 3 of the code
      # WARNING: Versions other than 3 represent mathematical variations that
      #       do not work as well or may have been only partially implemented.
      p = Plant(version=3)
      #set biomasses at start for all modules of left sector
      p.left.fineroot.biomass=0.78
      p.left.coarseroot.biomass=0.25
      p.left.stemlist[0].biomass=0.046
      p.left.stemlist[1].biomass=0.049
      p.left.stemlist[2].biomass=0.052
```

```
p.left.stemlist[3].biomass=0.054
p.left.stemlist[4].biomass=0.057
p.left.branch.biomass=0.22
p.left.leaf.biomass=0.5

#set labile carbon masses (WC) at start for all modules of left sector
p.left.leaf.WC=0.13
p.left.branch.WC=0.17
p.left.stemlist[0].WC=0.029
p.left.stemlist[1].WC=0.023
p.left.stemlist[2].WC=0.018
p.left.stemlist[3].WC=0.013
p.left.stemlist[4].WC=0.0078
p.left.coarseroot.WC=0.0052
p.left.fineroot.WC=0.027

# set phloem carbon masses (phloemC) at start for
                                    #all modules of left sector
p.left.leaf.phloemC=0.0047
p.left.branch.phloemC=0.0016
p.left.stemlist[0].phloemC=0.00032
p.left.stemlist[1].phloemC=0.00032
p.left.stemlist[2].phloemC=0.00032
p.left.stemlist[3].phloemC=0.00031
p.left.stemlist[4].phloemC=0.00031
p.left.coarseroot.phloemC=0.0011
p.left.fineroot.phloemC=0.0015

# set label nitrogen masses (WN) at start for all modules of left sector
p.left.leaf.WN=0.00022
p.left.branch.WN=0.00003
p.left.stemlist[0].WN=0.0000083
p.left.stemlist[1].WN=0.000012
p.left.stemlist[2].WN=0.000017
p.left.stemlist[3].WN=0.000028
p.left.stemlist[4].WN=0.000053
p.left.coarseroot.WN=0.0050
p.left.fineroot.WN=0.0046

# set water content (Wwater) for leaf module of left sector
p.left.leaf.Wwater=3.0


# set biomasses at start for all modules of right sector
p.right.fineroot.biomass=0.78
p.right.coarseroot.biomass=0.25
p.right.stemlist[0].biomass=0.046
p.right.stemlist[1].biomass=0.049
p.right.stemlist[2].biomass=0.052
p.right.stemlist[3].biomass=0.054
p.right.stemlist[4].biomass=0.057
p.right.branch.biomass=0.22
p.right.leaf.biomass=0.5

# set carbon masses (WC) at start for all modules of right sector
```

```
p.right.leaf.WC=0.13
p.right.branch.WC=0.17
p.right.stemlist[0].WC=0.029
p.right.stemlist[1].WC=0.023
p.right.stemlist[2].WC=0.018
p.right.stemlist[3].WC=0.013
p.right.stemlist[4].WC=0.0078
p.right.coarseroot.WC=0.0052
p.right.fineroot.WC=0.027

# set phloem carbon masses (phloemC) at start
   #for all modules of right sector
p.right.leaf.phloemC=0.0047
p.right.branch.phloemC=0.0016
p.right.stemlist[0].phloemC=0.00032
p.right.stemlist[1].phloemC=0.00032
p.right.stemlist[2].phloemC=0.00032
p.right.stemlist[3].phloemC=0.00031
p.right.stemlist[4].phloemC=0.00031
p.right.coarseroot.phloemC=0.0011
p.right.fineroot.phloemC=0.0015

# set nitrogen masses (WN) at start for all modules of right sector
p.right.leaf.WN=0.00022
p.right.branch.WN=0.00003
p.right.stemlist[0].WN=0.0000083
p.right.stemlist[1].WN=0.000012
p.right.stemlist[2].WN=0.000017
p.right.stemlist[3].WN=0.000028
p.right.stemlist[4].WN=0.000053
p.right.coarseroot.WN=0.0050
p.right.fineroot.WN=0.0046

# set water content for leaf module of right sector
p.right.leaf.Wwater=3.0

# for left and right root environments, define values for high and low N
p.left.fineroot.NrNEW_High=0.5
p.right.fineroot.NrNEW_High=0.5
p.left.fineroot.NrNEW_Low=0.05
p.right.fineroot.NrNEW_Low=0.05

# initialize both root environments with low N
p.left.fineroot.NrNEW=p.left.fineroot.NrNEW_Low
p.right.fineroot.NrNEW=p.right.fineroot.NrNEW_Low

# define how nutrient environment will dynamically vary
#  (see definition of NrNEW_Mode above)
p.left.fineroot.NrNEW_Mode=NrNEW_Mode
p.right.fineroot.NrNEW_Mode=NrNEW_Mode

# define patch duration for each root environment, based on value
#  for this cycle through the nested for-loop
p.left.fineroot.altinterval=altinterval
p.right.fineroot.altinterval=altinterval
```

```
        # define light level for each leaf environment
        p.left.leaf.Ls=2.0
        p.right.leaf.Ls=2.0

        # define xylem and phlome tangential resistance parameters for this
        #  cycle through nested for-loop
        p.k_tangx = k_tangx
        p.k_tangp = k_tangp

        # create a unique name for the output file for this plant's data
        p.setOutfile(filename="TimeSeries"+NrNEW_Mode+
                     str(round(p.left.fineroot.altinterval,1))+
                     "_k_tangx"+str(round(k_tangx,2))+"_k_tangp"+
                     str(round(k_tangp,2))+".csv",printinterval=1.0)

        # make sure that variable definitions are incorporated into
             # other aspects of plant traits
        p.update_derived()

        # Add our new plant p to the plant list "plants"
        plants.append(p)
#END OF LOOPS

# Defines day at which nutrient patch will be added
time0=5

# Applies growthOutput function (defined above) to all individuals in the
#   list "plants".  Here, each plant is grown for "time0" days, and data is
#   output to a unique file for graphing using the R "pyramid" package.
[growOutput(p,time0,"BiomassDistrLonger"+p.left.fineroot.NrNEW_Mode+
   str(round(p.left.fineroot.altinterval,1))+"_ktangx"+str(p.k_tangx)+
   "_ktangp"+str(p.k_tangp)+"_time"+str(round(p.time-time0,3))+".csv")
   for p in plants]

# Introduces nutrient patch:
for p in plants:
  p.left.fineroot.NrNEW=p.left.fineroot.NrNEW_High

# Runs simulation for 60 days
[growOutput(p,60,"BiomassDistrLonger"+p.left.fineroot.NrNEW_Mode+
   str(round(p.left.fineroot.altinterval,1))+"_ktangx"+str(p.k_tangx)+
   "_ktangp"+str(p.k_tangp)+"_time"+str(round(p.time-time0,3))+".csv")
   for p in plants]

# Closes file
for p in plants:
  p.closeOutfile
```

References

Andrews, M., J. A. Raven, P. J. Lea, and J. I. Sprent. 2006. A role for shoot protein in shoot-root dry matter allocation in higher plants. Annals of Botany **97**:3–10.

Anten, N. P. R., and F. Schieving. 2010. The role of wood mass density and mechanical constraints in the economy of tree architecture. The American Naturalist **175**:250–260.

Babst, B. A., R. A. Ferrieri, D. W. Gray, M. Lerdau, D. J. Schlyer, M. Schueller, M. R. Thorpe, and C. M. Orians. 2005. Jasmonic acid induces rapid changes in carbon transport and partitioning in Populus. New Phytologist **167**:63–72.

Babst, B. A., R. A. Ferrieri, M. R. Thorpe, and C. M. Orians. 2008. *Lymantrial dispar* herbivory induces rapid changes in carbon transport and partitioning in *Populus nigra*. Entomologia **128**:117–125.

Bledsoe, T. M., and C. M. Orians. 2006. Vascular pathways constrain C-13 accumulation in large root sinks of Lycopersicon esculentum (Solanaceae). American Journal of Botany **93**:884–890.

Bliss, K. M., R. H. Jones, R. J. Mitchell, and P. P. Mou. 2002. Are competitive interactions influenced by spatial nutrient heterogeneity and root foraging behavior? New Phytologist **154**:409–417.

Breshears, D. D., P. M. Rich, F. J. Barnes, and K. Campbell. 1997. Overstory-imposed heterogeneity in solar radiation and soil moisture in a semiarid woodland. Ecological Applications **7**:1201–1215.

Caldwell, M. M., T. E. Dawson, and J. H. Richards. 1998. Hydraulic lift: consequences of water efflux from the roots of plants. Oecologia **113**:151–161.

Cambui, C. A., H. Svennerstam, L. Gruffman, A. Nordin, U. Ganeteg, and T. Näsholm. 2011. Patterns of Plant Biomass Partitioning Depend on Nitrogen Source. PLoS ONE **6**:e19211.

Campbell, B. D., J. P. Grime, and J. M. Mackey. 1991. A trade-off between scale and precision in resource foraging. Oecologia **87**:532–538.

Canham, C. D. 1985. Suppression and Release during Canopy Recruitment in Acer saccharum. Bulletin of the Torrey Botanical Club **112**:134–145.

Caraco, T., and C. K. Kelly. 1991. On the Adaptive Value of Physiological Integraton in Colonal Plants. Ecology **72**:81–93.

Chiou, T. J., and D. R. Bush. 1998. Sucrose is a signal molecule in assimilate partitioning. Proceedings of the National Academy of Sciences **95**:4784–4788.

Choat, B., A. R. Cobb, and J. S. 2007. Structure and function of bordered pits: New discoveries and impacts on whole plant hydraulic function. New Phytologist **177**:608–626.

Choat, B., S. Jansen, M. A. Zwieniecki, E. Smets, and N. M. Holbrook. 2004. Changes in pit membrane porosity due to deflection and stretching: the role of vestured pits. Journal of Experimental Botany **55**:1569–1575.

Collatz, G. J., J. T. Ball, C. Grivet, and J. A. Berry. 1991. Physiological and environmental regulation of stomatal conductance, photosynthesis and transpiration: A model that includes a laminar boundary layer. Agricultural and Forest Meteorology **54**:107–136.

Collet, C., M. Fournier, F. Ningre, A. Houzandji, and T. Constant. 2011. Growth and posture control strategies in *Fagus sylvatica* and *Acer pseudoplatanus* saplings in response to canopy disturbance. Annals of Botany **107**:1345–1353.

Dale, V. H., J. L. A., S. McNulty, R. P. Neilson, M. P. Ayres, M. D. Flannigan, P. J. Hanson, L. C. Irland, A. E. Lugo, C. J. Peterson, D. Simberloff, F. J. Swanson, B. J. Stocks, and B. M. Wotton. 2001. Climate change and forest disturbances. Bioscience **51**:723–734.

Davis, S. D., J. S. Sperry, and H. U. G. 1999. The relationship between xylem conduit diameter and cavitation caused by freezing. American Journal of Botany **86**:1367–1372.

De Groot, C. C., L. F. M. Marcelis, R. van den Boogaard, and H. Lambers. 2002. Interactive effects of nitrogen and irradiance on growth and partitioning of dry mass and nitrogen in young tomato plants. Functional Plant Biology **29**:1319–1328.

de Kroon, H., H. Huber, J. F. Stuefer, and J. M. van Groenendael. 2005. A modular concept of phenotypic plasticity in plants. New Phytologist **166**:73–82.

Dewar, R. C. 1993. A Root-Shoot Partitioning Model Based on Carbon-Nitrogen-Water Interactions and Munch Phloem Flow. Functional Ecology **7**:356–368.

Dupuy, L., P. J. Gregory, and A. G. Bengough. 2010. Root growth models: towards a new generation of continuous approaches. Journal of Experimental Botany **61**:2131–2143.

Ellmore, G. S., A. E. Zanne, and C. M. Orians. 2006. Comparative sectoriality in temperate hardwoods: hydraulics and xylem anatomy. Botanical Journal of the Linnean Society **150**:61–71.

Erb, M., C. Lenk, J. Degenhardt, and T. C. Turlings. 2009. The underestimated role of roots in defense against leaf attackers. Trends in plant science **14**:653–659.

Esau, K., 1969. The Sieve Element. Pages 17–115 *in* The Phloem, volume 5 of *Encyclopedia of Plant Anatomy*. Gebruder Borntraeger, Berlin, Germany.

Fransen, B., H. De Kroon, C. G. F. De Kovel, and F. Van Den Bosch. 1999. Disentangling the effects of root foraging and inherent growth rate on plant biomass accumulation in heterogeneous environments: a modelling study. Annals of Botany **84**:305–311.

Getzin, S., and K. Wiegand. 2007. Asymmetric tree growth at the stand level: Random crown patterns and the response to slope. Forest ecology and management **242**:165–174.

Gloser, V., K. Libera, and C. M. Orians. 2008. Contrasting below-and aboveground responses of two deciduous trees to patchy nitrate availability. Tree physiology **28**:37.

Gloser, V., M. A. Zwieniecki, C. M. Orians, and N. M. Holbrook. 2007. Dynamic changes in root hydraulic properties in response to nitrate availability. Journal of Experimental Botany .

Golubski, A. J., K. L. Gross, and G. G. Mittelbach. 2008. Competition among plant species that interact with their environment at different spatial scales. Proceedings of the Royal Society B: Biological Sciences **275**:1897–1906.

Gómez, S., R. A. Ferrieri, M. Schueller, and C. M. Orians. 2010. Methyl jasmonate elicits rapid changes in carbon and nitrogen dynamics in tomato. New Phytologist **188**:835–844.

Gorska, A., Q. Ye, M. Holbrook, and M. A. Zwieniecki. 2008. Nitrate Control of Root Hydraulic Properties in Plants: Translating Local Information to Whole Plant Response. Plant Physiology **148**:1159–1167.

Greenidge, K. N. H. 1955. Studies in the Physiology of Forest Trees. III. The Effect of Drastic Interruption of Conducting Tissues on Moisture Movement. American Journal of Botany **42**:582–587.

Guo, S. W., R. Kaldenhoff, N. Uehlein, B. Sattelmacher, and H. Brueck. 2007. Relationship between water and nitrogen uptake in nitrate- and ammonium-

supplied Phaseolus vulgaris L. plants. Journal of plant nutrition and soil science **170**:73–80.

Gupta, M. L., and S. Bhambie. 1977. Studies in Lamiaceae I. The node. Proceedings of the Indian Academy of Sciences **86**:281–286.

Hacke, U. G., J. S. Sperry, J. K. Wheeler, and L. Castro. 2006. Scaling of angiosperm xylem structure with safety and efficiency. Tree Physiology **26**:689.

Hacke, U. G., V. Stiller, J. S. Sperry, J. Pittermann, and K. A. McCulloh. 2001. Cavitation Fatigue. Embolism and Refilling Cycles Can Weaken the Cavitation Resistance of Xylem. Plant Physiology **125**:779–786.

Hangarter, R. P. 1997. Gravity, light and plant form. Plant, Cell and Environment **20**:796–800.

Hodge, A. 2004. The plastic plant: root responses to heterogeneous supplies of nutrients. New Phytologist **162**:9–24.

Hodge, A. 2006. Plastic plants and patchy soils. Journal of Experimental Botany **57**:401–411.

Hodge, A. 2009. Root decisions. Plant, Cell & Environment **32**:628–640.

Hodge, A., D. Robinson, B. S. Griffiths, and A. H. Fitter. 1999. Why plants bother: root proliferation results in increased nitrogen capture from an organic patch when two grasses compete. Plant, Cell & Environment **22**:811–820.

Holton, N., A. Cano-Delgado, K. Harrison, T. Montoya, J. Chory, and G. J. Bishop. 2007. Tomato BRASSINOSTEROID INSENSITIVE1 is required for systemin-induced root elongation in Solanum pimpinellifolium but is not essential for wound signaling. The Plant Cell Online **19**:1709–1717.

Horton, M., and E. P. Lacey. 1994. Carbon integration in Plantago aristata (Plantaginaceae): the reproductive effects of defoliation. American Journal of Botany **81**:278–286.

Hutchings, M. J., and I. K. Bradbury. 1986. Ecological perspectives on clonal perennial herbs. Bioscience **36**:178–182.

Hutchings, M. J., and E. A. John. 2004. The effects of environmental heterogeneity on root growth and root/shoot partitioning. Annals of Botany **94**:1–8.

IPCC (Intergovernmental Panel on Climate Change), 2007. Summary for Policymakers. Climate Change 2007: The Scientific Basis.

Jansen, C., M. M. L. van Kempen, G. M. Bogemann, T. J. Bouma, and H. de Kroon. 2006. Limited costs of wrong root placement in Rumex palustris in heterogeneous soils. New Phytologist **171**:117–126.

Javot, H., and C. Maurel. 2002. The role of aquaporints in root water uptake. Annals of Botany **90**:301–313.

Jones, T. J., C. D. Luton, L. S. Santiago, and G. Goldstein. 2010. Hydraulic constraints on photosynthesis in subtropical evergreen broad leaf forest and pine woodland trees of the Florida Everglades. Trees—Structure and Function **24**:471–478.

Kembel, S. W., and J. F. Cahill. 2005. Plant phenotypic plasticity belowground: a phylogenetic perspective on root foraging trade-offs. The American Naturalist **166**:216–230.

Kembel, S. W., H. De Kroon, J. F. Cahill Jr, and L. Mommer. 2008. Improving the scale and precision of hypotheses to explain root foraging ability. Annals of Botany .

King, D. A. 2001. Stem orientation is related to growth rate, leaf dimensions, and the deciduous habit in temperate forest saplings. Botany **79**:1282–1291.

Kitin, P. B., T. Fujii, H. Abe, and R. Funada. 2004. Anatomy of the vessel network within and between tree rings of Fraxinus lanuginosa (Oleaceae). American Journal of Botany **91**:779–788.

Knapp, A. K. 1992. Leaf gas exchange in Quercus macrocarpa (Fagaceae): Rapid stomatal responses to variability in sunlight in a tree growth form. American Journal of Botany **79**:599–604.

Kobe, R. K., S. W. Pacala, J. A. Silander, and C. D. Canham. 1995. Juvenile Tree Survivorship as a Component of Shade Tolerance. Ecological Applications **5**:517–532.

Kozlowski, T. T., and C. H. Winget. 1963. Patterns of Water Movement in Forest Trees. Botanical Gazette **124**:301–311.

Lamb, E. G., J. J. Haag, and J. F. Cahill Jr. 2004. Patch-background contrast and patch density have limited effects on root proliferation and plant performance in Abutilon theophrasti. Ecology **18**:836–843.

Lang, A. C., W. Härdtle, H. Bruelheide, C. Geißer, K. Nadrowski, A. Schuldt, M. Yu, and G. von Oheimb. 2010. Tree morphology responds to neighbourhood competition and slope in species-rich forests of subtropical China. Forest Ecology and Management .

Larson, D. W., J. Doubt, and U. Matthes-Sears. 1994. Radially sectored hydraulic pathways in the xylem of *Thuja occidentalist* as revealed by the use of dyes. International Journal of Plant Sciences **155**:569–582.

Loepfe, L., J. Martinez-Vilalta, J. Pinol, and M. Maurizio. 2007. The relevance of xylem network structure for plant hydraulic efficiency and safety. Journal of Theoretical Biology **247**:788–803.

Mackay, J. F. G., and P. E. Weatherly. 1973. The Effects of Transverse Cuts Through the Stems of Transpiring Woody Plants on Water Transport and Stress in the Leaves. Journal of Experimental Botany **24**:15–28.

Maurel, C., T. Simonneau, and S. Moira. 2010. The significance of roots as hydraulic rheostats. Journal of Experimental Botany **61**:3191–3198.

McConnaughay, K. D. M., and J. S. Coleman. 1999. Biomass allocation in plants: ontogeny or optimality? A test along three resource gradients. Ecology **80**:2581–2593.

McNickle, G. G., and J. F. Cahill. 2009. Plant root growth and the marginal value theorem. Proceedings of the National Academy of Sciences **106**:4747–4751.

Meziane, D., and B. Shipley. 1999. Interacting determinants of specific leaf area in 22 herbaceous species: effects of irradiance and nutrient availability. Plant, Cell & Environment **22**:447–459.

Middlesex Fells Reservation, accessed on Sept 28, 2011. Massachusetts Department of Conservation and Recreation. URL `http://www.mass.gov/dcr/parks/metroboston/fells.htm`.

Murphy, N., and M. A. Watson. 1996. Sectorial root growth in cuttings of Coleus rehneltianus in response to localized aerial defoliation. Vegetatio **127**:17–23.

Muth, and Bazzaz. 2002. Tree canopy displacement at forest gap edges. Canadian Journal of Forest Research-Revue Canadienne De Recherche Forestiere **32**:247–254.

Muth, C., and F. Bazzaz. 2003. Tree canopy displacement and neighborhood interactions. Canadian Journal of Forest Research-Revue Canadienne De Recherche Forestiere **33**:1323–1330.

Nadezhdina, N. 2010. Integration of water transport pathways in a maple tree: responses of sap flow to branch severing. Annals of forest science **67**.

Nardini, A., and S. Salleo. 2000. Limitation of stomatal conductance by hydraulic traits: sensing or preventing xylem cavitation? Trees - Structure and Function **15**:14–24.

Newman, E. I. 1973. Permeability to water of the roots of five herbaceous species. New Phytologist **72**:547–555.

Niinemets, U., and F. Vallaraes. 2006. Tolerance to shade, drought, and waterlogging of temerate Northern Hemisphere trees and shrubs. Ecological Monographs **76**:521–547.

Nowacki, G. J., and M. D. Abrams. 1997. Radial-Growth Averaging Criteria for Reconstruction Disturbance Histories from Presettlement-Origin Oaks. Ecological Monographs **67**:225–249.

Oborny, B., T. Czárán, and A. Kun. 2001. Exploration and exploitation of resource patches by clonal growth: a spatial model on the effect of transport between modules. Ecological modelling **141**:151–169.

Orians, C. M. 2005. Herbivores, Vascular Pathways, and Systemic Induction: Facts and Artifacts. Journal of Chemical Ecology **31**:2231–2242.

Orians, C. M., M. Ardón, and B. A. Mohammad. 2002. Vascular architecture and patchy nutrient availability generate within-plant heterogeneity in plant traits important to herbivores. American Journal of Botany **89**:270–278.

Orians, C. M., B. Babst, and A. E. Zanne, 2005*a*. Vascular constraints and long distance transport in dicots. Pages 355–371 *in* N. M. Holbrook and M. A. Zwieniecki, editors. Vascular Transport in Plants. Physiological Ecology, Elsevier Academic Press, San Diego.

Orians, C. M., and C. G. Jones. 2001. Plants as resource mosaics: a functional model for predicting patterns of within-plant resource heterogeneity to consumers based on vascular architecture and local environmental variability. Oikos **94**:493–504.

Orians, C. M., J. Pomerleau, and R. Ricco. 2000. Vascular architecture generates fine scale variation in systemic induction of proteinase inhibitors in tomato. Journal of Chemical Ecology **26**:471–485.

Orians, C. M., S. D. P. Smith, and L. Sack. 2005*b*. How are leaves plumbed inside a branch? Differences in leaf-to-leaf hydraulic sectoriality among six temperate tree species. Journal of Experimental Botany **56**:2267–2273.

Orians, C. M., A. Thorn, and S. Gómez. 2011. Herbivore-induced resource sequestration in plants: Why bother? Oecologia .

Orians, C. M., M. M. I. van Vuuren, N. L. Harris, B. A. Babst, and G. S. Ellmore. 2004. Differential sectoriality in long-distance transport in temperate tree species: evidence from dye flow, 15N transport, and vessel element pitting. Trees - Structure and Function **18**:501–509.

Paschold, A., R. Halitschke, and I. T. Baldwin. 2007. Co-ordinating defenses: NACI1 mediates herbivore-induced resistance in *Nicotiana attenuata* and reveals the role of herbivore movement in avoiding defenses. The Plant Journal **51**:79–91.

Pate, J., and W. Jeschke, 1995. The Role of Stems in Transport, Storage, and Circulation of Ions and Metabolites by the Whole Plant. Pages 177–204 *in* Plant Stems: Physiology and Functional Morphology. Academic Press, Inc., San Diego, gartner edition.

Pearce, G., D. S. Moura, J. Stratmann, and C. A. Ryan. 2001. RALF, a 5-kDa ubiquitous polypeptide in plants, arrests root growth and development. Proceedings of the National Academy of Sciences of the United States of America **98**:12843–12847.

Pearcy, R. W., L. J. Gross, and D. He. 1997. An improved dynamic model of photosynthesis for estimation of carbon gain in sunfleck light regimes. Plant, Cell and Environment **20**:411–424.

Peel, A. J. 1963. Tangential movement of ^{14}C-labelled assimilates in stems of willow. Journal of Experimental Botany **15**:104–113.

Polley, H. W., H. B. Johnson, C. R. Tischler, and H. A. Torbert. 1999. Links between transpiration and plant nitrogen: Variation with atmospheric CO_2 concentration and nitrogen availability. International Journal of Plant Science **160**:535–542.

Postlethwait, S. N., and B. Rogers. 1958. Tracing the Path of the Transpiration Stream in Trees by the use of Radioactive Isotopes. American Journal of Botany **45**:753–757.

Preston, K. A. 1998. The effects of developmental stage and source leaf position on integration and sectorial patterns of carbohydrate movement in an annual plant, Perilla frutescens (Lamiaceae). American Journal of Botany **85**:1695–1703.

Price, E. A., and M. J. Hutchings. 1992. Studies of growth in the clonal herb *Glechoma hederacea*. II. The effects of selective defoliation. Journal of Ecology **80**:39–47.

Price, E. A., C. Marshall, and M. J. Hutchings. 1992. Studies of growth in the clonal herb *Glechoma hederacea*. I. Patterns of physiological integration. Journal of Ecology **80**:25–38.

Rinne, R. W., and R. G. Langston. 1960. Studies on lateral movement of phosphorous 32 in peppermint. Plant Physiology **35**:216–219.

Robinson, D. 1994. The responses of plants to non-uniform supplies of nutrients. New Phytologist **127**:635–674.

Rodriguez-Saona, C. R., L. E. Rodriguez-Saona, and C. J. Frost. 2009. Herbivore-induced volatiles in the perennial shrub, Vaccinium corymbosum, and their role in inter-branch signaling. Journal of chemical ecology **35**:163–175.

Roitsch, T. 1999. Source-sink regulation by sugar and stress. Current Opinion in Plant Biology **2**:198–206.

Roslin, T., S. Gripenberg, J. Salminen, M. Karonen, R. B. O'Hara, K. Pihlaja, and P. Pulkkinen. 2006. Seeing the trees for the leaves—Oaks as mosaics for a host-specific moth. OIKOS **113**:106–120.

Sack, L., P. D. Cowan, N. Jaikumar, and N. M. Holbrook. 2003. The "hydrology" of leaves: co-ordination of structure and function in temperate woody species. Plant, Cell & Environment **26**:1343–1356.

Sack, L., and H. N. M. 2006. Leaf hydraulics. Annual Review of Plant Biology **57**:361–381.

Salguero-Gómez, R., and B. B. Casper. 2011. A hydraulic explanation for size-specific plant shrinkage: developmental hydraulic sectoriality. New Phytologist **189**:229–240.

Scarpella, E., and A. H. Meijer. 2004. Pattern formation in the vascular system of monocot and dicot plant species. New Phytologist **164**:209–242.

Schamp, B. S., M. Schurer, and L. W. Aarssen. 2007. Testing Hypotheses for Stem Bending in Tree Saplings. International Journal of Plant Sciences **168**:547–553.

Schenk, H. J., S. Espino, C. M. Goedhart, M. Nordenstahl, H. I. M. Cabrera, and C. S. Jones. 2008. Hydraulic integration and shrub growth form linked across continental aridity gradients. Proceedings of the National Academy of Sciences **105**:11248–11253.

Schulte, P. J., and D. G. Costa. 2010. Xylem anisotropy and water transport—a model for the double sawcut experiment. Tree Physiology **30**:901–913.

Seidel, D., C. Leuschner, et al. 2011. Crown plasticity in mixed forests—Quantifying asymmetry as a measure of competition using terrestrial laser scanning. Forest Ecology and Management .

Shea, M. M., and M. A. Watson. 1989. Patterns of leaf and flower removal: their effect on fruit growth in Chamaenerion angustifolium (fireweed). American Journal of Botany **76**:884–890.

Shemesh, H., A. Arbiv, M. Gersani, O. Ovadia, A. Novoplansky, and H. H. Bruun. 2010. The Effects of Nutrient Dynamics on Root Patch Choice. Plos One **5**:e10824.

Shipley, B., D. Vile, E. Garnier, I. J. Wright, and H. Poorter. 2005. Functional linkages between leaf traits and net photosynthetic rate: reconciling empirical and mechanistic models. Functional Ecology **19**:602–615.

Siebrecht, S., K. Herdel, U. Schurr, and R. Tischner. 2003. Nutrient translocation in the xylem of poplar–diurnal variations and spatial distribution along the shoot axis. Planta **217**:783–793.

Singsaas, E. L., D. R. Ort, and E. H. DeLucia. 2000. Diurnal regulation of photosynthesis in understory saplings. New Phytologist **145**:39–49.

Sperry, J. S. 2003. Evolution of Water Transport and Xylem Structure. International Journal of Plant Science (3 Suppl.) **164**:S115–S127.

Sperry, J. S., N. N. Alder, and S. E. Eastlack. 1993. The Effect of Reduced Hydraulic Conductance on Stomatal Conductance and Xylem Cavitation. Journal of Experimental Botany **44**:1075–1082.

Sprugel, D. G. 2002. When branch autonomy fails: Milton's Law of resource availability and allocation. Tree Physiology **22**:1119.

Stark, J. M., 1994. Causes of soil nutrient heterogeneity at different scales. Pages 255–284 *in* M. M. Caldwell and P. R. W., editors. Exploitation of environmental heterogeneity by plants. Academic Press, San Diego.

Steppe, K., V. Cnudde, C. Girard, R. Lemeur, J. P. Cnudde, and P. Jacobs. 2004. Use of X-ray computed microtomography for non-invasive determination of wood anatomical characteristics. Journal of structural biology **148**:11–21.

Stoll, P., and B. Schmid. 1998. Plant foraging and dynamic competition between branches of *Pinus sylbestris* in contrasting light environments. Journal of Ecology **86**:934–945.

Suomela, J., P. Kaitaniemi, and A. Nilson. 1995. Systematic within-tree variation in mountain birch leaf quality for a geometrid, Epirrita autumnata. Ecological Entomology **20**:283–292.

Taiz, L., and E. Zeiger. 2002. Plant Physiology. 3rd edition. Sinauer Associates, Inc., Sunderland, MA.

Takahashi, H. 1994. Hydrotropism and its interaction with gravitropism in roots. Plant and Soil **165**:301–308.

Takano, M., H. Takahashi, T. Hirasawa, and H. Suge. 1995. Hydrotropism in roots: Sensing of a gradient in water potential by the root cap. Planta **197**:410–413.

Takenaka, A. 2000. Shoot growth responses to light microenvironment and correlative inhibition in tree seedlings under a forest canopy. Tree physiology **20**:987.

Takeuchi, H., M. P. Zalucki, and M. J. Furlong. 2009. *Crocidolomia pavonana* larval foraging: Behavior and feeding site preferences on cabbage, *Brassica olericea*. Entomologia Experimentalis et Applicata **133**:154–164.

Tans, P., 2009. Trends in atmospheric carbon dioxide – Mauna Lao. National Oceanic and Atmospheric Administration/Eearth System Research Laboratory. http://www.esrl.noaa.gov/gmd/ccgg/trends.

Thomas, L. P., and M. A. Watson. 1988. Leaf removal and the apparent effects of architectural constraints on development in Capsicum annuum. American journal of botany **75**:840–843.

Thompson, M. V., and N. M. Holbrook. 2003. Scaling phloem transport: water potential equilibrium and osmoregulatory flow. Plant, Cell & Environment **26**:1561–1577.

Thorn, A. M., and C. M. Orians. 2011*a*. Modeling the influence of differential sectoriality on the photosynthetic responses of understory saplings to patchy light and water availability. Trees **25**:833–845.

Thorn, A. M., and C. M. Orians. 2011*b*. Partial defoliation and hydraulic integration in *Ocimum basilicum*: Testing a model for sectored xylem flow using 15N labeling. American Journal of Botany **98**:1816–1824.

Thorn, A. M., and C. M. Orians. 2011*c*. Patchy nitrate promotes inter-sector flow and 15N allocation in *Ocimum basilicum*: A model and an experiment. Functional Plant Biology **38**:879–887.

Thornley, J. H., and I. R. Johnson. 2000. Plant and Crop Modelling: A Mathematical Approach to Plant and Crop Physiology. Blackburn Press, Caldwell, New Jersey.

Thornley, J. H. M. 1996. Modelling water in crops and plant ecosystems. Annals of Botany **77**:262–275.

Thorpe, M., P. Minchin, N. Gould, and J. McQueen, 2005. The stem apoplast: A potential communication channel in plant growth regulation. Pages 201–220 *in* N. M. Holbrook and M. A. Zwieniecki, editors. Vascular Transport in Plants. Physiological Ecology, Elsevier Academic Press, San Diego.

Thorpe, M. R., A. P. Ferrieri, M. M. Herth, and R. A. Ferrieri. 2007. 11 C-imaging: methyl jasmonate moves in both phloem and xylem, promotes transport of jasmonate, and of photoassimilate even after proton transport is decoupled. Planta **226**:541–551.

Tyree, M. T., and F. W. Ewers. 1991. Tansley Review No. 34. The hydraulic architecture of trees and other woody plants. New Phytologist **119**:345–360.

Tyree, M. T., and M. H. Zimmerman. 2002. Xylem Structure and the Ascent of Sap. Springer, Berlin.

Van Arendonk, J., E. Karanov, V. Alexieva, and H. Lambers. 1998. Polyamine concentrations in four Poa species, differing in their maximum relative growth rate, grown with free access to nitrate and at limiting nitrate supply. Plant Growth Regulation **24**:77–89.

van Vuuren, M., A. Muir, and C. Orians. 2003. Growth and nutrient uptake by birch and maple seedlings on soil with patchy or homogeneous distribution of organic matter. Canadian Journal of Forest Research—Revue Canadienne de Recherche **33**:2019–2026.

Volder, A., D. R. Smart, A. Bloom, and D. Eissenstat. 2005. Rapid decline in nitrate uptake and respiration with age in fine lateral roots of grape: Implications for root efficiency and competitive effectiveness. New Phytologist **165**:493–501.

Wangermann, E. 1967. The effect of the leaf on differentiation of primary xylem in the internode of *Coleus blumei* Benth. New Phytologist **66**:747–754.

Watson, M. A., and B. B. Casper. 1984. Morphogenetic constraints on patterns of carbon distribution in plants. Annual Review of Ecology and Systematics **15**:233–258.

Webster, C. R., and N. R. Jensen. 2007. A shift in the gap dynamics of Betula alleghaniensis in response to single-tree selection. Canadian Journal of Forest Research **37**:682–689.

West, G. B., J. H. Brown, and B. J. Enquist. 1999. A general model for the structure and allometry of plant vascular systems. Nature **400**:664–667.

Yang, Z., and D. J. Midmore. 2005. Modelling plant resource allocation and growth partitioning in response to environmental heterogeneity. Ecological modelling **181**:59–77.

Yang, Z., and D. J. Midmore. 2009. Self-organisation at the whole-plant level: a modelling study. Functional Plant Biology **36**:56–65.

Young, and Hubbell. 1991. Crown asymmetry, treefalls, and repeat disturbance of broad-leaved forest gaps. Ecology **72**:1464–1471.

Zanne, A. E., S. S. Lower, Z. G. Cardon, and C. M. Orians. 2006*a*. 15N partitioning in tomato: vascular constraints versus tissue demand. Functional Plant Biology **33**:457–464.

Zanne, A. E., K. Sweeney, M. Sharma, and C. M. Orians. 2006*b*. Patterns and consequences of differential vascular sectoriality in 18 temperate tree and shrub species. Functional Ecology **20**:200–206.

Zanne, A. E., M. Westoby, D. S. Falster, A. D. D., L. S. R., A. S. E. J., and C. D. A. 2010. Angiosperm wood structure: Global patterns in vessel anatomy and their relation to wood density and potential conductivity. American Journal of Botany **54**:1399–1405.

Zwieniecki, M. A., P. Melcher, and N. Holbrook. 2001. Hydrogel Control of Xylem Hydraulic Resistance in Plants. Science **291**:1059–1062.

Zwieniecki, M. A., C. M. Orians, P. J. Melcher, and N. M. Holbrook. 2003. Ionic control of the lateral exchange of water between vascular bundles in tomato. Journal of Experimental Botany **54**:1399–1405.